From Chitosan Thiomers to Polyoxometalate-Chitosan Nanocomposites for Medical Applications

---

Dissertation

zur

Erlangung der naturwissenschaftlichen Doktorwürde
(Dr. sc. nat.)

vorgelegt der

Mathematisch-naturwissenschaftlichen Fakultät

der

Universität Zürich

von

Matteo Croce

aus

Italien

Promotionskommission

Prof. Dr. Greta R. Patzke (Vorsitz)

Prof. Dr. Caroline Maake

Prof. Dr. Roland K. O. Sigel

Prof. Dr. Gilles Gasser

Zürich, 2018

«Ognuno sta solo sul cuor della terra

trafitto da un raggio di sole:

ed è subito sera.»

Salvatore Quasimodo, 1930

To Samuel

Summary

Acknowledgements

This manuscript is the final step of a journey that lasted four years, during which I met many people who helped me in various ways, sharing their ideas and suggestions and giving help and support when I needed it most.

I would like to thank my supervisors Prof. Dr. Greta Patzke and Prof. Dr. med. Caroline Maake for the trust they placed in me to run such a complex and interdisciplinary project. I thank Greta for her wise advice, for her help in choosing the best ideas worthy to be pursued and for the freedom and independence she granted during the project. Moreover, I wish to thank her for understanding the necessities of young parents and that the working place was not only in the office. Nevertheless, I wish to thank her for the prompt and very constructive revision of this thesis. I would like to thank Caroline for her support and enthusiasm and for her guaranteed availability for scientific discussions, especially in the moment when my faith in science was more challenged. I thank her, especially, for the trust placed in my skills, for the time spent in patiently listen to all the ideas I was coming up with and for the final revision of this thesis.

Many thanks go to Prof. Dr. Roland Sigel and Prof. Dr. Gilles Gasser for accepting to be part of my doctoral committee and for all the nice discussions and suggestions exchanged during these years.

The biggest thanks go definitely to my partner (in life and in this project) Simona Conti. The list of things for which I would like to thank her is enormously long, but I will keep it short. Simona, thank you for reading this thesis from bottom to top and for your effort in improving it. Thank you to accept to work with me, even knowing my special character and impatience. Thank you for the countless biological experiments you performed on the compounds I was synthesizing. Thank you for your tolerance when I was bringing the work at home discussing possible ways to solve research related issues all evening long, sometimes still in the morning. Last but not least, thank you for letting me know the joy of fatherhood.

I would like to thank all people that helped me with technical and administrative support. I thank Dr. Kim von Allmen and Fangyuan Song for performing the single-crystal X-ray diffraction measurements. I thank Dr. Thomas Fox for the solid-state ^{13}C-NMR spectroscopy and liquid-state ^{183}W-NMR spectroscopy experiments. I thank Nadja Bross for the instructions on the NMR

spectrometer. I thank Prof. Dr. Jean-Christophe Leroux (ETH Zurich) for allowing me to measure gel permeation chromatography in his laboratories. I thank all the members of the Center for Microscopy and Image Analysis (ZMB) and especially Dr. Moritz Kirschmann, Dr. Andres Käch and Lucca Andreoli for their introduction on electron microscopy. I thank Ramona Erni, Sabine Stockhause, Nathalie Fichter, Beatrice Spichtig and Larissa Mostacciuolo for their help in administrative matters.

I would like to thank Rafael Müller who turned out to be an inspirational, original colleague and friend for all the time of my PhD. Thanks for hearing me and to be always ready to cheer me up when the office was too silent. I would like to thank all the other colleagues from the E-floor downstairs for the nice jokes and science discussions. Thanks to Lukas, Kim, Peter, Doris, Sandra, Kathrin, Lara, Renè, Felix, Chen and Esmael. I thank also all the other group members for the nice moments together, especially the boat trip and the group meetings.

Special thanks go to Dr. Elena Alberti for her friendship and our nice discussions. Together we shared some very special moments, like the supervision of the students during the *Praktikum*, the cooking in Vinzenz and the organization of the CMSZH Retreat, where I enjoyed very nice moments.

Many thanks to Yvonne Forster for the correction of the *Zusammenfassung* and for the attempts on the determination of tungsten via ICP-MS. Thanks also for the nice breaks and walks.

I would like to thank my parents for supporting me all the time on following my dreams and to babysitting Samuel. Thank you, Samuel, for your happiness when you see me and for making all the days authentic. I would like to thank those friends which even if living far, were always present: among them Damiano and Giulia (remember - without you I would have never be here).

I would like to acknowledge the University of Zurich and the graduate school of Chemical and Molecular Sciences Zurich (CMSZH) for the good work facilities and the stimulating scientific environment. Financial support by the Swiss National Science Foundation (Grant No. 205321_146849) is finally gratefully acknowledged.

Abbreviations

AAs	amino acids
AC	acyl chloride
AIDS	acquired immune deficiency syndrome
Ala	alanine
AsPC-1	type of human pancreatic cancer cells
BHI	brain heart infusion
BOC	tert-butyloxycarbonyl
BSA	bovine serum albumin
CFU	colony forming units
CLSM	confocal laser scanning microscopy
CMC	carboxymethyl chitosan
COSY	correlation spectroscopy
CP-MAS	cross polarization-magic angle spinning
CYS	cysteine
d	duplet
DD	degree of deacetylation
DLS	dynamic light scattering
DMEM	Dulbecco's modified eagle medium
DMF	dimethylformamide
DMSO	dimethyl sulfoxide
DNA	deoxyribonucleic acid
DS	degree of substitution
$DTNB^{2-}$	5,5'-dithiobis(2-nitrobenzoic acid)
EDC	1-ethyl-3-(3-dimethylaminopropyl)carbodiimide hydrochloride
EDTA	ethylenediaminetetraacetic acid
EDX	energy-dispersive X-ray spectroscopy
EPR	enhanced permeability and retention
FCS	fetal calf serum
FMN	flavin mononucleotide
FT-IR	Fourier transform infrared
GPC	gel permeation chromatography
HAS	N-hydroxysuccinimide
HeLa	type of cervical cancer cell line
HIV	human immunodeficiency virus
HMW	high molecular weight
HPA-23	heteropolyanion-23 (ammonium-21-tungsto-9-antimoniate)
HPLC	high performance liquid chromatography
IC_{50}	effective concentration of 50% inhibition of cell growth
ICP-MS	inductively coupled plasma mass spectrometry
ICSD	inorganic crystal structure database
IMI	2-iminothiolane
kDa	kiloDalton

LB	Luria-Bertani
LMW	low molecular weight
m	multiplet
MBA	mercaptobutyric acid
MBeA	mercaptobenzoic acid
MHA	mercaptohexanoic acid
MIC	minimum inhibitory concentration
MMA	mercaptoacetaldehyde
MMW	medium molecular weight
MOA	mercaptooctanoic acid
MPA	mercaptopropionic acid
MRC-5	type of lung tissue cell line
MSPA	2-methyl-3-sulfanylpropanoic acid
MTT	3-(4,5-dimethylthiazol-2-yl)-2,5-diphenyltetrazolium bromide
MW	molecular weight
NADH	nicotinamide adenine dinucleotide (reduced form)
NMR	nuclear magnetic resonance
NPs	nanoparticles
PBS	phosphate buffered saline
PCA	plate counting agar
PDI	polydispersity index
PI	propidium iodide
POM	polyoxometalate
RNA	ribonucleic acid
RT	room temperature
s	singlet
SAR	structure-activity relationship
SEM	scanning electron microscopy
Ser	Serine
SPIONs	superparamagnetic iron oxide nanoparticles
t	triplet
TBA	tetrabutylammonium
TEM	transmission electron microscopy
TGA	thioglycolic acid
TLA	thiolactic acid
TMC	trimethyl chitosan
TNB^{2-}	5-thio-2-nitrobenzoic acid
TPH	tris(2-carboxyethyl)phosphine
TPP	sodium tripolyphosphate
UV-Vis	ultraviolet-visible
VDW	van der Waals
XRD	X-ray diffraction
ζ-potential	zeta-potential

Publications

The following parts of this PhD thesis have been published:

Chapter 2

M. Croce, S. Conti, C. Maake, G. Patzke, *Carbohydr. Polym.,* **2016,** *151*, 1184-1192.
https://doi.org/10.1016/j.carbpol.2016.06.014

Chapter 3

M. Croce, S. Conti, C. Maake, G. Patzke, *Eur. J. Inorg. Chem.*, **2018,** in press.
https://doi.org/10.1002/ejic.201800268

The synthesis and the characterization of the major part of the investigated compounds were performed by Matteo Croce, the author of this work. The following exceptions are herewith specified:

The single-crystal X-ray diffraction analyses were performed by Dr. Kim von Allmen and Fangyuan Song.

The solid-state ^{13}C-NMR and liquid-state ^{183}W-NMR measurements were performed by Dr. Thomas Fox.

The syntheses of two chitosan-TGA samples (SC-1 and GG-B-23) were performed by Simona Conti and Georg Geisberger.

The major parts of the biological experiments were performed by Simona Conti (Chapter 2: sections 2.2.4 and 2.3.2; Chapter 3: sections 3.2.5-3.2.9 and sections 3.3.4, 3.3.5.1 and 3.3.5.3; Chapter 4: section 4.3; Chapter 5: section 5.1.1). Flow cytometry experiments (section 3.3.5.2) and some preliminary cytotoxicity evaluations were performed by myself.

During our work, Simona Conti and I supported each other on a regular basis, especially in high-throughput work periods, and while performing the most complex experiments.

1. Introduction

1.1 The antibiotic resistance problem

Bacteria are monocellular prokaryotic microorganisms. Compared to the eukaryotic cells, bacterial cells are characterized by an absence of organelles in the cytoplasm, the absence of a nucleus and the consequent presence of DNA in a free form. Bacteria can be defined more precisely observing their molecular characteristics, to strictly distinguish their domain from the ones of Archaea and Eucarya.[1]

Thanks to millions of years of adaptation bacteria can be found in many different environments on earth, from the common soil to less usual environments like acidic spring waters, depth soil and seas.[2] Moreover, bacteria can be found in our body[3] and especially in the gut, where their population can partially change depending on the diet:[4] some bacteria species can establish a commensal and/or symbiotic relationship with humans, influencing for examples their immune functions, as well as the processing of nutrients.[5]

Certain strains of bacteria can act as pathogens and caused the plethora of diseases which marked our history. *Yersinia pestis was* responsible for the big epidemy in the Middle age known as "black death", which led to the death of 25 to 50% of the European population and was triggering many social and political changes, among others the start of the Secularization in Europe.[6] Tuberculosis, caused by the bacterium *Mycobacterium tuberculosis,* is one of the most widespread and persistent infectious diseases, which caused many victims in the previous centuries, and continue to be a lethal disease even nowadays, especially in the developing countries, with almost one third of human population supposedly being infected.[7] The memory of this disease in the occidental culture is still vivid in the mass culture and it plays an essential role in several books, movies, as well as theater's plays and operas like the famous "La Traviata" of *Giuseppe Verdi*. Furthermore, during the 19th century, bacterial infections such as pneumonia, diarrhea and diphtheria represented the main causes of death.[8] Bacteria were also limiting the positive outcome of surgical operations, even after the introduction of antisepsis procedures, due to post-surgical infections.[9]

The discovery of penicillins in 1928 by Fleming[10] and of the sulfonamides in 1932 by Domagk[11] made the extensive treatment of bacterial infections possible for the first time. This

revolutionized the medical field and significantly increased the human life expectancy. After World War II several classes of effective antibiotics were discovered, and a wave of optimism emerged between many physicians which can be adequately summarized by the presumable statement of the US Surgeon General William H. Stewart

"[it] is time to close the book on infectious diseases and declare the war against pestilence won."

Curiously, background research later showed that this sentence was never actually stated - on the contrary Stewart insisted to never underestimate the danger of infectious diseases.[12] The first appearance of antibiotic resistant bacteria in the hospitals was already documented in the years after the first use of sulfonamides and penicillin in Germany in the 1930s and in the United Kingdom in the 1940s.[13] Later on, the first multi-drug resistant strains (*Escherichia coli* and *Salmonella* species) were isolated in Africa during the 1950s and 60s.[14] Antibiotic resistance is an ancient phenomenon:[15] phylogenetic reconstruction highlights the rise of antibiotic resistance genes well before the production of antibiotics as pharmaceutical drugs.[16] Furthermore genomic sequencing data acquired from several strains collected in a Mexican cave dated 4 million years, evidenced the presence of some strains resistant to up of 14 different commercially available antibiotics, highlighting how resistance phenomenon existed well before antibiotics were discovered and in an environment isolated from the anthropogenic impacts.[17]
The antibiotics resistance phenomenon has been accelerated by the excessive and/or inappropriate use of antibiotics.[18] In many countries worldwide, antibiotics can be purchased without medical prescription, can be prescribed without any diagnosis or confirmation on the ongoing bacterial infection and/or consumed for an ineffective period of time. Misbehaviors, both on the physicians and on the patients sides, led to the quick development of genetic resistance by the survived bacterial populations and to their diffusion in the environment.[19] The use of antibiotics in intensive breeding and aquaculture, not only as prevention, but also as growth promotion agents is a further source of serious concern, even though the risks that this practice bears are known since the 1960s.[20] In this way, antibiotics are assumed by healthy individuals through nutrition and furthermore are spread in the environment by animal dejections, altering the soil microbiota and favoring the development of antibiotics resistant strains.

Antimicrobial resistance can be acquired as result of chromosomal mutation or inductive expression of a latent chromosomal gene or transmitted by genetic exchange through transformation (the exchange of DNA), transduction (bacteriophage), or conjugation by plasmids (extrachromosomal DNA).[21] Particularly, bacteria can become immune to the effects of antibiotics in several ways,[22] for example, by modifying/reprogramming the target structures (proteins),[23] deactivating enzymatically the antibiotic[24] such in the case of the beta lactamase,[25] limiting the antibiotic penetration inside the cells[26] or increasing its efflux.[27]

Antibiotic resistance strains were isolated for many different bacterial species.[28] The gram-positive methicillin-resistant *Staphylococcus aureus*, responsible for serious infections like pneumonia, infective endocarditis and bone/joint infections especially in hospitalized patients,[29] is estimated to be responsible of 19.000 fatalities per year solely in the USA.[30,31] Additional antibiotics resistant strains which are commonly isolated in hospitals are *Klebsiella pneumoniae, Pseudomonas aeruginosa, Enterococcus faecalis, Clostridium difficile*, and the above mentioned *M. tuberculosis*.[28,30] Particularly, gram-negative bacteria have the ability to quickly develop resistance to multiple antibiotics: in fact organisms can be isolated which are resistant to nearly all the available antibiotics.[19] Even some strains of the normally harmless *E. coli* showed ampicillin resistance increasing the difficulty of treatments.

Antimicrobial resistant strains are becoming a serious plague for human health and, from the economic point on view, an heavy burden for many healthcare systems.[32] The occurrence of infections caused by antibiotic resistant bacteria is dramatically rising in the clinics all over the world.[33,34] As representative example, the incidence of *P. aeruginosa* with combined antibiotics resistance, i.e. resistant to at least three classes of commercial antibiotics, isolated in the European Union countries in 2016 is reported in Figure 1.1. It is clear how the antimicrobial resistance problem is generally spreading.[35]

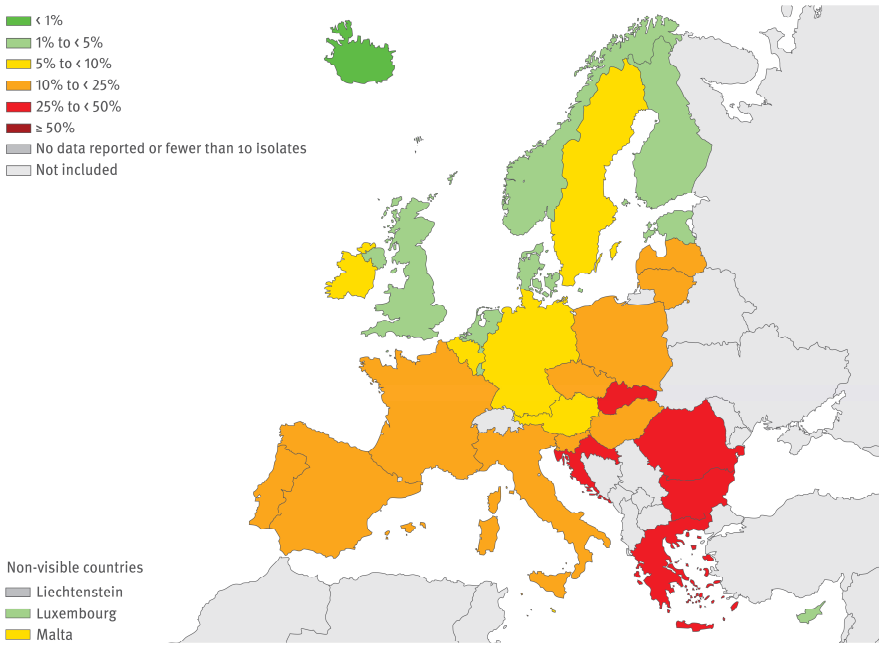

Figure 1.1. Incidence of P. aeruginosa with combined antibiotics resistance isolated in 2016 in the European Union.[35]

In "the review on antimicrobial resistance" *O'Neill* reported that 700.000 deaths every year are caused by antibacterial resistant strains.[36] Furthermore, considering the current behavior and attitude toward antibiotics, a vertiginous increase in fatalities caused by bacterial infections has been predicted: fatalities are expected to reach 10 million per year by 2050, exceeding the dimensions caused nowadays yearly by cancer.[36] The losses are huge also from an economical point of view. As example, the costs supported by the healthcare system only for methicillin-resistant *S. aureus* infections is estimated in $3-4 billion per year in the USA,[31] while the total loss in household income due to resistant species is $35 billion yearly only in the USA.[37] The economic burden is so heavy that if serious measures are not taken in account, the cumulated loss to the global economic output could reach $100 trillion by 2050.[36]

The Infectious Disease Society of America suggested possible solutions which include frequent meetings and workshops for better distribution of the available information about antibiotic resistant bacteria in the medical community, and a maximized prevention together with a more accurate and selective application of antibiotics. Other suggested actions that could limit the diffusion of antibiotic resistance are the improvement of diagnosis, tracking and prescription

practices, as well as the optimization of the therapeutic regimens and the adoption of antibiotic stewardship programs.[38] Furthermore, pharmaceutical industries and academy have to put continuous efforts in research and development programs to be able to offer new classes and new compounds effective against bacteria which can be resistant to all the commercial antibiotics.[34] Of crucial importance is the strategy to preserve the efficacy of the newly discovered drugs by keeping them as reservoir, used therefore to treat only the serious cases and kept out of the market.

The majority of the lead compounds of a certain class of antibiotic are natural products, which were discovered from fungi or bacteria, e.g. actinomycetes to gain advantage against their antagonists during the evolutionary race. Often these natural products were chemically tailored by pharmaceutical companies to achieve better pharmacological properties.[39] Nowadays, over ten classes of antibiotics are actually on the market, among them the most used are beta-lactams (which include penicillins, cephalosporins and carbapenems), tetracyclines, quinolones, sulfonamides, glycopeptides and aminoglycosides. Each class of antibiotic inhibits or competes with the natural substrate, such as proteins or DNA/RNA involved in essential pathways of the bacterial cell. Beta-lactams are known to inhibit the bacterial cell wall formation, by targeting the enzyme responsible for the crosslinking of the peptidoglycan, which leads to instability and destruction of the entire bacterial cell wall.[40] Tetracyclines, on the other hand, inhibit the synthesis of bacterial proteins by preventing the association of aminoacyl-tRNA within the bacterial ribosome,[41] while quinolones inhibit the enzyme DNA gyrase essential for DNA replication[42] and sulfonamides inhibited the enzyme involved in the folate synthesis.[43]

Since the decades after the World War II, known as the golden era of antibiotic discoveries, only three totally new classes of antibiotics were discovered since the 1970s.[44] The discovery, the development and the optimization of new effective antibiotics, which require several years before approval and therefore commercialization, led to an innovation gap where no new classes of antibiotics were introduced in the market (Figure 1.2). In the years of the innovation gap, most of the new drugs introduced were achieved by the synthetic tailoring of the already well known scaffolds.[30,45] The discovery of new effective classes of antibiotics in the era of antibiotics resistance phenomenon will provide much-needed time to elaborate strategies to reduce the incidence of infections and to increase the awareness of the public about this problem.

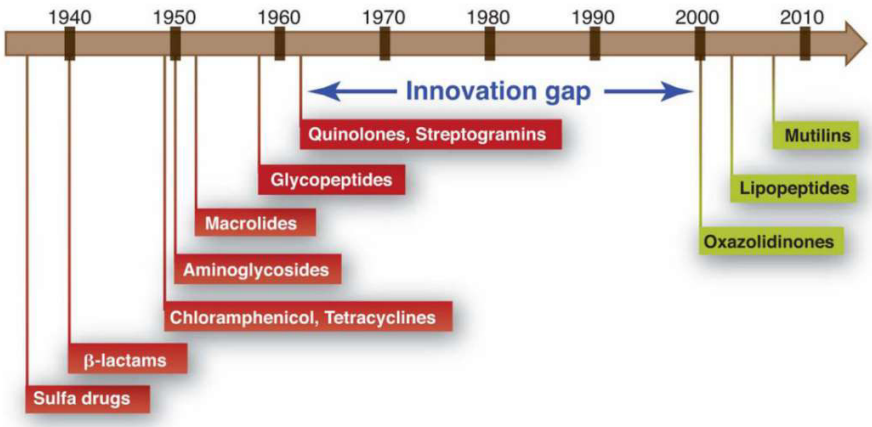

Figure 1.2. Year of market introduction of antibiotics classes with the innovation gap from the sixties to the new century.[30]

In March 2017, forty-one new antibiotic drugs, which could be an effective treatment for dangerous bacterial infections were in clinical development,[46] however the investments in the development of new antibiotics is limited compared to other classes of drugs.[36] Treatments with antibiotics are short-term therapies and therefore, from the economic point of view, the production of such compounds is not remunerative:[47] pharmaceutical industries prefer to invest in the treatment of chronic diseases, which are long-term therapies and therefore request continuous supply of according drugs.[48] Governments worldwide try to develop solutions, such as allocating public funding for the research on new antibiotics, however, further measures are necessary to provide new incentives for investments into antibiotic drugs research.

Among other antimicrobial candidates, the biopolymer chitosan and its derivatives emerged for contemporary antimicrobial research because of their outstanding antimicrobial properties. In this thesis, the antibacterial properties of chitosan and some of its functionalized derivatives (chitosan thiomers) were investigated, and progress was made in understanding and maximizing their efficiency against relevant pathogen strains. Chitosan and chitosan thiomers will be introduced in the sections 1.3 and 1.4.

1.2 The economic burden of treating cancer

While bacteria represent an increasing threat for our future, cancer still remains the second most urgent medical problem with over 600.000 deaths to be expected only for the year 2017 in the USA.[49] Thanks to innovative therapies and early diagnostics, cancer is becoming a more and more treatable disease. Due to the high costs, cancer treatments can be hardly affordable even for citizens of wealthy countries, such as the USA,[50] not to mention the population of the poor countries. Surprisingly, the price of anticancer drugs (and other medications) is significantly higher in the USA compared to its neighbors Canada and Mexico, or the European Union. The prices of anticancer drugs in the USA from 2000 until now showed a 5 to 10-fold increase that does not seem to stop, far ahead of the current inflation. Particularly, some of the anticancer drugs recently introduced in the market are priced more than $100.000 per year of treatment, and even when having a copayment of 20% the drug still remains hardly affordable also for well insured patients.[51] The study of *Dusetzina et al.* evidenced that high copayment costs often result in discontinuous treatments.[52] The high prices of anticancer drugs force many patients (10-20%) to not undergo treatment or to compromise significantly the treating plan.[50] The reasons for the high costs of anticancer treatments are attributed mainly to companies who are holding the monopoly for a certain drug and can thus control the price, which is associated with the development and production of the product and with the necessity and the demand dictated by the patients. On the other hand, it is convenient that pharmaceutical companies can fix the price of anticancer drugs, because in the case prices are controlled by a third party the stimulus for innovation will be impaired. However, these motivations seem not to be solid enough and the high prices in the USA appear to be unreasonable and without a real justification.

Fortunately, the situation is different in the other developed countries like Australia, Canada Germany and other European Union countries. In fact, consortiums formed of experts in cancer, as well as patients' and pharmaceutical industries' representatives have established agreements, like the Pharmaceutical Benefits Scheme in Australia[53] or the Pharmaceutical Market Restructuring Act in Germany, where the available cancer drugs were evaluated based on their benefits and reasonable prices were established. In this way drugs are more affordable for the

patients and their price are based on their benefits, while still granting a reasonable profit for the pharmaceutical industry.[53]

The problem of anticancer prices is especially serious in the low-income countries in Africa and Asia. A large part of the population of these countries is generally without a medical insurance and does not have the financial means to purchase basic medications, let alone costly anticancer drugs, without which the destiny of certain death is inevitable.

To render anticancer therapies affordable to everyone, more cost efficient anticancer treatments are needed. For this purpose, economic and bioactive inorganic cluster compounds, namely polyoxometalates (POMs), have been investigated as potential anticancer agents and tested against different types of cell lines. POMs could represent a valuable alternative to the available expensive anticancer drugs, due to the cost and time efficient preparation processes. To investigate the feasibility of POMs as anticancer drugs, the biological properties of some bioactive representatives were studied. Moreover, the biological properties of such compounds have been investigated either in pristine and in chitosan nanocomposite form. In the present work, evidences for the improved selective toxicity against cancer cells of these new materials are provided. The presented results pave the way for future in depth *in vivo* investigations. Some general information about POMs and nanoparticles are given in the sections 1.5 and 1.6.

1.3 Chitosan

Chitosan is a carbohydrate biopolymer composed of randomly distributed β-(1→4)-linked D-glucosamine and N-acetyl-D-glucosamine. This polymer is processed from chitin, so that a lower degree of acetylated units leads to its solubility in acidified aqueous solutions. Their different degree of deacetylation is responsible for the different solubility of the two polymers, and for the higher crystallinity of chitin. The degree of deacetylation (DD) correlates the number of deacetylated units to the total number of units: when DD is less than 50% the polymer is becoming soluble in acidic solution, and it is referred to as chitosan (Figure 1.3).[54]

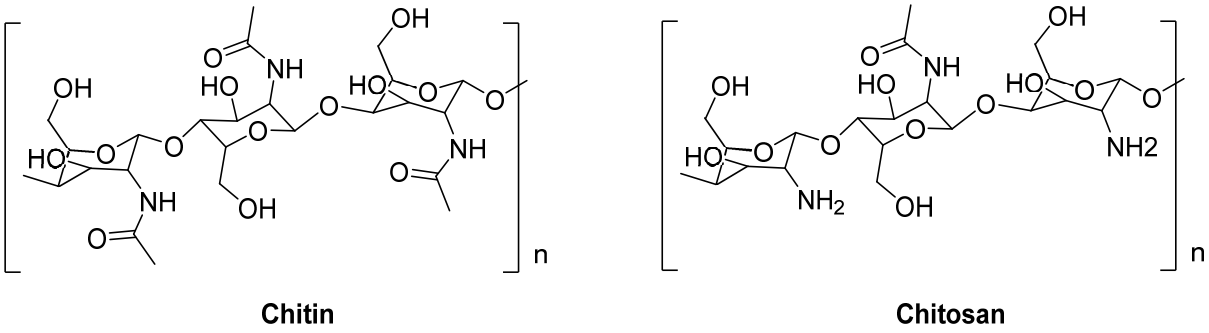

Figure 1.3. Chitin and chitosan structures.

The protonation of the amine groups of chitosan in acidic conditions allows its solubilization in water and renders chitosan the only positively charged natural polymer.[54] Chitin is present in many invertebrates and microorganisms where it has a protective role. Essentially isolated from the shells of some shellfish, and from particular shrimps, chitin is an abundant side-product of the fishing industry.[55] Chitosan is generally produced by industrial deacetylation of chitin: the heterogeneous reaction is conducted at high temperatures (120-150 °C) in alkaline media, generally sodium hydroxide. However, in this way the obtained material has variable physicochemical characteristics, and its production generates a large volume of industrial waste. A greener alternative can be the direct extraction from the mycelium of fungi that have chitosan in their fungal cell wall. Following this biorefinery approach, chitosan with reproducible characteristics, depending on the fermentation conditions, is produced.[56]

1.3.1 Characterization

To understand and predict the properties of chitosan, the degree of deacetylation and the molecular weight should be investigated. Together they are responsible for different properties of chitosan such as solubility, metal chelation and antibacterial activity.

1.3.1.1 Degree of deacetylation

The degree of deacetylation (DD) of chitosan corresponds to the number of free amine groups present: it determinates the pK_a of the polymer (generally about 6.3) and therefore the overall charge of chitosan at a given pH. Several methods were proposed to determine the DD, such as FT-IR[57] and Raman spectroscopy,[58] elemental analysis,[59] or UV-Vis spectroscopy.[60] However ^{13}C-NMR[61] and ^{1}H-NMR[62,63] spectroscopy are currently the most widely used and reliable

techniques. The ^{1}H-NMR and ^{13}C-NMR spectra of chitosan were described for the first time by *Hirai et al.*, who assigned the chemical shifts of the protons and of the carbon atoms using 2D-NMR spectroscopy.[62] A representative ^{1}H-NMR spectrum of chitosan and the proton assignments are shown in Figure 1.4.

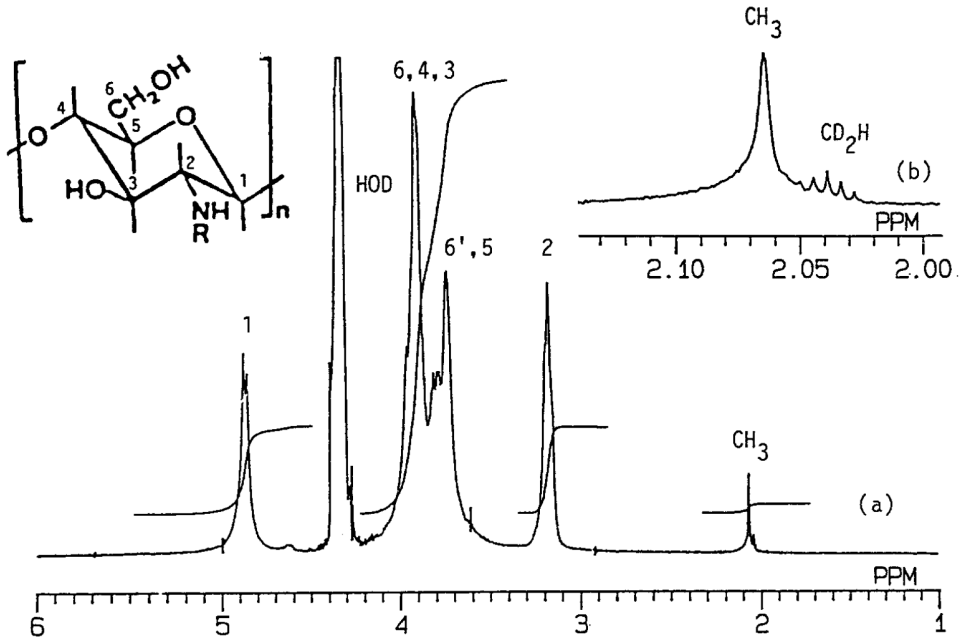

Figure 1.4. Chitosan ^{1}H-NMR spectrum and structure with the assigned protons.

^{1}H-NMR spectroscopy requires low sample quantities and it is fast, reliable and sensitive.[63] The signals were assigned as following:

δ 2.07 ppm	Methyl unit of the acetyl groups
δ 3.18 ppm	$H2_{deacetylated}$
δ 3.90, 3.81, 3.78, 3.74 ppm (broad)	$H2_{acetylated}$ H3, H4, H5, H6 and H6’
δ 4.65 ppm	$H1_{acetylated}$
δ 4.87, 4.85 ppm (doublet)	$H1_{deacetylated}$

^{1}H-NMR spectroscopy can be performed at room temperature or at 75 °C, in the last case the water peak shifts and the proton signal H1 of the acetylated unit is revealed. Depending on the temperature used for the NMR measurement, two formulas were proposed to calculate the DD:

$$\boldsymbol{DD}\ (\%) = \left\{\mathbf{1} - \left[\frac{\frac{1}{3}\boldsymbol{I_{CH_3}}}{\frac{1}{6}\boldsymbol{I_{(H2-H\ )}}}\right]\right\} \cdot \mathbf{100} \qquad \textbf{(1)}$$

$$\boldsymbol{DD}\ (\%) = \left\{\mathbf{1} - \left[\frac{\frac{1}{3}\boldsymbol{I_{CH_3}}}{\boldsymbol{I_{(H1DA+H1A)}}}\right]\right\} \cdot \mathbf{100} \qquad \textbf{(2)}$$

The formula (1) does not involve the H1 signal and therefore can be used for room temperature measurements, while (2) requires higher temperatures to be able to visualize both the H1 signals. The DDs calculated with the different formulas are usually in good agreement.

1.3.1.2 Molecular weight

Several methods were proposed to evaluate the MW of chitosan, such as viscosity measurements, laser light scattering[64] and HPLC,[65] but the currently most used technique is gel permeation chromatography (GPC), also known as size exclusion chromatography. The GPC is usually equipped with different types of detector.[66] Generally a viscometer is coupled with a differential refractometer and a right angle (90°) light scattering.[67] The eluent is a acetic acid/sodium acetate buffer which assures good solubility of chitosan and absence of aggregates.[68] Once the viscosity is measured it is possible to determinate the MW using the Mark-Houwink equation:[55]

$$[\boldsymbol{\eta}] = \boldsymbol{K} \cdot \boldsymbol{MW^{a}} \qquad \textbf{(3)}$$

The so-called Mark-Houwink constants (K) and (α) depend on the type of polymer, solvent and the temperature used during the viscosity measurement. The constants depend both on the MW and the DD of the polymer and consequently, if an accurate MW determination is desired, the measurement of the viscosity alone is not enough. Depending on the MW chitosan can be divided in oligo-chitosan, low MW chitosan (LMW), medium MW chitosan (MMW) and high MW chitosan (HMW). The classification is not universally recognized, but in this thesis the one proposed in a recent review is used:[69] chitosan oligomers have a MW of ≤ 16 kDa, LMW-chitosans range from > 16 kDa up to 190 kDa, MMW-chitosan > 190 kDa up to 300 kDa and HMW-chitosan covers all polymers above 300 kDa.

1.3.2 Chitosan properties and applications

Chitosan is a cheap and abundant raw material, which was largely investigated for practical applications in different fields like pharmacy, cosmetics, food processing, agriculture and waste water treatment.[54] Chitosan is nontoxic, biocompatible, and biodegradable by enzymes present in the human body, mainly by lysozyme.[70] All these characteristics are prerequisites for a material to be pharmaceutically applicable. Moreover, the possibility to process chitosan in different forms like sponge, hydrogels, fibers and films renders it extremely attractive for pharmaceutical uses. The most promising applications of chitosan are wound healing and regeneration of bones and tissues, thanks to its anti-inflammatories properties, cell growth promotion, antimicrobial activity and hemostatic action.[71] Moreover, chitosan and its micro/nanospheres, as well as some chitosan derivatives were deeply investigated for drug and gene delivery.[72]

Chitosan is also used as additive in cosmetics, for example, for its water retention properties and in hair care due to electrostatic reduction.[73] Moreover chitosan is a legal dietary supplement for weight loss in many countries, such as Italy, Norway and Japan,[74] although doubts about its effectiveness were reported.[75]

As chitosan has well documented antimycotic activities,[69,76] it was also investigated as food preserver or material for food packaging.[77]

Chitosan also has enormous potential in agriculture where it was investigated as seed coating, resistance elicitor inducing plant defense responses and soil amendment.[78] The ability of chitosan to chelate metal ions[79] and other pollutants is currently used in the treatment of wastewater.[80]

Many of the applications of chitosan are directly connected to its antimicrobial activity that is discussed in detail in the section 2.1.1.

1.3.3 Functionalization of chitosan

Chitosan can be easily functionalized on both its alcohol and its amine groups. The functionalization is intended to improve chitosan properties, including its solubility, mucoadhesivity and antibacterial activity. Chitosan can be selectively functionalized on one moiety or on both. This is feasible both protecting the undesired functional group or performing

a reaction that targets selectivity the desired moiety.[69] The amine group can undergo a Schiff reaction with aldehydes or ketones yielding the corresponding aldimines and ketimines, while chitosan hydroxyl groups can be functionalized through esterification or etherification. The formation of amide bonds between the amine groups of chitosan and the carboxylic acid of different biologically active molecules is a frequently used functionalization pathway and will be widely addressed in chapter 2 and 4.

A wide variety of chitosan derivatives were reported,[81] including quaternized chitosans that are functionalized with alkyl chains and showed improved antibacterial properties,[82] the phosphorylated chitosans, with improved solubility and used for metal chelation and tissue regeneration,[83] the sugar chitosans, that are recognized by the corresponding specific lectins and are quite promising for drug targeting,[84] the carboxyalkylated chitosans, that are soluble also at physiological or basic pH,[85] the chitosan thiomers (briefly thiomers), functionalized with thiolic groups to increase the mucoadhesive properties[86] and many others.

The present thesis is focused on chitosan as (1) the starting material for the synthesis of thiomers, (2) the positively charged organic constituent of polyoxometalate-chitosan nanoparticles and (3) the starting material for the carboxymethyl chitosan, which is herein used to prepare further polyoxometalate nanoparticles. The positive charge, the biocompatibility and antibacterial properties of chitosan are the main reasons why this polymer was chosen. In the following paragraphs, both thiomers and polyoxometalates will be introduced from a general point of view.

1.4 Chitosan thiomers

Chitosan thiomers are prepared through the reaction between mercapto substituents and the amine groups of chitosan. Chitosan thiomers were developed principally in *Bernkop-Schnürch*'s group, as non-invasive drug carriers, due to their excellent mucoadhesive properties.[86]

The first chitosan thiomer to be developed was chitosan substituted with thioglycolic acid (chitosan-TGA).[87] Chitosan-TGA showed 10-fold improved mucoadhesion compared to pristine chitosan, while exhibiting a good swelling behavior and maintaining its biodegradability. Thiomer mucoadhesion is due to the interaction of the sulfhydryl groups with cysteine-rich subdomains of mucus glycoproteins of the mucus gel layer. These interactions are based on thiol/disulfide

exchange reactions, an oxidation process, or on the formation of disulfide bonds, leading to an increased residence time that allows a time dependent release of the carried drug.[86]

Different thiomers were further developed for specific applications as drug carriers.[88] Alkyl chain thiols can be attached through amide bonds, like cysteine, N-acetylcysteine and glutathione, or amidine bonds, such as thioethylamidine and thiobuthylamidine. Typically, the pK_a values of these thiols are in the range of 8-10.

Aryl thiols such as 6-mercaptonicotinic acid and 4-mercaptobenzoic acid were also used to functionalize chitosan due to their lower pK_a (5-7), and therefore higher reactivity. Particularly 6-mercaptonicotinic acid-chitosan showed the highest mucoadhesive properties, measured *in vitro* via the rotating cylinder method and via tensile studies. Thiomers also display good *in situ* gelling properties due to the oxidation of the thiols in physiological conditions.[88]

The last trend about thiomers are the S-protected thiomers.[89] They consist of a chitosan-TGA whose thiol groups are protected through a sulfur bridge with 6-mercaptonicotinic acid. In this way, the thiols are still active in sulfur exchange reactions and are not oxidized before reaching the mucosa, thus exhibiting even better mucoadhesion properties.

In 2014, the first product containing a chitosan-N-acetylcysteine conjugate for treatment of dry eye syndrome was launched on the European market.[90] The antibacterial properties of the thiomers, as well as their synthesis and characterization will be further discussed in the second and fourth chapter of this thesis.

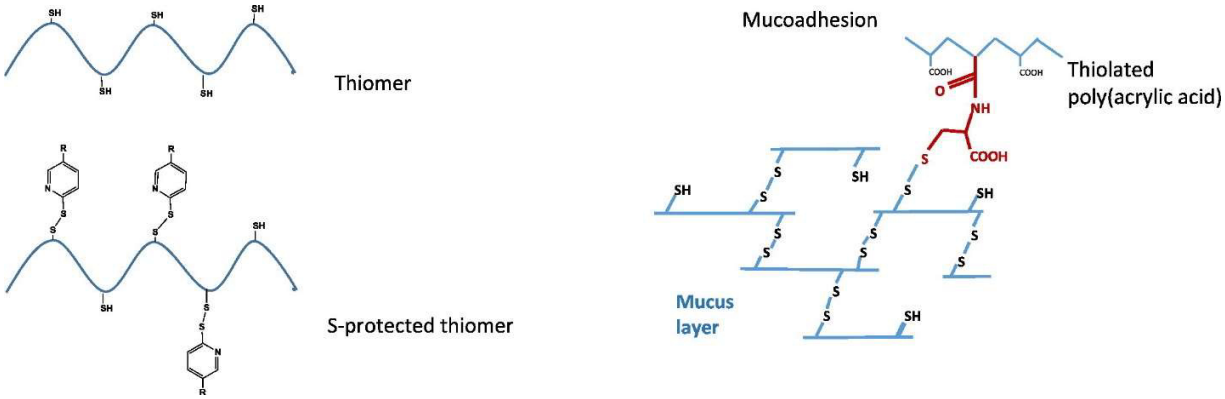

Figure 1.5. Schematic structure of a thiomer and S-protected thiomer and schematic interaction of a thiomer with a mucus layer.[90]

1.5 Polyoxometalates

Polyoxometalates (POMs) are discrete, negatively charged polyoxoclusters of group 5 and 6 of transition metals, mainly of molybdenum, tungsten and vanadium and less commonly of tantalum and niobium, in their high oxidation states.

POMs are formed from octahedral subunits of these metal oxides (MO_6) which condense together to form larger polyanions with a well-defined geometrical structure which is dependent on the metal.[91,92]

These compounds are known since 1826 when Berzelius first isolated some molybdenum compounds with phosphate and arsenates, while it was Marignac that discovered the first heteropolytungstates in 1862.[91] The first structure was assigned by Keggin from powder X-ray diffraction data to the heteropolyacid $H_3PW_{12}O_{40}$, that was named Keggin structure in honor of its discoverer.[93] Since the 1990s, due to the improvement in characterization techniques, such as single-crystal X-ray diffraction, NMR spectroscopy and mass spectrometry, the enormous variety of structures and functionalization possibilities of POMs has grown steadily.[92]

POMs can generally be divided into isopolyanions, only formed by a single metal type and oxygen atoms, and heteropolyanions which contain an additional heteroatom. Isopolyanions are generally less stable than heteropolyanions. By tuning the synthesis conditions, it is possible to produce a large library of possible building blocks for each of the transition metals, as summarized in Figure 1.6.

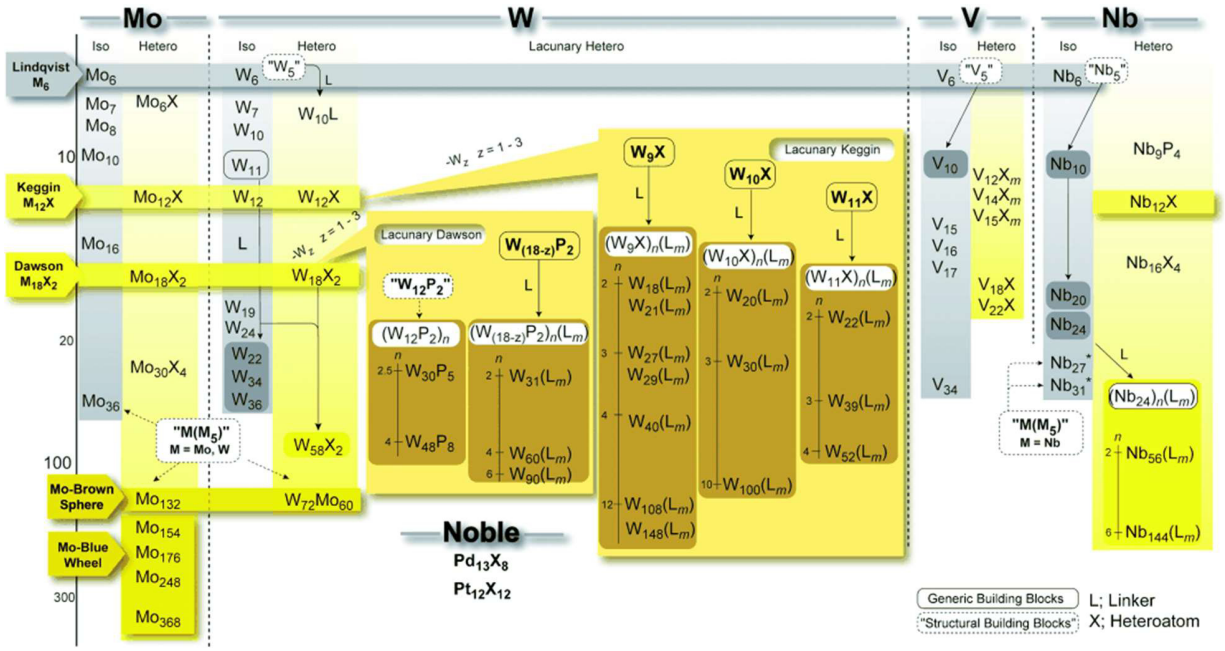

Figure 1.6. A classification of known POM building blocks. Black lines: POMs isolated as stable clusters. Dashed lines: POM building blocks that could not be isolated to date. Isopolyanions are shown in grey, heteropolyanions are colored (taken from reference[92]).

Each building block corresponds to a distinct geometrical structure, that can also be achieved by varying the chemical composition. The most typical POM structure motifs are summarized in Figure 1.7, with the Keggin and Wells-Dawson being the most common and generally stable structures. The Keggin structure is characterized by a general formula $[XM_{12}O_{40}]^{n-}$, where X is the heteroatom (most commonly P^{5+} or Si^{4+}), M is the metal atom (generally Mo or W). The heteroatom is placed in the center and surrounded by 4 oxygen to form a tetrahedron. The heteroatom is caged by 12 MO_6 corner sharing units, that form four M_3O_{13} sets of three edge-sharing octahedra. They are linked to the central heteroatom and among themselves through oxygen atoms.[94,95]

The Wells-Dawson structure has been defined by *Dawson* via X-ray analysis in 1953.[96] It is characterized by a general formula of $[X_2M_{18}O_{62}]^{n-}$, where X is the heteroatom (most commonly P^{5+}, but also Si^{4+}, As^{5+} and S^{6+}), M is the metal (generally Mo or W). The Wells-Dawson cluster has a mirror plane: the heteroatoms are located in the center of the respective lacunary units and

surrounded by 4 oxygen atoms forming two tetrahedra that are caged by 9 MO_6 corner sharing units, to form the two lacunary XM_9O_{36} moieties connected by six bridging oxygens.

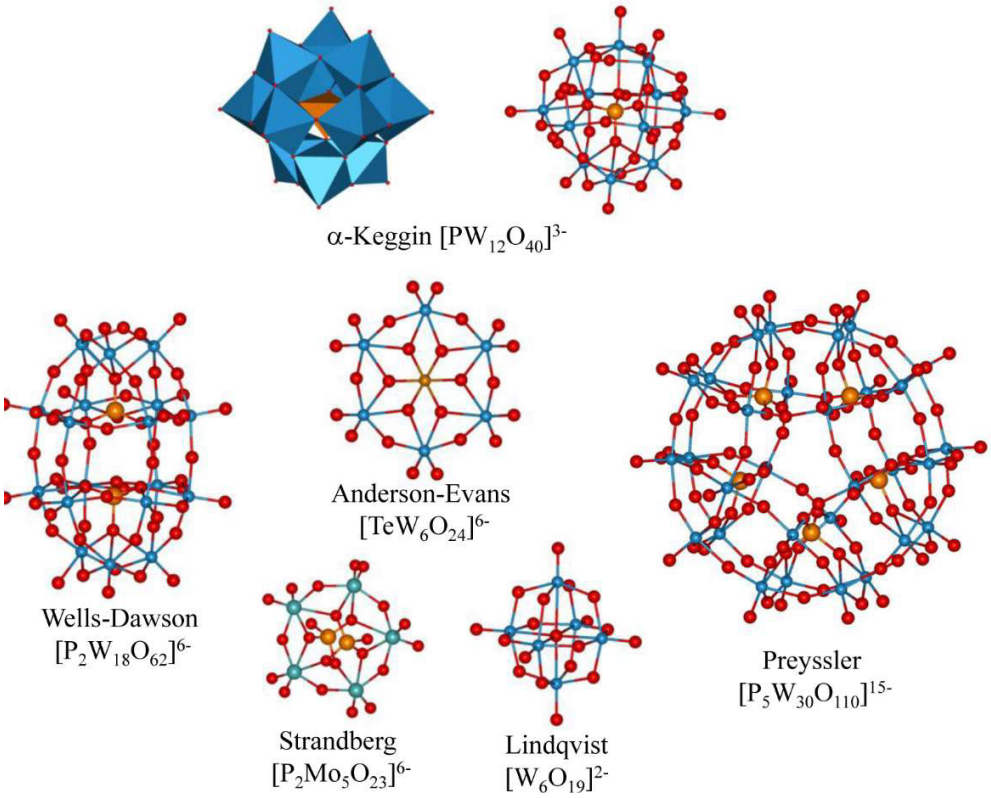

Figure 1.7. Most frequent structural motifs of smaller POMs.[97]

The synthesis of POMs is often simple and economical, involving just a few steps and inexpensive starting materials such as Na_2WO_4 for the tungsten-based POMs. Generally, the synthesis starts with dissolving the starting material and the addition of a mineral acid. After the acidification MO_6 units start to form and polycondensation sets in to produce large POM frameworks.[98] To achieve heteropolyanions, heteroatoms are included in the system through addition of specific reagents, for example H_3PO_4 when phosphorous is desired in the structure. The precipitation of the products is then triggered by adding the counteranion, such as alkali metal or ammonium cations. The different reaction conditions such as temperature, pH, heating method (hydrothermal, microwave or reflux), time, the different ratio between the elements, and the addition order, often influences the outcome of the synthesis and leads to diverse final products.[92,98] Sometimes

the raw products consists of a mixture of different POMs, or mostly of one POM together with some minor impurities.

While POM synthesis is simple, their purification is not trivial. Repeated recrystallizations are the only possible method to isolate pure products which results in low yields and long purification times.[99,100]

The possibility to isolate lacunary structures, where some of the cage atoms are removed to create vacancies that can be coordinated with transition metals or organic molecules, paves the way to the synthesis of a multitude of inorganic-organic hybrid materials. They can be prepared in different ways, starting from lacunary or normal POMs and involving electrostatic, covalent and non-covalent interactions.[98,100]

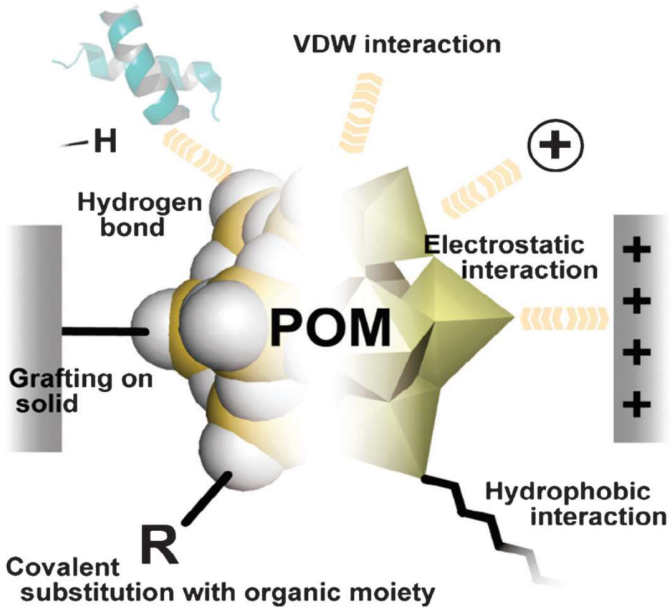

Figure 1.8. Schematic representation of various interaction modes in POM-based materials.[101]

POMs are usually strong acids as well as oxidation reagents and their reduced forms have a dark blue color, often referred to as “heteropoly blues” or “poly blues”. Their reduction does not lead to decomposition and they can undergo multiple reversible electrochemical or photochemical redox reactions. POMs are generally more stable in acidic aqueous solutions due to their high oxidation states, but they often decompose in basic environments.[102] POMs exhibit d^0 and d^1 configurations of their metal centers and thus display properties comparable to those of the classical solid-state metal oxides. Most importantly, POMs are water soluble and therefore

suitable for applications in solution, especially for homogeneous catalysis. When combined with organic counter ions, POMs are also soluble in some polar organic solvents, like acetonitrile or dimethylformamide, thus broadening the scope of possible applications.

Due to the great variety in structure and possible targeted modifications, the application of POMs in various fields[103] such as catalysis,[101,104] molecular magnetism,[105] and medicine[106,107] was deeply investigated. The application of POMs in medicine and the possibility to create nanocomposites with biopolymers that lead to improved biological properties will be further addressed in chapter 3 in more detail.

1.6 Nanoparticles

Nanoparticles are particles, which should exhibit at least two of their dimensions in the range between > 1 nm and < 100 nm. The lower limit is introduced to avoid single and small groups of atoms from being designated as nano-objects, and the upper one is sometimes extended to larger sizes, depending on the properties under consideration.

The peculiar properties of nanoparticles are related to their size limits. Considering the same mass, nanoparticles exhibit a higher surface area compared to bulk materials, which generally leads to higher activity and accessibility in catalysis. Their size is also responsible for the preferential accumulation of nanodrugs in cancer tissue, due to the enhanced permeability and retention (EPR) effect.[108]

Different types of nanoparticles were investigated for medical purposes, principally as drug-delivery systems and as *in-vivo* imaging agents.[109] The different application possibilities include the following particle types:

- Polymeric nanoparticles are matrix like colloidal nanoparticles that can be prepared with different biodegradable polymers such as polylactide-polyglycolide copolymers, polyacrylates, alginate and chitosan. They are generally used as drug carriers.[110]
- Polymeric micelles are generally composed of amphiphilic or oppositely charged copolymers that form a spherical structure, with the drug, protein, or DNA placed in their inner core.

- Quantum dots are semiconductor particles, generally consisting of hundred to thousand atoms. Their optical and electronical properties strictly depend on their size.[111] Their chemical composition can include different elements such as CdS, CdSe, InAs, PbSe. They are promising tools for *in vivo* imaging and diagnostics.[112]
- Gold nanoparticles are biocompatible, easy to functionalize and to produce with definite morphology and size, and they display outstanding bioconjugation properties.[113]
- Superparamagnetic iron oxide nanoparticles (SPIONs) are nanoparticles of Fe_2O_3 and Fe_3O_4, generally with 6-15 nm sizes, that display magnetic properties. Upon interaction with an external magnetic field, they can be accumulated in a specific target in the human body and be used in magnetic resonance imaging or magnetic-field-assisted physical drug targeting for cancer therapy.[114] When exposed to an alternate magnetic field, the magnetic moment of SPIONs oscillates, producing heat that could be used in the hyperthermic treatments of cancer.
- Silica and organically modified silica nanoparticles are mesoporous structures, with well-defined surface properties and tunable pore sizes. They can carry drugs or dyes for imaging therapies in their inner core.[115]
- Liposome based nanoparticles were developed and are currently used in medicine and pharmacy as drug carriers,[116] although some studies indicate that they could accumulate in the liver and cause hypersensitivity.[117]
- Engineered viral nanoparticles and artificial viruses have been widely investigated as delivery vectors in gene therapy due to their high transfection efficiencies, and also as imaging and target delivery systems.[118] Their effective application is complicated due to the possibilities of host infections and immunological reactions.

Some of the described nanoparticles structures are shown in Figure 1.9.

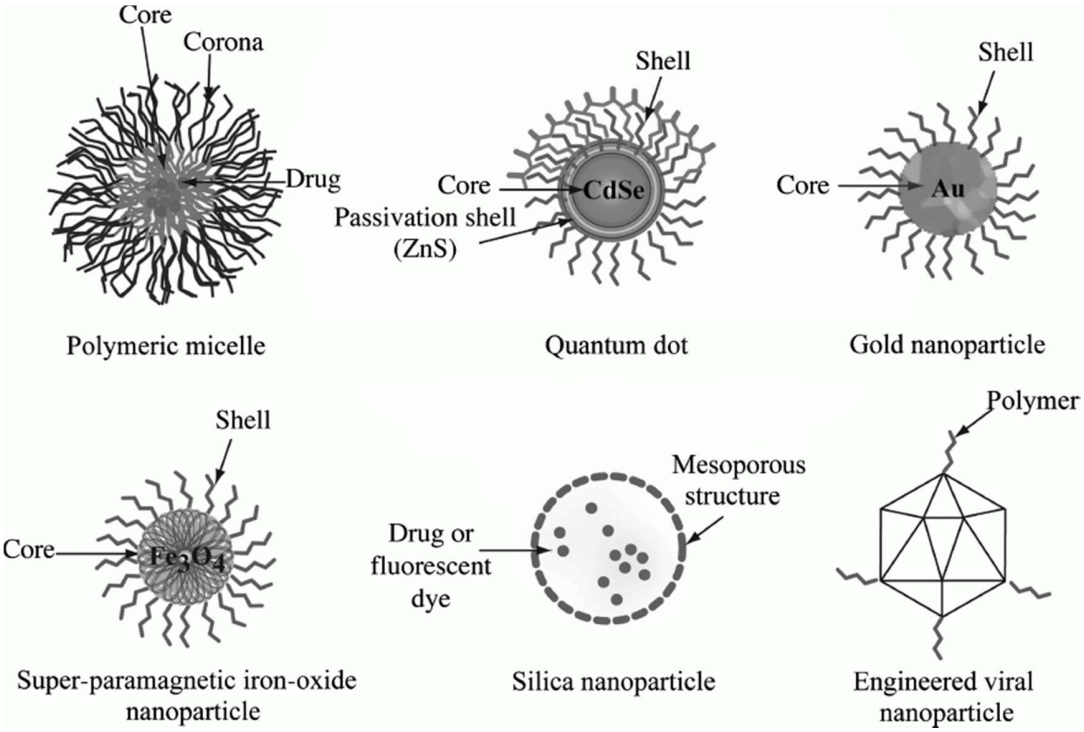

Figure 1.9. Classes of nanoparticles with potential use in medicine.[109]

Nanoparticles could be functionalized for higher target selectivity by attachment of various peptide ligands,[119] small molecules[120] or antibodies.[121] Many nanoparticle-based drugs are currently on the market, or in clinical or pre-clinical investigations.[109,116]

However, nanoparticles still present some issues which limit their applications, such as their stability in and outside the body and their potential toxicity. The ideal nanocarrier should be stable until it reaches its target, then release its drug there and be subsequently degraded and excreted from the organism. The stability of nanoparticles is dependent on their composition and the characteristics of the external environment, e.g. pH and ionic strength.

The potential toxicity of nanoparticles for the patients and the effect that they can have on environmental pollution are in the focus of public concerns. A complete characterization of nanoparticles to verify the absence of impurities, together with a complete investigation of their interaction with the cells are necessary to determine their possible toxicity.[122] Depending on their characteristics, nanoparticles could harm the organism by various mechanisms such as generation of reactive oxygen species,[123] membrane perturbation[124] and direct physical damage. Most nanoparticles within a biological system undergo transformations. Typically, they

are chelated by molecules, mostly proteins, present in the organism forming a kind of corona that influences their behavior. It is possible that nanoparticles form aggregates that could be sequestered by the reticuloendothelial system and not reach their desired targets. The fate of the nanoparticles, between the excretion from the body or their bioaccumulation in certain organs is not perfectly clear. Ratios of between 40-50% of elimination through the urinary system were measured,[125] but further long-term studies are necessary to exclude the possibilities that nanoparticles cause chronic damage to the organism.

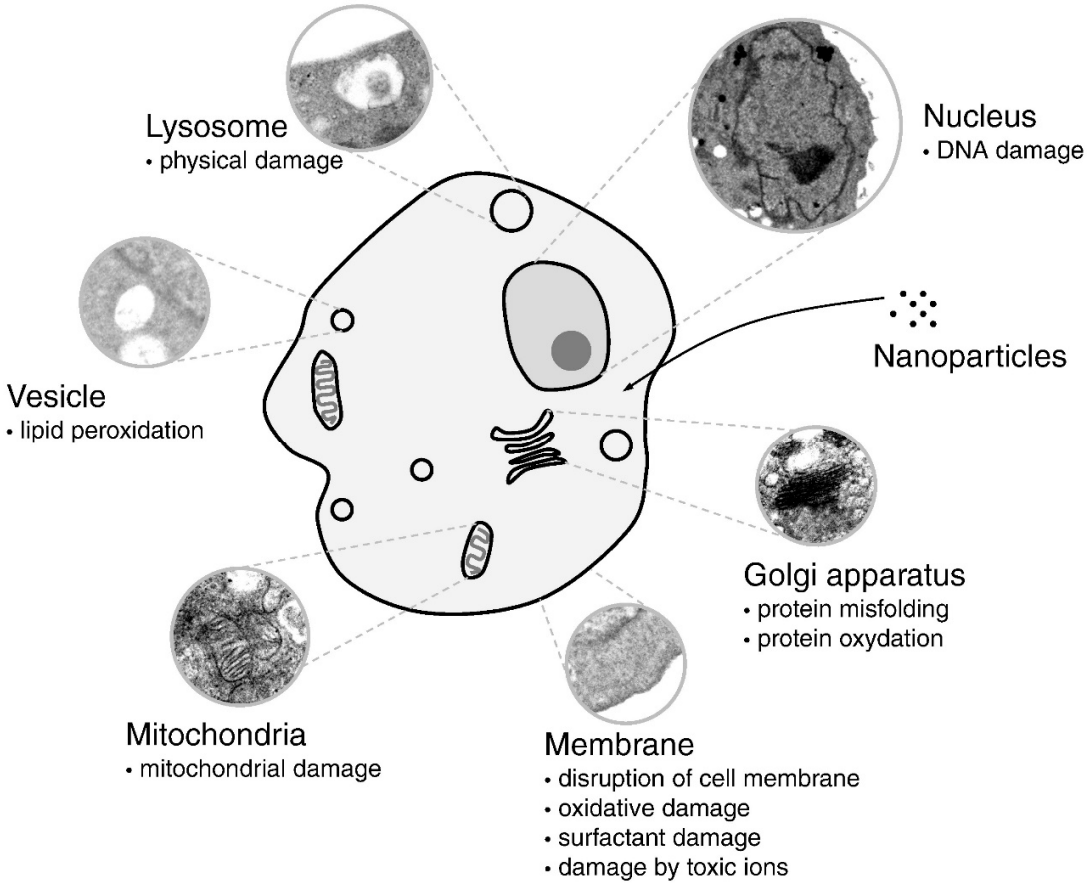

Figure 1.10. Interaction of nanoparticles with cells: possible targets and nanotoxicity mechanisms.[122]

1.7 Goal and strategy of this work

The main goal of this work was to explore the biological properties of chitosan thiomers and of polyoxometalate-chitosan nanocomposites paving the way to potential future clinical applications as easily accessible alternative drug types. Consequently, the present work can be divided into three parts. In the first part, chitosan thiomers were synthesized, and their antibacterial properties investigated, as well as their cytotoxicity on immortalized cell lines. A series of different derivatives was synthesized and carefully characterized to determine their structure-activity relationships (SAR). In the second part LMW-chitosan and its derivative carboxymethyl chitosan (CMC) were used to prepare nanocomposites with inorganic POMs. Their biological activities against bacteria and mammalian cells were screened to evaluate the different behavior of the composites compared to their pristine components. Finally, the efficiency of the thiomer functionalization was evaluated, focusing on the synthesis of chitosan-TGA, and some initial attempts to functionalize chitosan with amino acids and other derivatives are also reported.

2. Chitosan thiomers as antibacterial agents

2.1 Introduction

Chitosan thiomers were developed as drug carriers as described in the introduction (see section 1.2) and their pronounced antibacterial properties were deeply investigated in previous studies. 2-iminothiolane- (IMI) and acetyl-cysteine-chitosan were investigated against *E. coli* and *S. aureus*, and IMI-chitosan showed a lower value of minimum inhibitory concentration (MIC) compared to chitosan. In the same study the authors proposed that the bactericidal mechanism of IMI-chitosan involved the destruction of the bacteria cell membrane.[126] In the same year, the antibacterial properties of four different chitosan derivatives, i.e. trimethyl chitosan (TMC), carboxymethyl chitosan (CMC) and chitosan-TGA (MMW and LMW) were investigated. From this study emerged the versatile antimicrobial agent LMW chitosan-TGA, that is effective after just 30 min against different microorganisms, namely the gram-positive *Streptococcus sobrinus*, the gram-negative *Neisseria subflava* and the fungus *Candida albicans*.[127] To investigate other possibilities for the enhancement of the antimicrobial activity along these lines, different thiol substitutions and starting material parameters (DD, MW) were investigated in this work. In the following chapters a survey on the antibacterial properties of chitosan and derivatives is reported to put the present work into perspective.

2.1.1 Antibacterial properties of chitosan

The antimicrobial properties of chitosan and its derivatives are known since the second half of the last century[128] and the efficiency of chitosan against different bacterial strains such as the gram-negative *E. coli*, *Pseudomonas fluorescens*, *P. aeruginosa*, *Salmonella typhimurium* and *Vibrio parahaemolyticus* and the gram-positive *Listeria monocytogenes*, *Bacillus megaterium*, *Enterococcus faecalis*, *S. aureus*, *Lactobacillus plantarum*, *L. brevis*, and *L. bulgaricus* was clearly established.[129,130] Although several mechanisms of action were proposed, nowadays there is no evidence for an unique and prevailing mechanism of action. The mechanism of action varies between gram-positive and gram-negative bacteria, due to the differences between the two categories, especially regarding their cell membrane structure, and depends on both the microorganism type and on the characteristics of the chitosan (MW and DD).[69] In gram-positive

bacteria, chitosan is supposed to target the cell membrane where it binds electrostatically to the teichoic acids incorporated in the peptidoglycan layer, thus leading to a destabilization of the membrane and to a partial leakage of cell constituents, inducing the death of the microorganism.[131] An alternative and possible concurrent mechanism involves the possible penetration of LMW chitosan into the cell cytoplasm, where it interacts with the nucleic acids, thereby interfering with the normal cellular metabolism.[132] In gram-negative bacteria, chitosan is supposed to interact mainly with the negative lipopolysaccharides of the outer membrane[133] or of the inner membrane.[134] The modifications to the membranes and the consequent leakage of cellular material is leading to cellular death. Furthermore, several studies confirmed the interference of chitosan oligomers with the nucleic acid synthesis of *E. coli*, which was also detected in the cytoplasm by fluorescent labelling.[132,135]

Another hypothesis is based on the ability of chitosan to chelate metals at pH higher than 6.5.[136] Chitosan can sequestrate metals from the outer barrier to destabilize it, as well as from the surrounding environment of the bacteria, causing an insufficient uptake of micronutrients and eventually bacterial death. However, this hypothesis is not supported by any recent study or evidence, and only two studies on the antifungal action of chitosan proposed this mechanism.[137] The metal chelation mechanism seems to be the one with least reported evidences and most controversial discussions in the chitosan community.[138]

Liu et al. considered both gram-negative and gram-positive bacteria and suggested that chitosan would deform the cell membrane of both, even if the specific target is depending on the microorganism, while afterwards LMW chitosan blocks the nucleic acids, thus interfering with protein synthesis.[139] A combination of both pathways, where chitosan attacks in different proportions both the membrane and the nucleic acids, depending on chitosan and strain characteristics, was proposed as the most evident conclusion.[140] In Figures 2.1 and 2.2 a survey of the mechanism of action and of the structure of the cellular wall of gram-positive and -negative bacteria, is reported.

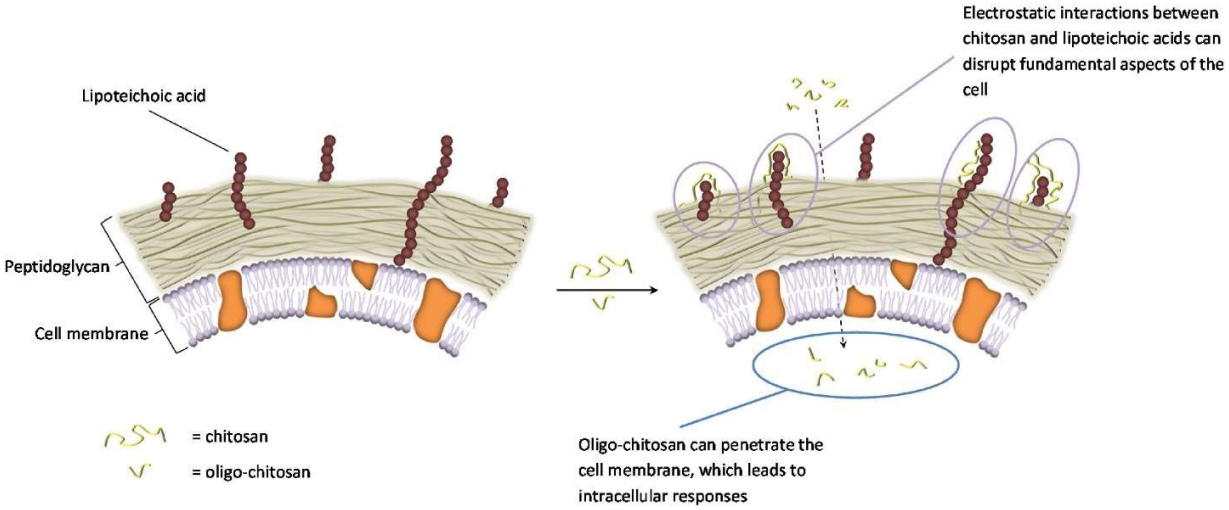

Figure 2.1. Mode of action against gram-positive bacteria for chitosan and oligo-chitosan.[69]

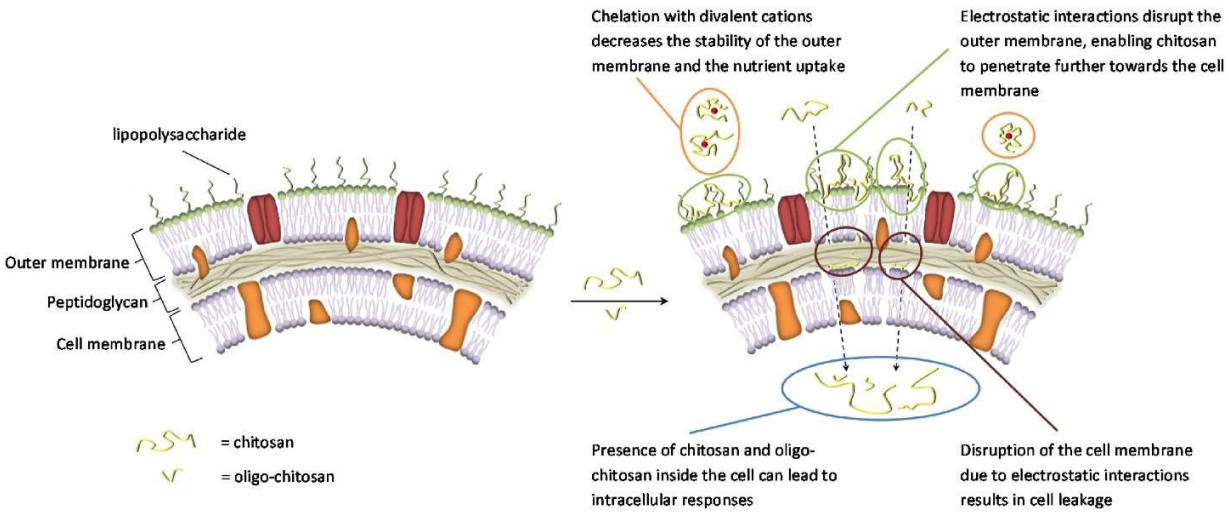

Figure 2.2. Mode of action against gram-negative bacteria for chitosan and oligo-chitosan.[69]

Regardless the mechanism of action, the data on the antimicrobial efficiency of chitosan and derivatives reported so far are sometimes controversial or substantially different among different studies. The antimicrobial properties of chitosan depend strongly on its characteristics (MW and DD),[141,142] on the environmental conditions (pH, temperature and ionic strength), as well as the microorganism species, which causes the above discrepancies between reported results.[69] Some studies thus correlate the mentioned characteristics of chitosan and the resulting antimicrobial activity. The impact of MW on the antimicrobial activity appears to be different for gram-negative and gram-positive bacteria:[130] LMW chitosan was superior in eliminating gram-negative bacteria,

while higher MWs exerted stronger effects against gram-positive bacteria,[141–143] probably due to the differences in cellular membrane structure or due to the involved mechanism. Chitosan with a higher DD bears, at the same pH value, a higher positive charge density due to the protonation of the amine groups which leads to an enhancement of the antimicrobial activity,[142–144] more markedly for the gram-negative strains, and to a lower extent for the gram-positive strains.[141] This behavior supports the hypothesis of the interaction of the positive charged ammonium group and the negatively charged components of the bacteria membranes and nucleic acids. Further findings on the enhanced antibacterial activity of quaternary amine chitosan derivatives, bearing permanent positive charges, compared to their pristine chitosan starting materials support this hypothesis.[82,145] Additionally, the antibacterial properties of chitosan are strictly dependent on the environmental pH. Chitosan displayed higher efficiency against bacteria at lower pH, because of the higher positive charge density.[130,132] Moreover, chitosan at pH > 6.5 is not soluble which reduces its applicability in physiological solution.

All the above operational parameters should be kept constant or considered when comparing the antimicrobial activity of different chitosans and chitosan derivatives.

2.1.2 Approach in the present work

The goal of the present project was to investigate the impact that both the substituent and the characteristics of the starting material exert on the antibacterial properties of chitosan thiomers. Therefore, four different starting materials were chosen for the investigation: three LMW chitosans (18, 55 and 90 kDa) and one MMW-chitosan (250 kDa), all of them having a high DD (87-94%). To evaluate the effect of chitosan substitution on the antibacterial activity, simple commercially available reagents bearing thiol moieties were selected to functionalize the chitosans. Five mercapto-carboxylic acids with different structural elements were applied, which could be attached to the amine group of chitosan through amide bond formation. Two of them bear linear alkyl chains (TGA and mercaptopropionic acid, MPA), one has a methyl group on the carbon in position 2 (thiolactic acid, TLA), one is equipped with an additional amine group (cysteine, Cys), while the last one displayed an aromatic ring, (mercaptobenzoic acid, MBeA). Finally, 2-iminothiolane (IMI) was used to form through ring-opening reaction an amidine bond

with a permanent positive charge. The chemical structures of the thiol reagents used for the functionalization are summarized in Figure 2.3.

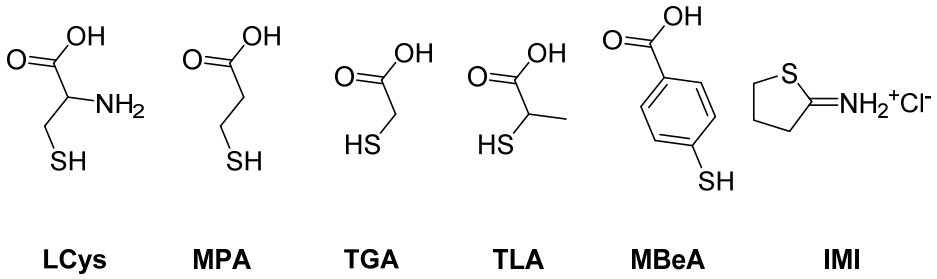

Figure 2.3. Thiol reagents used to functionalize chitosan.

To investigate the structure-activity relationships (SAR), a comprehensive analytical characterization of all chitosan thiomers is mandatory. Special efforts have been made for the determination of DD, MW and degree of substitution (DS). To screen the efficiency of the antimicrobial activity of the synthesized chitosan derivatives, a MTT assay, which is normally used for viability assessment on mammalian cells, was adapted for bacterial tests. The method was first optimized on the gram-negative *E. coli* and afterwards on the gram-negative *P. aeruginosa* and the two gram-positive strains *S. sobrinus* and *Streptococcus mutans.* The results evidenced the superior efficacy of the derivatives produced with the starting material chitosan 85/20 (MW ~ 90 KDa and DD ~ 93%), probably because of their higher DD. Among the derivatives produced from chitosan 85/20, chitosan-TGA, -MPA and -TLA had most pronounced antibacterial effect. To evaluate the effect of the alkyl chain length on the antimicrobial activity, we decided to systematically increase the number of carbon atoms of the alkyl chain substituent. Therefore the following chitosan thiomers were synthesized and characterized: chitosan-2-methyl-3-sulfanylpropanoic acid (MSPA), -mercaptobutyric acid (MBA), -mercaptohexanoic acid (MHA) and -mercaptooctanoic acid (MOA). The reaction scheme as well as the chemical structure of the mentioned thiomers are reported in Figure 2.4.

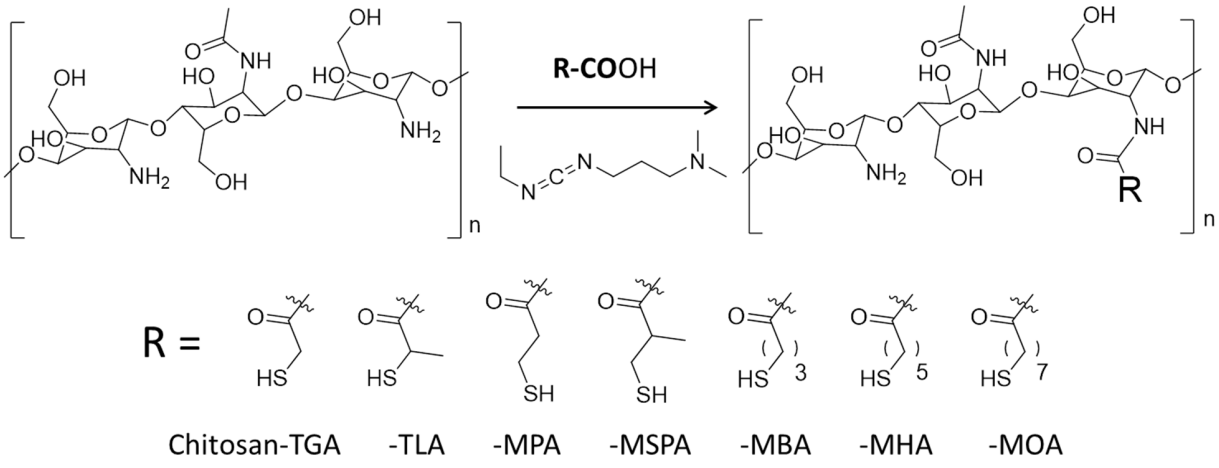

Figure 2.4. Synthetic approach and survey of the characterized and tested alkyl thiolated chitosans.

The antibacterial properties of the proposed series of thiomers were in depth investigated, preliminarily with MTT assay and afterwards with the more precise and accurate plate counting agar (PCA). The tendency of chitosan thiomers to exert a bactericidal effect was further investigated microscopically using the LIVE/DEAD assay. Bacteria cells were treated with chitosan-MPA as representative compound. Chitosan-MPA was used as reference thiomer for the assessment of the cytotoxicity on mammalian cells and the determination of the IC_{50} (i.e. the half maximal inhibitory concentration, namely the concentration of a compound needed to inhibit the cellular metabolism by half).

2.2 Experimental section

2.2.1 Materials

Unless otherwise specified, reagents were purchased from Sigma-Aldrich (Buchs, Switzerland) and used as received. Chitosan with different DD and MW was purchased from Heppe Medical Chitosan (Halle (Saale), Germany). They are referred to as 85/5, 85/10, 85/20, and 85/100, with the first number indicating the DD and the second number indicating the viscosity of the material at 1% (w/v) in 1% acetic acid at 20 °C measured in mPa·s. Thioglycolic acid (97%), mercaptopropionic acid (99%) and tris(2-carboxyethyl)phosphine hydrochloride (TPH 99%) were purchased from abcr GmbH (Karlsruhe, Germany). N-(3-dimethylaminopropyl)-N'-ethylcarbodiimide hydrochloride (EDC 98%, 99%, and crystalline) was purchased from Sigma-

Aldrich and abcr GmbH (98%). 3-(4,5-dimethylthiazol-2-yl)-2,5-diphenyltetrazolium bromide (MTT) was purchased from Alfa Aesar (Heysham, UK).

2.2.2 Thiomer synthesis

2.2.2.1 Amide bond formation: Reaction with mercapto-carboxylic acids

Published synthesis protocols[87,146] were first applied to synthesize chitosan-TGA. Due to an unsatisfactory degree of substitution (DS), the reaction time, the temperature as well as the order of the reagents addition were then modified. A detailed paragraph describing all the attempts to increase the DS of chitosan-TGA can be found in chapter 4. Chitosan-MBeA synthesis was performed as described in a previously published procedure,[147] while halving the concentration of EDC due to the low solubility of the highly substituted product. The syntheses of all the other thiomers involving the formation of amidine bond were adapted from reported protocols for chitosan-TGA and -MBeA. The synthesis conditions for the most representative derivatives are summarized in Table 2.1.

Table 2.1. Synthesis conditions for the most representative thiomers.

Substituent	Start. Mat.	Reagent (g)	EDC (g)	T (°C)	Time (h)
TGA-A	85/100	0.5	1	Room T	2
TGA-B	85/20	0.5	1.6	Room T	3
TLA-A	85/5	0.5	1.2	55	3
TLA-B	85/20	0.5	1.24	55	3
MPA-A	85/10	0.5	1.26	Room T	68
MPA-B	85/5	0.5	1.2	55	3
MPA-C	85/20	0.6	1.26	40	23
MSPA	85/20	0.5	1.4	40	21
MBA	85/20	0.5	1.2	40	24
MHA	85/20	1	1.24	40	20
MOA	85/20	1	1.4	40	19.5
MBeA-A	85/10	0.625	1.2	Room T	66
MBeA-B	85/10	0.65	0.6	Room T	66
MBeA-C	85/5	0.65	1.2	Room T	66
L-Cys-A	85/5	0.55	1.3	Room T	3
L-Cys-B	85/20	0.67	1.1	55	3

The typical synthesis procedure for the thiomers is described below in detail. The synthesis was performed in inert conditions under nitrogen flow. 500 mg chitosan were dissolved in 4 mL 1 M HCl for 15 min, and 46 mL water were added to obtain a 1% (w/v) chitosan solution. After chitosan was completely dissolved, the functionalizing reagent was added to the solution. EDC was added after 10 min while maintaining the temperature of the system for the applied reaction time (cf. Table 2.1). The pH of the reaction was adjusted to 5. 300-400 mg reducing agent (TPH) were eventually added during the final 30 min. The product was dialyzed in cellulose membrane tubing with a molecular cut-off of 12 kDa in the dark at 4 °C against different media, as described below, for at least 75 h. The following media were used and changed twice a day: 5 mM HCl (day 1), 5 mM HCl + 1% (w/v) NaCl (day 2 and day 3), and 1 mM HCl (day 4). The product was then freeze dried for 48 h and stored in the dark at -20 °C until further use. A chitosan sample processed without the addition of any reagents was used as a reference in the antimicrobial tests.

2.2.2.2 Ring-opening reaction: Chitosan-IMI

The synthesis procedure was adapted from previously reported protocols[126,148] and it was modified to achieve a higher DS of chitosan. The reaction was conducted in inert atmosphere and in the dark. 500 mg of chitosan reacted with 4 mL of HCl 1 M for 15 min and then 46 mL of water were added to achieve a 1% (w/v) chitosan solution. After 10 min, chitosan was well dissolved, and the pH was adjusted to 6.5 with a solution of 0.5 M NaOH, followed by the addition of 140 mg of DTT and after 10 min of 500 mg of 2-iminothiolane. The pH changed to 5.8 and it was adjusted to 6.5 with NaOH 0.5 M. The reaction was continued for 3 h at 55 °C. The solution was dialyzed in the dark at 4 °C against different media for 76.5 h. The following media were used and changed twice a day: 5 mM HCl (day 1), 5 mM HCl + 1% (w/v) NaCl (day 2 and day 3), and 1 mM HCl (day 4 and day 5). The product was freeze dried for 48 h and stored in the dark at -20 °C until further use. The scheme of the reaction is reported in Figure 2.5.

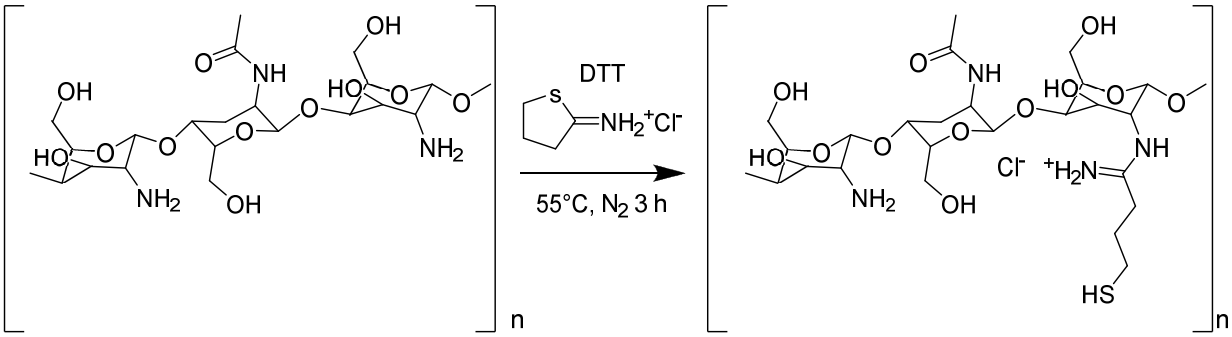

Figure 2.5. Reaction scheme for the synthesis of chitosan-TBA.

2.2.3 Characterization

2.2.3.1. NMR spectroscopy

^{1}H-NMR spectra were recorded at RT or at 75 °C on a 300 or 400 MHz Bruker Avance Spectrometer (Billerica, USA) with CP-MAS technology (Cross Polarization-Magic Angle Spinning). The DD of chitosan and of the thiomers was calculated according to *Hirai*.[62] Samples were prepared in D_2O at a concentration of ≥ 10 mg/mL.

2D-^{1}H-NMR was recorded for chitosan-IMI, -TGA and -MBeA at 75 °C on a 400 MHz Bruker Avance Spectrometer (Billerica, USA) with CP-MAS technology.

Solid-state ^{13}C-NMR was recorded for chitosan-IMI at RT on a 400 MHz Bruker Avance Spectrometer (Billerica, USA) with CP-MAS technology.

2.2.3.2. ζ-potential measurements

All samples at a concentration of 4 mg/mL in Phosphate Buffer Saline pH 7.3 (PBS) were analyzed with a Zetasizer Nano ZS90 (ZEN3690, Malvern Instruments Ltd, Malvern, UK) using Malvern disposable folded capillary cells.

2.2.3.3. Aqueous Gel Permeation Chromatography (GPC)

MW determination was performed in acetate buffer (0.15 M, pH 4.6-4.7) using a Viscotek GPC Max system equipped with a VE 2001 GPC solvent/sample module (Malvern). The separation was achieved with one A Guard (Malvern) and two GMPWXL 08025 (Tosoh Bioscience LLC, King of Prussia, USA) columns.

The detectors used were Viscotek 270 Dual Detector for light scattering and viscosity measurements, and Viscotek VE 3580 RI detector or Viscotek UV detector 2600 (Malvern) for refractive index and UV measurements, respectively. Methods were calibrated with polyethylene oxide and dextran Malvern standards. For each chitosan thiomer weight-average and number-average MW were determined and the polydispersity index (PDI) calculated. Each sample was dissolved in the buffer within a concentration range of 4.5-5.5 mg/mL and filtered through a 0.22 µm filter before injection.

2.2.3.4. Elemental analysis

Elemental analysis was performed on a Truespec CHNS-microanalyzer (LECO Corporation, St. Joseph, USA). To evaluate the DS of each chitosan thiomers, the molar amount of sulfur was correlated with molar nitrogen content, dividing their percentage in weight by their MW.

2.2.3.5. Thiol group determination

5,5'-dithiobis-(2-nitrobenzoic acid), $DTNB^{2-}$ or Ellman's reagent, was used to determine thiol group concentrations according to literature protocols.[149] Cysteine (concentration range 75-350 µM) was used as standard. Absorbance at 405 and 450 nm was measured with a 96-well plate reader (Synergy 2 Multi-Mode Reader, BioTek Instruments, Winooski, USA).

2.2.3.6 FT-IR spectroscopy

FT-IR spectra were recorded in solid-state sample with a Bruker VORTEX 70 spectrometer.

2.2.4. Antibacterial activity determination

2.2.4.1. Bacterial strains and media

*Escherichia coli (*ATCC 11775) *and Pseudomonas aeruginosa* (ATCC 27853) (German Collection of Microorganisms and Cell Cultures GmbH DSMZ, Braunschweig, Germany) were subcultivated in Luria-Bertani (LB) broth pH 7.0 ± 0.2 (10 g/L tryptone, 5 g/L yeast extract, and 5 g/L sodium chloride) at 37 °C under constant rotation (220 rpm). *Streptococcus sobrinus* (OMZ 176) and *Streptococcus mutans* (OMZ 918) (Institute of Oral Microbiology, University Hospital Zurich, Zurich, Switzerland) were subcultivated in Brain Heart Infusion (BHI) broth pH 7.4 ± 0.2 (5 g/L beef heart, 12.5 g/L calf brains, 2.5 g/L disodium hydrogen, 2 g/L phosphate, D(+)-glucose, 10 g/L peptone, 5 g/L sodium chloride) at 37 °C under constant rotation (220 rpm). All the bacteria were

grown in agar plates composed 10% agar in the cultivation medium. Plate Counting Agar (PCA) containing 5.0 g/L tryptone, 2.5 g/L yeast extract, 1.0 g/L D(+)-glucose and 12.0 g/L bacteriological agar was used for plate counting experiments. All the media were autoclaved before use.

2.2.4.2 MTT viability assays

A log-phase bacteria suspension containing around 10^8 colony forming units (CFU)/mL was incubated with chitosan thiomers (dissolved in medium/0.9% NaCl (1:1) to reach 2 mg/mL or 4 mg/mL) at 37 °C and 220 rpm. After 30 or 60 min, aliquots were taken and mixed to a ratio of 1:10 with 3-(4,5-dimethylthiazol-2-yl)-2,5-diphenyltetrazolium bromide (MTT) (5 mg/mL). After 1 h at 37 °C, 220 rpm, samples were centrifuged for 10 min at 13300 rpm, the insoluble product formazan was dissolved in 1 mL DMSO and the absorbance was measured at 550 and 570 nm with a 96-well plate reader (Synergy 2 Multi-Mode Reader, BioTek). To ensure sterility of chitosan samples, aliquots of chitosan solutions were plated onto LB agar and incubated for 16 h at 37 °C. Assays were performed as biological triplicates with technical quadruplicates.

2.2.4.3. Plate Counting

A log-phase bacterial suspension was adjusted to 0.5 McFarland turbidity standard (around 10^8 CFU/mL) with medium and incubated for 30 or 60 min with chitosan thiomers (final concentrations 20 and 40 µM, in 1:1 medium/0.9% NaCl) at 37 °C and constant rotation. *P. aeruginosa*, *S. sobrinus* and *S. mutans* reactions were serial diluted 10-10^2-fold and aliquots were plated onto PCA. *E. coli* were serial diluted 10^6-10^8-fold and aliquots were plated onto PCA. Bacterial cultures that received culture medium instead of chitosan thiomers served as positive controls and were serially diluted to 10^6-10^8-fold. All plates were incubated for 24 h at 37 °C before colony counting. Only plates containing between 300 and 10 colonies were used for enumeration. Experiments were performed in triplicates. Statistical calculation was performed with GraphPad Prism using one-way ANOVA including Tukey's test and Mann-Whitney t-test ($p < 0.05$).

2.2.4.4. LIVE/DEAD assays

LIVE/DEAD® BacLight™ Bacterial Viability Kit (Molecular Probes, Oregon, USA) was used according to the manufacturer's protocol. Briefly, bacterial suspensions containing around 10^8 CFU/mL were

incubated with 40 µM chitosan-MPA (in 0.9% NaCl) for 30 min at 37 °C, washed twice with 0.9% NaCl (13000 rpm for 2 min) and the dye mixture of the kit was added. After 15 min in the dark 10 µL of the sample were immobilized on a glass slide coated with 2% agarose. Imaging was performed with a confocal laser scanning microscope (CLSM SP5 Mid UV-VIS Leica, Wetzlar, Germany). Imaris (Bitplane, Zurich, Switzerland) was used as software for image processing.

2.2.4.5. Cultivation of CAL-33 and HeLa cells

CAL-33 and HeLa cell lines (tongue squamous cell carcinoma ACC 447; human cervical cell adenocarcinoma CCL-2) were purchased by DSMZ or ATCC and were cultivated in RPMI-1640 supplemented with 1% GlutaMAX™ and 10% heat inactivated FCS (Fetal Calf Serum) and DMEM supplemented with 10% heat inactivated FCS, respectively. The cells were subcultivated every 3- 4 d at 80% confluency by trypsinization with 0.05% trypsin-EDTA (0.05% trypsin and 0.02% EDTA) (Thermo Fischer, Waltham, USA) and incubated at 37 °C, 5-6% CO_2 in a humidified atmosphere.

2.2.4.6. MTT cytotoxicity assay

CAL-33 or HeLa cells were seeded onto 96-well plates at a density of 12000 cells per well in RPMI-1640 or DMEM and incubated overnight under standard conditions (37 °C, 5-6% CO_2, humidified atmosphere). The cells were treated with different RPMI-1640/DMEM solutions containing chitosan-MPA at different concentrations (100, 50, 25, 12.5, 6.25, 3.12, 1.56 and 0.78 µM) and incubated for 24 h in standard conditions. After the cells were washed twice with complete medium 10 µL of MTT (5 mg/mL, final concentration 0.5 mg/mL) were added to each well and the plated incubated for 4 h. The insoluble metabolic product formazan was solubilized with 100 µL of SDS solution 10% (w/v) in 0.01 N HCl and incubated overnight. The optical density was recorded at 570 nm using a 96-well plate reader (Synergy 2 Multi-Mode Reader, BioTek). For each concentration sextets were performed to determine the standard deviation. Results are expressed as mean ± SD. Non-linear regression of the curve was performed with GraphPad Prism5.

2.3 Results and discussion

2.3.1 Thiomers synthesis and characterization

To study the effect of the substitution on the antibacterial activity, chitosan was functionalized with aryl, alkyl and amino acids, all of them equipped with a thiol group. The focus was placed on the influence of the alkyl chain length of the substituent: starting from thioglycolic acid, the alkyl chain length was increased to 2, 3, 4, 6 and 8 carbon atoms, including two branched substituents (Figure 2.4). Most of the alkyl thiomers were newly synthesized and they were screened for antimicrobial activity with respect to deriving SAR.

Two different kind of reactions were used, one involves the formation of an amide bond: the carboxylic group of the TGA is activated by the carbodiimide EDC forming an O-acyl urea derivative as intermediate product, which reacts with chitosan primary amino groups. Even if for EDC the best reactivity should be in the pH range from 2.5 to 4.5,[150] the functionalization of chitosan was performed at pH 5, because it was reported as the pH leading to the best functionalization with thiols.[87] Additional considerations about this reaction or possible alternatives will be discussed in the chapter 4 of this thesis.

The second reaction is an ring-opening reaction involving 2-iminothiolane, proceeding without using any catalyst or activator by targeting directly the amine groups of chitosan with the introduction of a cationic amidine substructure.

All produced materials, including the pristine chitosan, were characterized in detail using different spectroscopic and analytical techniques to correlate their specific structural properties to the observed antibacterial behavior.

2.3.1.1 Ellman test and degree of substitution

Special emphasis was placed on the quantification of the amount of sulfur present in the samples through Ellman's reagent assay and elemental analysis. The extent of the functionalization is proportional to the amount of sulfur attached to the polymer. Ellman's reagent[151] 5,5'-dithiobis(2-nitrobenzoic acid) ($DTNB^{2-}$) is able to react stoichiometrically with the thiolate anion ($R\text{-}S^-$), producing the yellow compound 5-thio-2-nitrobenzoic acid (TNB^{2-}), which exhibits intense light absorption at a wavelength of 410-420 nm and is directly proportional to the sulfur content.[152] A scheme of the reaction is shown in Figure 2.6.

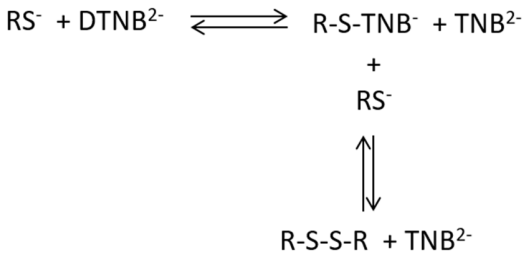

Figure 2.6. Scheme of Ellman's reaction.[149]

To quantify the sulfhydryl groups in the polymer, calibration curves of cysteine were freshly prepared and measured each time to achieve the highest possible accuracy. The concentration of sulfhydryl groups was calculated only for the samples with absorbance in the linearity range of the calibration curve. Typically, all the concentrations below 80 µmol/g were outside of the linearity range and therefore considered as not substituted. A representative calibration curve is reported in Figure 2.7.

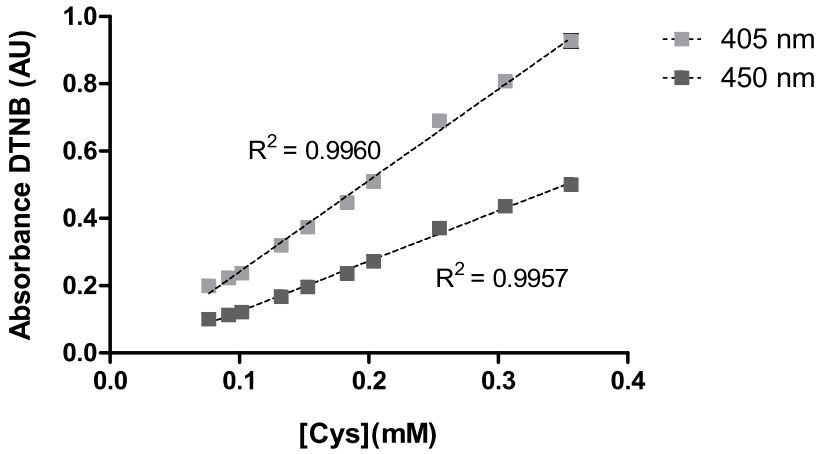

Figure 2.7. Ellman test calibration curves.

As Ellman's reagent reacts only with sulfhydryl groups (-SH), the real sulfur contents might be underestimated because of the formation of disulfide bridges. Therefore S/N molecular ratios were calculated from elemental analysis data. The results of both the Ellman test and of the elemental analysis were compared to verify the consistency of the results (see Table 2.2).

Table 2.2. Characterization of the synthesized thiomers (n. d. = not detectable).

Substituent	**Start. Mat.**	**DD** (%)	**Mw** (kDa) ± SD	**PDI**	**DS** (%)	**SH** (µmol/g) ± SD	**ζ pot.** (mV) ± SD
Chitosan	85/20	93.1	92.5 ± 1.1	1.06	n. d.	n. d.	29.9 ± 1.0
TGA-A	85/100	91.1	252.6 ± 0.3	2.17	0.7	91.5 ± 0.5	31.4 ± 0.9
TGA-B	85/20	93.7	103.2 ± 3.4	1.31	0.5	90.2 ± 0.5	27.6 ± 1.4
TLA-A	85/5	87.5	25 ± 0.4	1.59	6.2	221.1 ± 2.0	20.6 ± 1.4
TLA-B	85/20	93.3	124.4 ± 4.4	1.1	3.1	186.7 ± 2.4	29.6 ± 0.9
MPA-A	85/10	87.1	83.5 ± 2.5	1.12	12.1	164.6 ± 3.9	26.5 ± 0.2
MPA-B	85/5	88.2	22.5 ± 1.1	1.24	7.3	174.9 ± 3.1	22 ± 0.9
MPA-C	85/20	93.2	97.6 ± 2.3	1.25	5.1	144.1 ± 2.7	32.5 ± 0.9
MSPA	85/20	93.1	104.6 ± 8.5	1.22	3.7	206.6 ± 1.7	38 ± 1.0
MBA	85/20	94.2	87.6 ± 3.9	1.32	1.0	168.3 ± 0.5	32.2 ± 0.8
MHA	85/20	92.8	96.2 ± 2.4	1.23	4.5	253.7 ± 14	30.3 ± 1.4
MOA	85/20	93.2	117.8 ± 2.6	1.14	4.3	254.6 ± 24	30.2 ± 0.3
L-Cys-A	85/5	86	15.6 ± 0.7	1.01	2.8	114 ± 2	13.0 ± 3.7
L-Cys-B	85/20	88	92.7 ± 9.6	1.19	5.1	152 ± 0.3	23.9 ± 3.5
IMI-A	85/5	86.9	33.7 ± 10.5	1.44	27.6	304 ± 7	//
IMI-B	85/10	85.5	109.9 ± 13.7	1.32	25.1	228.3 ± 21	//
MBeA-A	85/10	81	//	//	//	524 ± 22	//
MBeA-B	85/10	86	//	//	//	224 ± 16	//
MBeA-C	85/5	84.9	//	//	35.0	305 ± 7	//

The extent of the functionalization, or in other words the DS and concentration of sulfhydryl groups, depends strongly on the reactivity of the substituent, on the starting material (lower MW seems to be functionalized more easily) and the conditions used in the synthesis (time, temperature, pH and inert atmosphere). Chitosan-TGA turned to be the less substituted of the synthesized thiomers, with a concentration of sulfhydryl groups of about 90 µmol/g and a DS of 0.5-0.7%. Multiple attempts to synthesize chitosan-TGA with a higher DS via novel or modified literature protocols were performed and more details are discussed in chapter 4. All other synthesized thiomers have a DS from 3 to 7% and a concentration of sulfhydryl groups from 150

to 250 µmol/g, depending on the reagent and on the reaction conditions. When the sulfhydryl groups content of only the thiomers prepared from the starting material 85/20 is considered, more uniform DS (from 3 to 5%) were achieved, except for chitosan-MBA which was less substituted.

Chitosan-MBeA and -IMI showed a high DS. The high substitution of the aryl thiomers could be explained by the higher reactivity of the carboxylic acid nearby the aromatic ring. If the substitution extent is too high, the chitosan-MBeA becomes insoluble. To achieve more soluble samples, it was necessary to reduce the amount of EDC. Nevertheless, it was easy to achieve a high degree of substitution up to 35% and thiol concentration up to 500 µmol/g. Regarding chitosan-IMI, details from two different procedures were incorporated in the synthesis.[126,148] In the second study highly substituted material was achieved while using small amounts of starting material, while larger amounts of chitosan were used in the first study. Therefore, the second reaction was scaled up in this work, still achieving a good DS and high concentration of sulfhydryl groups. Taking advantage of the easily achievable substitution, this synthesis is recommended when high DS are desired, but chitosan-IMI it is probably not stable (see discussion below).

2.3.1.2 ^{1}H and ^{13}C-NMR spectroscopy

The successful functionalization of the chitosan backbone can be investigated with NMR spectroscopy. When the DS is high enough, the protons of the substituent can be detected by ^{1}H-NMR spectroscopy. The ^{1}H-NMR spectrum of chitosan-MSPA is reported as representative example (Figure 2.8) together with its molecular structure and the assignment of the chemical shifts either of the chitosan backbone and either of the substituent. The spectrum displays a well-defined peak at δ 1.76 ppm related to the methyl group in alpha position. In the case of chitosan-MSPA the degree of substitution can be evaluated using the integral of the methyl group (δ 1.76 ppm), however with this method we obtain a DS of 23.4% that does not agree with the one calculated using elemental analysis data. Furthermore, if the DD of chitosan is calculated from the integrals of the peaks of the ^{1}H-NMR spectra at 75°C, a lower DD of 88.21% is estimate. Anyway, comparing the DD calculated at 75 °C and at room temperature, it was possible to verify that the differences between the DD of the single samples are retained at both temperatures.

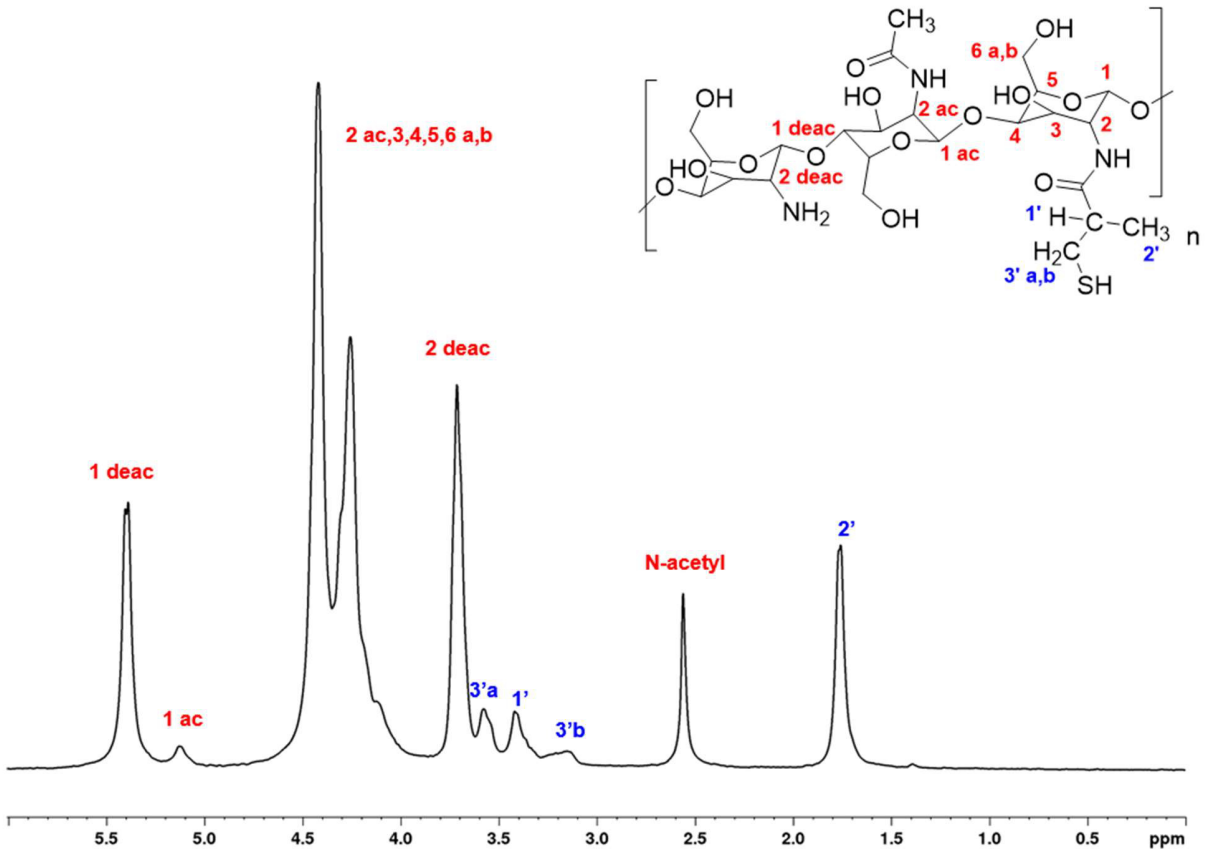

Figure 2.8. Chitosan-2-methyl-3-sulfanylpropanoic acid ^{1}H-NMR spectrum (400 MHz, D_2O, 348 K, with suppression of water): δ 1.76 (d, J= 6.3 Hz, 3H2'), 2.56 (s, N-acetyl), 3.14, 3.58 (m, 2H3'), 3.42 (m, H1'), 3.71 (s, H2 deac.), 4.25-4.42 (broad, H2 ac., H3, H4, H5, H6a,b), 5.12 (d, J = 6.5 Hz, H1 ac.), 5.40 (d, J = 7.9 Hz, H1 deac.).

In the case of chitosan-TGA, no chemical shifts related to the CH_2 of the substituent are visible, most probably because of their overlap with the chitosan signal (Figure 2.9).[153] Despite this the weak signal related to the sulfhydryl group is visible at δ 1.39 ppm. On the other hand, in the case of chitosan-TLA, -MSPA, -MPA, -MBA, -MHA and -MOA, the signals related to the substituents were clearly visible in the ^{1}H-NMR spectra (Figure 2.10-2.14). The weak signal of the amine group was also visible at δ 1.77 ppm.

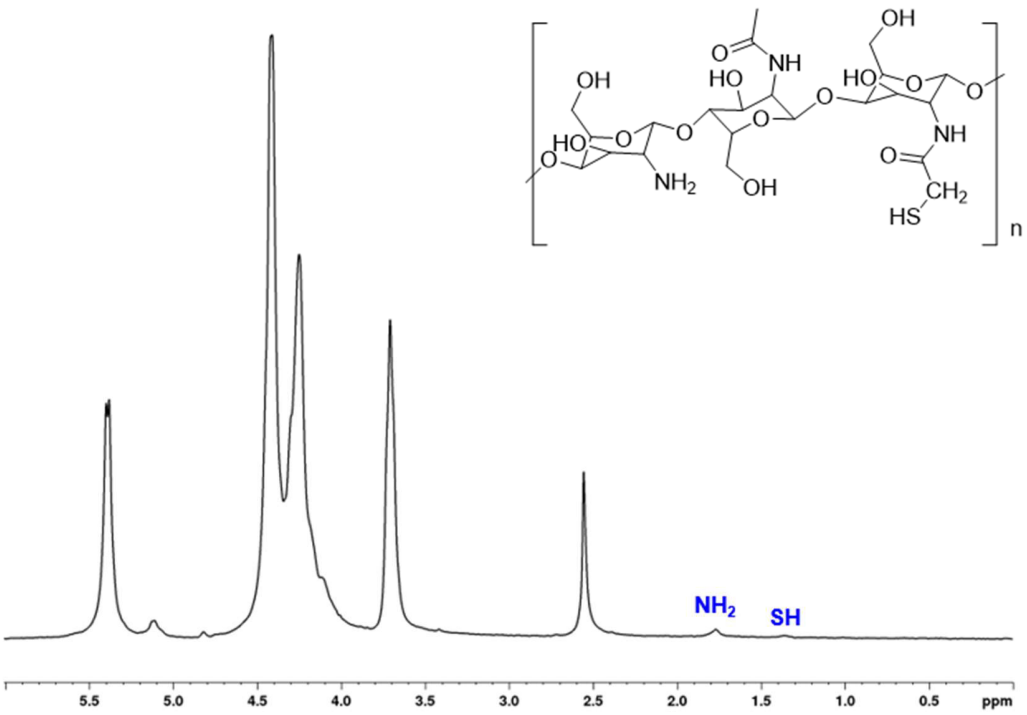

Figure 2.9. Chitosan-TGA ^{1}H-NMR spectrum recorded at 348 K in D_2O with suppression of water signal.

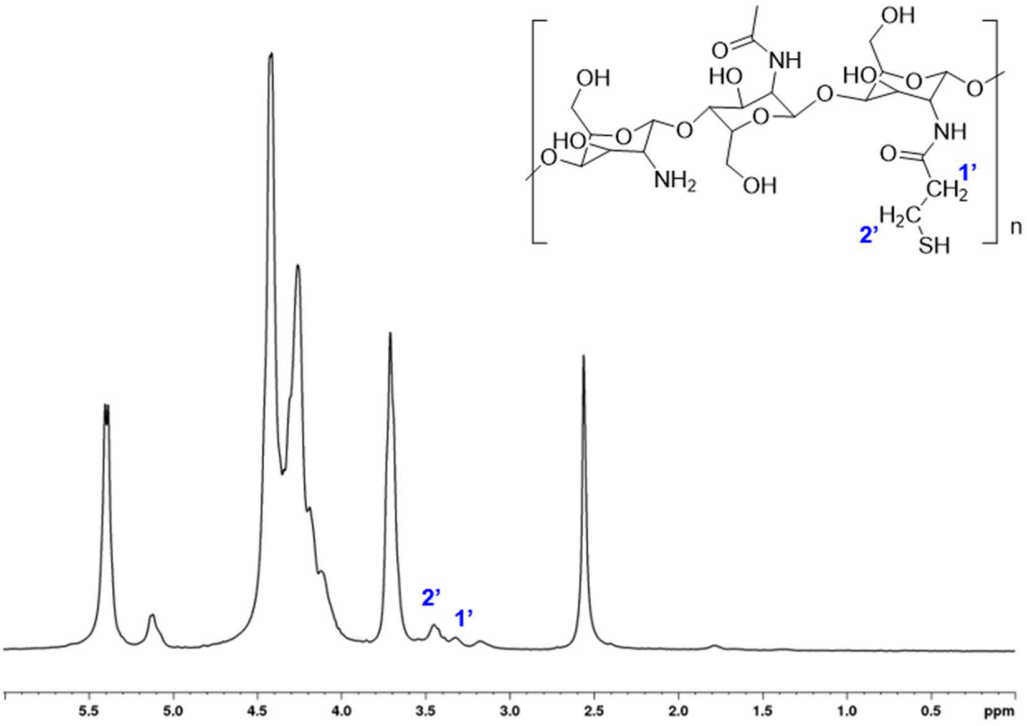

Figure 2.10. Chitosan-MPA ^{1}H-NMR spectrum recorded at 348 K in D_2O with suppression of water signal.

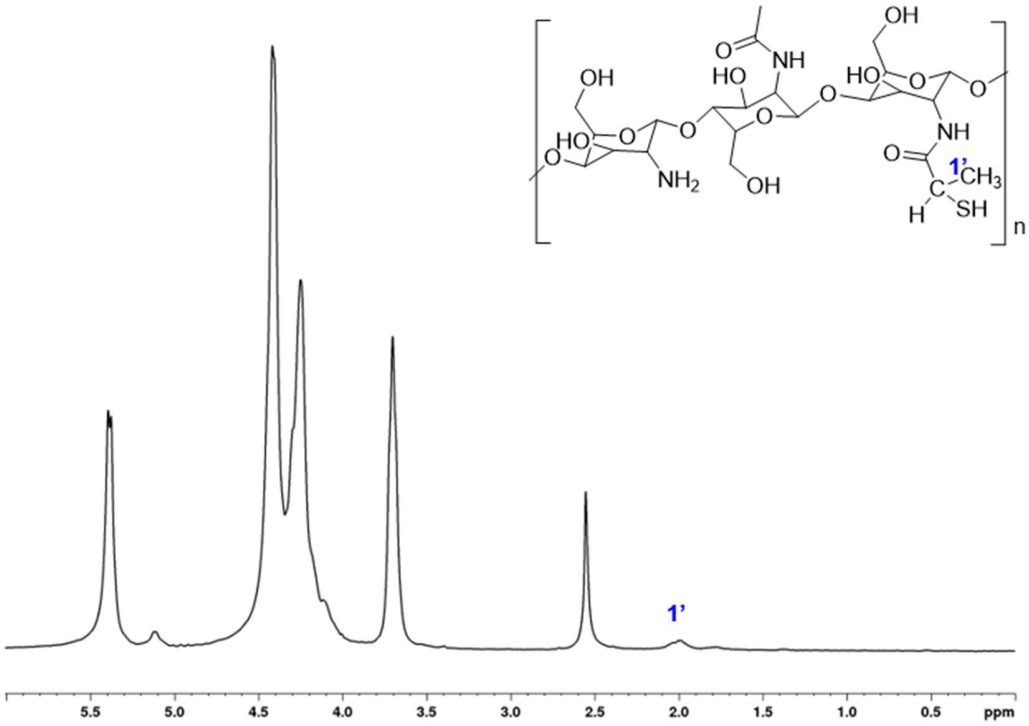

Figure 2.11. Chitosan-TLA ^{1}H-NMR spectrum recorded at 348 K in D_2O with suppression of water signal.

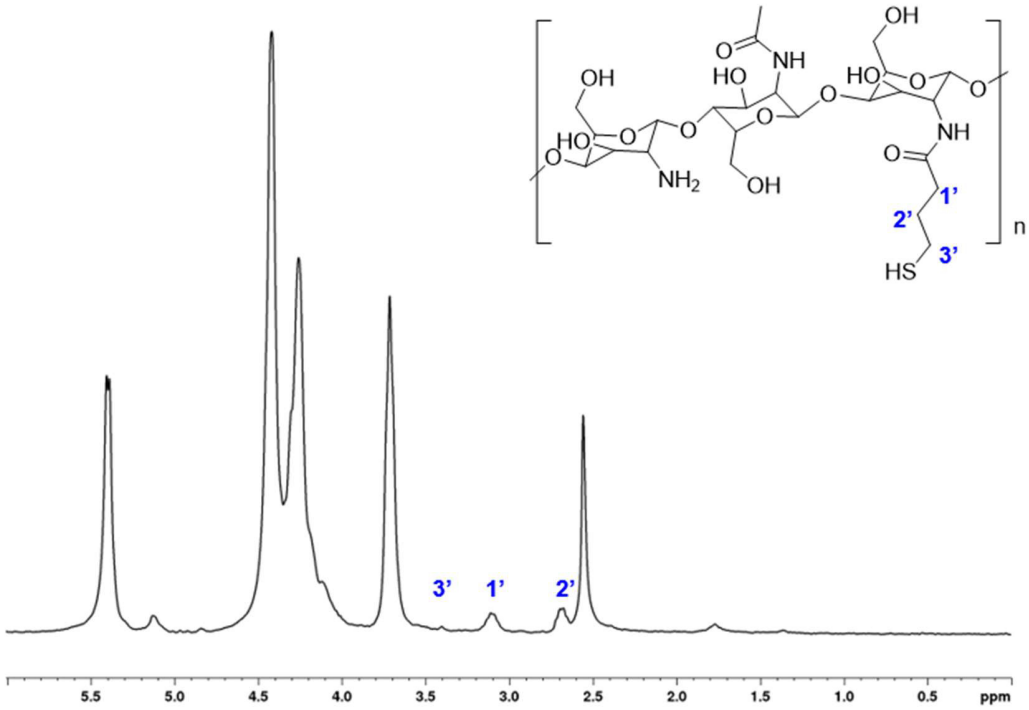

Figure 2.12. Chitosan-MBA ^{1}H-NMR spectrum recorded at 348 K in D_2O with suppression of water signal.

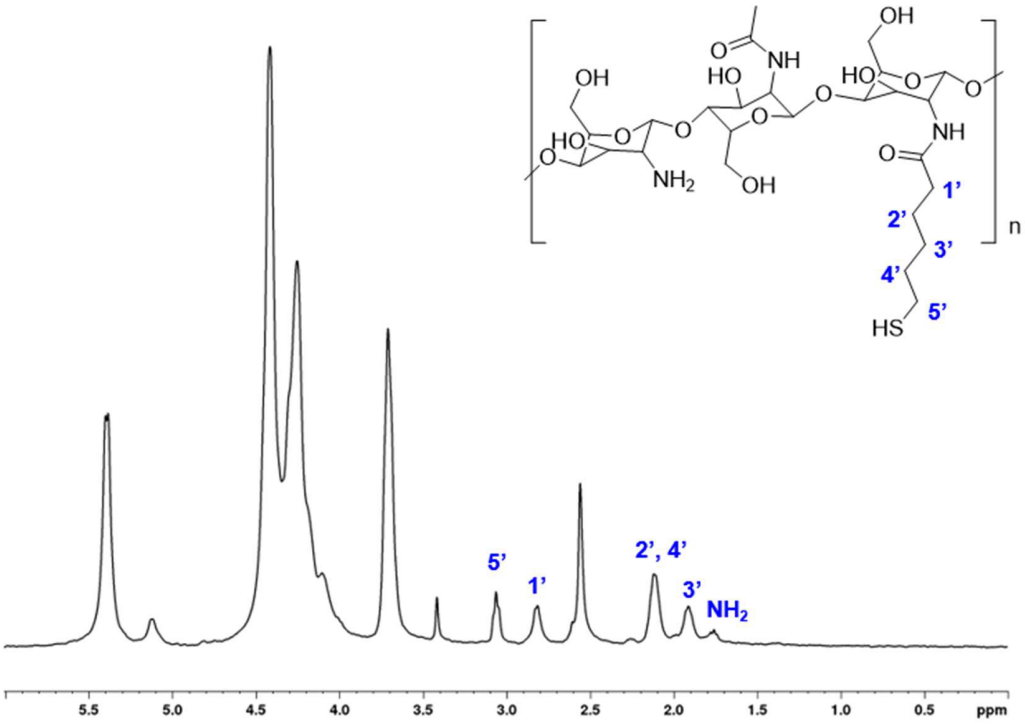

Figure 2.13. Chitosan-MHA ^{1}H-NMR spectrum recorded at 348 K in D_2O with suppression of water signal.

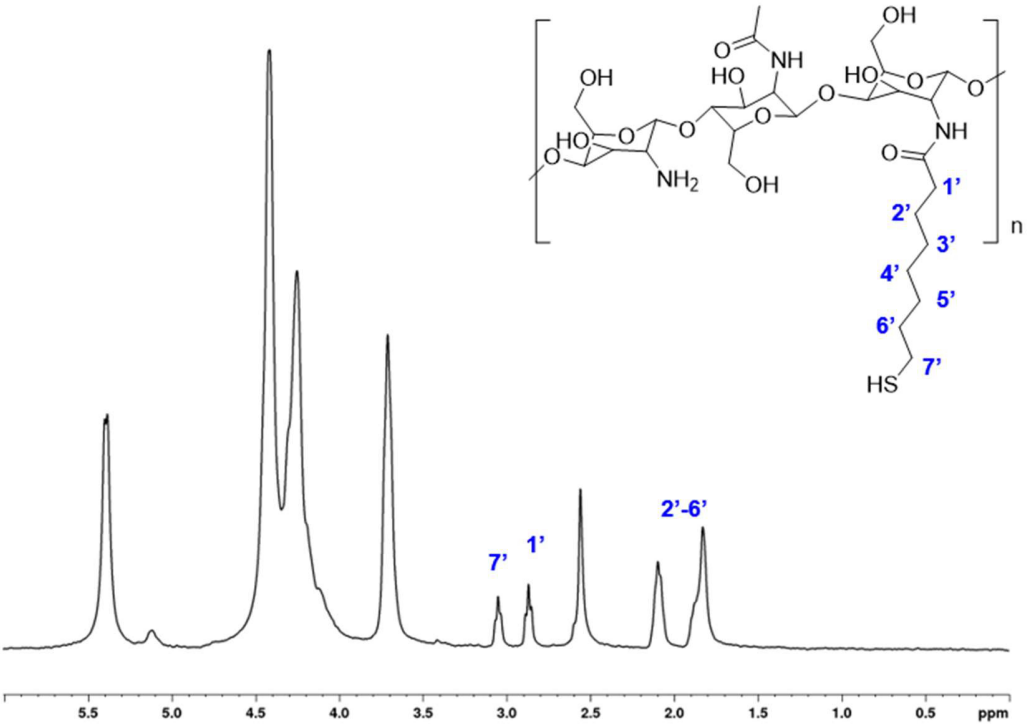

Figure 2.14. Chitosan-MOA ^{1}H-NMR spectrum recorded at 348 K in D_2O with suppression of water signal.

The stability of chitosan-IMI was investigated via ^{1}H-NMR spectroscopy at 75 °C recording a spectrum when the sample was freshly prepared and when the sample was left in solution for one month, to investigate any possible changes. In the spectrum of the freshly prepared sample the signals related to the substituent are clearly visible at δ 2.5, 2.4 and 1.8 ppm, while the signal at δ 2.0 ppm is attributed to the hydrogen atoms of the acetyl group (Figure 2.15). Note the presence of the broad peak at δ 2.3 ppm and at δ 4.7 ppm for which no suitable assignment could be found. The peak at δ 4.7 ppm could be related to the H1 proton bound to the substituent. After one month, the ^{1}H-NMR spectrum of chitosan-IMI does not show the peaks at δ 2.3 ppm and at δ 4.7 ppm (Figure 2.15b). It was reported that this could be due to loss of the substituent through a ring-closure reaction.[154] However, the results of the Ellman test on the same sample showed a very high concentration of free sulfur, which is in contrast with the ring-closure hypothesis. Interestingly, 4 years after synthesis, chitosan-IMI was not soluble anymore in water, thus providing further evidence in favor of the ring-closing decomposition.

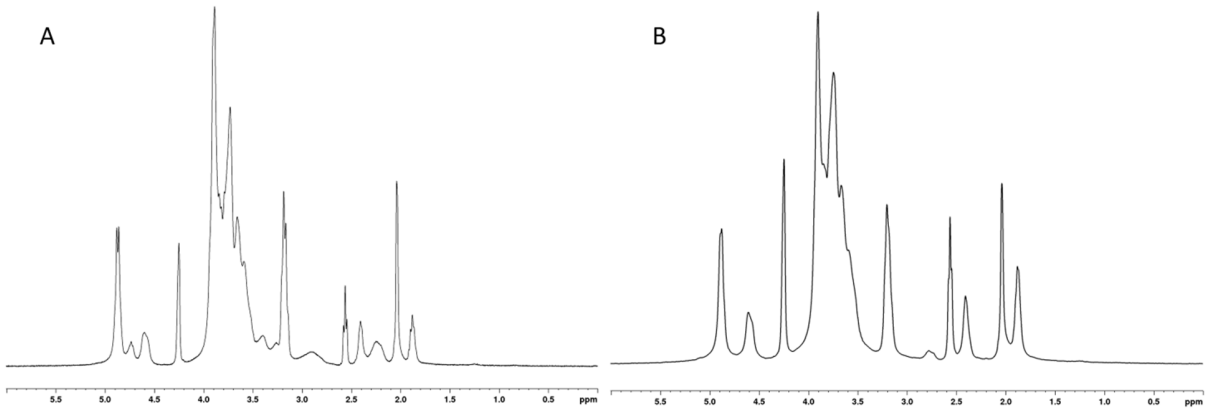

Figure 2.15. ^{1}H-NMR spectrum of chitosan-IMI freshly prepared (A) and after 1 month (B) recorded at 348 K in D_2O.

Chitosan-IMI was also investigated by COSY-^{1}H-NMR. This technique is useful to attribute the correlation between the protons of the substituent and those of the chitosan backbone: it is, for example, possible to establish that the signal at δ 1.8 ppm is due to the CH_2β in the middle of the alkyl chain, because it interacts with both the signals at δ 2.5 and δ 2.4 ppm, that are relative to the protons at the beginning (CH_2α) and at the end of the chain(CH_2γ) (N-C-CH_2α-CH_2β-CH_2γ-SH; Figure 2.16).

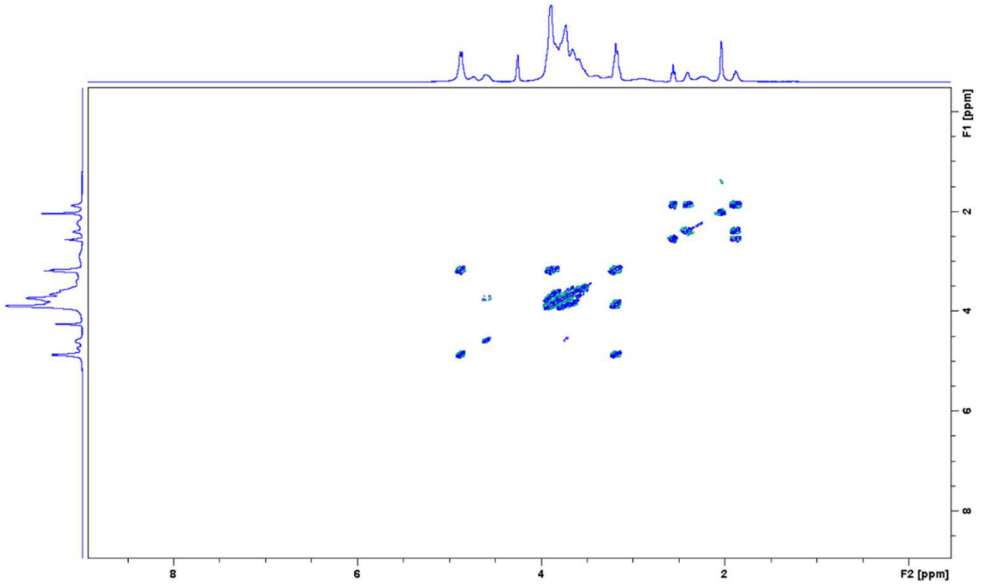

Figure 2.16. COSY- ^{1}H-NMR spectrum of freshly prepared chitosan-IMI recorded at 348 K in D_2O.

Chitosan-IMI was characterized by ^{13}C-NMR spectroscopy that also confirmed the presence of the substituent displaying the three chemical shifts related to IMI at δ 43.2, 37.8 and 31.1 ppm (Figure 2.17b).

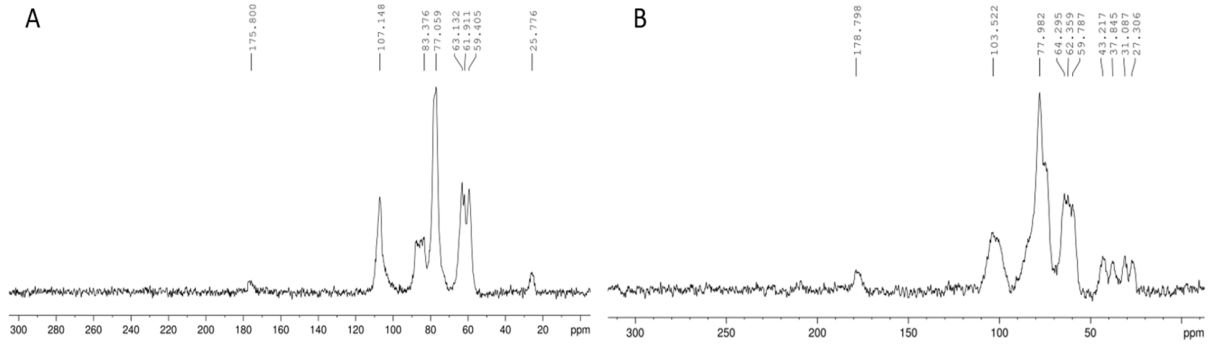

Figure 2.17. Solid ^{13}C-NMR spectra of pristine chitosan (A) and freshly prepared chitosan-IMI (B).

The ^{1}H-NMR spectrum of chitosan-MBeA displays the characteristic signals related to the chitosan backbone and additionally the signals of the protons of the aromatic ring (δ 8.3 ppm) and two signals at δ 1.6 and δ 3.65 ppm related to the dioxane which is a residue from the synthesis (Figure 2.18).

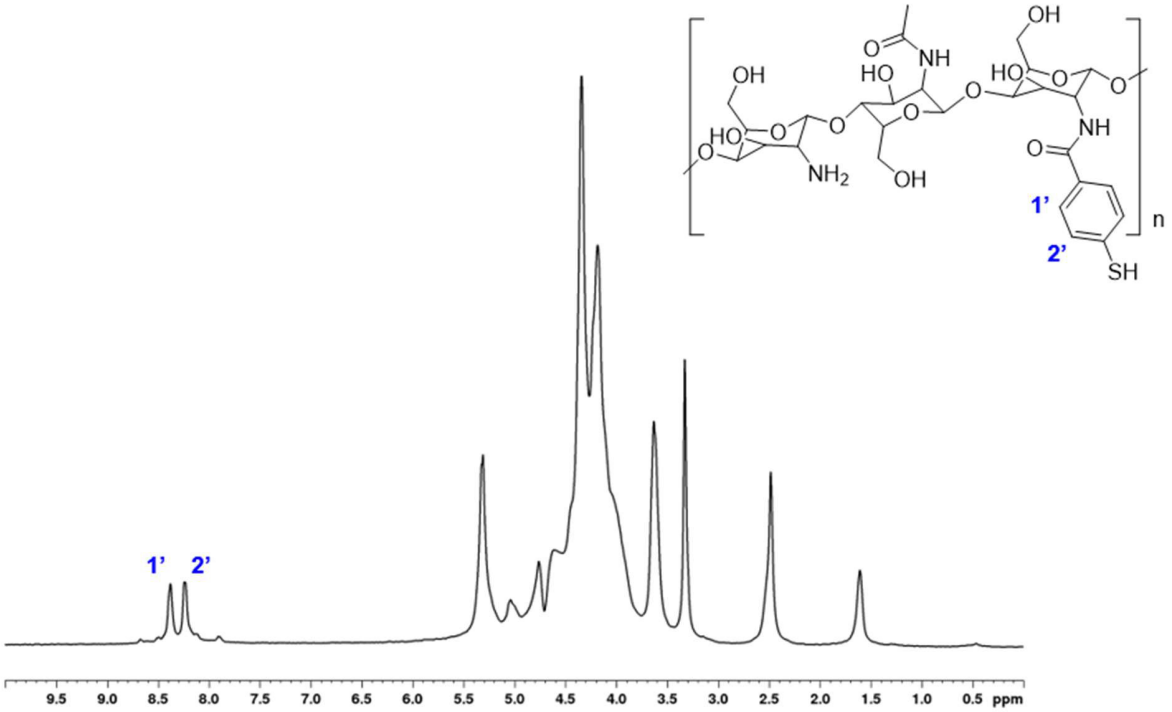

Figure 2.18. Chitosan-MBeA ^{1}H-NMR spectrum recorded at 348 K in D_2O with suppression of water signal.

The ^{1}H-NMR spectra acquired at room temperature were used to calculate the DD of all the synthesized thiomers: according to the formula of *Hirai et al.* the integrals of the signals related to the three protons of the acetyl group are correlated with the signals of the chitosan backbone.[62] The DD were depending on the chitosan starting material and ranged from 85 to 94%. All the derivatives synthesized from chitosan 85/20 had a DD higher than 92.8%.

2.3.1.3 Gel Permeation Chromatography

Gel permeation chromatography was used to determine the MW of the majority of the thiomers. The MW is important for the antibacterial properties of chitosan as stated before. Furthermore, comparing the MW of the thiomers with the one of the pristine starting materials, is possible to verify if some depolymerization was occurring during the synthesis, or on the contrary, if the substitution was increasing the MW. All the alkyl thiomers and chitosan-Cys synthesized from chitosan 85/20 (92.5 kDa) had MW between 90 to 120 kDa (Table 2.2), which supports the hypothesis that the functionalization increases the MW. Chitosan-IMI achieved from chitosan 85/5 and 85/10 showed a marked increase in the MW, especially for chitosan-IMI-B whose MW

increases from 55 kDa to 110 kDa. Chitosan-MBeA MW was not measured because of solubility issues; however, it could be speculated that due to its high DS the MW increases compared to the starting material. Both the number-average and the weight-average MW were determinate with GPC experiments and the PDI was calculated. PDI values, which indicate the polydispersity of the polymer, were ranging from 1.1-1.3 for the thiomers synthesized from chitosan 85/10 and 85/20 indicating a good uniformity of the polymer chain mass. A polydispersity index higher than 2 was calculated for the derivatives synthesized from chitosan 85/100 highlighting the irregular length of the polymer chains. This is true in a lesser extent, also for the derivatives of chitosan 85/5. The differences in the PDI could either be due to the characteristics of the starting material or be a consequence of the reaction conditions.

2.3.1.4 ζ-potential

As mentioned above, the pH value exerts a major influence on the antimicrobial efficacy of chitosan and its derivatives. Therefore, to exclude this influence, chitosan thiomers were dissolved in PBS before to be screened against bacteria. Furthermore, to remain as close as possible to the biological conditions, chitosan thiomers were dissolved in PBS to measure their ζ-potential and their pH. The pH values after dissolution were around 5.5-6.0 with measured ζ-potentials around +30 mV due to the residual protonated ammonium groups. The thiomers achieved from 85/5 were the only ones with a low ζ-potential in the range of +10 to +20 mV.

2.3.1.5 FT-IR spectroscopy

FT-IR spectroscopy was not as efficient and insightful as other analytical techniques to characterize the different thiomers or to confirm the substitution, except for chitosan-IMI and MBeA, which had a high DS. The signal corresponding to the amine vibration at 1587 cm^{-1} present in the starting material (data not shown) disappears in all the alkyl thiomers and in the reference chitosan spectra and it is substituted by two signals at 1515 and 1620 cm^{-1} assigned to the protonation of the amine group. The change in the spectra is probably due to the conditions of the reaction and dialysis environment (Figure 2.19a) The spectrum of chitosan-IMI displays a shift of the bands at 1515 and 1620 cm^{-1} to 1521 and 1627 cm^{-1} (Figure 2.19b) because of the formation of the amidine bond. Chitosan-MBeA spectrum shows also shifts of the bands at 1515 and 1620 cm^{-1} to 1521 and 1627 cm^{-1}, respectively, that could be attributed to the formation of the

amide bond. Additionally, two shoulders at 1596 and 1490 cm^{-1} are attributable to the aromatic ring of the substituent.[155]

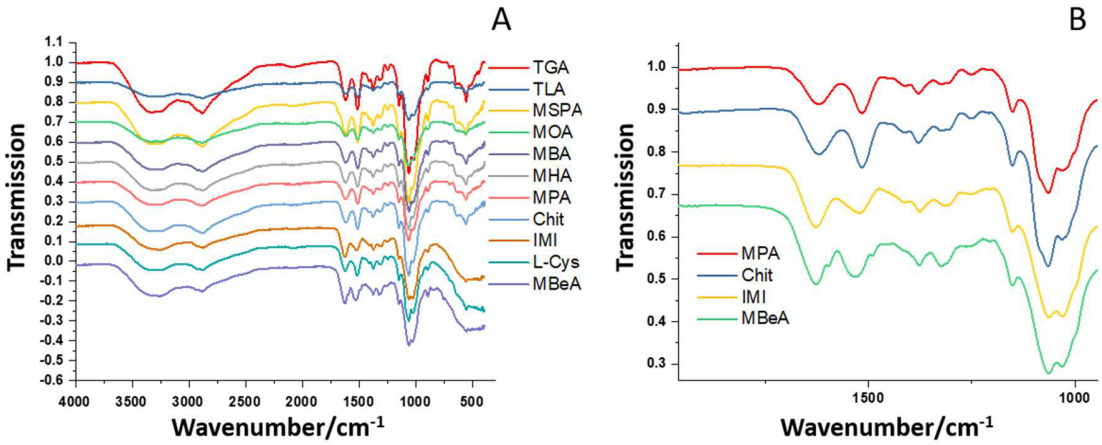

Figure 2.19. FT-IR spectra of the chitosan thiomers: all thiomers in the entire range of measurement (A) and focus on the region between 2000 to 1000 cm^{-1} for chitosan, chitosan-MPA, -IMI and -MBeA (B).

2.3.1.6 Conclusion

The goal of this work was to define a SAR between the alkyl chain length and the antimicrobial activity of the chitosan thiomers. Therefore, we aimed to standardize the influence of DS, DD, MW and positive charge density, which could affect the antimicrobial properties of the materials, to the maximum possible extent. These parameters were successfully kept in a narrow range and their contribution on the antimicrobial activity can thus be assumed as fairly constant.

2.3.2 Biological activity tests

Several chitosan thiomers have been thoroughly characterized, and they were screened for antimicrobial activity against the gram-negative strain *E. coli* to identify the most promising derivatives, and the corresponding chitosan starting materials. After the initial selection, the most effective thiomers were tested against two representatives gram-negative (*E. coli* and *P. aeruginosa*) and two representatives gram-positive (*S. sobrinus* and *S. mutans*) strains. *E. coli* and *P. aeruginosa*, among others, are responsible for the increased antibiotic resistance phenomenon which is a heavy burden for many health systems worldwide. [156] These two strains were selected because of their biological relevancy and ubiquity.[157] In contrast, *S. sobrinus* and *S. mutans* are

normal components of the oral flora, which play a fundamental role in the balance of the oral plaque and in the formation of dental caries.[158] Control over these strains would thus be beneficial for the oral health.

2.3.2.1 MTT assays screening

To determine which characteristics of the chitosan starting materials have a major influence on the antibacterial behavior and which derivatives show the highest efficacy, an easy and low-cost screening assay was set up by adapting and optimizing the well-known MTT-based cytotoxicity assay.[159] In contrast to previously described MTT procedures, a protocol that permits a quick processing of numerous compounds in many replicates was developed, using a 96-well plates to detect the absorbance with a standard plate reader. The modified MTT assay allows the quantification of alive bacteria after treatment with chitosans, because of the proportionality between the absorbance of the formazan crystals produced by the MTT metabolism and the number of viable cells. The linearity of the method was proved under experimental conditions (Figure 2.20).

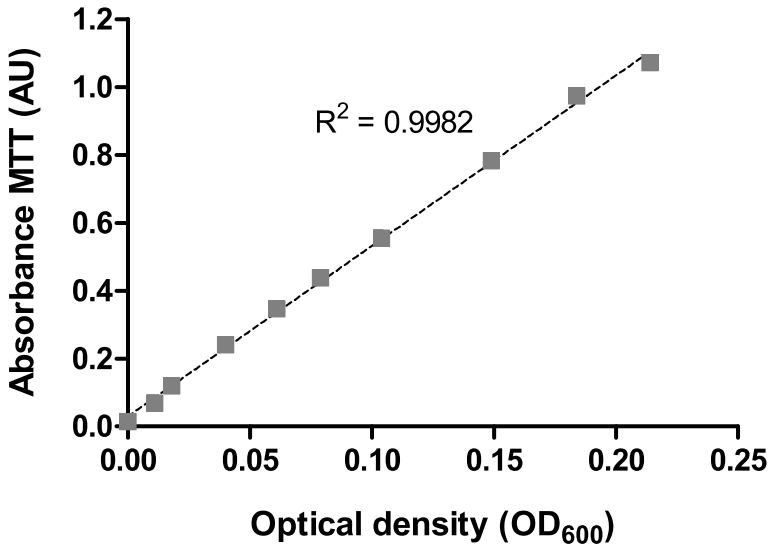

Figure 2.20. Linearity of the MTT reduction assay.

The derivatives synthesized from different starting materials were tested at two concentrations (2 and 4 mg/mL) and two incubation times (30 and 60 min). The MTT assay results highlighted the

remarkable improvements in the antimicrobial effect of chitosan-TGA and -MPA (and to a lower extent of chitosan-TLA) synthesized from chitosan 85/20 in comparison to the others synthesized from chitosan 85/5, 85/10, and 85/100 (Figure 2.21). The DD of 85/20 chitosan thiomers determined by ^{1}H-NMR spectroscopy was around 93%, thus suggesting that this starting material affords chitosan thiomers with higher DD, which is well known to enhance the antimicrobial activity. Therefore, chitosan 85/20 was used as starting material for the synthesis of chitosan-MSPA, -MBA, -MHA and -MOA, which have been tested with MTT assay as well. The MTT assay results under the mildest conditions (2 mg/mL and 30 min incubation) showed that the derivatives chitosan-TGA and -MPA exerted the highest antimicrobial activity (Figure 2.21). However, to draw more reliable conclusions further antimicrobial investigations with more precise methods were required.

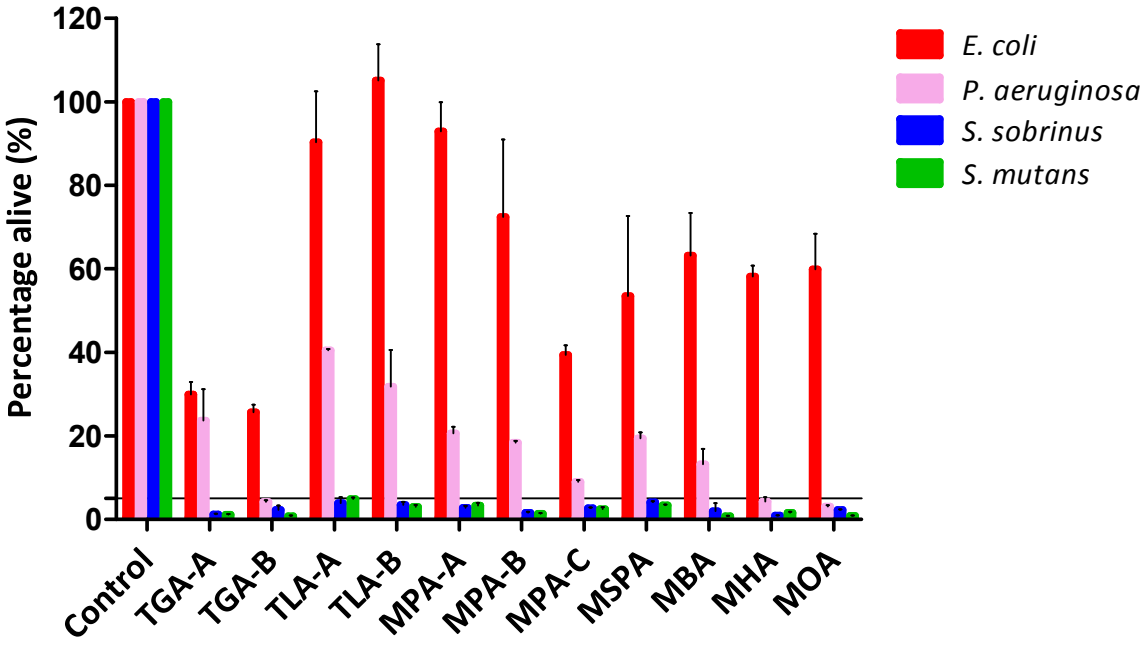

Figure 2.21. MTT results for chitosan thiomers at 2 mg/mL, 30 min of incubation for E. coli, P. aeruginosa, S. sobrinus and S. mutans.

Chitosan-MBeA was tested only against *E. coli*, while chitosan-IMI was only tested against *E. coli* and *P. aeruginosa*. Despite the high DS of these chitosans, the bacteria were not affected by the treatment, showing instead an increase in the population compared to the control (Figure 2.22).

This may suggest that a high DS may not be fundamental to maximize the antibacterial activity of chitosan thiomers – on the contrary, it is important to provide enough free amine groups on the chitosan backbone to allow the interaction between the positive ammonium groups with the bacterial targets. Chitosan-L-Cys did not display any outstanding activity in the MTT assay (Figure 2.22), however chitosans substituted with amino acids and as well with the D isomer of cysteine will be briefly considered in chapter 5.

As the goal was the identification of a broad spectrum antimicrobial agent among the chitosan thiomers, chitosan-IMI, -L-Cys and -MBeA with low antimicrobial activity on gram-negative strains were not further tested on the gram-positive strains.

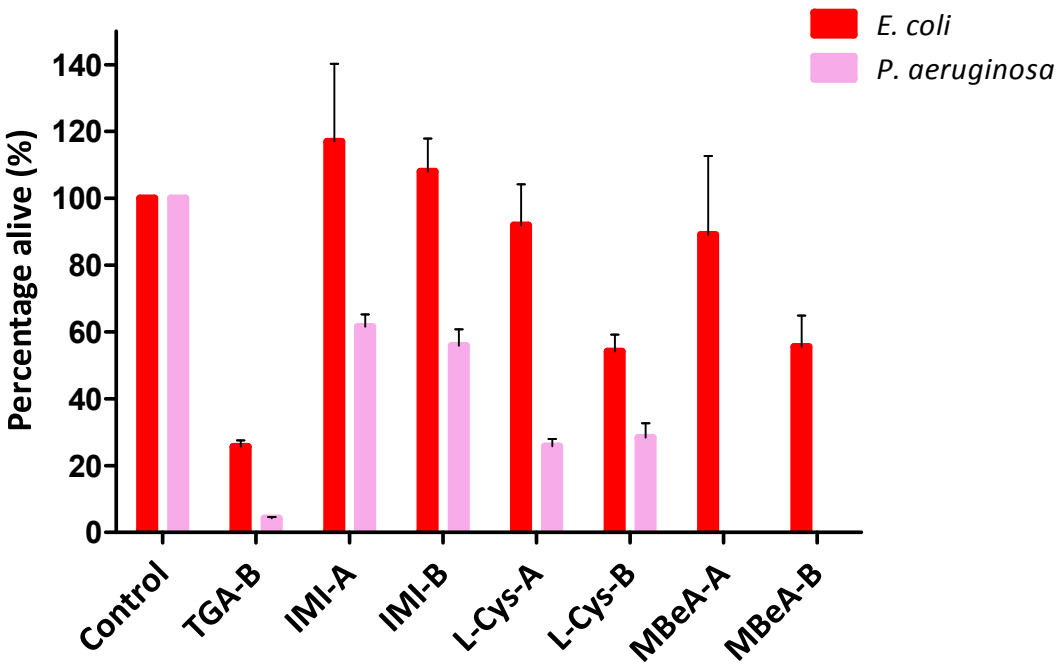

Figure 2.22. MTT results for chitosan-TGA, -IMI, -L-Cys and MBeA at 2 mg/mL, 30 min of incubation for E. coli and P. aeruginosa.

2.3.2.2 Plate counting experiments

Whereas the MTT assay allows for a rapid and convenient screening, the quantitative assessment of the antimicrobial efficiency requires more precise methods: plate counting experiments were therefore performed. This method is based on counting the bacteria which survive after treatment and are able to form a colony onto agar plates after 24 h. Plate counting experiments permit through different dilutions of the bacterial suspension to detect a reduction up to 8 log

(1 survived over 1 billion cells), which justifies the longer operational time. Plate counting experiments were performed for chitosan-TGA, -TLA, -MPA, -MSPA, -MBA, -MHA and -MOA prepared from chitosan 85/20 and their activity was compared with the reference chitosan. Two different concentrations, 20 and 40 µM and two different incubation times, 30 and 60 min were tested. After the bacteria were plated and incubated for 24 h, the post-treatment capability of bacterial cells to form colonies was evaluated. The results revealed that for all strains tested higher concentrations and prolonged treatment times did not exert a significantly stronger antimicrobial effect than the milder conditions. Therefore, results after treatment for 30 min with 20 µM chitosan thiomers are reported in Figure 2.23 and discussed in the following lines.

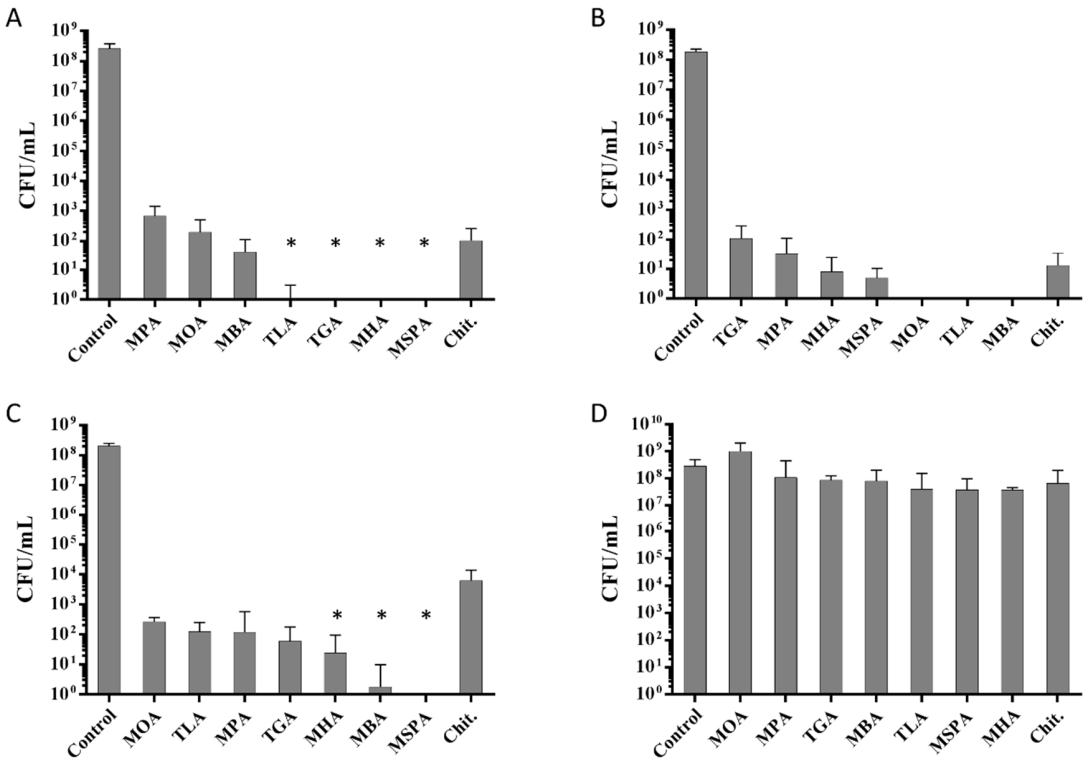

Figure 2.23. Plate counting results: colony forming units (CFU) per mL for P. aeruginosa (A), S. sobrinus (B), S. mutans (C) and E. coli (D) (20 µM, 30 min incubation). Thiomers marked with an asterisk were statistically significant compared to chitosan ($p < 0.05$).

Interestingly, the experiments show that none of the investigated thiomers had a significant effect on the reduction of the *E. coli* population (Figure 2.23d), suggesting that both chitosan and its derivatives are not suitable for the depletion of this strain. The strong resistance of *E. coli*

towards the thiomers and chitosan could be useful when the target is only a certain pathogenic strain which is growing in biofilms, for example. In fact, several *E. coli* strains are normally present in the flora of the gut,[157] where they are in a symbiotic relationship within the organism: their depletion would not bring any health benefits, just causing discomfort eventually.

On the contrary, the antimicrobial activity of the chitosan thiomers on the other three tested strains is outstanding. All the derivatives, as well as reference chitosan, had a strong impact on the population of the gram-negative *P. aeruginosa* and both gram-positive strains *S. sobrinus* and *S. mutans (*Figure 2.23 *a, b and c)*. It is important to highlight that chitosan alone led to at least a 4.5-log reduction of colonies for all the three strains, but not to complete eradication of the population. In previous reports on *P. aeruginosa*, however, chitosan inhibition rates were not as high as in our study, even at higher concentrations or longer incubation times: chitosans with 30 and 120 kDa was able to reduce the population of this strain of 94.9%,[160] or of 99.9% when chitosans 49 kDa (DD 53%), 285 kDa (DD 76%) and 1080 kDa (DD 98%) were used.[161] Furthermore, minimal inhibitory concentration (MIC) values of chitosan on *S. mutans* have been reported to range from 1.25 to 5 mg/mL.[162] The variance of these results illustrates how different characteristics of the polymer as well as different applied conditions and methodology affect a reported chitosan antibacterial activity.

Whereas the treatment with pristine chitosan already significantly reduced the number of alive bacteria, the substitution of chitosan with the thiol-alkyl chains could enhance the antimicrobial activity, presumably through hydrophobic interactions between the alkyl chain and the bacterial wall proteins.[163] Furthermore, the reaction of the sulfhydryl group with the cysteine of membrane proteins could exert a detrimental effect on bacteria.[88] These combined features of the chitosan thiomers could lead to a prolonged interaction with the bacterial cell wall, thus enhancing the antibacterial activity. All the alkyl thiomer compounds induced at least a 5.6-log colony reduction compared to untreated controls. However, a single thiomer which was able to eradicate completely all the three strains was not present among the tested derivatives, with the efficiency of the single thiomers depending on the selected strain. This is in good agreement with previous reports for pristine chitosan[129,130] and for quaternary N-alkyl derivatives.[164] Even apparently small differences may have strong implications (such as on the repopulation of infected sites) due to the short generation times of most bacteria. Chitosan-TLA, -TGA, -MHA and

-MSPA worked equally excellent for gram-negative *P. aeruginosa* leading to a complete eradication of the bacteria (8.4-log reduction) and the results were statistically significant compared to pristine chitosan (Figure 2.23a). The gram-positive Streptococci displayed an inconsistent pattern, with a superiority of chitosan-MOA, chitosan-TLA and chitosan-MBA vs *S. sobrinus* (Figure 2.23b) and of chitosan-MSPA against *S. mutans* (Figure 2.23c). Advantages of chitosan thiomers were clearly visible in *S. mutans*, where chitosan-MHA, -MBA, and -MSPA all displayed a statistically significant effect compared to pristine chitosan, and especially chitosan-MSPA incubations resulted in 8.3-log reduction and the complete eradication of the bacterial population (Figure 2.23c). However, even if certain thiomer effects were not statistically significant, elimination of all present bacteria in 30 min is key to prevent a recolonization from surviving cells. Our findings were supported by the work of *Geisberger et al.*, where chitosan-TGA exerted a 5-log CFU reduction on *S. sobrinus*.[127] In contrast, previous studies on *E. coli* and *S. aureus* found chitosan-TGA[165] and chitosan-acetylcysteine[126] to be less effective than pristine chitosan, probably because of the high substitution degree, which removes the amine groups essential for the antibacterial action. Numerical differences in the antimicrobial activity often arise from different tested strains, chitosan characteristics and test protocols, which render direct comparisons difficult.

2.3.2.3 LIVE/DEAD Assays

To verify the actual bactericidal action of chitosan thiomers and exclude the metabolic inhibition of the bacteria as a possible pathway, a viability assay was performed.[166] Two fluorescent dyes were used to discriminate between alive and dead cells, with SYTO 9 generally labelling all bacteria in green, regardless of intact or damaged membranes. In contrast, propidium iodide (PI) penetrates only bacteria with damaged membranes, causing a reduction in SYTO 9 fluorescence when both dyes are present, and therefore giving the cells a red color. Chitosan-MPA was chosen as a representative sample and its effect on bacteria was observed with confocal laser scanning microscopy. Untreated cells showed only the incorporation of SYTO 9, whereas PI fluorescence was detected after treatment with chitosan-MPA. With killing rates of 99-100% the microscopic analyses support the above results from plate counting experiments for *P. aeruginosa*, *S. sobrinus* and *S. mutans* (Figure 2.24f-2.26f). The case of *E. coli* is different with both alive and dead cells in

a ratio around 70% present in the overlay (Figure 2.27f), in line with our previous investigations. The results provide further evidence that chitosan derivatives eliminate bacteria by disrupting the cell membrane, as one major cause of death. The exclusive presence of agglomerates after chitosan-MPA treatment was detected for both gram-positive bacteria (Figure 2.25d and Figure 2.26d), in line with what was also observed in previous publications.[167]

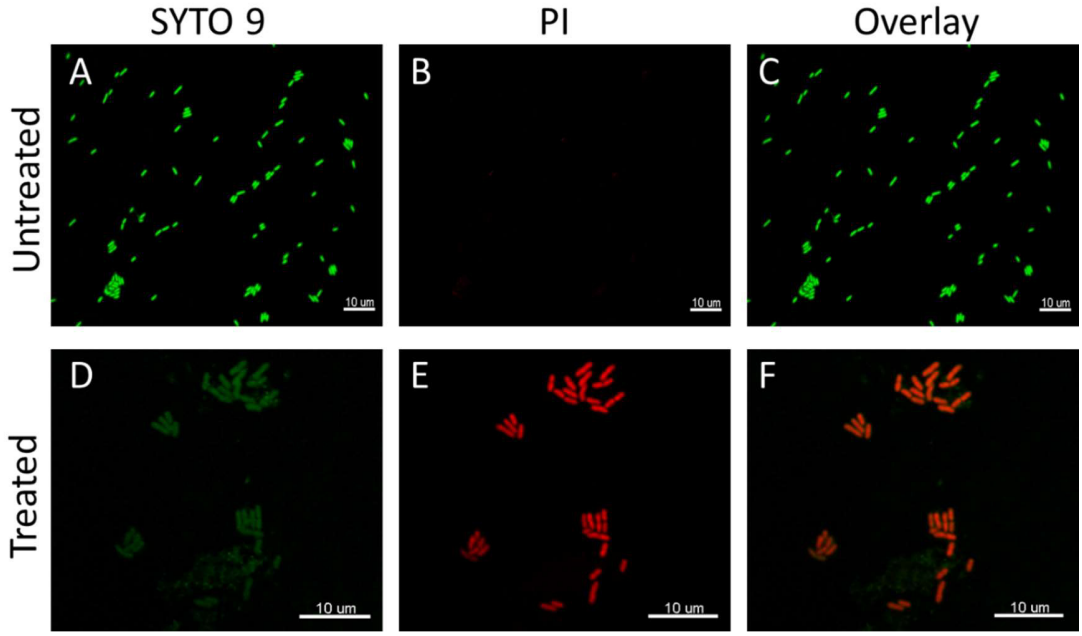

Figure 2.24. Effects of chitosan-MPA treatment on P. aeruginosa analyzed with confocal laser scanning microscopy: untreated control (A-C), treated (D-F); SYTO 9 fluorescence (A, D); propidium iodide fluorescence (B, E), and overlay (C, F).

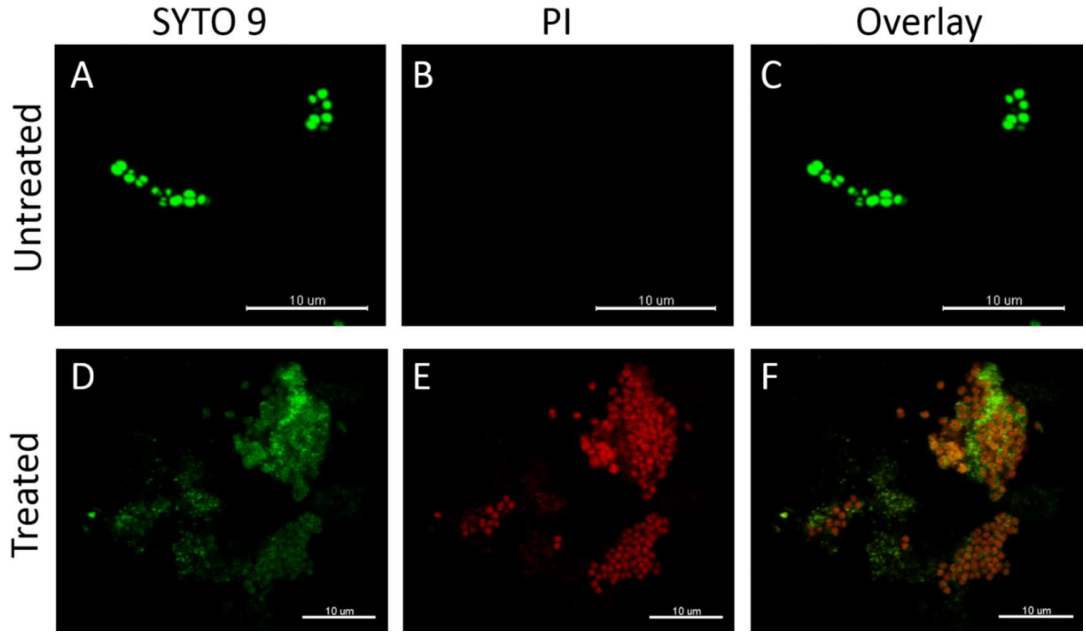

Figure 2.25. Effects of chitosan-MPA treatment on S. sobrinus analyzed with confocal laser scanning microscopy: untreated control (A-C), treated (D-F); SYTO 9 fluorescence (A, D); propidium iodide fluorescence (B, E), and overlay (C, F).

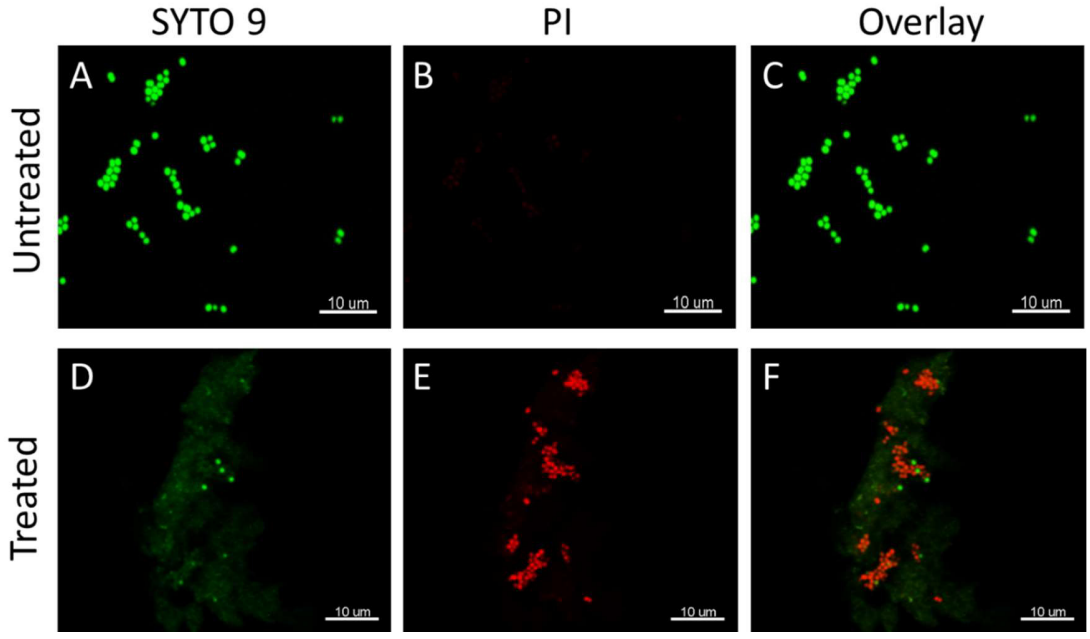

Figure 2.26. Effects of chitosan-MPA treatment on S. mutans analyzed with confocal laser scanning microscopy: untreated control (A-C), treated (D-F); SYTO 9 fluorescence (A, D); propidium iodide fluorescence (B, E), and overlay (C, F).

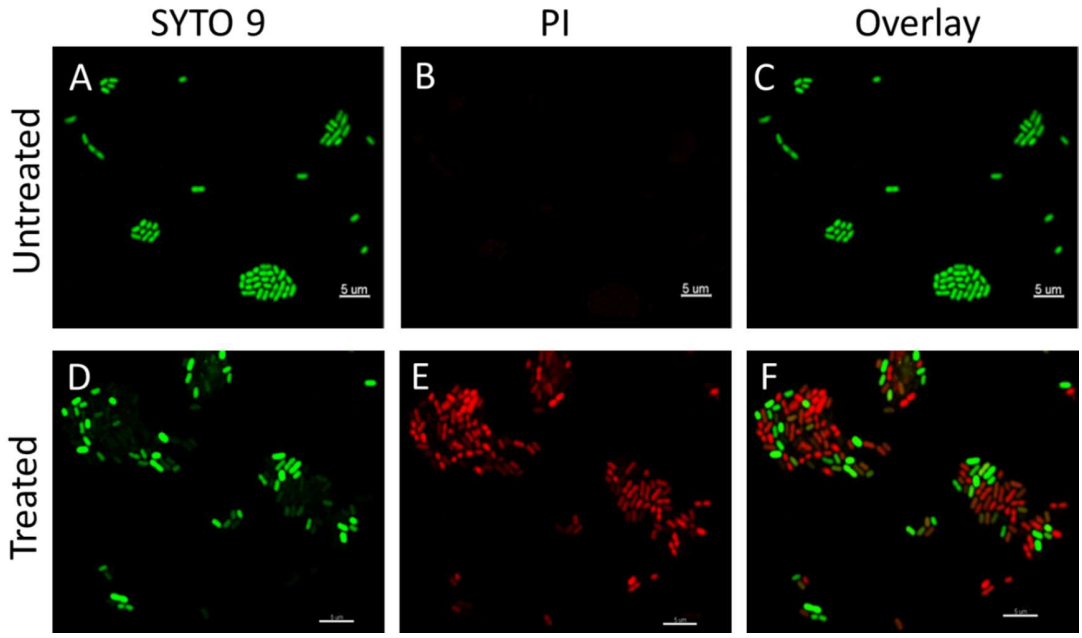

Figure 2.27. Effects of chitosan-MPA treatment on E. coli analyzed with confocal laser scanning microscopy: untreated control (A-C), treated (D-F); SYTO 9 fluorescence (A, D); propidium iodide fluorescence (B, E), and overlay (C, F).

2.3.2.4 CAL-33 and HeLa cytotoxicity

Cytotoxicity of chitosan-MPA after 24 hours has been assessed through the MTT viability assay on CAL-33 and HeLa cell lines. The cell viability percentage was plotted against the logarithm of the concentration and afterwards a non-linear regression curve was fitted to the acquired data, from which the IC_{50} of the compound was determined. For chitosan-MPA an IC_{50} of 14.8 ± 1.1 µM, corresponding to 1.27 mg/mL, was calculated. The IC_{50} is lower than the concentration used to treat the bacteria in our experiments, however the incubation time on the mammalian cells was longer than on bacteria. It may thus be hypothesized that the treatment time on bacteria is so short that we can exclude any cytotoxic effect on mammalian cells.

Further experiments to confirm the safety of chitosan thiomers as antimicrobial agents should be performed (e.g. toxicity on somatic cells) to confirm their safe applicability.

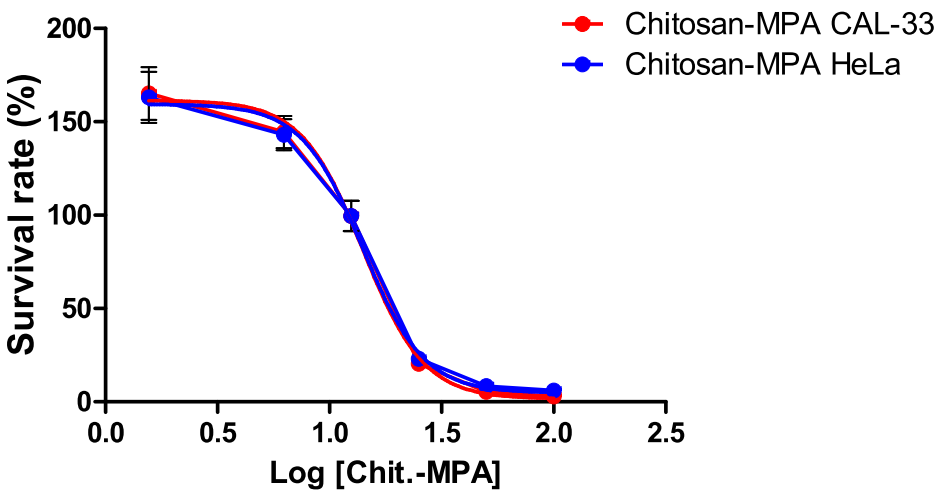

Figure 2.28. Nonlinear regression curve fit for the viability MTT assay of chitosan-MPA treatment on CAL-33 (red) and HeLa (blue) for 24 h (IC_{50} 14.87 µM; R^2 = 0.9999).

2.4 Conclusion and prospective of chitosan thiomers

A comprehensive systematic investigation of the antimicrobial efficacy of several thiolated chitosans was conducted. Special emphasis was placed on the characterization of chitosan thiomers bearing increasing alkyl chain length and their SAR with respect to antimicrobial activity. The MTT-based screening evidenced that functionalization, especially when conducted to a high extent, does not generally improve the antibacterial activity of pristine chitosan, suggesting that a certain amount of free amine groups is necessary to generate antimicrobial effects. In parallel, experiments on *E. coli*, *P. aeruginosa*, *S. sobrinus* and *S. mutans* evidenced the enhanced bactericidal effect of moderately substituted chitosan alkyl thiomers compared to pristine chitosan. Chitosan was not able to eliminate the bacterial population completely, while for three out of four investigated strains, at least one chitosan thiomer per strain was able to do so. The ability to eradicate completely a bacterial population is a key feature to be considered for clinical applications: even minor amounts of remnant bacteria may turn out to be detrimental over time due to their rapid growth which can re-infect the site. Under our experimental conditions *E. coli* was scarcely affected by the treatment of alkyl thiomers. This resistance could be useful in the treatment of chitosan thiomer-sensitive pathogen bacteria, without harming the commensal *E. coli* population.

The cytotoxicity of chitosan-MPA, as representative chitosan thiomer, was investigated on mammalian cells and an IC_{50} below the concentration applied against bacteria was found. However, it is reasonable to assume that the same concentration used for bacteria would not be toxic for somatic cells during short exposure times (e.g. 30-60 min).

The above investigation emphasizes the outstanding antimicrobial properties of N-acyl thiolated chitosans and paves the way to the design of new highly efficient, biocompatible and cost-effective antimicrobial compounds.

3. Polyoxometalates and their nanocomposites with chitosan as new candidates for biomedical applications

3.1 Introduction

Over the past years, polyoxometalates emerged as a promising class of biologically active compounds and were investigated against different targets, e.g. bacteria, cancer cells and viruses.[106,107,168] However, the clinical use of POMs is not yet feasible, because of their frequently undefined stability at physiological conditions and their high unspecific cytotoxicity. A strategy to improve the stability and the selectivity of POMs in the physiological environment is based on their encapsulation within a biocompatible polymer matrix. The encapsulation would enhance POM stability and, at the same time, increase the uptake by specific targets, e.g. cancer cells. In this study, well-known biologically active POMs were encapsulated with chitosan and its derivative carboxymethyl chitosan (CMC) to investigate their cytotoxicity profile upon encapsulation with the biocompatible matrix. In the next sections, a survey on biological activity of POMs when used as pristine component or nanocomposite is provided. In particular, the changes upon encapsulation in different biomatrices are considered, focusing on chitosan and its derivatives.

3.1.1 POMs in medicine

The first investigations of POMs on biological targets highlighted their strong antiviral properties.[169] The most famous antiviral POM was $(NH_4)_{17}Na[NaSb_9W_{21}O_{86}]$, a tungsten heteropolyanion containing antimony, known as HPA-23 and hereafter abbreviated as $\{Sb_9W_{21}\}$. $\{Sb_9W_{21}\}$ was identified as very promising antiviral compound, active against the murine Leukemia and Sarcoma viruses[170] through inhibition of their RNA-dependent DNA polymerase.[171] The uptake of $\{Sb_9W_{21}\}$ in C3HBi fibroblasts was investigated and evidences of accumulation after 48 h of incubation in the cytoplasm were provided.[172] Furthermore, $\{Sb_9W_{21}\}$ was active against HIV-1 virus inhibiting its reverse transcriptase *in vitro*.[173] The *in vitro* results were very promising and therefore $\{Sb_9W_{21}\}$ was chosen to be tested on patients with acquired immune deficiency syndrome (AIDS) in the 1980s. In the first screening, $\{Sb_9W_{21}\}$ caused a reduction of the surrogate

markers for HIV in four patients.[174] In the first study, after eight weeks of trial, no decisive improvements were observed and a third of the patients had to interrupt the treatment because of the severe side effects and dose-related haematological abnormalities.[175] In the second trial, a persistence or even increase of antigenemia was observed for all the patients together with thrombocytopenia for nine of twelve patients, confirming that pristine $\{Sb_9W_{21}\}$ is not a suitable anti-HIV drug.[176] Shortly after the first trial, a polarographic study on $\{Sb_9W_{21}\}$ was published revealing poor stability of the compound in water solution over the entire pH range and an antimony leakage,[177] thus interrupting any further experiments of POMs on humans.

Polyoxometalates were investigated as anticancer drugs with promising results. The most extensively studied anticancer POM was the polyoxomolybdate $[TBA]_6[Mo_7O_{24}]\cdot 3H_2O$ (abbreviated as $\{Mo_7O_{24}\}$), where TBA is tert-butyl ammonium, synthesized by *Yamase* and co-workers.[178] $\{Mo_7O_{24}\}$ was found to be active against different cancer cell lines, e.g. MX-1 murine mammary cancer cell line, Meth A sarcoma and MM46 adenocarcinoma. The proposed mechanism is based on the formation of a 1:1 complex between $\{Mo_7O_{24}\}$ and flavin mononucleotide (FMN) in mitochondria. Since FMN is the prosthetic group in flavoproteins and acts as an electron carrier for the electron transfer (from NADH to coenzyme Q) coupled with ATP generation, the formation of the complex could inhibit the synthesis of ATP[179] with a resultant antitumor activity. Moreover, $\{Mo_7O_{24}\}$ exhibits higher cytotoxicity in cancer cells compared to normal cells because of the selective reduction of $\{Mo_7O_{24}\}$ in the mitochondrial system of the cancer cells to the more cytotoxic reduced species ($H_xMo_7O_{24}$).[180] Flow cytometry studies conducted on human pancreatic cancer cells suggested a dose dependent growth inhibition and cellular death pathway occurring by apoptosis.[181] A further study about the anticancer activity of a photo reduced product of $\{Mo_7O_{24}\}$, precisely $[Me_3NH]_6[H_2Mo_{12}O_{28}(OH)_{12}(MoO_3)_4]$, evidenced that apoptosis and autophagy pathways have a role in the death of the cell.[182] Besides *in vitro* inhibition experiments on pancreatic cancer cells, tumor expansion rate was studied on mice *in vivo*. The inhibition of tumor growth at doses of 125 mg and 500 mg per body-weight was 33.5 and 68.3%, respectively, and the mouse body weight was not affected, pointing to good tolerability of the compound. In view of the previously reported data $\{Mo_7O_{24}\}$ and its reduced species were proposed as promising molecules in the treatment of cancer.

Many other POMs were proposed as promising anticancer in original works, such as $K_7Na_3[Cu_4(H_2O)_2(PW_9O_{34})_2]_{20}H_2O$[183] and $[CoW_{11}O_{39}(CpTi)]^{7-}$ (Cp = η5-C_5H_5).[184]

Enzymatic inhibition by POMs has been observed in several different enzyme classes.[185] $(NH_4)_6[P_2Mo_{18}O_{62}]$ was found to be a potent enzymatic inhibitor, with particularly high selectivity and an IC_{50} of 1.5 nM against the protein kinase CK2, a multifunctional kinase which is dysregulated in many cancers.[186] The selectivity of POMs in inhibiting certain enzymes was suggested to be the responsible feature for the observed biological activity. Furthermore, $Na_{10}[H_2W_{12}O_{42}]$ and $Na_{33}[H_7P_8W_{48}O_{184}]$ were selectively inhibiting alkaline phosphatases displaying profound anticancer and amoebicidal activity with low cytotoxicity *in vitro* on normal cells (immortalized human corneal epithelial cells).[187]

Polyoxometales were investigated against bacteria alone or in combination with β-lactam antibiotics. In particular, highly negative charged POMs like $K_{27}[KAs_4W_{40}O_{140}]$ and $K_{18}[KSb_9W_{21}O_{86}]$ as well as the Keggin-type POM $K_5[SiVW_{11}O_{40}]$ showed minimum inhibitory concentration (MIC) values of less than 256 µg/mL against 17 different *Helicobacter pylori* strains,[188] while vanadium containing POMs, such as $[tert\text{-}BuNH_3]_4[V_4O_{12}]$, were active against *Streptococcus pneumoniae.*[189]

Among other investigated POMs, $K_7[PTi_2W_{10}O_{40}]$, $K_4[SiMo_{12}O_{40}]$ and $K_6[P_2W_{18}O_{62}]$ were the most efficient ones in enhancing the antibacterial activity of β-lactam antibiotics against the methicillin-resistant *S. aureus.*[190]

Particularly, $K_7[PTi_2W_{10}O_{40}]$, from now on abbreviated as $\{PTi_2W_{10}\}$, was found to be active against several enveloped DNA and RNA viruses, inhibiting their replication.[191] Moreover, $K_6[P_2W_{18}O_{62}]$, henceforth abbreviated as $\{P_2W_{18}\}$, the first representative of the Wells-Dawson structure type,[96] displayed a broad spectrum biological activity against bacteria,[192] viruses[193] and cancer cells.[194]

Despite the promising results *in vitro*, the application of POMs in pharmaceutics is still far from implemented. A key strategy to render POMs more applicable for medical purposes is based on their encapsulation into a biocompatible polymeric matrix, e.g. starch, liposomes or chitosan.

3.1.2 POM-biopolymer composites

The encapsulation of POMs with different biomatrices was investigated with respect to the influence on POM cytotoxicity. The nanocomposites of $K_6H_2[CoW_{11}TiO_{40}]$ and $K_6[SiW_{11}TiO_{40}]$, two POMs with promising anticancer activity, were prepared using starch microspheres through an enveloping method.[195] The encapsulation preserved the structure of the POM and increased its stability, while improving the uptake of the POM by cancer cells and reducing the cytotoxicity against normal cells. After several hours, a leakage from the microspheres was observed together with a partial decomposition of POMs in buffer conditions, highlighting the need for better encapsulating agents.

$K_6H_2[CoW_{11}TiO_{40}]$ and $K_6[SiW_{11}TiO_{40}]$ were encapsulated into liposomes showing results comparable to the POM-starch nanocomposites: increased POMs stability and higher cancer cellular uptake together with a decreased cytotoxicity, but a partial leakage was again detected.[196] More recently $[Si_2W_{18}Ti_6O_{77}]$-starch nanoparticles were used for an *in vivo* study, where the POMs were released in a time dependent way, thus prolonging the life span of mice bearing cancer and resulting negative in a mutagenicity test.[197]

A valid alternative to starch and liposomes is chitosan, which generates more stable nanocomposites with POMs,[198] even if they were generally larger and more polydispersed. Chitosan encapsulation is also known to stabilize POMs which undergo structural modifications and degradations under certain conditions.[199] It has been observed that the association with chitosan could improve the cancer cellular uptake of $\{PTi_2W_{10}\}$[198] and enhances the anticancer activity of $[Cs\subset Eu_6As_6W_{63}O_{218}(H_2O)_{14}(OH)_4]^{25-}$-chitosan nanoparticles compared to the pristine POM.[200] In our group, chitosan water soluble derivatives (carboxymethyl chitosan (CMC) and trimethyl chitosan), were used to prepare nanoscale POM composites with tunable morphology and surface charge, and their cellular uptake and anticancer profiles were studied on HeLa cells.[199]

The cytotoxicity and the inhibition of two alkaline phosphatase enzymes of $[NaP_5W_{30}O_{110}]^{14-}$-, $[V_{10}O_{28}]^{6-}$- and $[TeW_6O_{24}]^{6-}$-chitosan nanoparticles were investigated.[201] Alkaline phosphatase enzymes are known to be overexpressed in different cancer types undergoing metastasis. The compound $[TeW_6O_{24}]^{6-}$ showed stronger inhibition against tissue non-specific alkaline phosphatase when used alone, and against calf intestine alkaline phosphatase when

encapsulated with chitosan, respectively. $[NaP_5W_{30}O_{110}]^{14-}$-chitosan nanoparticles displayed the highest cytotoxicity (88 ± 10%) at a POM concentration of 10 μM. A follow up study of the same group investigated the activity of three different Keggin-type POMs (i.e. $[PW_{12}O_{40}]^{3-}$, $[CoW_{11}TiO_{40}]^{7-}$, and $\{PTi_2W_{10}\}$,) and corresponding chitosan nanoparticles against HeLa cells.[202] $[CoW_{11}TiO_{40}]$-chitosan displayed the highest cytotoxicity against HeLa cells, providing further evidence for its anticancer properties, which had been observed elsewhere for its nanocomposites with starch and liposomes. Furthermore, $[CoW_{11}TiO_{40}]$-chitosan displayed low cytotoxicity on normal cells (Vero cells), as the prerequisite for as promising anticancer drug.

Since chitosan is a well-known antimicrobial agent, synergistic effects on its antimicrobial activity were evaluated for POM-chitosan nanocomposites. Capsules obtained via the supramolecular assembling of polyoxometalates, chitosan and the surfactant cetyltrimethylammonium bromide were investigated against *E. coli* using a growth inhibition assay. Specifically, $[H_3PMo_{12}O_{40}]$ and $(NH_4)_{15}\{Na[(Mo_2O_4)_6(\mu_2\text{-}SO_3)_3\text{-}(\mu_2\text{-}SO_3)]_2\}$ were able to reduce the growth of *E. coli* up to 80%, while $[H_3PW_{12}O_{40}]$-capsules and the pristine POMs were not as efficient.[203] The different shape and size of the capsules within the POMs containing molybdenum, were reported as possible explanation for their higher activity. *Fiorani et al.* tested $[H_5PMo_{10}V_2O_{40}]$-chitosan nanoparticles against *E. coli,* showing a synergic activity that led to the complete eradication of the bacterial population at a POM concentration of 0.6 mg/mL.[204] In summary, POM-chitosan nanoparticles were proven to be promising antibacterial agents, however, further experiments on different bacterial strains are required to draw more general conclusions.

3.1.3 Approach of the present study

In this work $\{Sb_9W_{21}\}$, $\{Mo_7O_{24}\}$ and $\{P_2W_{18}\}$, were chosen as representative biologically active POMs and promising candidates for medical applications for a deeper exploration of their biological activity. Special efforts were dedicated to the modification of POM cytotoxicity by the encapsulation in chitosan matrices. The association of chitosan and POMs led to the formation of nanocomposites, which were characterized in detail with dynamic light scattering (DLS) and electron microscopy. Moreover, the stability of POMs in physiological conditions was addressed as a key issue for their application. Consequently, the stability of $\{Sb_9W_{21}\}$ and $\{P_2W_{18}\}$ was newly investigated before and after the encapsulation processes.

The cytotoxicity of the pristine POMs as well as of the nanocomposites was evaluated against bacteria (the gram-positive *S. sobrinus* and the gram-negative *E. coli*) as well as for different cell lines, namely HeLa and MRC-5. HeLa represents an immortal cell line derived from cervical cancer cells, while the MRC-5 cell line was derived from normal lung tissue of a 14-week-old male fetus. Furthermore, $(TBA)_4[Mo_8O_{26}]$, $K_7[PTi_2W_{10}O_{40}]$, $K_4[SiMo_{12}O_{40}]$ and $(NH_4)_6[P_2Mo_{18}O_{62}]$, and their nanocomposites with chitosan or CMC, were prepared and their cytotoxicity was tested. However, they were tested on HeLa as part of a screening plan and therefore no in-depth studies were conducted. The focus of our research investigations was mainly on the first three well-known POMs ($\{Sb_9W_{21}\}$, $\{Mo_7O_{24}\}$ and $\{P_2W_{18}\}$), which were more extensively characterized, with respect to their cytotoxicity vs. their nanocomposites with chitosan and CMC. Consequently, the other investigated POMs will be addressed separately in the next sections.

3.2 Material and methods

3.2.1 Materials

Reagents, including the reference material $(NH_4)_6[Mo_7O_{24}]$, were purchased from Sigma-Aldrich (Buchs, Switzerland) and unless otherwise specified used as received. Chitosan 90/5 (DD 90%, MW 20 kDa) was purchased from Heppe Medical Chitosan (Halle (Saale), Germany). 3-(4,5-dimethylthiazol-2-yl)-2,5-diphenyltetrazolium bromide (MTT) was purchased from Alfa Aesar (Heysham, UK).

3.2.2 Instrumental details

^{1}H-NMR spectra at 10, 25 and 75 °C and ^{183}W-NMR spectra were recorded on a 500 MHz Bruker Avance Spectrometer (Billerica, USA) with CP-MAS technology, and ^{31}P-NMR spectra were obtained at 25 °C using a 400 MHz Bruker Avance Spectrometer (Billerica, USA) with CP-MAS technology. UV-Vis absorption spectroscopy was performed using a Lambda 650 S PerkinElmer UV-Visible spectrometer in the range λ=225-800 nm equipped with a Quartz SUPRASIL precision cell (10 mm). FT-IR spectra were recorded with a Bruker VORTEX 70 spectrometer. XRD patterns were recorded on a STOE STADI P diffractometer in transmission mode (flat sample holders, Ge monochromator, and $CuK_{\alpha 1}$ radiation) by using a position-sensitive detector. Suitable crystals for single-crystal XRD analysis were selected under polarized light, coated with Paratone-N oil,

mounted inside a small fiber loop and placed under nitrogen gas flow at 183 K for protection of crystals from air. Crystallographic data collection was performed with an Oxford Xcalibur Ruby CCD single-crystal diffractometer (Mo-K_α radiation, λ = 0.71073 Å). Hydrodynamic size and ζ-potential were measured with a Zetasizer Nano ZS90 (ZEN3690, Malvern Instruments Ltd, Malvern, UK) using polystyrene disposable cuvettes (Sarstedt AG & Co, Germany) and Malvern disposable folded capillary cells, respectively. A field emission scanning electron microscope Zeiss Supra 50 VP, equipped with secondary, backscattered electron and EDX detectors, a transmission electron microscope FEI Tecnai G2 Spirit 120-kV equipped with two digital CCD cameras for image acquisition and diffraction analysis and a scanning transmission electron microscopy with corresponding detector, as well as Oxford EDX system for elemental analysis were used for the acquisition of the images. Elemental analyses were performed at "Mikroanalytisches Labor Pascher" (Remagen/Germany).

3.2.3 Synthesis and characterization of the starting material

$(NH_4)_{17}Na[NaSb_9W_{21}O_{86}]$[170,205] and the pure α-isomer,[206] as well as a mixture of the α-, β- and γ-isomers[207] of $K_6[P_2W_{18}O_{62}]$ were prepared following the previously reported procedures. $\{Sb_9W_{21}\}$ was characterized by single-crystal and powder X-ray diffraction, elemental analysis and FT-IR spectroscopy. The stability of $\{Sb_9W_{21}\}$ was investigated by monitoring the pH changes in aqueous solution (4 mg/mL) and recording UV-Vis spectra from 225 to 800 nm over 4 d. $K_6[P_2W_{18}O_{62}]$ isomers were characterized by single-crystal and powder X-ray diffraction, elemental analysis, FT-IR spectroscopy, and ^{31}P-NMR and ^{183}W-NMR spectroscopy. The stability of the $\{P_2W_{18}\}$ isomers was investigated at different pH values (3.5, 7.4 and 12) by recording the ^{31}P-NMR spectra, monitoring the pH trend (4 mg/mL) and the UV-Vis absorption from 800 to 225 nm at pH 7.2-7.4 for 4 d. $(TBA)_4[Mo_8O_{26}]$,[208] $H_4[SiMo_{12}O_{40}]$,[95,209] $K_7[PTi_2W_{10}O_{40}]$[210] and $(NH_4)_6[P_2Mo_{18}O_{62}]$[211] were prepared following the previously reported procedures. All POMs were characterized by FT-IR spectroscopy and powder X-ray diffraction. $(NH_4)_6[P_2Mo_{18}O_{62}]$ and $K_7[PTi_2W_{10}O_{40}]$ were further characterized by ^{31}P-NMR spectroscopy.

Carboxymethyl chitosan was synthesized following the procedure proposed by *Geisberger et al.*.[212] After the synthesis and lyophilization, CMC was newly dissolved in water and filtered

through a 0.22 µm filter to remove the unreacted chitosan. CMC was characterized by ^{1}H-NMR and FT-IR spectroscopy.

3.2.4 Preparation and characterization of the nanoparticles

POM-chitosan nanoparticles were produced as follow: 1 mL of chitosan solution (8 mg/mL, pH 5.5, solubilized in water with HCl) was sonicated at room temperature for 5 min, afterwards 1 mL of POM solution (4 mg/mL) was added and the mixture was sonicated for further 20 min. POM-chitosan nanoparticles were produced at pH 4 using chitosan solubilized with acetic acid. POM-CMC nanoparticles were prepared at pH 7.1-7.3 as follows: 1 mL CMC solution (8 mg/mL), 0.5 mL POM solution (4 mg/mL) and 0.5 mL ultrapure water or PBS buffer were stirred for at least 30 min before dropwise addition of 0.4 mL $CaCl_2$ (3.5 mg/mL); the mixture was stirred for one additional hour before DLS measurements. Chitosan pristine nanoparticles were achieved through dropwise addition of sodium tripolyphosphate (TPP) to a stirred solution of chitosan, while CMC pristine nanoparticles were produced through addition of $CaCl_2$ to a stirred solution of CMC.

Nanoparticles were further analyzed by SEM and TEM. Prior to SEM characterization, the nanoparticles were extensively washed with ultrapure water using a 4 kDa cut-off centrifuge filter and resuspended by ultrasonication. For SEM analysis the nanoparticles were deposited on a sample holder with a carbon sticky surface and coated with a 4 nm Pt layer. For TEM analysis, the nanoparticle solution was deposited for 1 min onto 300 mesh copper grids activated by glow discharge. The grids were afterwards incubated 3 times for 15 s with uranyl acetate (1% w/v in water).

Size and ζ-potential of the nanoparticles were measured by DLS, and size as well as pH measurements were repeated daily over 3 d to confirm their stability.

3.2.5 Bacterial strains and media

Escherichia coli (ATCC 11775, German Collection of Microorganisms and Cell Cultures (DSMZ) GmbH, Braunschweig, Germany) was cultivated in Luria-Bertani (LB) broth pH 7.0 ± 0.2 (10 g/L tryptone, 5 g/L yeast extract, and 5 g/L sodium chloride) at 37 °C under constant rotation (220 rpm). *Streptococcus sobrinus* (OMZ 176, Institute of Oral Microbiology, University Hospital Zurich, Zurich, Switzerland) was cultivated in Brain Heart Infusion (BHI) broth pH 7.4 ± 0.2 (5 g/L

beef heart, 12.5 g/L calf brains, 2.5 g/L disodium hydrogen, 2 g/L phosphate, D(+)-glucose, 10 g/L peptone,5 g/L sodium chloride) at 37 °C under constant rotation (220 rpm). Plate Counting Agar (PCA) containing 5.0 g/L tryptone, 2.5 g/L yeast extract, 1.0 g/L D(+)-glucose and 12.0 g/L bacteriological agar was used for plate counting experiments.

3.2.6 Plate counting experiments

Bacterial suspensions were adjusted to 0.5 McFarland turbidity standard with medium and incubated for 30 min with pristine POMs and POM-chitosan nanoparticles (final concentration 2 mg/mL) at 37 °C and constant rotation. After preparation of proper dilutions, aliquots were plated onto PCA. Bacterial cultures that received medium instead of the tested compounds served as positive controls and were serially diluted 10^6-10^7-fold and then plated. All plates were incubated for 24 h at 37 °C before counting of colonies. Only plates containing between 300 and 10 colonies were used for enumeration. Experiments were performed in triplicates.

3.2.7 Cultivation of HeLa and MRC-5

HeLa cells (human cervical adenocarcinoma cell line CCL-2) and MRC-5 cells (normal lung fibroblast cell line CCL-171), purchased by DSMZ, were cultivated in DMEM supplemented with 10% heat inactivated Fetal Calf Serum (FCS) at 37 °C, 6% CO_2 and humidified atmosphere. The cells were passaged at 80% confluence by trypsinization with 0.05% trypsin-EDTA (0.05% trypsin and 0.02% EDTA) (Thermo Fischer, Waltham, USA).

3.2.8 MTT cytotoxicity assay

HeLa and MRC-5 cells were seeded onto 96-well plates at a density of 1.2 and 3.0 x 10^4 cells/well, respectively, in DMEM and incubated overnight under standard conditions (37 °C, 6% CO_2, humidified atmosphere). The medium was replaced by different DMEM solutions containing POMs and POM-chitosan nanoparticles at different concentrations. The controls received only medium. For POM-chitosan nanoparticles the pH of DMEM was adjusted to 6.5, which was used as medium for the controls. The cells were incubated under standard conditions for 24 h. After three washing steps with complete medium the cells were allowed to recover for further 24 h. After recovery, 10 µL of MTT (5 mg/mL, final concentration 0.5 mg/mL) were added to each well and the plate was incubated for 4 h at 37 °C, 6% CO_2, in humidified atmosphere in the dark. The

insoluble metabolic product formazan was solubilized with 100 µL of a solution of SDS 10% w/v in 0.01 N HCl and incubated overnight in standard conditions. The optical density was recorded at 570 nm using a 96-well plate reader (Synergy 2 Multi-Mode Reader, BioTek). For each concentration sextets were performed to determine the standard deviation. Results are expressed as mean ± SD. Statistical analysis of the data was performed with GraphPad Prism 5.

3.2.9 Flow cytometry

HeLa cells were seeded onto 6-well plates at a density of 18 x 10^4 cells/well in DMEM and incubated overnight under standard conditions (37 °C, 6% CO_2, humidified atmosphere). The cells were treated for 24 h with 10 µM of P_2W_{18} isomeric mixture diluted in DMEM, while untreated cells were used for negative controls and heat-treated cells were used as positive control (2 min, 80 °C). Cells were washed with PBS and trypsinized. Cells were isolated by centrifugation, washed with PBS and resuspended with the Binding Buffer and stained with FITC-Annexin V, propidium iodide and Hoechst 33342 (Apoptotic, Necrotic, and Healthy Cells Detection Kit, Genecopoeia USA), as suggested by the manufacturer. The stained cells were analyzed with the LSR II Fortessa flow cytometer (BD Biosciences) using the 450/50, 530/30 and 610/20 filters for fluorescence detection.

3.3 Results and discussion

3.3.1 Synthesis and characterization of POMs

Our research focused on {Sb_9W_{21}}, {Mo_7O_{24}} and {P_2W_{18}}, because among the multitude of well-known biologically active polyoxometalates, their well-documented specific activity against different targets renders them very attractive for future medical applications. Furthermore, other biologically interesting POMs, namely $(TBA)_4[Mo_8O_{26}]$, $H_4[SiMo_{12}O_{40}]$, $K_7[PTi_2W_{10}O_{40}]$ and $(NH_4)_6[P_2Mo_{18}O_{62}]$, were synthesized (and their cytotoxicity was basically explored, as discussed in section 3.3.5.3).

The acclaimed anticancer compound {Mo_7O_{24}}[213] was selected as reference. The antitumoral activity of {Mo_7O_{24}} was previously investigated for its isopropyl ammonium salt, and *Yamase et al.* reported that the countercation does not influence the antitumor activity.[214] Therefore, the commercially available $(NH_4)_6[Mo_7O_{24}]$ was selected for the present study. {Sb_9W_{21}}[170,205] and

$\{P_2W_{18}\}$[206,207] were synthesized according to previously reported procedures. Their syntheses were reproducible, fast and cost-efficient, which are all important prerequisites for future drug production. Single-crystal X-ray characterizations were performed for both $\{Sb_9W_{21}\}$ and α-$\{P_2W_{18}\}$, and their determined crystal structures were consistent with the ones previously reported.[96,215] Therefore, countercations for $\{Sb_9W_{21}\}$ were not assigned given the difficulties to distinguish between Na, NH_4 and water molecules. Furthermore, as stated before, the presence of different counterions does not affect the biological activity of the POMs.

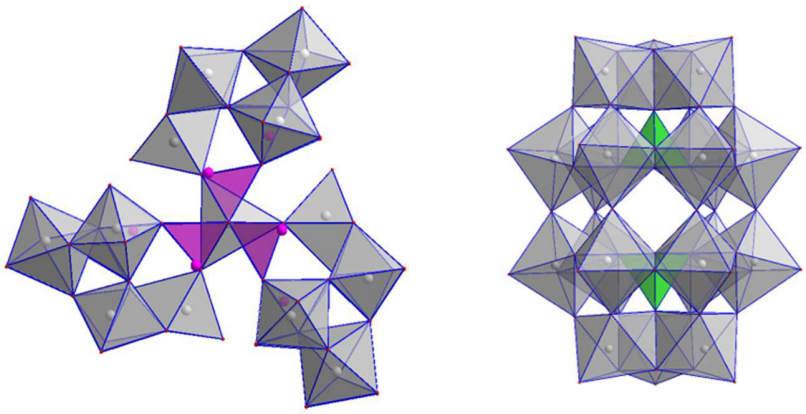

Figure 3.1. Crystal structure of $\{Sb_9W_{21}\}$ (left) and of α-$\{P_2W_{18}\}$ (right).

The phase purity of $\{Sb_9W_{21}\}$ was determined by single-crystal and powder X-ray diffraction (XRD) measurements. The acquired powder-XRD pattern was compared with the one calculated from single-crystal data, revealing a good overlap and therefore phase purity (figure 3.2b). To the best of our knowledge the powder-XRD spectrum of $\{Sb_9W_{21}\}$ is not currently present in the literature and could be useful to easily verify the purity of the freshly synthesized POM. The FT-IR spectrum of $\{Sb_9W_{21}\}$ is discussed in detail in section 3.3.3 (Figure 3.2a).

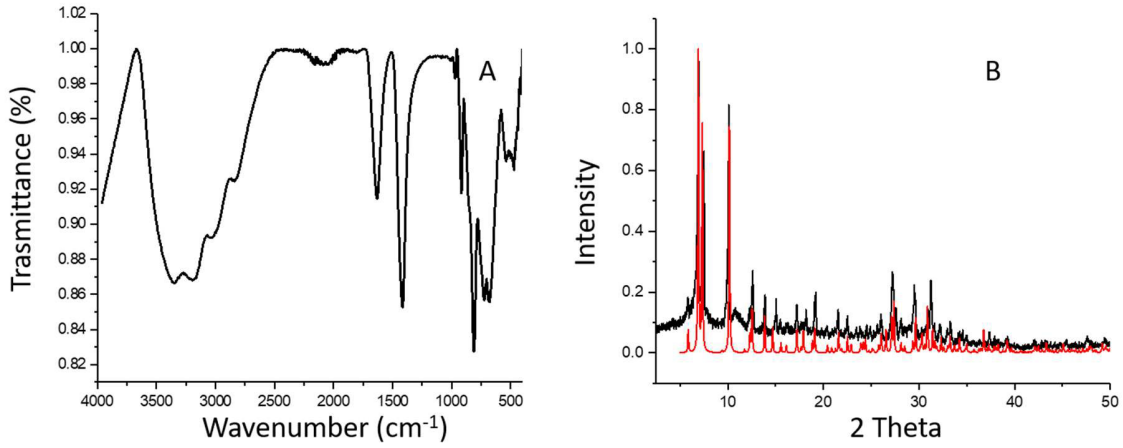

Figure 3.2. FT-IR spectrum (A) and powder-XRD pattern of {Sb_9W_{21}} (black) vs. calculated pattern from single-crystal XRD data (red).

{P_2W_{18}} was isolated both as the pure α-isomer and as a mixture of the α-, β- and γ-isomers, which differ with respect to their orientation of the W_3O_{13} triads. The isomeric mixture was produced according to the procedure from *Finke et al.*,[207] while the pure α-isomer was obtained following a new reagent-saving procedure suggested by *Mbomekalle et al.,* that consisted in leaving the reaction mixture for 3 d at 80 °C, followed by slow recrystallization at 5 °C.[206] The ^{31}P-NMR spectrum of α-{P_2W_{18}} was consistent with the ones previously reported.[206,216] ^{31}P-NMR spectroscopy allows an easy determination of the isomeric ratio by comparison of the NMR peak integrals. The α-isomer spectrum showed a single peak at δ -13.0 ppm,[206] confirming the absence of impurities and of the other isomers (Figure 3.3a). The Isomeric mixture of α-, β- and γ-{P_2W_{18}} displayed a sharp and intense peak at δ -13.0 ppm related to the α-isomer, two smaller peaks at δ -11.5 ppm and δ -12.3 which are characteristic of the β-isomer and a small peak at δ -10 ppm, corresponding to the γ-isomer.[217] The calculated ratio was 10:2:1 for α-, β- and γ-isomer, respectively (Figure 3.3b).

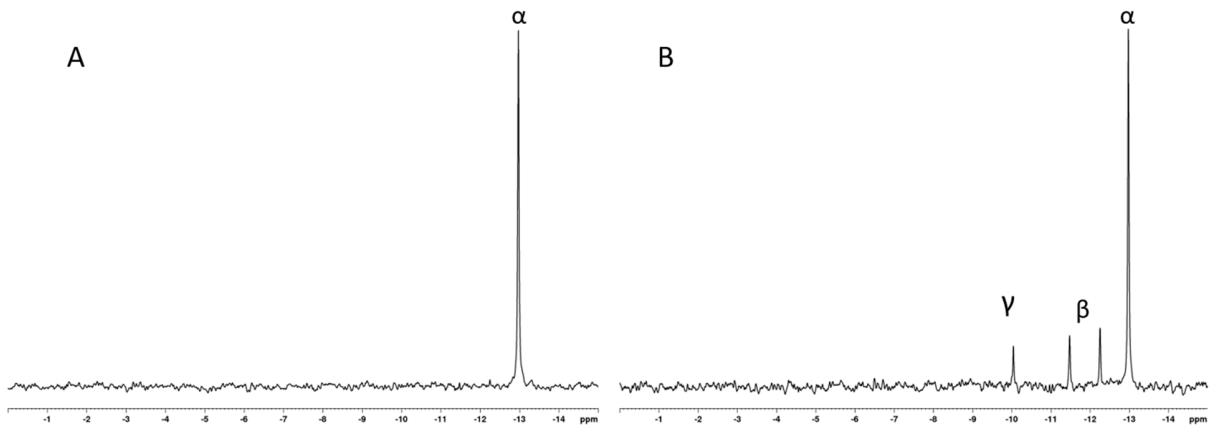

Figure 3.3. ^{31}P-NMR spectra of the α-{P_2W_{18}} and of the α-, β- and γ-isomer mixture of {P_2W_{18}}.

The recorded ^{183}W-NMR spectra were consistent with the ones reported in literature.[217] In the spectrum of the α-isomer the two signals at δ -126.9 and at δ -172.3 ppm further confirmed its identity and the absence of other compounds (Figure 3.4).

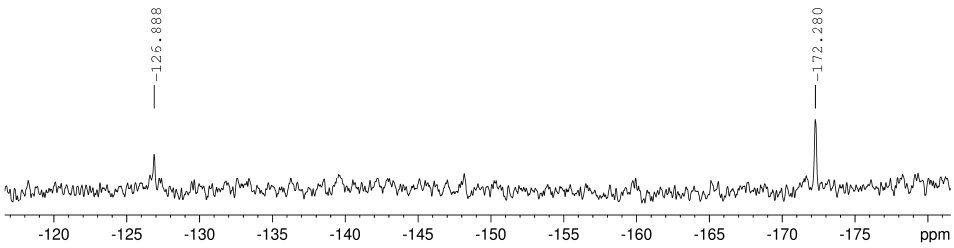

Figure 3.4. ^{183}W-NMR spectrum of the α-isomer of {P_2W_{18}}.

In the ^{183}W-NMR spectrum of the isomeric mixture of α-, β- and γ-{P_2W_{18}} the signals relative to the α-isomers and two signals relative to the β-isomer at δ -170.5 and δ -189.9 ppm are shown (Figure 3.5). Interestingly the signals relative to the α- and β-isomers are duplets. The duplets in the ^{183}W-NMR spectroscopy could either be an evidence for a scalar coupling with one spin-half nucleus of 100% natural abundance (such as W-F, W-P, W-H, W-Rh,) or could be due to the presence of isomers with a quite similar structure, which is more likely in the present case.

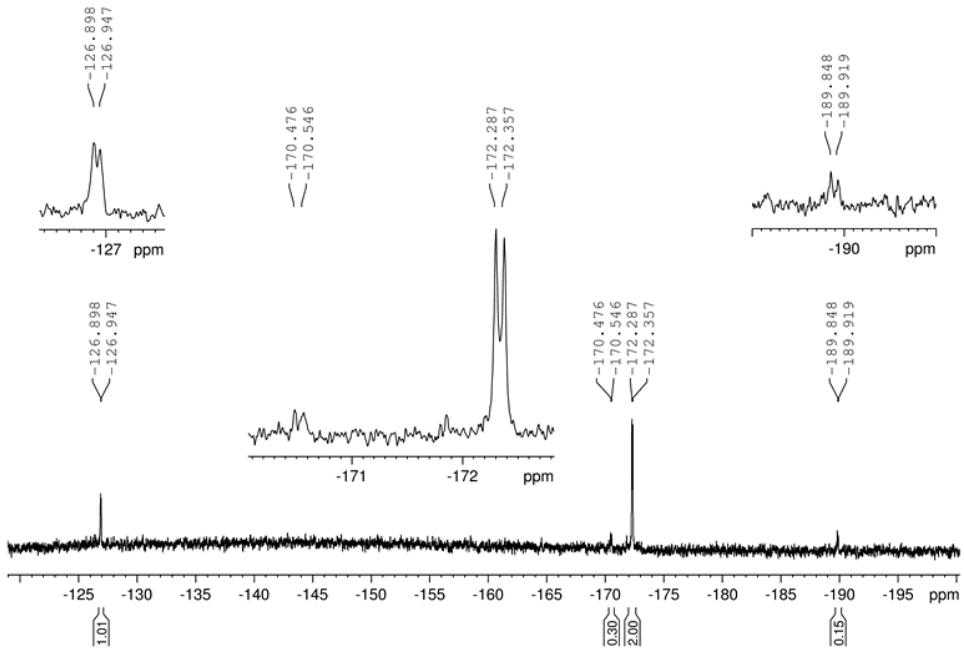

Figure 3.5. ^{183}W-NMR spectra of the α-, β- and γ-isomer mixture of {P_2W_{18}}.

The FT-IR spectra recorded for both the α-isomer and the isomeric mixture of α-, β-, and γ-{P_2W_{18}} were consistent with the one previously reported,[206,207] and details are discussed in section 3.3.3. The FT-IR spectra of the α-isomer and the isomeric mixture differed among each other exclusively for the peak at 1162 cm^{-1} which is present only in the isomeric mixture of α-, β-, and γ-{P_2W_{18}} (Figure 3.6a). The powder-XRD pattern revealed a high crystallinity of the α-isomer while the α-, β- and γ-isomer mixture represented an amorphous material. Surprisingly, the comparison between the measured powder-XRD pattern and the one calculated from the acquired single-crystal XRD data showed low phase purity of the material (Figure 3.6b), probably because of the differences in the water content between the crystals and the presence of some residual sodium counterions (see elemental analysis in section 3.3.3).

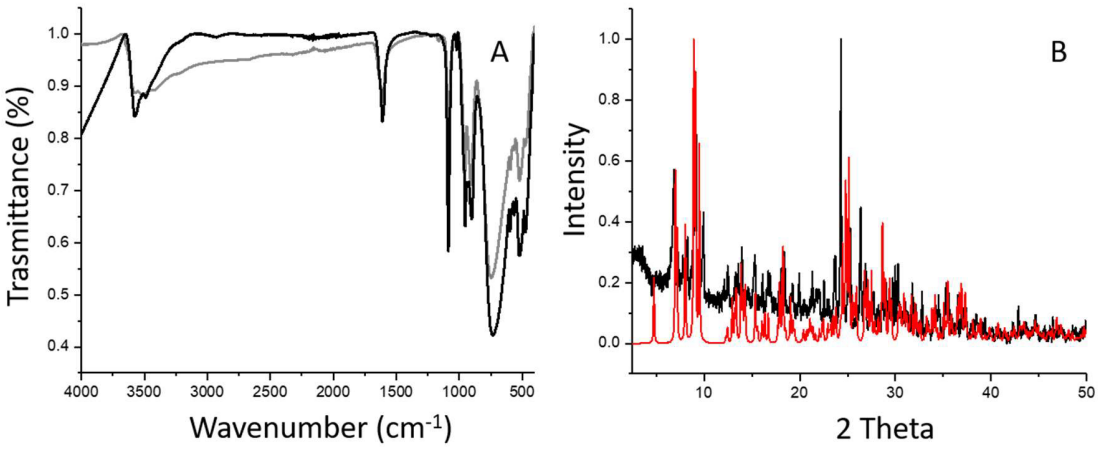

Figure 3.6. FT-IR spectra (A) (black α-isomer; grey α-, β- and γ-isomers mixture) and powder-XRD pattern (B) of {P_2W_{18}} (black) vs. calculated pattern from single-crystal X-ray data (red).

3.3.1.1 Stability of {Sb_9W_{21}}, {P_2W_{18}} and {Mo_7O_{24}}

Stability assessment of POMs is crucial for any future clinical applications.[218] The reference compound {Mo_7O_{24}} was reported to be stable at pH values 5-7:[219] the stability at pH 7.3 over 6 d was confirmed by UV-Vis spectroscopy measurements (Figure 3.7).

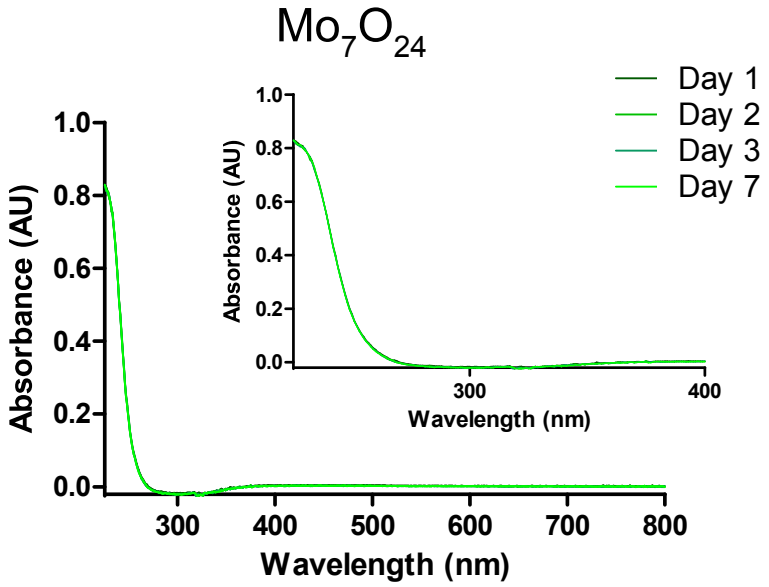

Figure 3.7. UV-Vis spectra of {Mo_7O_{24}} recorded over several days.

The stability of $\{Sb_9W_{21}\}$ and $\{P_2W_{18}\}$ was investigated measuring the change of the pH of their solutions as well as the UV-Vis spectra over 3 d. ^{31}P-NMR spectra were recorded for $\{P_2W_{18}\}$ as additional evidence. The reported instability of $\{Sb_9W_{21}\}$ in the entire pH range[177] was confirmed by our experiments. In fact, despite the low pH change when dissolved in water from 7.8 to 6.5 in 50 h, the UV-Vis spectra showed a decrease in intensity of about 15% per day, thus confirming the instability of the POM (Figure 3.9). On the contrary, the ^{31}P-NMR spectra of the isomeric mixture of α-, β- and γ-$\{P_2W_{18}\}$ recorded under acidic, physiologic or basic pH for 5 d showed no changes, either in position nor in intensity. Concordantly, the ^{31}P-NMR spectrum of α-$\{P_2W_{18}\}$ measured at pH 7.8, close to physiological conditions, showed no change after 7 d (Figure 3.8).

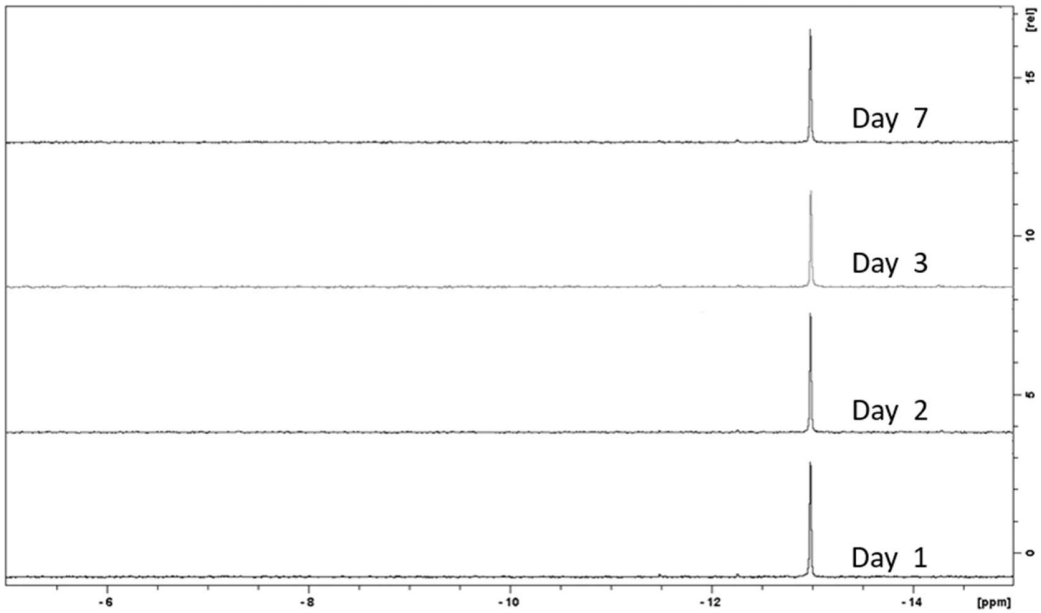

Figure 3.8. ^{31}P-NMR spectra of α-$\{P_2W_{18}\}$ measured at pH 7.8 for several days.

Furthermore, the ^{31}P-NMR spectrum of α-$\{P_2W_{18}\}$ recorded in D_2O (pH around 4) showed no variation after several months left in solution. The UV-Vis spectra of the α-, β- and γ-$\{P_2W_{18}\}$ at pH 7.3 showed no significant reduction in intensity in four d (Figure 3.9), as well as the one of α-$\{P_2W_{18}\}$ at pH 7.2. During the same period, the pH value of the solution of the α-, β- and γ-$\{P_2W_{18}\}$ isomers dissolved in water shifted from 6.3 to 4.9, and for α-$\{P_2W_{18}\}$ from 6.4 to 5.4, showing a partial acidic behavior of $\{P_2W_{18}\}$. (Please see section 3.3.3. for the effect of encapsulation on the POM stability.)

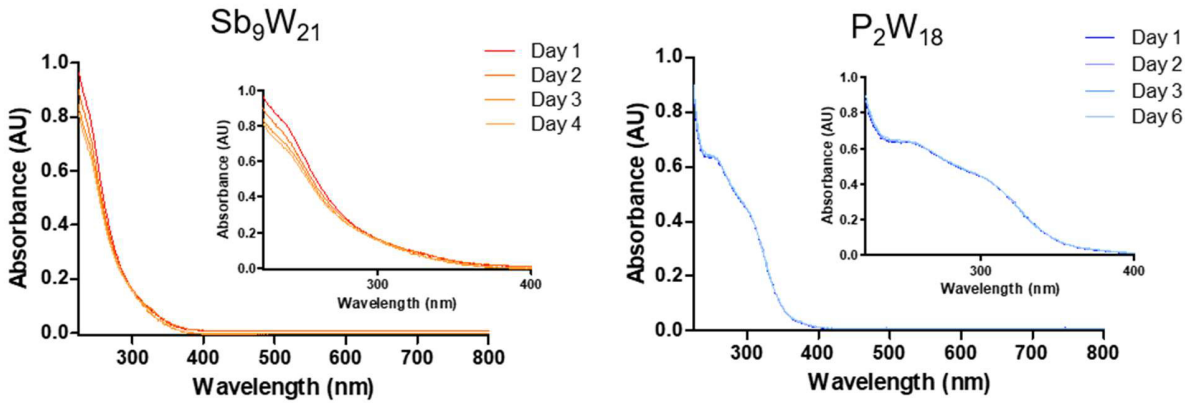

Figure 3.9. UV-Vis spectra of {Sb_9W_{21}} and of {P_2W_{18}} recorded over several days.

3.3.1.2 Synthesis and characterization of other biologically investigated POMs

$(TBA)_4[Mo_8O_{26}]$,[208] $H_4[SiMo_{12}O_{40}]$,[95,209] $K_7[PTi_2W_{10}O_{40}]$[210] and $(NH_4)_6[P_2Mo_{18}O_{62}]$[211] were synthesized according to previously reported procedures and their identity and purity was assessed via FT-IR spectroscopy, powder-XRD and, for the POMs containing P, ^{31}P-NMR spectroscopy.

The identity of $(TBA)_4[Mo_8O_{26}]$ (abbreviated as {Mo_8O_{26}}) was confirmed by FT-IR spectroscopy, and the spectrum was consistent with the one reported by *Roman at al.*[208] The FT-IR spectrum presented the typical signals of the β-octamolybdate compounds: at 945 cm^{-1} a very strong band related to the terminal Mo-O bond and three bands at 916, 896 and 844 cm^{-1} related to the stretching of the $[Mo_2O_2]$ units (Figure 3.10a). Moreover, the powder-XRD pattern of {Mo_8O_{26}} was in good agreement with the calculated one from the single-crystal data in the Inorganic Crystal Structure Database (ICSD; database code 56356) (Figure 3.10b).

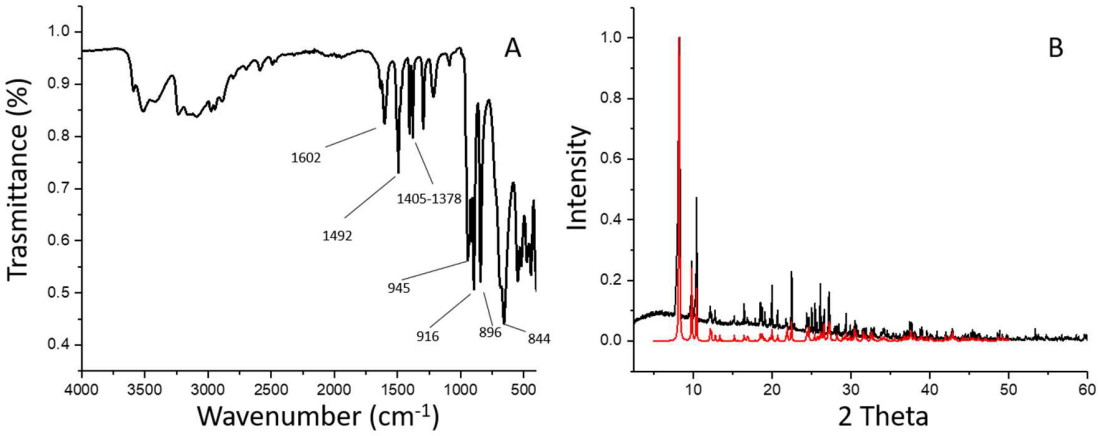

Figure 3.10. FT-IR spectrum (A) and powder-XRD pattern (B) of {Mo_8O_{26}} (black) vs. calculated pattern from single-crystal XRD data (red).

The identity and phase purity of $H_4[SiMo_{12}O_{40}]$ (abbreviated as {$SiMo_{12}$}) were confirmed through the powder-XRD pattern which matched well with literature data (PDF number: 84-0228) (Figure 3.11b). The material displayed good crystallinity and its FT-IR spectrum was consistent with the one previously reported.[95] In particular, the peaks related to the symmetric (1014 cm^{-1}) and asymmetric stretching (977 and 750 cm^{-1}) of Mo-O bonds and the peak related to the asymmetric stretching of Si-O (910 cm^{-1}) were present (Figure 3.11a).

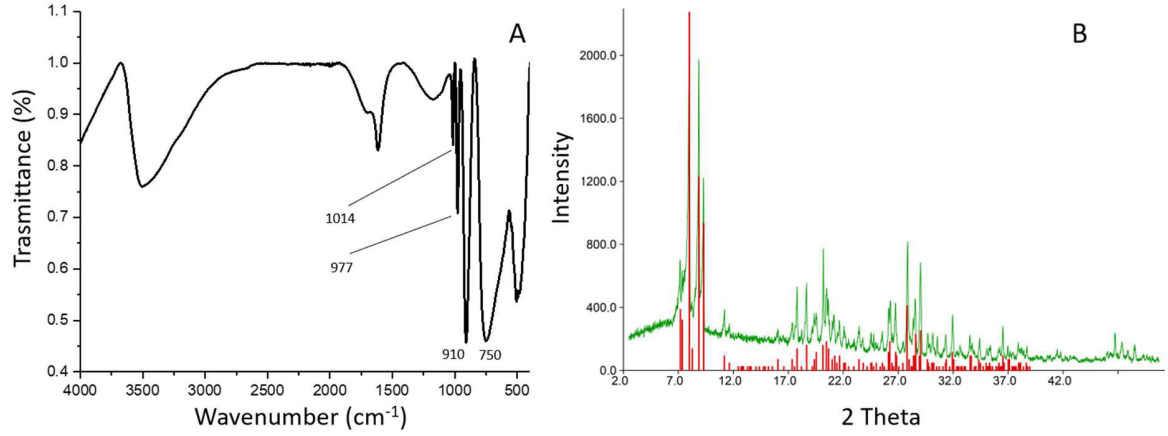

Figure 3.11. FT-IR spectrum (A) and powder-XRD pattern (B) of {$SiMo_{12}$} (green) vs. calculated pattern from single-crystal XRD data (red).

The identity of $K_7[PTi_2W_{10}O_{40}]$ (abbreviated as $\{PTi_2W_{10}\}$) was confirmed by FT-IR spectroscopy (Figure 3.12a): the vibration bands at 1081, 1062 and 1043 cm^{-1} could be assigned to ν_{as} (P-O; O central tetrahedron), 950, 873 and 765 cm^{-1} are assigned to ν_{as} (W=O; terminal O), ν_{as} (W-O_b-W; O corner-sharing) and ν_{as} (W-O_c-W; O edge-sharing), respectively.[210,220] The ^{31}P-NMR spectrum showed two peaks: δ -12.16 ppm belongs to the more abundant isomer, while δ -12.71 ppm belongs to another isomer present in negligible quantity (Figure 3.12b).

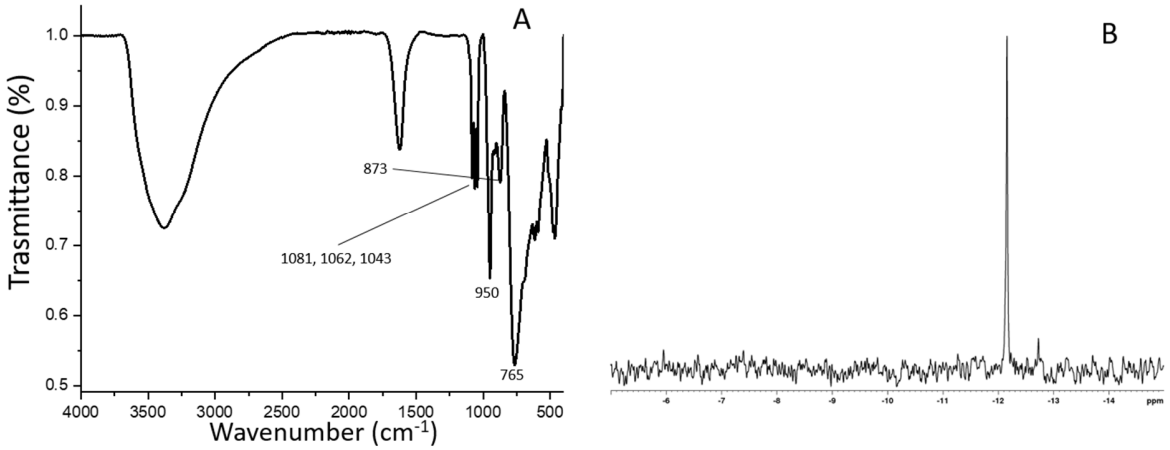

Figure 3.12. FT-IR spectrum (A) and ^{31}P-NMR spectrum (B) of $\{PTi_2W_{10}\}$.

$(NH_4)_6[P_2Mo_{18}O_{62}]$, (abbreviated as $\{P_2Mo_{18}\}$), was characterized by FT-IR spectroscopy, and the signals of the recorded spectrum were in good agreement with the one reported: the band at 1602 cm^{-1} corresponds to the OH stretching and the one at 1415 cm^{-1} to the vibration of NH_4^+, while the signals from 600 to 1001 cm^{-1} arise from the Mo-O bond vibrations (Figure 3.13a).[211] ^{31}P-NMR spectroscopy was performed, and the measured spectrum confirmed the identity of the product displaying the signal at δ -3.14 ppm, plus the presence of a little amount of impurities, with their peaks appearing at δ 0.06 ppm and δ 1.33 ppm, respectively (Figure 3.13b).

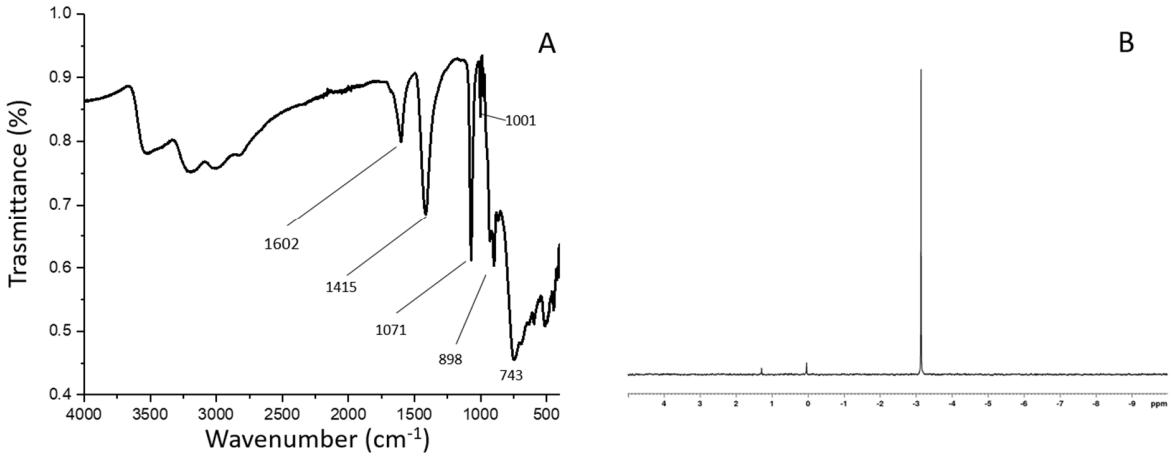

Figure 3.13. FT-IR spectrum (A) and ^{31}P-NMR spectrum (B) of {P_2Mo_{18}}

3.3.2 Synthesis and characterization of CMC

Carboxymethyl chitosan was synthesized according to the procedure previously used in our group.[212] The FT-IR and the ^{1}H-NMR spectra were consistent with the one previously reported in the literature (Figure 3.14).[212,221] ^{1}H-NMR spectrum was measured at different temperatures in order to shift the OH signal of the water and to be able to integrate all the peaks relative to the CH_2COO^- substitution. The main peak regarding the substitution at δ 3.11 ppm belongs to the protons of N-CH_2-COO^-. The degree of substitution was calculated according to the formula proposed by *Chen and Park,*[221] and 1.49 carboxymethyl unit per sugar ring was determined. The FT-IR spectrum is discussed in detail in section 3.3.3. The as-prepared CMC was soluble in water at pH values > 7.

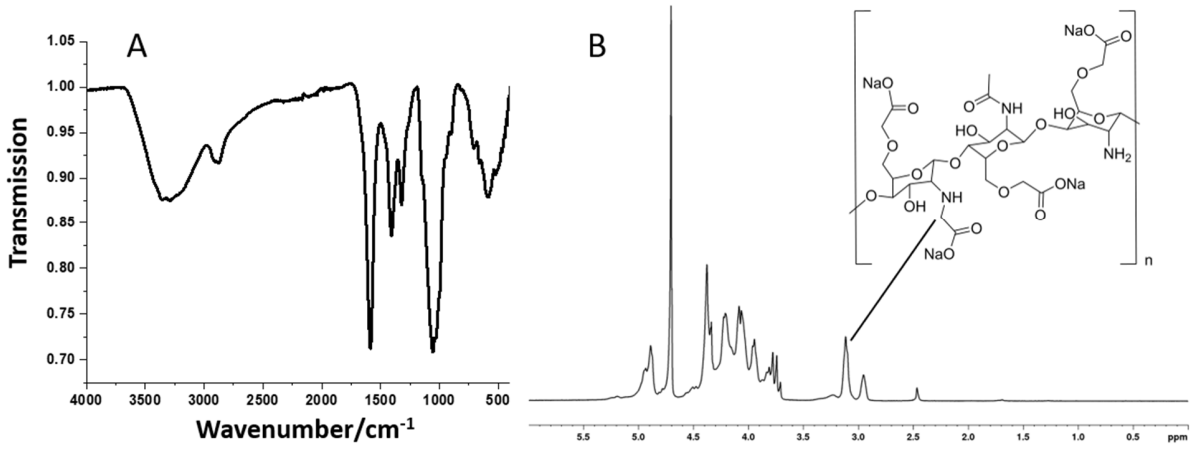

Figure 3.14. FT-IR (A) and ^{1}H-NMR spectrum together with the structural formula (B; 500 MHz, D_2O, 348 K, with suppression of water) of CMC.

3.3.3 Preparation and characterization of the nanocomposites

To investigate the effect of the encapsulation on the cytotoxicity of $\{Mo_7O_{24}\}$, $\{Sb_9W_{21}\}$ and $\{P_2W_{18}\}$, their nanocomposites with chitosan and CMC were prepared. Chitosan and CMC solubility cover the entire pH range: the former is soluble in water at pH < 6.5, while the latter at pH values above 7. The use of both biopolymers as encapsulating agents allowed the preparation of nanocomposites with pH dependent stability covering a wide range of values, thus extending the possible applications in the medical field. $\{Mo_8O_{26}\}$, $\{SiMo_{12}\}$, $\{PTi_2W_{10}\}$ and $\{P_2Mo_{18}\}$ were encapsulated with chitosan or CMC in order to investigate the feasibility of particles preparation and to study their change in cytotoxicity after the encapsulation.

POM-chitosan nanoparticles were produced via cross-linking interaction between the positively charged chitosan and the negatively charged POMs under constant sonication. POM-CMC nanoparticles were prepared under constant stirring using Ca^{2+} (from $CaCl_2$) as cationic cross-linker between the negatively charged CMC and POM.

The as-prepared nanoparticles were investigated by DLS to determine average size (from now on simplified referred to as size), number and polydispersity index (PDI). The size of the nanoparticles is measured as hydrodynamic volume as an average of three independent measurements. Different parameters affect the size and the polydispersity of the nanoparticles. The characteristics of the polymer, e.g. the degree of deacetylation, the degree of substitution and

the molecular weight, are important parameters to be considered regarding the size of the nanocomposites. The molecular weight of the polymer will change the size of the nanoparticles in a directly proportional manner. The degree of deacetylation and of substitution are essential parameters in the formation of the nanoparticles, because they mediate the electrostatic interactions between the components. In addition to the polymer, the concentration and the nature of the POM as well as the reaction conditions (ionic strength and temperature) influence the characteristics of the final particles. The quality of nanoparticles produced at different temperatures was investigated, and the particles produced at 20 °C had smaller size and PDI compared to the one prepared at lower or higher temperatures. POM-chitosan nanoparticles were generally smaller and less polydispersed than POM-CMC nanoparticles, whereas the nanoparticles of the pristine polymers exhibited the opposite behavior.

The nanoparticles used in the biological experiments ranged from 90 to 230 nm with a polydispersity index of 0.170-0.260, while chitosan nanoparticles produced with TPP were typically larger. The characteristics of the most representative nanoparticles tested on different biological targets are summarized in Table 3.1.

The characteristics of the nanoparticles such as size, surface charge and type of polymer are very important parameters which influence the metabolism *in vivo*. According to previous studies, the mechanism of the cellular uptake could depend on the nanoparticle size, and nanoparticle around 150 nm would be preferably internalized via non-phagocytic mechanism.[222] Furthermore, nanoparticles of different sizes will be metabolized and accumulated differently,[223] e.g. particles below 400 nm could be accumulated in the tumor via the “enhanced permeability and retention” (EPR) effect.[224]

The surface charge of the nanoparticles plays a relevant role in the cellular uptake. Chitosan nanoparticles have a ζ-potential typically around +20 mV while CMC nanoparticles have a ζ-potential of around -20mV. Negatively charged POM-CMC nanoparticles, when injected directly in the blood stream, would accumulate most likely in the tumor cells via EPR effect, while positively charge POM-chitosan nanoparticles would be recognized mainly by the mononuclear phagocyte system.[225]

Table 3.1. Summary of the characteristics summary of some nanoparticles used in this work.

Label	**POM**	**Chitosan**	**Size** (nm)	**PDI**	**Tested on**
137	Mo_8O_{26}	Chit	105	0.214	HeLa
158	$SiMo_{12}$	Chit	166	0.222	HeLa
174	Sb_9W_{21}	Chit	99	0.167	Bacteria
216	Sb_9W_{21}	Chit	171	0.172	Bacteria
179	P_2W_{18}	Chit	188	0.205	Bacteria
217	P_2W_{18}	Chit	178	0.226	Bacteria
193	/	Chit	381	0.155	Bacteria
151	Sb_9W_{21}	Chit	152	0.193	HeLa
206	Mix-P_2W_{18}	Chit	117	0.252	HeLa
211	Mix-P_2W_{18}	Chit	99	0.259	HeLa
256	/	Chit	595	0.203	HeLa
287	Sb_9W_{21}	Chit	134	0.185	HeLa
290	α-P_2W_{18}	Chit	213	0.197	HeLa
297	Mo_7O_{24}	Chit	161	0.178	HeLa
298	P_2Mo_{18}	Chit	178	0.195	HeLa
300	α-P_2W_{18}	Chit	233	0.235	MRC-5
301	Sb_9W_{21}	Chit	182	0.183	MRC-5
304	α-P_2W_{18}	Chit	122	0.21	HeLa
305	Mo_7O_{24}	Chit	187	0.179	MRC-5
CMC 29	Mo_8O_{26}	CMC	225	0.141	HeLa
CMC 34	Mix-P_2W_{18}	CMC	216	0.387	HeLa
CMC 42	Sb_9W_{21}	CMC	96	0.195	HeLa
CMC 43	PTi_2W_{10}	CMC	188	0.361	HeLa
CMC 48	Mix-P_2W_{18}	CMC	168	0.223	HeLa
CMC 78	α-P_2W_{18}	CMC	105	0.381	HeLa
CMC 79	Sb_9W_{21}	CMC	180	0.335	HeLa
CMC 82	Sb_9W_{21}	CMC	173	0.246	MRC-5
CMC 83	α-P_2W_{18}	CMC	148	0.313	MRC-5
CMC 86	/	CMC	313	0.227	MRC-5
CMC 88	/	CMC	276	0.19	HeLa
CMC 94	Mo_7O_{24}	CMC	124	0.277	MRC-5
CMC 95	Sb_9W_{21}	CMC	173	0.415	HeLa
CMC 98	Mo_7O_{24}	CMC	127	0.188	HeLa
CMC 102	Sb_9W_{21}	CMC	109	0.347	HeLa

The successful encapsulation of the POM inside the polymer was confirmed by FT-IR spectroscopy. The FT-IR spectra showed the characteristic IR vibrations of both components (Figure 3.15).

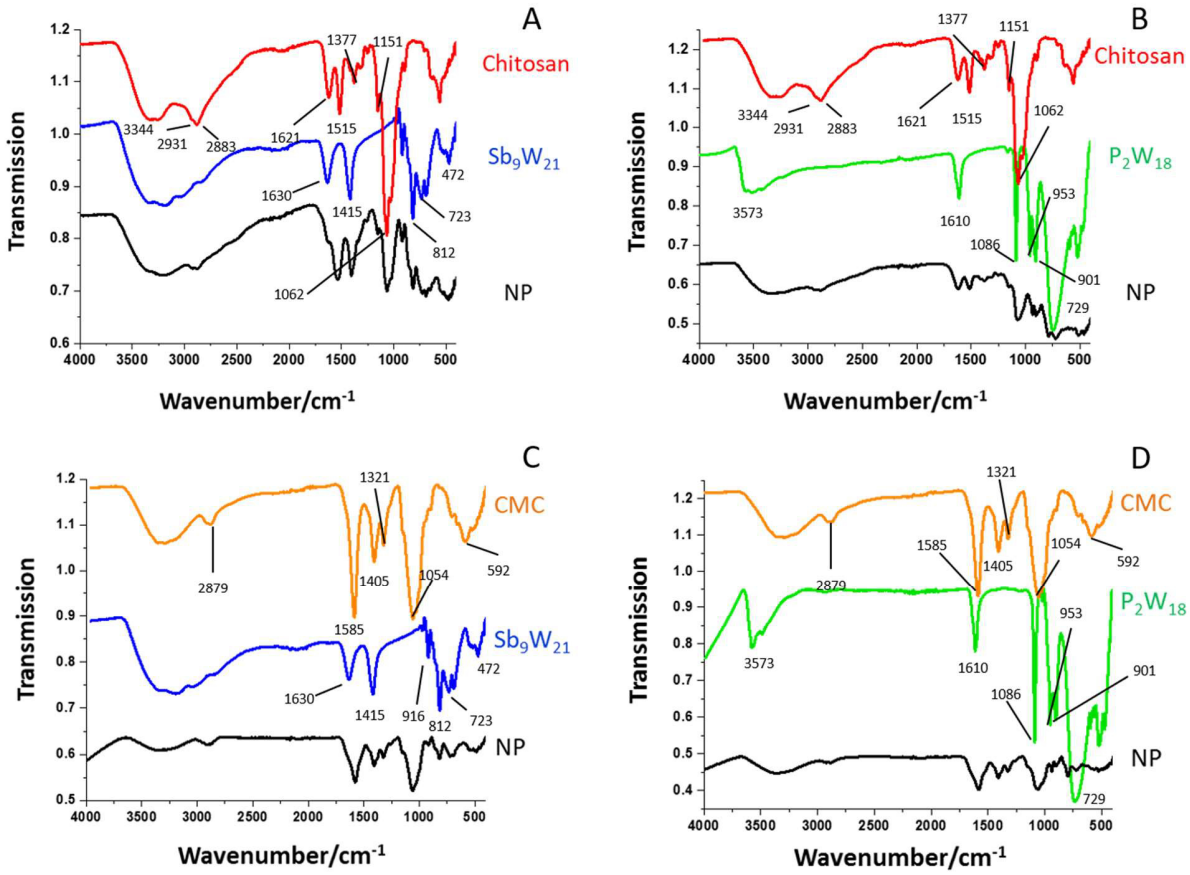

Figure 3.15. FT-IR spectra overview of chitosan, {Sb_9W_{21}} and nanocomposites (A), of chitosan, α-{P_2W_{18}} and the nanocomposites (B) of CMC, {Sb_9W_{21}} and nanocomposites (C) and of CMC, α-{P_2W_{18}} and the nanocomposites (D).

The FT-IR spectrum of chitosan displayed the characteristic bands of the polymer from 3344 to 3261 cm^{-1} (OH and NH overlapped stretching), 2931 and 2883 cm^{-1} (CH stretching), 1621 cm^{-1} ($-NH_3^+$), 1515 cm^{-1} (amide bending), 1151 cm^{-1} (bridging -O-) and 1062 cm^{-1} (-CO and CH-OH stretching).

The FT-IR spectrum of CMC displayed the characteristic bands from 3355 to 3288 cm^{-1} (OH and NH overlapped stretching), 2879 cm^{-1} (CH stretching), 1585 and 1405 cm^{-1} corresponding to the asymmetric and symmetric stretching of the COO^- group, respectively, 1321 cm^{-1}, assigned to the CH_2 wagging, and 1054 cm^{-1} assigned to the CH-OH stretching.

α-{P_2W_{18}} could be easily identified by four characteristic IR bands in the 1100-770 cm^{-1} range: 1087, 955, 913 and 729 cm^{-1} which correspond to the ν_{as} (P-O_a), ν_{as} (W-O_d), ν_{as} (W-O_b-W) and ν_{as} (W-O_c-W) bands, respectively.

The spectrum of {Sb_9W_{21}} displayed the characteristic ν_{as} (W-O) bands at 916, 812, and 723 cm^{-1}, and at 1415 cm^{-1} a vibration related to NH_4^+.

The encapsulation efficiency was determined by UV-Vis spectroscopy. The UV-Vis spectrum of the filtrate of the nanoparticles after centrifugation through a 10 kDa centrifuge filter was recorded and compared to the spectrum of the pristine POMs. The ratio between the absorbance of the filtrate and the absorbance of the pristine POM permits to calculate the encapsulation efficiency. Encapsulation efficiencies of 99.7 and of 99.4% were found for α-{P_2W_{18}}- and {Sb_9W_{21}}-chitosan nanoparticles, respectively. Encapsulation efficiency of about 99.7% was calculated for α-{P_2W_{18}}- and {Sb_9W_{21}}-CMC nanoparticles.

The encapsulation in the polymeric matrix improved the stability of {Sb_9W_{21}} and did not reduce significantly the one of {P_2W_{18}}, either as α-isomer or as the mixture of α-, β- and γ-isomers, as shown in Figure 3.16.

The UV-Vis data suggest that {P_2W_{18}} undergoes partial modification upon encapsulation: after some time, the nanoparticle suspension probably displays a partial reduction, as indicated by the visible light blue coloration of the reduced POM. However, the reversible partial reduction does not change the structure of the POM and thus might not be the only factor. The partial alteration of {P_2W_{18}} takes place within the first h after encapsulation, so that the UV-Vis spectra remain stable after the first day.

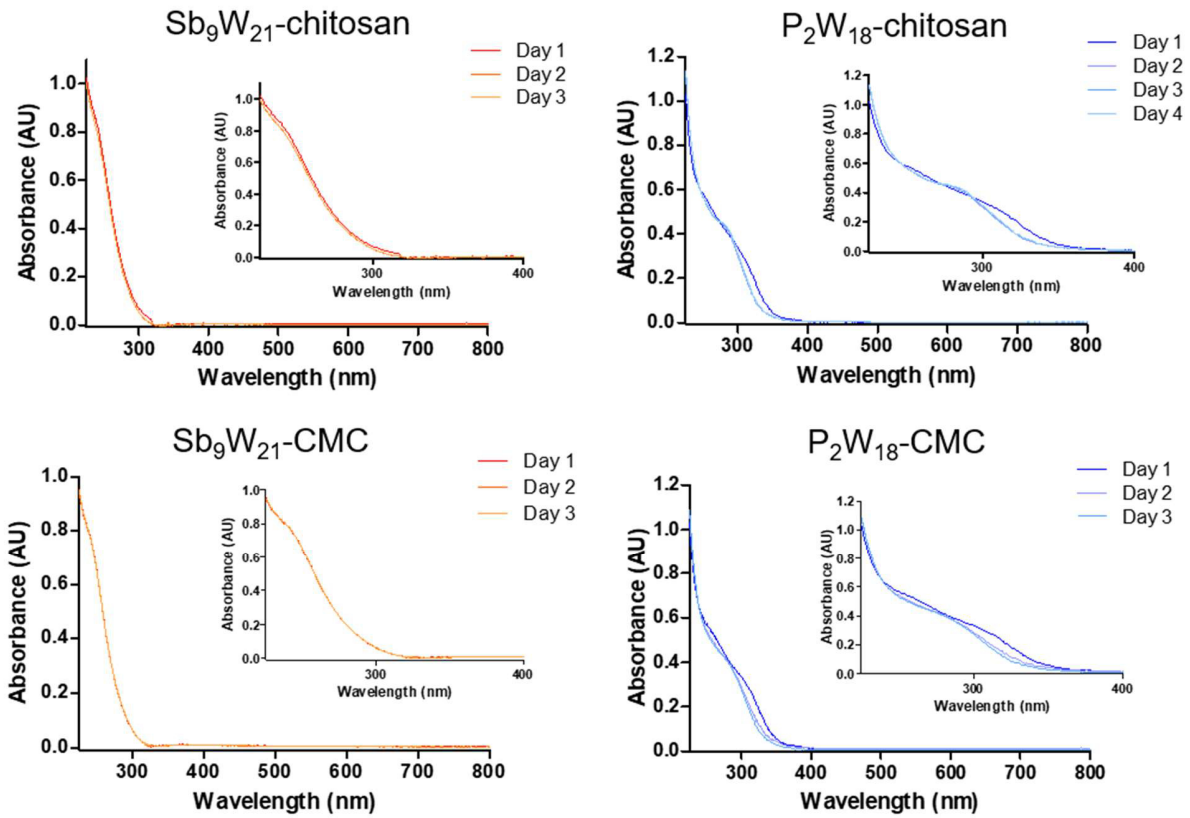

Figure 3.16. UV-Vis spectra of {Sb_9W_{21}}- and {P_2W_{18}}- chitosan and CMC nanoparticles over 3-4 days.

Elemental analysis confirmed the presence of the main elements in both POMs and nanoparticles in good correlation with calculated values (Table 3.2). For {Sb_9W_{21}}, the ratio W/Sb did not significantly change before (3.58) and after the encapsulation with chitosan (3.61), and furthermore it is in good agreement with the theoretical value (3.57). Likewise, for α-{P_2W_{18}} the W/P ratio (53.4) remained after encapsulation (53.7), in good agreement with the theoretical value (53.3). In comparison, the ratio between W/K (13.7) was somewhat higher than the theoretical value (13.4), probably due to the presence of some residual sodium as counterion.
In case of α-, β- and γ-{P_2W_{18}}, the ratio W/P (48.3) differed from the theoretical value (53.3) and slightly changed upon chitosan encapsulation (from 48.3 to 55).

Table 3.2. Elemental analysis of {Sb_9W_{21}} and {P_2W_{18}} and their nanoparticles with chitosan.

	P Mass-%	W mass-%	K mass-%	W/P	W/K	Sb mass-%	W mass-%	W/Sb
α-, β- and γ-P_2W_{18}	1.39	67.2		48.3				
NP α-, β-, γ-P_2W_{18}	0.30	16.5		55				
α-P_2W_{18}	1.28	68.4	4.99	53.4	13.7			
NP α-P_2W_{18}	0.35	18.8		53.7				
Sb_9W_{21}						14.4	51.5	3.58
NP Sb_9W_{21}						3.43	12.4	3.61
Theoretical	1.28	68.23	5.10	53.3	13.4	16.4	57.7	3.57

The stability of the nanoparticles was investigated by monitoring the pH of the solution as well as the size of the particles over 72 h. The stability of {P_2W_{18}}- and {Sb_9W_{21}}-chitosan nanoparticles was confirmed by the constant pH value of 5.4 over the entire monitoring period, while the pH of the CMC nanoparticles remained constant around 7.1 for {P_2W_{18}}-CMC and 7.2 for {Sb_9W_{21}}-CMC. POM-chitosan nanoparticles are stable at pH < 6.5, while at higher pH values aggregation sets in due to the deprotonation of the ammonium groups. In contrast, CMC nanoparticles are stable at pH above 7 due to the deprotonation of the carboxylic groups. The size of {Sb_9W_{21}}-chitosan nanoparticles remained almost constant over a period of 3 d (from 107 to 114 nm), while for {P_2W_{18}}-chitosan nanoparticles the size increased during the observation period, from 131 to 151 nm and from 160 to 188 nm for the isomeric mixture and the α-isomer, respectively, thus revealing a partial tendency to agglomerate.

The tendency to form agglomerates is even more pronounced when POM-CMC are considered: the size increased over 3 d from 95 to 113 nm, from 180 to 230 nm and from 187 to 875 nm for {Sb_9W_{21}}-CMC, α-{P_2W_{18}}-CMC and α-, β- and γ-{P_2W_{18}}-CMC nanoparticles, respectively.

3.3.3.1 Electron microscopy of the nanocomposites

POM-chitosan and -CMC nanoparticles were investigated with electron microscopy, namely scanning electron microscopy (SEM) and transmission electron microscopy (TEM), to characterize their morphology and to confirm the size calculated by DLS. Sample preparation is a key step for

the successful analysis of the nanoparticles by SEM that presented some difficulties for as-prepared nanoparticles: the deposition of a drop of the nanoparticles resulted in a polymeric surface, due to the aggregation of the nanoparticles in the drying process (Figure 3.17a). Moreover, the presence of large quantities of sodium chloride even after dilution did not allow the proper observation of the POM-chitosan nanoparticles, as they were completely included within the salt crystals (Figure 3.17b). NaCl was formed during the preparation process of the nanoparticles from HCl used to solubilize chitosan and from NaOH used for pH adjustment.

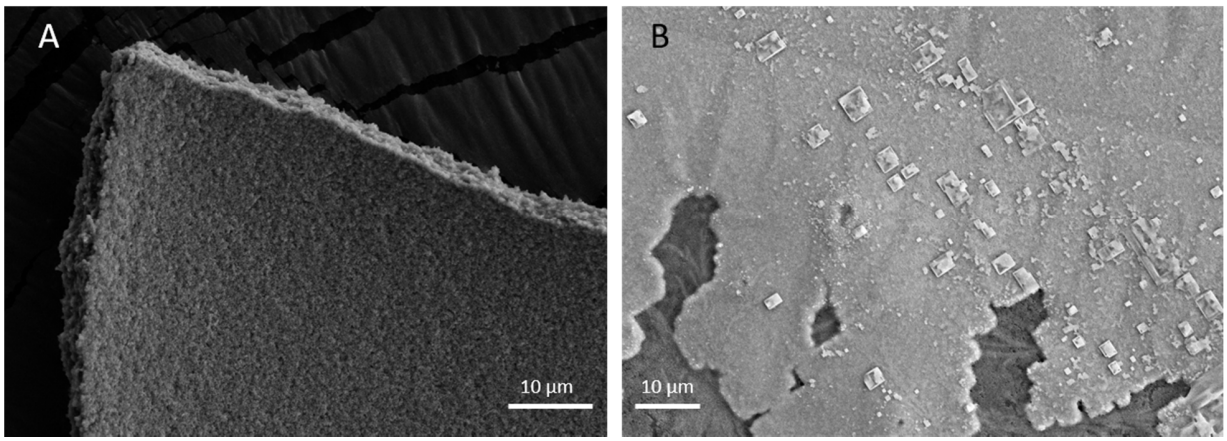

Figure 3.17. SEM micrographs of polymer like surface (A) and residual crystals of NaCl (B).

In order to remove the salt, the nanoparticles were extensively washed with ultrapure water with a 10 kDa centrifuge filter and resuspended via sonication before deposition on the sample holder. In the SEM micrograph of α-{P_2W_{18}}-chitosan nanoparticles the persistent presence of NaCl is still evident (Figure 3.18), as confirmed by the energy-dispersive X-ray spectroscopy (EDX) analysis that also showed the signals of the characteristic elements of the α-{P_2W_{18}}-chitosan nanocomposites. The observed shape of the nanoparticles was irregular, with sharp borders, probably due to the residual NaCl, while the size was in good agreement with DLS measurements. A similar morphology was previously observed for $(NH_4)_{15}\{Na[(Mo_2O_4)_6(\mu_2\text{-}SO_3)_3\text{-}(\mu_2\text{-}SO_3)]_2\}$-chitosan nanoparticles embedded in gelatin instead of NaCl.[203] NaCl does not affect negatively the size and the morphology of the POM-chitosan nanoparticles: on the contrary an higher ionic strength is known to lead to smaller and less polydispersed nanoparticles.[226] The effect is the

opposite for POM-CMC nanoparticles, which are generally larger and more polydispersed in the presence of NaCl.[227]

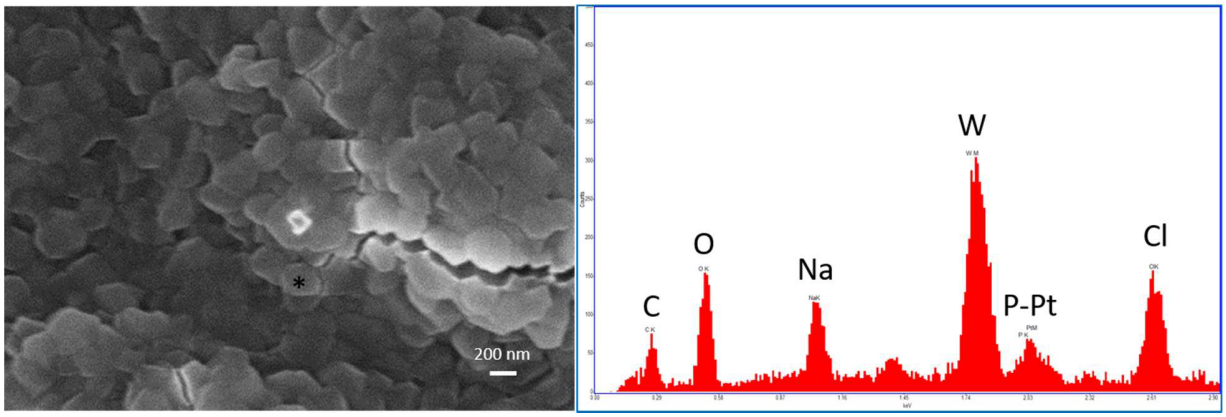

Figure 3.18. SEM micrograph of α-{P_2W_{18}}-chitosan nanoparticles and corresponding EDX analysis (measured spot).*

{Sb_9W_{21}}-chitosan microparticles were isolated after the washing steps as single particles and furthermore no salt was present (Figure 3.19). They presented a spherical shape even though their size was larger than calculated by DLS, probably due to the isolation procedure. The EDX confirmed the presence of characteristic elements present in chitosan and {Sb_9W_{21}}.

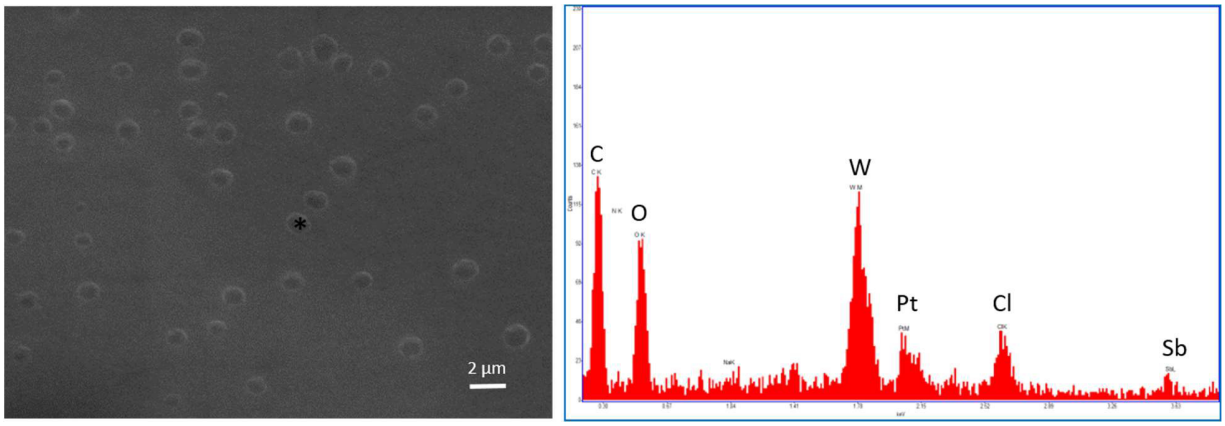

Figure 3.19. SEM micrograph of {Sb_9W_{21}}-chitosan microparticles and corresponding EDX analysis (measured spot).*

The {Sb_9W_{21}}- and α-{P_2W_{18}}-CMC nanoparticles did not require a washing procedure due to the minor salt content. They were morphologically comparable to α-{P_2W_{18}}-chitosan isolated

particles. Their size was in good agreement with the DLS mesaurements and the EDX analysis confirmed the presence of all the involved elements (Figure 3.20).

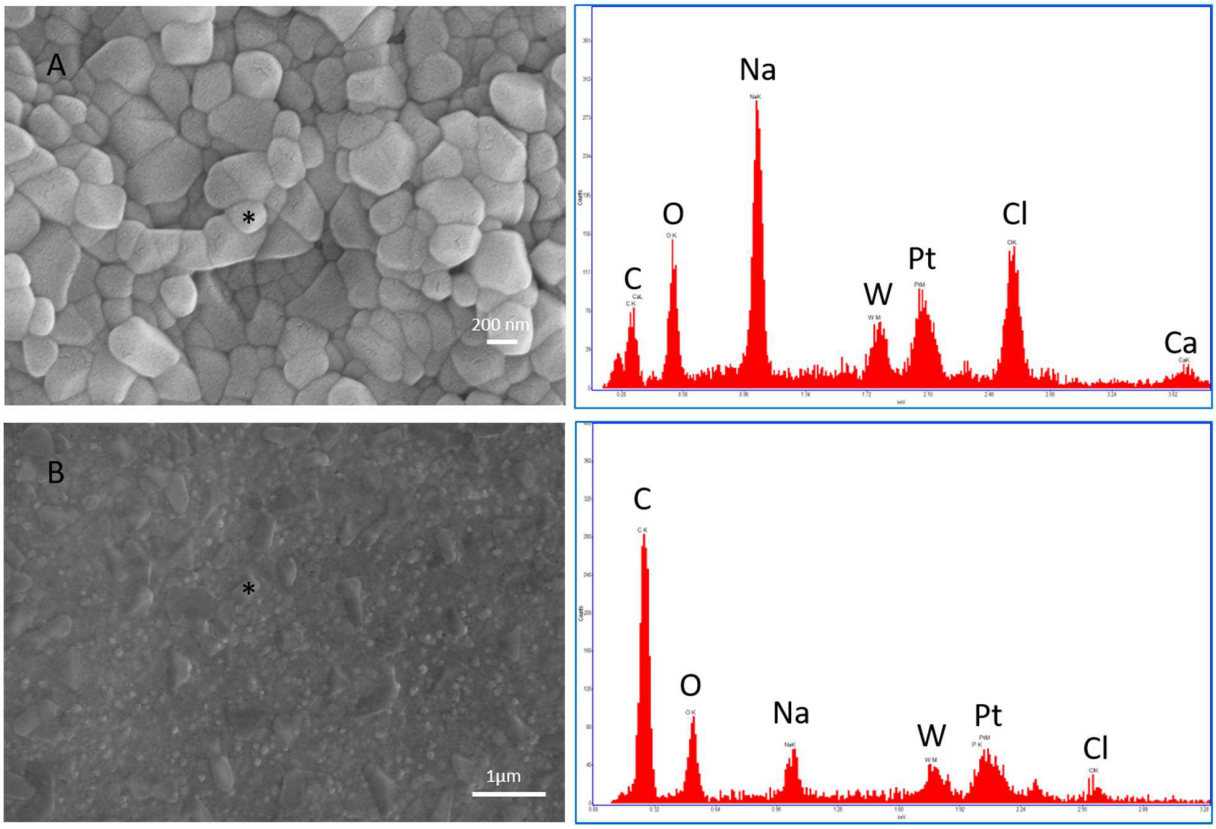

Figure 3.20. SEM micrographs of nanoparticles {Sb_9W_{21}}-CMC nanoparticles (A) and α-{P_2W_{18}}-CMC nanoparticles (B) with related EDX spectra (measured spot).*

A way to visualize the POM-chitosan nanoparticles directly after their preparation, which does not require any further treatment, was developed. To this end, chitosan was solubilized with acetic acid and, after addition of water, the pH of the solution was 4.5. In this way, the immediate preparation of the particles was possible, avoiding the pH setting procedure. The as-prepared nanoparticles of α-{P_2W_{18}} and chitosan solubilized with acetic acid were deposited upon dilution on a SEM sample holder. The size distribution estimated from SEM images was in good agreement with DLS measurements, ranging from 100 nm up to 800 nm, with the distribution peak around 220 nm (Figure 3.21). In the SEM micrograph, the chitosan nanoparticles presented a spherical jagged shape, which may have been concealed by remnant NaCl after the other sample preparation route.

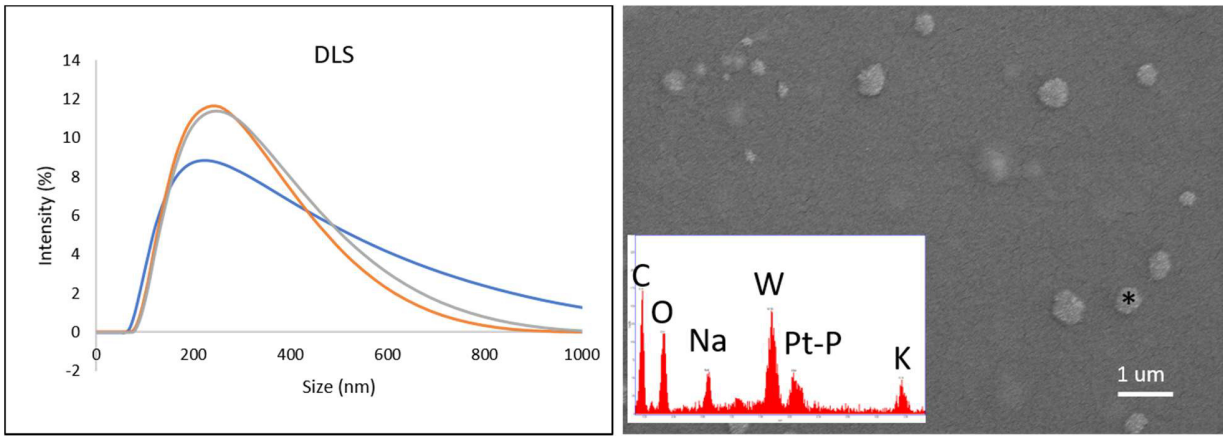

*Figure 3.21. DLS and SEM micrograph with EDX analysis of α-{P_2W_{18}}-chitosan nanoparticles (chitosan dissolved with acetic acid; * measured spot).*

The nanoparticles subjected to TEM analyses were not washed for the removal of the salt, because of the different sample preparation procedure. The morphology of {Sb_9W_{21}}- and α-{P_2W_{18}}-chitosan nanoparticles revealed by SEM was confirmed by TEM observations. {Sb_9W_{21}}-chitosan nanoparticles were more rounded, while the α-{P_2W_{18}} ones appeared to have sharper edges. The observed size for both the nanoparticles was in good agreement with the one measured by DLS and the EDX analysis confirmed the presence of all the expected elements of the components.

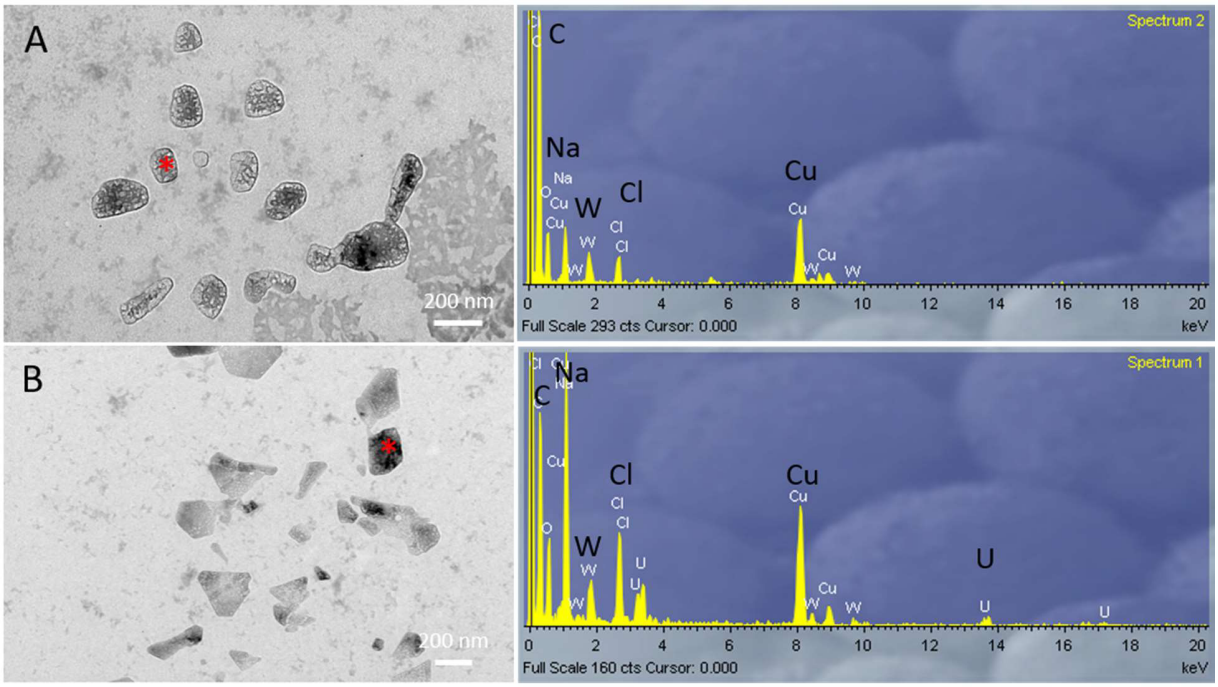

Figure 3.22. TEM micrographs of {Sb_9W_{21}}-chitosan nanoparticles (A) and α-{P_2W_{18}}-chitosan nanoparticles (B), with corresponding EDX analyses (measured spot).*

Interestingly, TEM images of {Sb_9W_{21}}-CMC and α-{P_2W_{18}}-CMC nanoparticles displayed an irregular fibrous morphology and partial tendency to agglomerate, which is more evident for α-{P_2W_{18}}-CMC. TEM micrographs of α-{P_2W_{18}}-CMC nanoparticles indicated a larger size compared to the one measured by DLS. DLS measurements performed over time confirmed the tendency to agglomerate. The irregular shape was previously observed by *Fiorani et al.* in the TEM micrographs of $[W_{10}O_{32}]^{4-}$-chitosan nanocomposites.[204] The irregular morphology could be attributed either to the properties of CMC or to the high vacuum conditions used in TEM observations. The EDX analyses confirmed the presence of all the elements of the nanocomposites, in addition to the copper of the sample grid and the uranium of the negative stain.

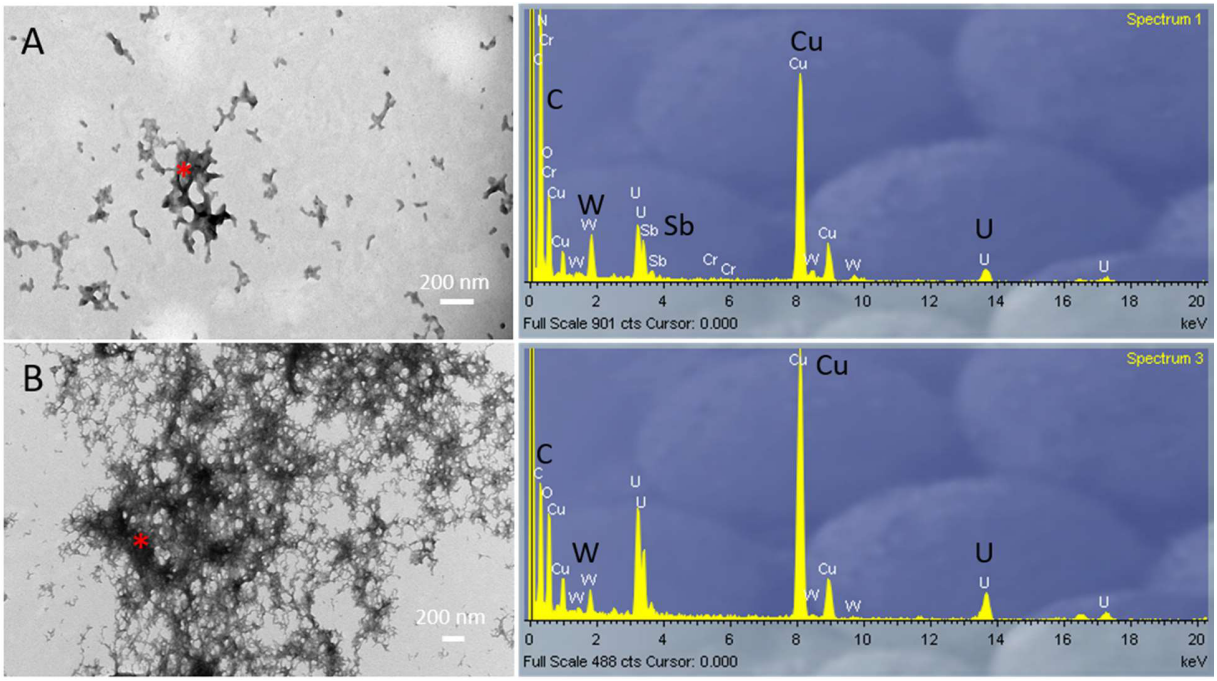

Figure 3.23: TEM micrographs of {Sb_9W_{21}}-CMC nanoparticles (A) and α-{P_2W_{18}}-CMC nanoparticles (B) with corresponding EDX analyses (measured spot).*

In summary, the size of the nanoparticles confirmed by DLS and electron microscopy was in most of the cases around 200 nm. The success of the encapsulation was confirmed by FT-IR spectroscopy and EDX analysis. The morphology of the nanoparticles was dependent on the type of the POMs and of the polymer used, as well as on the preparation procedure. In the following two sections, the cytotoxicity of the POM-chitosan and POM-CMC nanoparticles as well as of the pristine components on bacteria and mammalian cells are discussed.

3.3.4 Cytotoxicity on bacteria

The antibacterial effect of POMs and chitosan-POM nanocomposites was investigated with plate counting experiments on two bacterial strains, the gram-negative *E. coli* and the gram-positive *S. sobrinus*. Results expressed as Colony Forming Unit per mL (CFU/mL) of the antibacterial effect of {Sb_9W_{21}} and {P_2W_{18}} (the isomeric mixture) and the respective chitosan-nanoparticles on the bacteria are reported in Figure 3.24.

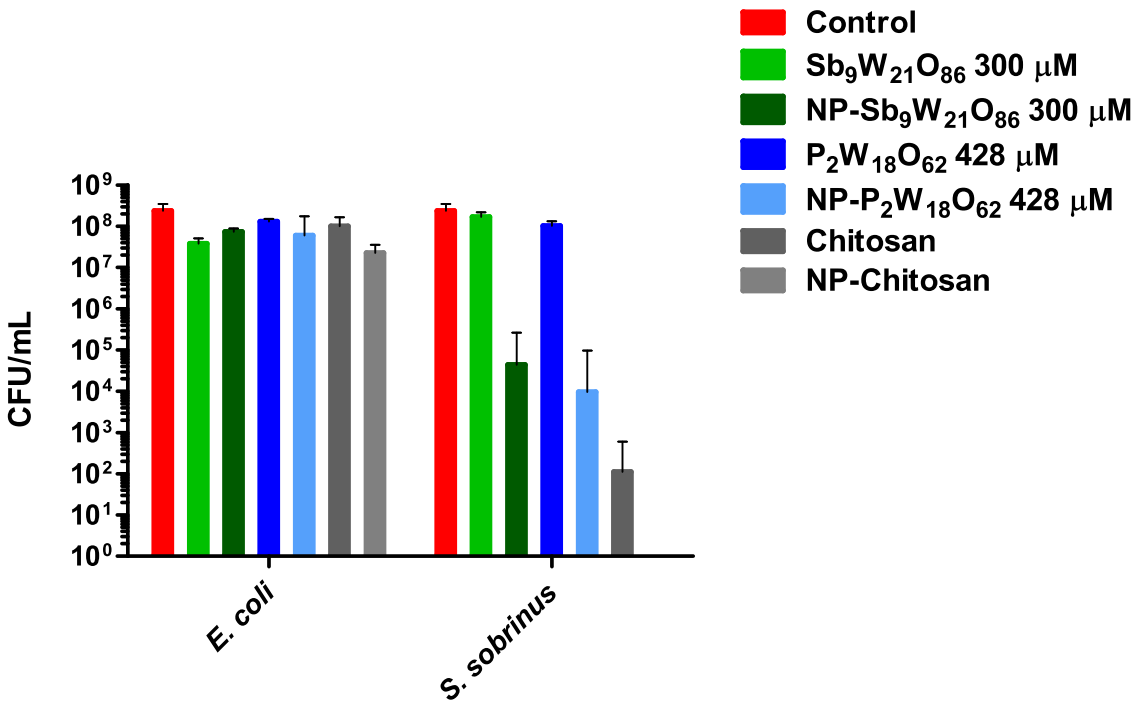

Figure 3.24. Results of plate counting experiment for {Sb_9W_{21}} and {P_2W_{18}} and the respective chitosan-nanoparticles (NP) on E. coli and S. sobrinus (2 mg/mL, 30 min incubation).

The antimicrobial activity depended on the strain, the type of POM and the polymer used for the encapsulation. The pristine POMs were less effective both on *E. coli* and *S. sobrinus* than the encapsulated analogues, with almost no reduction of the bacterial population. The encapsulation of {Sb_9W_{21}} with chitosan exerted higher antimicrobial activity than the two separate components on *E. coli*, with a 2-log reduction clearly due to the joint antimicrobial effect. In contrast, the treatment with encapsulated {P_2W_{18}} barely resulted in a 1-log reduction, while chitosan alone reached at best only a 1-log reduction of colonies. On *S. sobrinus* {Sb_9W_{21}}-chitosan and {P_2W_{18}}-chitosan exerted 4-log and 4.5-log reduction respectively, but pristine chitosan alone achieved on *S. sobrinus* a 6.5 log-reduction, when in solution, and completely eradicated the bacterial population when applied as nanoparticles. These data clearly illustrate the low influence that the tested POMs have on this bacteria strains and were contextualized with the data previously reported as follows. {P_2W_{18}} was never tested on *E. coli*, but was used to treat vancomycin resistant *S. aureus* and in co-treatment with β-lactam antibiotic (oxacillin).[228] *Inoue et al.* found out that {P_2W_{18}} enhances the effect of oxacillin at a concentration of 100 μM and 50 μM

rendering the strain susceptible. However, no plate counting experiments have been performed rendering the comparison of the antimicrobial activity difficult.

To the best of our knowledge, $\{Sb_9W_{21}\}$ with NH_4^+ and Na^+ as counter anions was never tested on *E. coli*. However, a similar study using K^+ as counter anion has been conducted on the gram-negative *H. pylori*.[229] In this study, a 6 log-reduction has been achieved treating the bacteria with 24 µM $\{Sb_9W_{21}\}$ for 12 h. When the bacteria were incubated less than 4 h no significant growth reduction appeared. In our work, a higher concentration of POM was used, but with much shorter incubation time (30 min). It is not possible to say if the reduction of 1 log is due to the higher concentration used or the effect of the counter anion. As far as we know, no studies have been conducted on the action of both pristine polyoxometalates on *S. sobrinus*, so direct comparison with our data is not possible.

In this work, the antimicrobial activity of pristine CMC and of its composites was also investigated, but no relevant antibacterial effect was observed, probably due to the functionalization of chitosan's amine groups, which are often referred to as the responsible group for the antibacterial properties exerted by chitosan.

The plate counting experiments evidenced that none of the pristine POMs as well as the composites exhibit a relevant antibacterial action against the two tested strains. However, the use of these materials could be of interest for application when is important to have cytotoxic action on a tissue, while keeping intact the natural microbial population (e.g. in the small and large intestine).

3.3.5 Cytotoxicity on mammalian cells

3.3.5.1 Cytotoxicity of $\{Sb_9W_{21}\}$, $\{P_2W_{18}\}$, $\{Mo_7O_{24}\}$ and nanocomposites

$\{Sb_9W_{21}\}$, α-$\{P_2W_{18}\}$ and $\{Mo_7O_{24}\}$ and respective nanocomposites have been tested on HeLa and MRC-5, cervical adenoma and normal lung fibroblast cell lines, respectively, and their viability was assessed by MTT assay. The results of $\{Sb_9W_{21}\}$ and α-$\{P_2W_{18}\}$ and their chitosan and CMC nanocomposites are reported in Figure 3.25 and in Figure 3.26 for HeLa and MRC-5 cell lines, respectively. The survival rates are expressed as percentage where 100% refers to the untreated control and the concentration expressed in µM refers to the concentration of the POM encapsulated into the nanocomposite. $\{Sb_9W_{21}\}$ and α-$\{P_2W_{18}\}$ chitosan encapsulation was

generally leading to a decrease in cytotoxicity compared to the POMs alone on both cell lines.

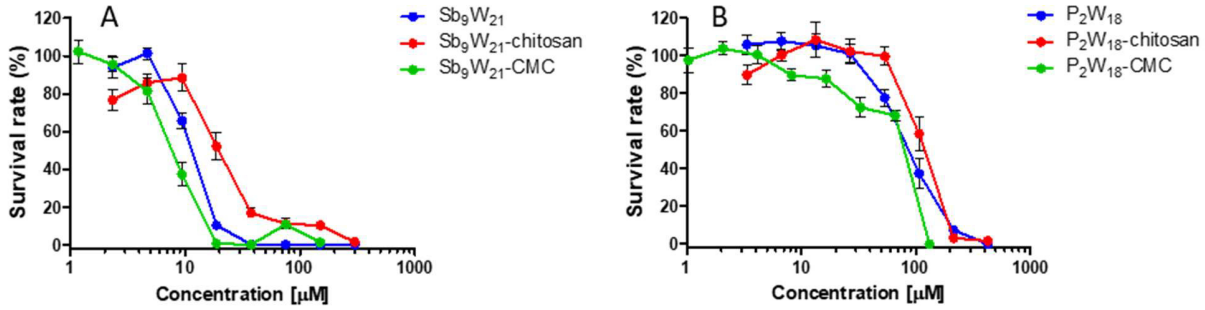

Figure 3.25. Cytotoxicity results on HeLa cells of {Sb_9W_{21}}, {Sb_9W_{21}}-chitosan and {Sb_9W_{21}}-CMC nanoparticles (A) and of α-{P_2W_{18}}, α-{P_2W_{18}}-chitosan and α-{P_2W_{18}}-CMC nanoparticles (B).

Our findings showed an opposite behavior compared to previous results on POM-chitosan nanocomposites as reported in the section 3.1.2. For example, pristine $[Cs\subset Eu_6As_6W_{63}O_{218}(H_2O)_{14}(OH)_4]^{25-}$ displayed higher cytotoxicity *in vitro* upon chitosan encapsulation.[200] In two consecutive studies by *Shah et al.* it was observed that the cytotoxicity of the POMs was enhanced upon encapsulation reaching 80-88% inhibition rate on HeLa[201] and IC_{50} ranging from 8 to 1 µM, i.e. 2-18 fold lower than the IC_{50} value for the respective POM.[202]

The profile of cytotoxicity of POM-CMC nanoparticles was depending both on the POM and the cell line. Either on HeLa and on MRC-5 cells {Sb_9W_{21}}-CMC exerted a higher toxicity compared to the pristine POM and its chitosan homologue: the change of polymer led to an opposite effect. The {Sb_9W_{21}}-CMC nanoparticles were surprisingly much more toxic on HeLa cells if compared to similar concentration of $[Co_4(H_2O)_2(PW_9O_{34})_2]^{10-}$-CMC nanoparticles, where encapsulation also led to reduced cytotoxicity compared to the pristine POM.[212]

Interestingly α-{P_2W_{18}}-CMC nanoparticles behaved differently depending on the tested cell lines. On HeLa cells α-{P_2W_{18}}-CMC composites were the most toxic of the tested compounds, while on MRC-5 cells they were, at concentrations below 100 µM, better tolerated than the α-{P_2W_{18}}-chitosan nanoparticles and the pristine α-{P_2W_{18}}.

Cases in which POMs cytotoxicity is unchanged by the encapsulation were also reported in the literature, e.g. $[Eu(SiW_{11}O_{39})_2]^{13-}$ nanocomposites with CMC,[230] and nanoparticles of

$K_7[P_2W_{17}(NbO_2)O_{61}]\cdot 13H_2O$ with trimethyl chitosan,[199] showed no difference in cytotoxicity compared to the pristine POMs.

The effect on the cytotoxicity of the POMs upon encapsulation seems to be dependent both on the POM and the polymer used for nanoparticle preparation.

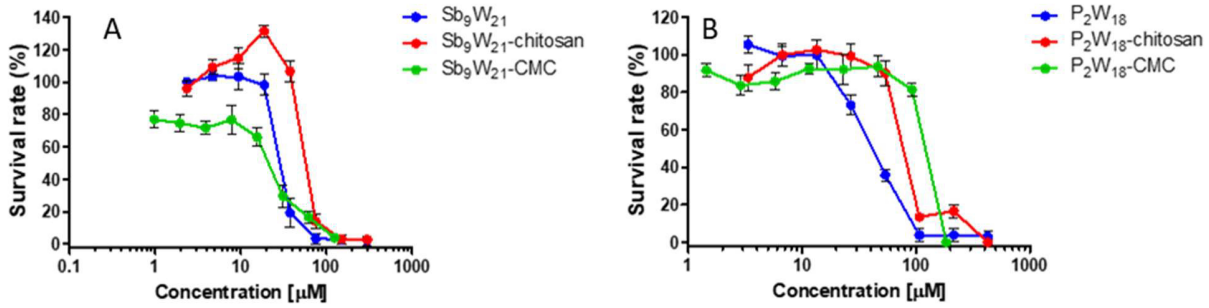

Figure 3.26. Cytotoxicity results on MRC-5 cells of {Sb_9W_{21}}, {Sb_9W_{21}}-chitosan and {Sb_9W_{21}}-CMC nanoparticles (A) and of α-{P_2W_{18}}, α-{P_2W_{18}}-chitosan and α-{P_2W_{18}}-CMC nanoparticles (B).

The cytotoxicity of pristine chitosan and CMC, either in solution either in nanoparticle form, was investigated. In Figure 3.27 the cytotoxicity results for pristine chitosan and CMC on HeLa cells are reported. Chitosan in solution and in nanoparticle form displayed a slightly different cytotoxic profile: chitosan in nanoparticle form exerted higher toxicity compared to chitosan in solution. Moreover, chitosan in both the investigated forms is more harmful for cells compared to CMC, which did not show any toxic effect at concentration below 4 and 2.5 mg/mL for dissolved and nanoparticle form, respectively.

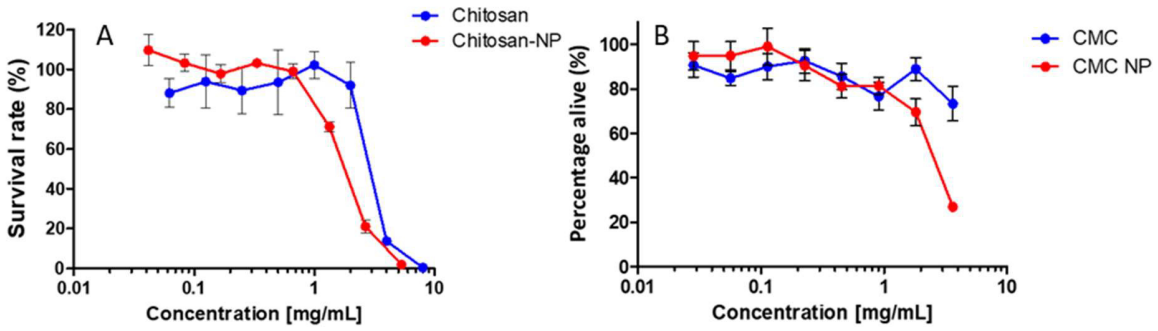

Figure 3.27. Survival rate on HeLa cells of chitosan in solution and as nanoparticles (A), as well as CMC in solution and CMC nanoparticles (B).

On MRC-5 the cytotoxicity of chitosan and CMC either in solution either in nanoparticle form was similar, with chitosan displaying again higher cytotoxicity compared to CMC (Figure 3.28). The higher cytotoxicity of the positively charged chitosan nanoparticles compared to CMC, which are negatively charged, is confirmed by similar studies. In fact gold particles functionalized with cationic side chains were found to be more cytotoxic compared to the one functionalized with anionic side chains.[231]

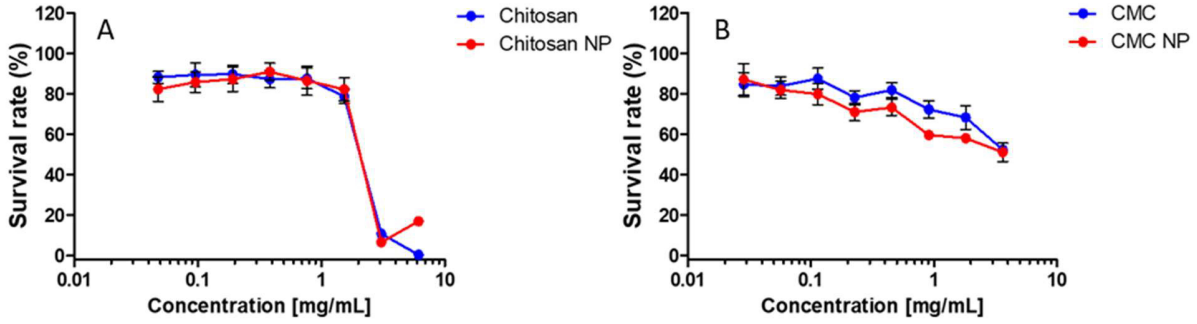

Figure 3.28. Survival rate on MRC-5 cells of chitosan in solution and as nanoparticles (A), as well as CMC in solution and CMC nanoparticles (B).

On that basis, the toxicity displayed by chitosan nanocomposites at the highest concentration is caused by the intrinsic toxicity of the polymer, however, at lower concentrations the exerted toxicity is related to the synergistic action of both components of the nanoparticle. In view of these results, future *in vivo* experiments should be planned, optimizing the concentration of POM and polymer used for the preparation of the nanocomposites, in order to exclude the toxicity of the latter.

The cytotoxic activity of $\{Sb_9W_{21}\}$ and α-$\{P_2W_{18}\}$ and their nanocomposites was compared to the reference anticancer compound $\{Mo_7O_{24}\}$. In both the cell lines $\{Mo_7O_{24}\}$ exhibited no significant activity even when high concentrations were applied (1 mM), while for $\{Sb_9W_{21}\}$ and α-$\{P_2W_{18}\}$ a much lower concentration was sufficient to descend below the detection limit of the method. For $\{Mo_7O_{24}\}$, however, the cytotoxicity dramatically increases upon encapsulation with both chitosan or CMC (Figure 3.29). The reason of the enhanced toxicity might be attributed to the reduction of $\{Mo_7O_{24}\}$ by chitosan. It has been in fact observed that the reduced species of $\{Mo_7O_{24}\}$ exerted significantly higher cytotoxicity on AsPC-1 and MNK-45 cell lines.[181,182]

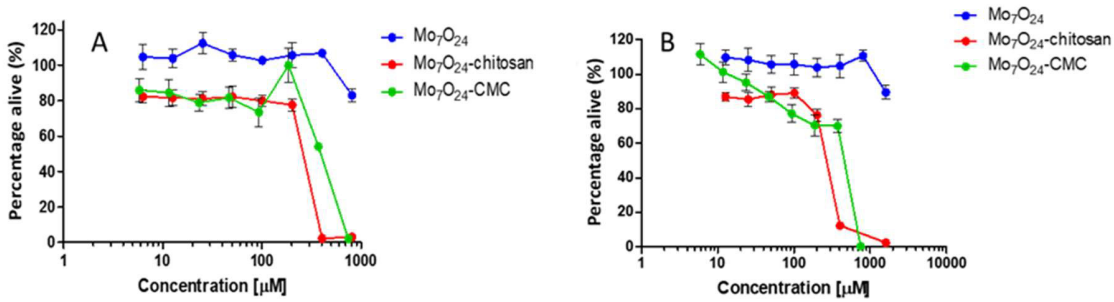

Figure 3.29. Survival rates expressed as percentage on HeLa (A) and MRC-5 (B) cells, after 24 h treatment with {Mo_7O_{24}}, {Mo_7O_{24}}-chitosan and {Mo_7O_{24}}-CMC.

{Mo_7O_{24}}-chitosan nanocomposites can open up applications in cancer therapy due to their selective targeting characteristics. Generally, cancer tissues are characterized by acidic extracellular pH (down to 5.7),[232] which allows them to enhance the uptake of nutrients and to proliferate inside the organism.[233] {Mo_7O_{24}}-chitosan nanoparticles could exert their cytotoxic effect on the cancer cells upon injection in the cancer tissue, where they are stable due to the acidic pH. The chitosan nanoparticles would diffuse out of the cancer cells and when the physiological pH (7.2-7.3) will be restored, the polymer might precipitate eventually impairing the transport of nutrients. The pristine POM would be gradually released from the chitosan nanoparticle, after enzymatic degradation/digestion of the polymer. The two separate components would be in the healthy tissue at not-cytotoxic concentration and would be then eliminated by the organism. Other POMs which exhibit and increased cytotoxicity upon chitosan encapsulation could also be applied in the treatment of cancer, according to the suggested approach.

An alternative approach involving CMC nanoparticles in anticancer therapy could consist in their injection into the blood stream. A good candidate among the investigated nanocomposites are the {P_2W_{18}}-CMC nanoparticles. {P_2W_{18}}-CMC nanoparticles exerted lower toxicity than the pristine POM on normal cells (Figure 3.26b). Due to their size below 200 nm and their negative charge, they would accumulate in the cancer tissue because of the EPR effect, thus reducing the damage of the healthy tissue. POM-CMC nanoparticles, which possess higher toxicity on cancer cells compared to normal cells (Figure 3.25) undergo precipitation at acidic pH and therefore further accumulation in the cancer area. There, CMC could be degraded by enzymes releasing the

pristine POM, e.g. α-{P_2W_{18}} or α-, β- and γ-{P_2W_{18}}, which would then eliminate the cancer cells due to their high cytotoxicity. A surprising difference in the cytotoxic effect between the α-isomer and the isomeric mixture of α-, β- and γ-{P_2W_{18}} was observed on HeLa cells (Figure 3.30). Moreover, the encapsulation of α-, β- and γ-{P_2W_{18}} in both chitosan and CMC reduced the cytotoxicity compared to the pristine mixture, whereas for the α-{P_2W_{18}} the cytotoxicity depended on the polymer.

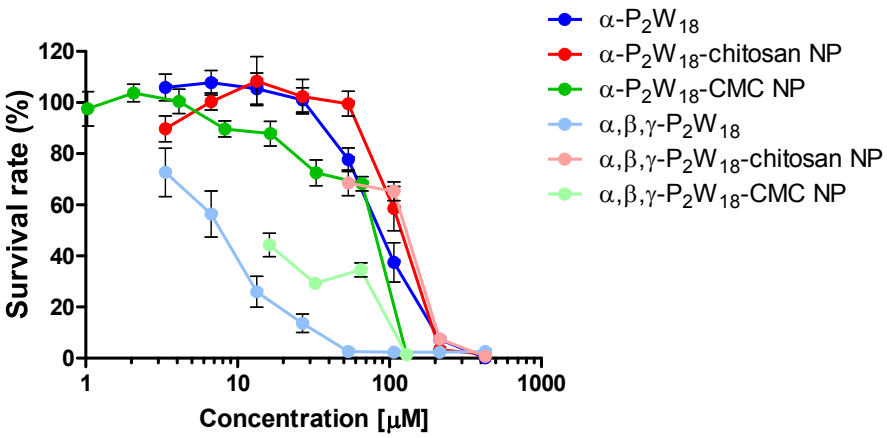

Figure 3.30. Survival rates expressed as percentage of HeLa cells after 24 h treatment with α-{P_2W_{18}} and α-, β- and γ-{P_2W_{18}} and correspondent nanocomposites with chitosan and CMC.

The IC_{50} values calculated for α-{P_2W_{18}} were 83.42 and 39.05 μM for HeLa and MRC-5 cell lines, respectively. Previously reported IC_{50} values were calculated around 20 μM for MCF-7, SKOV-3 and HepG2 cancer cell lines, much lower than for HeLa and MRC-5 cell lines.[194] In the same study the mechanism of action of α-{P_2W_{18}} was investigated, suggesting an influence on the cellular redox reactions for the energy production by mitochondria which finally induces cellular death by apoptosis.

α-{P_2W_{18}} and α-, β- and γ-{P_2W_{18}} tested on HeLa cells showed a significant difference between their IC_{50} values (83.42 and 16.26 μM), which is most probably due to the change in the position of {WO_3} triad. In a computational study, the isomer α-1,2-{PTi_2W_{10}} exhibited a higher inhibition potential against the neuraminidase of a subtypes of the influenza virus A compared to the other isomers of {PTi_2W_{10}}.[234] The different orientation of the upper {WO_3} triad might enhance the interaction of the β- or γ-isomer with some cellular enzymes, causing an acute cytotoxic effect.

ICP-MS analysis is appropriate to quantify α-, β- and γ-{P_2W_{18}} uptake by the cells, which quantifies the total W content upon acidic digestion of the treated cells. In case of intracellular POM localization, another appropriate method for the isolation of the different organelles would be necessary to establish the cellular target of the POM. Moreover, cytotoxicity studies should be performed also on the pure β- and γ- isomers in order to correctly attribute the responsible one for bioactivity.

To better understand the mechanism responsible for the high cytotoxicity of α-, β- and γ-{P_2W_{18}} flow cytometry experiments were performed.

3.3.5.2 Flow cytometry experiments

To further investigate the death mechanism of HeLa cells upon POM treatment, flow cytometry experiments were performed. The isomeric mixture of α-, β-, and γ-{P_2W_{18}} was chosen as representative compound due to the high cytotoxicity exerted on HeLa cells. After incubation for 24 h with α-, β- and γ-{P_2W_{18}} the cells were stained with three dyes, which emit in a specific wavelength range. Each dye provides information about the condition of the cell as well as about death mechanism: Annexin stains apoptotic cells, propidium iodide the necrotic one, whereas Hoechst stains all the cells.

The flow cytometer separates and counts single cells using the diffraction of light to evaluate the size and granulometry. Consequently, different cell populations are identified, and the eventual presence of unrelated particles and cell clusters can be excluded from the final plot. At the same time, the fluorescence signal of the stain is related to a defined cellular population. An untreated sample was used as negative control and a heat-treated sample as positive control. In the bivariate dot plot of the untreated cells 80% of the population was found to be alive (below left), while around 20% of the cells suffered from the trypsinization and were dead (Figure 3.31a). The positive control showed a population of 30% of surviving cells, revealing that the used conditions (2 min, 80 °C) were too mild to kill the entire cellular population (Figure 3.31b). The sample treated with α-, β- and γ-{P_2W_{18}} at a concentration close to the IC_{50} showed that 99% of the cell population was dead (Figure 3.31c). The death pathway evidenced by flow cytometry involves both necrosis and apoptosis, even if necrosis seems to be the major mechanism involved. These findings on the death mechanism associated with α-, β- and γ-{P_2W_{18}} complement the results

obtained in a previous study, where only apoptosis was detected.[194] To improve the quality of the data for more precise conclusions on the α-, β- and γ-{P_2W_{18}}-associated death mechanism, further experiments would be necessary where the effect of the concentration of the POM and the contribution of each dye are considered.

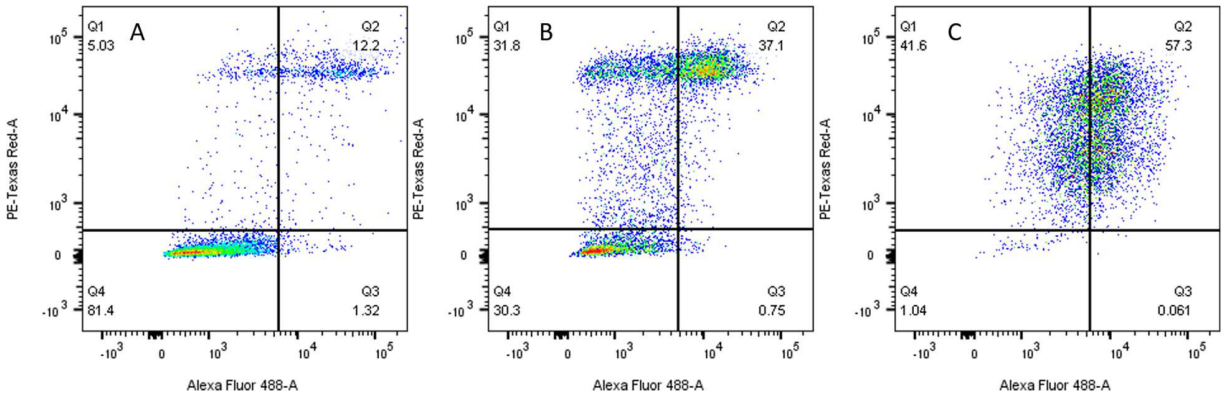

Figure 3.31. Bivariate dot plot of the negative control (A), the positive control (B) and of the cells treated with 10 µM α-, β- and γ-{P_2W_{18}} (C).

3.3.5.3 Cytotoxicity of other POMs

Alongside the cytotoxicity of {P_2W_{18}}, {Sb_9W_{21}} and {Mo_7O_{24}}, other synthesized POMs and their respective chitosan or CMC nanoparticles were tested on HeLa cells.

The Wells-Dawson {P_2Mo_{18}}, an isostructural form of α-{P_2W_{18}}, was encapsulated into chitosan and tested on HeLa cells. The cytotoxicity of the pristine and encapsulated form of both Wells-Dawson was compared (Figure 3.32). {P_2Mo_{18}} and corresponding chitosan nanoparticles showed lower cytotoxicity compared to {P_2W_{18}}, the cytotoxicity dropped to zero at concentrations below 100 µM. Interestingly, chitosan encapsulation enhanced the toxicity of {P_2Mo_{18}}, whereas for {P_2W_{18}} the opposite behavior is observed. It can be concluded that the Wells-Dawson structure is not the only parameter which influences the cytotoxicity, but that also the size of the POM and the elemental composition contribute to the final cytotoxicity of both the pristine POM and of the nanocomposites.

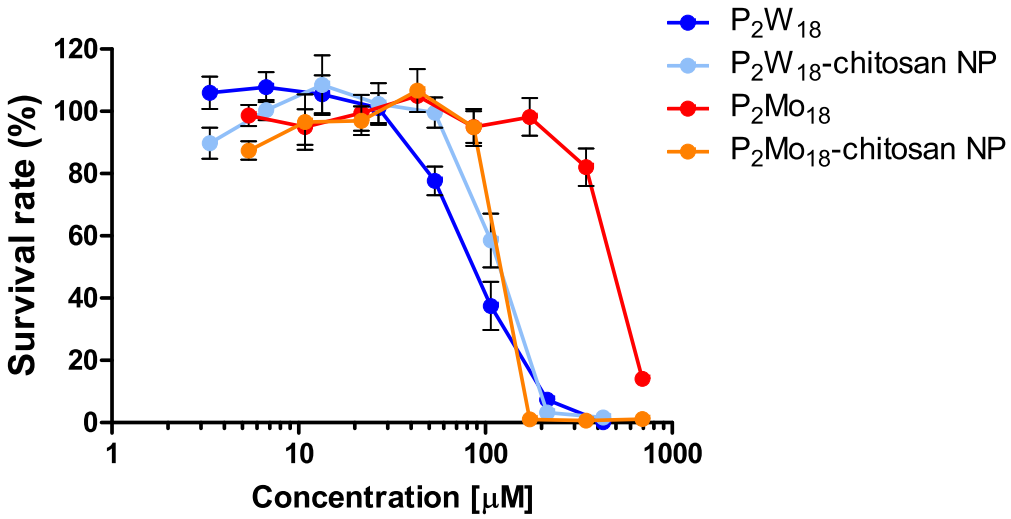

Figure 3.32. Cytotoxicity results for HeLa of {P_2Mo_{18}}, {P_2Mo_{18}}-chitosan nanoparticles, α-{P_2W_{18}} and α-{P_2W_{18}}-chitosan nanoparticles.

{Mo_8O_{26}} showed no cytotoxic effect on HeLa cells at the tested concentrations (Figure 3.33), as well as {Mo_7O_{24}}. The encapsulation either with chitosan or CMC led to an increased toxicity, as in the case of {Mo_7O_{24}}. In view of these findings, it can be concluded that the encapsulation of hepta- and octa-molybdates originates more cytotoxic species. The formation of the reduced species formed from the interaction of the polymolybdate and the chitosan may explain the enhanced toxicity of the chitosan nanocomposites.[181,182]

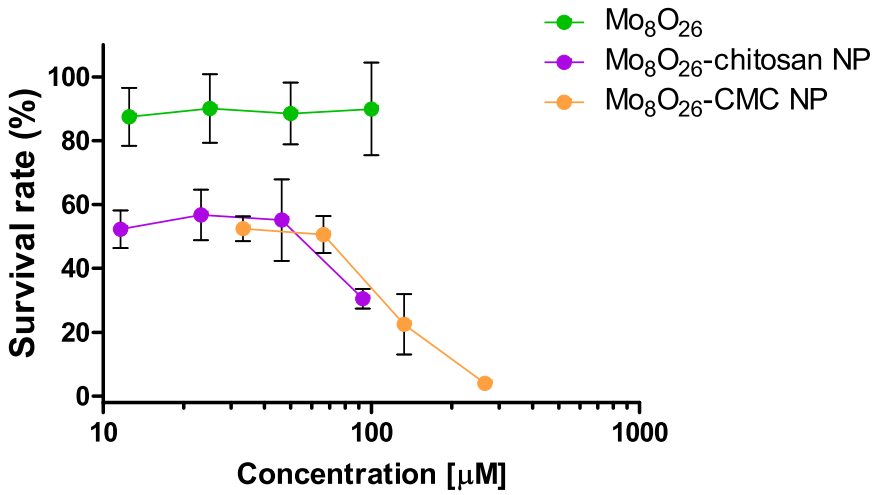

Figure 3.33. Cytotoxicity results for HeLa of {Mo_8O_{26}}, {Mo_8O_{26}}-chitosan and {Mo_8O_{26}}-CMC.

Two Keggin-type POMs, namely $\{SiMo_{12}\}$ and $\{PTi_2W_{10}\}$, were tested and both exhibited low cytotoxicity at the tested concentrations. Likewise, $\{PTi_2W_{10}\}$ toxicity tested on rats after 14 d of treatment was considered reversible and not severe.[235] Pristine $\{SiMo_{12}\}$ was more cytotoxic than the corresponding chitosan nanoparticles, whereas $\{PTi_2W_{10}\}$ showed an opposite behavior compared to its CMC nanoparticles. Further investigations on a broader range of concentrations would be necessary to confirm these observations.

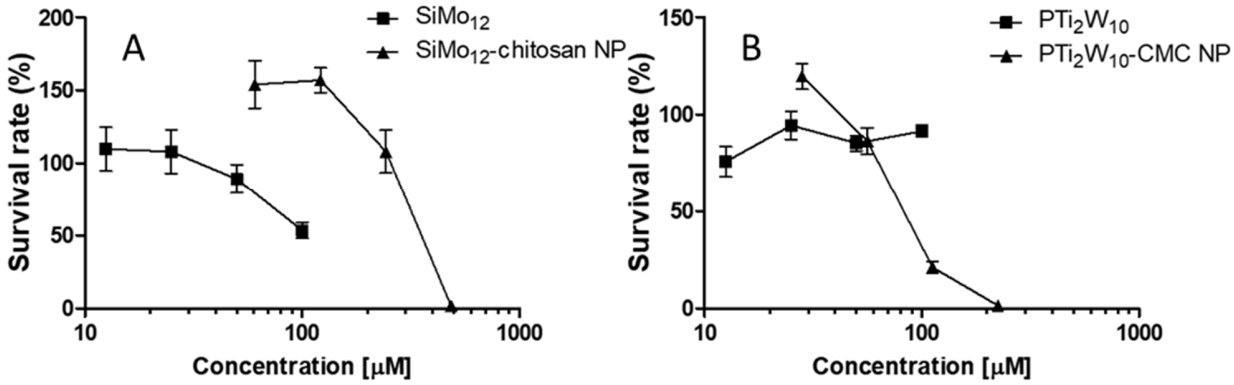

Figure 3.34. Cytotoxicity results for HeLa of $\{SiMo_{12}\}$ and -chitosan nanoparticles (A) and $\{PTi_2W_{10}\}$ and -CMC nanoparticles (B).

3.4 Conclusions

The polyoxometalates $\{Sb_9W_{21}\}$, α-$\{P_2W_{18}\}$, as well as other POMs with interesting and promising properties for medical applications, were synthesized and characterized in detail. The preparation of nanoparticles combining the above POMs with chitosan and CMC was improved and nanocomposites with a narrow size range (around 100-200 nm) were achieved. Moreover, the protocol for a clean visualization of POM-chitosan nanoparticles through electron microscopy (SEM) was optimized: acetic acid is a more convenient medium for the solubilization of chitosan, because it prevents NaCl precipitations.

$\{Sb_9W_{21}\}$ and $\{P_2W_{18}\}$ and the prepared nanocomposites did not show any particular antibacterial activity, thus highlighting their possible use for bacteria-friendly applications, where the local flora should not be harmed during, for example, anticancer or antiviral treatment.

POMs and their nanocomposites were tested on HeLa and MRC-5 cell lines. $\{Mo_7O_{24}\}$ was used as reference compound because of its well documented anticancer properties. However, $\{Mo_7O_{24}\}$

showed lower cytotoxicity against both the tested cell lines, while α-{P_2W_{18}} and {Sb_9W_{21}} exhibited higher toxicity. Surprisingly, the isomeric mixture of α-, β- and γ-{P_2W_{18}} exerted higher cytotoxicity compared to the pure α isomer. Further experiments should be performed for in depth investigation of the anticancer activity of the isomeric mixture by isolating the pure isomers and performing ICP-MS analysis on treated cells for cellular uptake.

The effect on the cytotoxicity of POMs upon encapsulation was investigated. However, the cytotoxic effect was not univocal: the cytotoxicity of the nanocomposite could be either increased or reduced, depending on the POM and the matrix used for the encapsulation. Furthermore, the tested cell lines play a role in defining the cytotoxicity. The rational design of POM-chitosan and POM-CMC nanocomposites is thus not yet feasible without further test experiments due to the many parameters involved in the overall cytotoxic effect. Any POM-chitosan and POM-CMC nanocomposites should be evaluated individually. Moreover, it is essential for biomedical applications to consider the intrinsic toxicity of the encapsulating agent. The cytotoxic effect should be attributed to the nanocomposite and the POM therein - and not by the encapsulating agent itself.

Two possible ways for selective cancer targeting were proposed and they benefit from the pH dependent stability of chitosan and CMC. Further in *vitro* and in *vivo* experiments could be performed to verify the feasibility of POM-chitosan and POM-CMC nanocomposites as pH sensitive drugs.

The synthesis and characterization of {Sb_9W_{21}}, α-{P_2W_{18}} and {Mo_7O_{24}} and respective nanocomposites, as well as their cytotoxicity on HeLa and MRC-5 are reported in a manuscript that will be submitted in the next months.

3.5 Appendix - crystallographic tables

Table 3.3. Crystallographic data of {Sb_9W_{21}}.

Empirical formula	Na O_{86} Sb_9 W_{21}
Formula weight	6355.46 g·mol^{-1}
Temperature	183 K
Radiation wavelength	0.71073 Å
Crystal system	hexagonal
Space group	*P*-62c
a	17.3851(4) Å
b	17.3851(4) Å
c	24.0907(16) Å
α	90°
β	90°
γ	120°
Volume	6305.7(5) $Å^3$
Z	2
Density calcd	3.347 g·cm^{-3}
Absorption coefficient	21.031 mm^{-1} (Gaussian)
Crystal size	0.311 × 0.184 × 0.047 mm^3
Independent reflections	4407 [R_{int} = 0.0660]
Reflections collected	40708
θ range	2.343-26.364°
Completeness to θ = 26.32°	0.9981
F(000)	5424
Data/restraints/parameters	4407/0/110
$R_1[I>2\sigma(I)]^a$	0.1251
$wR_2[I>2\sigma(I)]^b$	0.3223
$R_1{}^a$ (all data)	0.1296
$wR_2{}^b$ (all data)	0.3347
Goodness-of-fit on F^2	1.245

Table 3.4. Crystallographic data of α-{P_2W_{18}}.

Empirical formula	$K_6P_2W_{18}O_{62}\cdot 14H_2O$
Formula weight	1337.54 g·mol^{-1}
Temperature	183 K
Radiation wavelength	0.71073 Å
Crystal system	triclinic
Space group	*P*-1
a	12.8118(5) Å
b	14.7165(6) Å
c	19.8231(7) Å
α	70.062(4) °
β	80.413(3) °
γ	64.400(4) °
Volume	3167.8(2) Å^3
Z	2
Density calcd	5.055 g·cm^{-3}
Absorption coefficient	33.108 mm^{-1}
Crystal size	0.317 × 0.138 × 0.136 mm^3
Independent reflections	21398 [R_{int} = 0.0586]
Reflections collected	39528
θ range	2.186-33.082°
Completeness to θ = 30.44°	0.999
F(000)	4168
Data/restraints/parameters	21398/0/939
$R_1[I>2\sigma(I)]^a$	0.0614
$wR_2[I>2\sigma(I)]^b$	0.1489
$R_1{}^a$ (all data)	0.0749
$wR_2{}^b$ (all data)	0.1584
Goodness-of-fit on F^2	1.105

4. Chitosan-TGA: synthetic approaches

The functionalization of chitosan with thioglycolic acid (TGA) turned to be one of the major challenges in the present thesis. The reported experimental conditions used to functionalize chitosan with TGA are straightforward and do not present any obvious issues. Notwithstanding, under these conditions the substitution degree for chitosan-TGA observed by different group members was extremely low compared to the results recently reported by *Bernkop-Schnürch et al.* in 2015.[236] Although several attempts were made to reproduce the results published for the reported procedures, the expected results were not achieved. This may be due to apparently minor, but effectively quite important parameter changes, so that the original synthesis was rationally modified to improve the DS.

The most important changes involve the use of inert reaction conditions, varying amounts of TGA and EDC, the activation of TGA by N-hydroxysuccinimide, the activation of TGA separately before the reaction, the addition of the reagents in a different order, in addition to the variation of pH, temperature and reaction time. The reaction between glucosamine, the monomeric form of chitosan, and thioglycolic acid was also investigated, unfortunately without any positive results. The DS was calculated from elemental analysis data. The modifications proposed could improve the extent of the substitution, however, alternative synthetic routes were explored to further enhance the functionalization of chitosan with the thiol moiety -CH_2SH. The Schiff reaction with mercaptoacetaldehyde and the reaction with the previously prepared TGA acyl chloride were performed to directly functionalize the amine groups of chitosan.

4.1 Materials and methods

4.1.1 Materials

Chitosan with different DD and MW (85/5, 85/10, 85/20, 85/100 and 95/20) was purchased from Heppe Medical Chitosan (Halle (Saale), Germany). Thioglycolic acid (97%) was purchased from abcr GmbH (Karlsruhe, Germany). TGA with purity > 99% was purchased from Sigma-Aldrich (Buchs, Switzerland), as well as all the reagents which are not here reported. N-(3-dimethylaminopropyl)-N'-ethylcarbodiimide hydrochloride, known as EDC or EDAC (98%, 99%, and crystalline) was purchased from Sigma-Aldrich or from abcr GmbH (98%).

Mercaptoacetaldehyde as mixture of monomer and dimer (8:2) was purchased from Proactive Molecular Research (Florida, USA). 3-(4,5-dimethylthiazol-2-yl)-2,5-diphenyltetrazolium bromide (MTT) was purchased from Alfa Aesar (Heysham, UK).

4.1.2 Reaction with EDC

To functionalize chitosan with TGA previously published protocols were accurately applied.[87,146] For clarity, the original procedure is briefly reported:

4 mL 1 M HCl were added to 500 mg of chitosan, stirred for 15 min, and 46 mL water were added to obtain a 1% (w/v) chitosan solution. After chitosan was completely dissolved, EDC was added to obtain a final concentration of 50 mM (1.246 g). After dissolution of EDC, 500 mg of TGA were added. The pH of the reaction was adjusted to 5. The reaction mixture was incubated for 3 h at room temperature under permanent stirring. The product was dialyzed in cellulose membrane tubing with a molecular cut off of 12 kDa in the dark at 4 °C against different media, as described below, for at least 75 h. The following media were used and changed twice a day: 5 mM HCl (day 1), 5 mM HCl + 1% (w/v) NaCl (day 2 and day 3), and 1 mM HCl (day 4). The product was then freeze dried for 48 h and stored in the dark at -20 °C until further use.

Several conditions were later modified: temperature, time, pH, type of chitosan, supplier and purity grade of EDC and TGA, order of addition of the reagents, use of N-hydroxysuccinimide (HAS) to activate TGA prior to reaction, as well as the external condition of the reaction set-up (dark and/or in inert atmosphere). The addition of undissolved chitosan to the reaction mixture was also tested. The conditions of the synthesis of selected chitosan-TGA samples are summarized in Table 4.1. The reactions were always performed with 500 mg of pristine chitosan.

Table 4.1. Synthesis conditions used for the preparation of selected chitosan-TGA samples.

Label	**Start. Mat.**	**TGA** (g)	**EDC** (g)	**HAS** (g)	**T** (°C)	**Time** (h)	**Comments**
MAC-A-1	85/5	0.5	1.2	//	RT	3.5	Water degassed
MAC-A-14	85/5	0.5	1.8	//	RT	3	Inert conditions
MAC-A-22	85/100	0.5	1	//	RT	2	Inert conditions
MAC-B-8	85/5	0.53	1.1	//	55	5	Inert conditions
MAC-B-20	85/10	0.5	1.2	//	RT	3	Normal with light
MAC-B-24	85/10	2.65	1.3	//	RT	21	Inert, EDC first
MAC-B-37	95/20	1	1.2	//	40	20	Dark and inert
MAC-B-38	95/20	1	1.2	//	40	20	Dark and inert
MAC-C-3	95/20	1	0.4	//	RT	3	Inert, TGA first
MAC-C-4	95/20	0.5	0.4	//	RT	3	
MAC-C-5	95/20	0.5	1	//	RT	3	
MAC-C-12	85/20	1	0.6	//	RT	3	
MAC-C-13	85/20	0.53	1	//	RT	3	New TGA, inert
MAC-C-20	95/20	0.5	0.5	//	RT	3	No pH setting, previous activation
MAC-C-21	95/20	0.5	1	//	RT	3	pH 4.5 setting, previous activation
MAC-C-30	95/20	1	2	//	RT	5	
MAC-C-33	95/20	1	1	1.24	RT	3	No pH setting
MAC-C-35	85/20	1	1	1.24	RT	3	TGA EDC controlled pH 4.2
MAC-C-41	95/20	1.3	1.2	//	RT	5	Solid chitosan, no pH setting
MAC-C-43	85/20	0.53	1	1.2	RT	3	Solid chitos., pH 4.5 activation TGA
MAC-C-47	95/20	4	1.5	//	RT	65	Large volume
SC-1	85/20	0.5	1.2	//	RT	3	Conducted by another researcher
MAC-D-8	90/20	0.02	0.2	0.12	RT	16	Anh, inert dark prev. activation
MAC-D-9	90/20	0.5	0.5	0.31	RT	16	Anh, inert dark prev. activation
MAC-D-13	90/20	0.52	0.6	0.35	RT	21.5	Previous activation
GG-B-23	85/20	0.5	1.2	//	RT	3	Conducted by another researcher

4.1.3 Schiff Reaction

Two chitosan-TGA samples were prepared by Schiff reactions with slightly varying procedures. MAC-C-31: 4 mL 1 M HCl were added to 500 mg of chitosan and left to stir for 15 min before 30 mL water were added. To this solution 1 g of mercaptoacetaldehyde dispersed in 20 mL water were added dropwise. The reaction mixture was warmed at 65 °C for 3 h, cooled to room temperature and dialyzed in cellulose membrane tubing with a molecular cut off of 12 kDa in the dark at 4 °C against different media, as described below, for at least 75 h. The following media were used and changed twice a day: 5 mM HCl (day 1), 5 mM HCl + 1% (w/v) NaCl (day 2 and

day 3), and 1 mM HCl (day 4). The product was then freeze dried for 48 h and stored in the dark at -20 °C until further use. The isolated material was a white polymer-like solid.

MAC-C-32: 4 mL 1 M HCl were added to 500 mg of chitosan and stirred for 15 min, and 30 mL water were added. After chitosan was completely dissolved, it was added dropwise to a previously prepared suspension of 2 g of mercaptoacetaldehyde in 20 mL water. The reaction mixture was warmed at 80 °C for 3 h, cooled to room temperature and left to stir during the weekend. Afterwards, the insoluble unreacted aldehyde was removed by filtration. The filtered solution was freeze dried for 48 h and stored in the dark at -20 °C until further use. The isolated material was a white polymer-like solid.

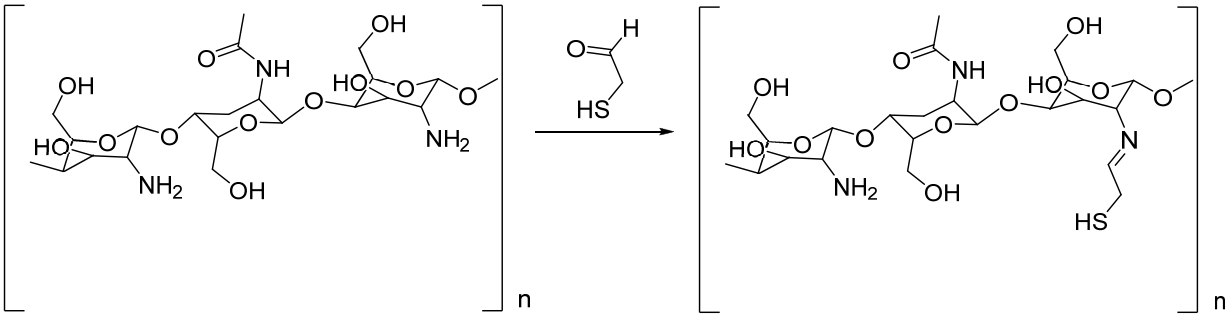

Figure 4.1. Reaction scheme of chitosan functionalization with mercaptoacetaldehyde.

4.1.4 Reaction of chitosan with TGA acyl chloride

Two chitosan-TGA samples were prepared with TGA acyl chloride following slightly varied procedures.

MAC-C-29: The reaction was performed under anhydrous and inert conditions. 12 mL of anhydrous dimethylformamide (DMF) were degassed in a round bottom flask with septum for 10 min prior to the addition of 1.29 g of $SOCl_2$. 1 g of TGA was added dropwise with a syringe. After 1 h, a solution of chitosan, prepared by dissolving 500 mg chitosan with 4 mL of HCl (1 M) in 20 mL of water, was added dropwise to the reaction mixture. After complete addition of chitosan, the reaction mixture was left at room temperature. After 3 h, 50 mL of water were added, and the pH of the solution was set to 9 to precipitate chitosan. The precipitate was washed

with deionized water and dried in air for 4 d. 5 mL of 1 M HCl were added to the dry product, left to react for 1 h and then 50 mL deionized water were added to solubilize the product. The dissolved product was dialyzed according to the protocol reported in section 4.1.3 and then lyophilized and stored in the dark at -20 °C until further use. A brownish fluffy solid was obtained.

MAC-C-36: The reaction was performed under anhydrous and inert conditions. 12 mL of anhydrous DMF and 1 g of TGA were degassed in a round bottom flask with nitrogen flow. After 10 min, 1.29 g of $SOCl_2$ were added dropwise to the reaction mixture. After 1 h a chitosan solution (300 mg of chitosan in 10 mL of acetic acid 1% v/v) was added dropwise. Precipitate formation was observed. After 1 h of reaction at RT the reaction mixture was dialyzed as described in section 4.1.3. After dialysis, a precipitate was removed by filtration and a brownish fluffy solid was isolated.

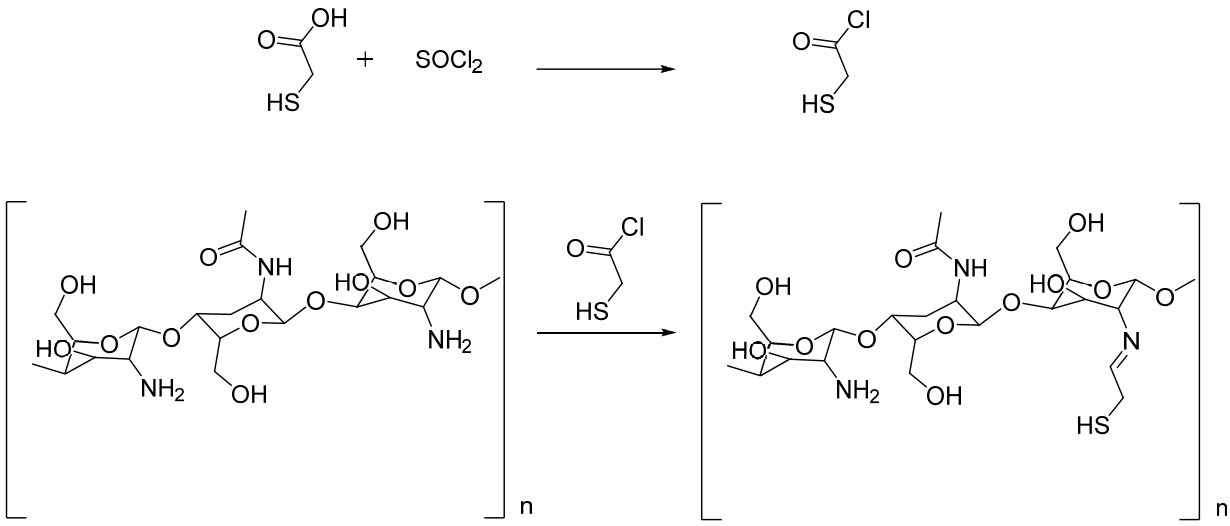

Figure 4.2. Reaction scheme for the preparation of TGA acyl chloride and its reaction with chitosan.

4.1.5 Characterization of the products

The products were characterized by ^{1}H-NMR spectroscopy, elemental analysis and Ellman test as described in section 2.2.3. Antimicrobial activity was tested with MTT (for bacteria cultivation and MTT assay conditions cf. section 2.2.4).

4.2 Results and discussion

In this section, the outcomes of the functionalization of chitosan with TGA are reported and correlated to the conditions used for the synthesis. Elemental analysis was performed to evaluate the DS and to quantify the total amount of sulfur bound to chitosan. TGA contains one sulfur atom and chitosan one nitrogen atom per sugar unit. Therefore, the molar ratio S/N can be calculated by dividing the percentage of each element by the molecular weight, which then affords the DS. The Ellman test was performed on representative derivatives to quantify and correlate the number of unreacted thiols to the conditions of the synthesis.

4.2.1 Considerations about the EDC reaction

The conditions which have major impact in the functionalization of chitosan-TGA were previously analyzed by *Bernkop-Schnürch et al.* during their first synthesis of such thiomers. In their first publication on chitosan-TGA, the impact of the pH and the ratio between chitosan and TGA on the concentration of sulfhydryl groups was investigated.[87] The highest concentration of sulfhydryl groups was achieved at pH 5, using a mass ratio of chitosan to TGA 1 : 1 (Figure 4.3).

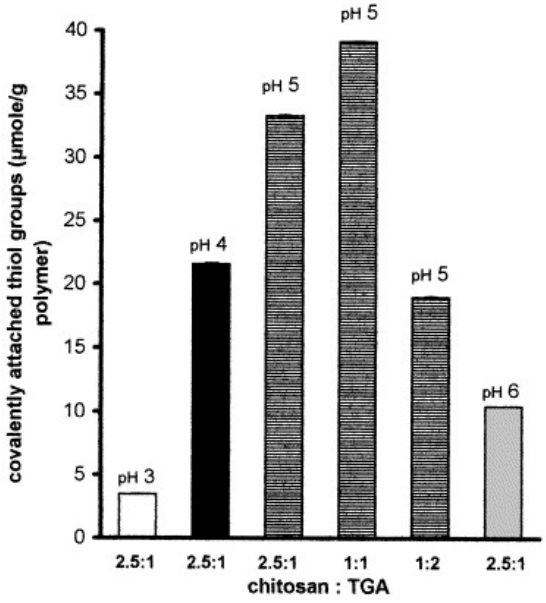

Figure 4.3. Concentration of thiol groups for chitosan-TGA correlated to the synthesis conditions.[87]

The functionalization of chitosan-TGA was evaluated by the Ellman test and a concentration of sulfhydryl groups of 40 µmol/g was calculated. All measured concentrations are very low and

would usually fall within the non-linear absorption range of the calibration curve typically recorded in our laboratory. Moreover, the authors did not report elemental analysis data in any of their publications. The conditions reported by *Bernkop-Schnürch* were reproduced by three different group members altogether: despite the operator change, the DS calculated by elemental analysis was always 1.3-1.5% (MAC-B-20, SC-1, GG-B-23) and the thiol concentrations were around 140 µmol/g. Although the thiol concentration was higher compared to the original paper, higher concentrations still appear to be possible to achieve, because in a more recent publication by *Bernkop-Schnürch at al.* the successful substitution of chitosan with higher TGA amounts was reported.[89] Although higher thiols concentrations (340 µmol/g) were achieved, no changes in the synthesis procedure were reported and the author always referred to the original synthesis of 2001.[87] However, higher amounts of TGA and EDC were used according to the experimental part[89] and the reaction procedure was slightly modified. For example, in a publication of 2015, TGA was previously activated by EDC and then dropwise added to the chitosan solution.[236] This rendered the reproduction of such procedures somewhat difficult. The pre-activation of TGA with and without the addition of N-hydroxysuccinimide (HAS) was also done in this work. HAS is usually adopted in peptide synthesis for the activation of carboxylic acids.[237] The reaction did not work as expected (MAC-C-20, -C-21 and -C-35) with achieved DS ranging from 0.1 to 1.5%.

It has been reported that the DS increases proportionally with the amount of TGA used in the reaction.[89,153,238] *Lee at al.* observed that a higher amount of TGA compared to the one used by *Bernkop-Schnürch's* group and a reaction time of 5 h led to a concentration of 360 µmol of thiol groups per gram of chitosan.[153] *Cathell at al.* prepared chitosan-TGA using a large excess of TGA (5 g) and a larger reaction volume (400 mL) obtaining a DS of 116% calculated from elemental analysis data.[238] A DS higher than 100 could signify that the hydroxy groups of chitosan were also functionalized or that the dialysis procedure was not successful. The synthesis conditions proposed by *Lee* and *Cathell* were reproduced as well, and DS values of 0.4 and 1.5% (MAC-C-30 and -C-47) were achieved.

In light of the above reproducibility issues, other less obvious parameters in the synthesis set-up which could influence the substitution degree were investigated. Both the absence of light and of oxygen in the reaction environment influenced the reaction outcome. However, other parameters such as the amount of TGA, time and temperature of the reaction had to be modified

to achieve higher DS. The chitosan-TGA samples with highest DS values were prepared under inert conditions, such as MAC-B-8 with a maximum DS of 3.54% and 140 µmol/g thiol concentration. The sample was prepared under nitrogen flow at 55 °C for 5 h using EDC of crystalline grade. The second highest DS of 2.52% (MAC-B-24) with a thiol concentration of 100 µmol/g was prepared using a higher amount of TGA (2.65 g) and a reaction time of 21 h. The low amount of free sulfur calculated from Ellman test results for both thiomers is probably due to the longer reaction times (and higher temperature) applied. In Table 4.2 the DS values of the most representative synthesized chitosan-TGA are summarized.

Table 4.2. DS of the most representative chitosan-TGA samples prepared with EDC activated reactions (bold: maximum degree of substitution).

Label	**Start. Mat.**	**DS** (%)
MAC-A-1	85/5	2.12
MAC-A-14	85/5	2.36
MAC-A-22	85/100	0.57
MAC-B-8	85/5	3.54
MAC-B-20	85/10	1.53
MAC-B-24	85/10	2.52
MAC-B-37	95/20	0.60
MAC-B-38	95/20	0.97
MAC-C-3	95/20	1.51
MAC-C-4	95/20	0.79
MAC-C-5	95/20	1.30
MAC-C-12	85/20	1.38
MAC-C-13	85/20	1.32
MAC-C-20	95/20	0.30
MAC-C-21	95/20	0.07
MAC-C-30	95/20	0.43
MAC-C-33	95/20	0.53
MAC-C-35	85/20	1.04
MAC-C-41	95/20	0.90
MAC-C-43	85/20	0.76
MAC-C-47	95/20	1.47
SC-1	85/20	1.42
MAC-D-8	90/20	1.06
MAC-D-9	90/20	0.84
MAC-D-13	90/20	1.48
GG-B-23	85/20	1.28

The functionalization of chitosan with TGA was successful to a certain extent. To investigate the effect of the substitution on the antimicrobial activity, higher DS were desired. Consequently, other synthetic approaches were investigated, i.e. the formation of a Schiff base and the reaction of chitosan with TGA acyl chloride (TGA-AC).

4.2.2 Other functionalization strategies

Several examples of chitosan functionalization with aldehydes were reported.[239] In fact, the amine groups of chitosan can form Schiff bases with aldehydes. The reaction between chitosan and mercaptoacetaldehyde (MAA) was performed and two products with DS of respectively 2.6 and 6.1% and thiol concentrations of 110 and 114 µmol/g, respectively, were achieved. The higher temperature and longer reaction time led to higher substitution degrees. The low amount of free sulfur is probably due to the presence of dimers in the starting material or to their possible formation under the conditions of reaction. The low solubility of MAA in water posed a reactivity issue. An alternative way to directly functionalize chitosan with TGA involves the formation of a TGA-AC intermediate, followed by its reaction with the amine groups of chitosan. The formation of the TGA-AC intermediate was performed with thionyl chloride in DMF which can as well catalyze the reaction under inert conditions.[240] The addition of the previously dissolved chitosan eliminates the excess of thionyl chloride, meanwhile TGA-AC also reacts with water to form TGA. The reaction is competitive with respect to the amine group of chitosan and water, which is present in excess. Nevertheless, DS values of 4.1 and 30.8 were achieved.

Table 4.3. Characteristics of chitosan derivatives synthesized via MAA and TGA-AC.

Label	**Start. Mat.**	**Reagent**	**SH** (µmol/g)	**DS**
MAC-C-29	95/20	TGA-AC	nd	4.1
MAC-C-36	95/20	TGA-AC	nd	30.8
MAC-C-31	95/20	MAA	110	2.6
MAC-C-32	95/20	MAA	114	6.1

For both chitosan-TGA samples synthesized via MAA and TGA-AC, the DS achieved could also be related to the residual starting material, which could not be removed by dialysis or filtration, because of the poor solubility in water. Moreover, the brownish color of the products isolated

from the acyl chloride synthesis could suggest the presence of some impurities. To verify the structure of the final products ^{1}H-NMR spectroscopy was performed. The presence of impurities was observed in the spectrum of sample MAC-C-36 with the highest degree of substitution, while in the spectra of MAC-C-29, -C-31 and -C-32 only the signals related to chitosan were present, while no signals related to impurities were observed. In view of these data, the Schiff base route can be considered as alternative to the reaction with EDC. To obtain higher DS values, the complete solubilization of both aldehyde and chitosan would be necessary, so that other solvent mixtures should be investigated. The purification process should also be improved to ensure the complete removal of the starting reagents.

4.3 MTT test results

Efforts to improve the DS of chitosan-TGA were made in the first place to investigate the effect on the antimicrobial activity compared to pristine chitosan or to less substituted chitosan-TGA. To this end, *E. coli* was preferred over the other strains testes in this work due to its high resistance towards chitosan. The MTT tests were performed under the same conditions as described in chapter 2, applying 2 and 4 mg/mL of compound and 30 and 60 min incubation time. Figure 4.4 shows the results of the MTT test at 2 mg/mL, 30 min of incubation on *E. coli* for selected chitosan-TGA samples.

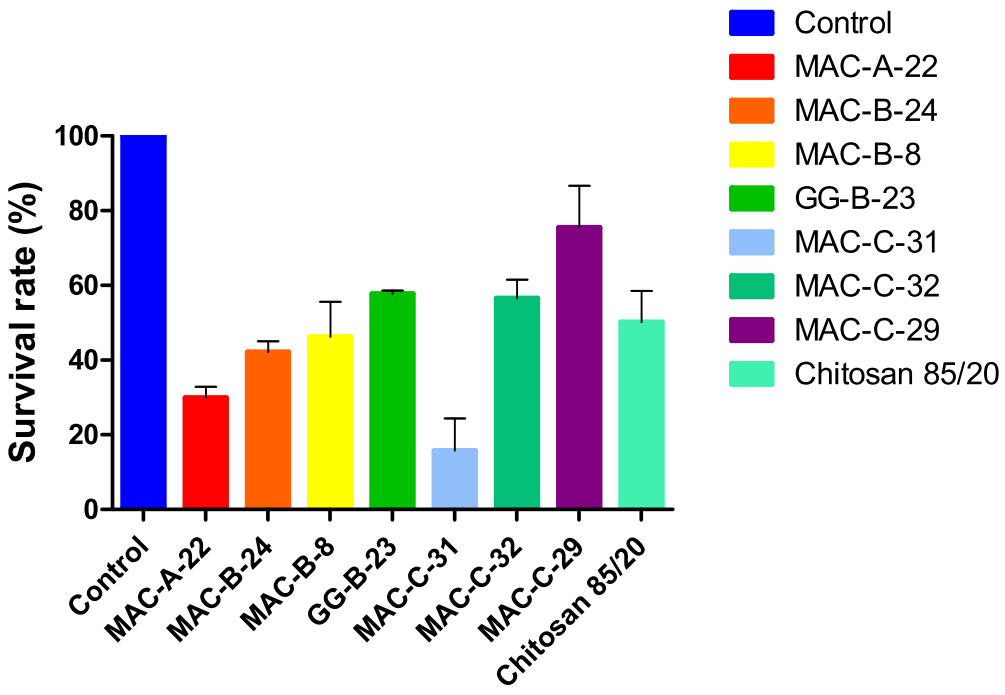

Figure 4.4. MTT results for different chitosan-TGA samples (2 mg/mL, 30 min of incubation vs. E. coli).

Focusing on the DS, the antimicrobial activity decreased with increasing DS (MAC-A-22, -B-24, -B-8). Surprisingly, the Schiff base MAC-C-31 with a DS of 2.63% was the most active compound of the series. The observed MAC-C-31 efficacy could also be due to the different starting material with a higher DD. The two samples with highest substitution degrees which were prepared from the same starting material (MAC-C-29, -C-32) display rather poor antimicrobial activity. MAC-C-29 showed lower antimicrobial activity, probably because of the low concentration of thiol groups. As mentioned in chapter 2, a high DS is not a necessary criterion for high antimicrobial activity: against certain strains, DS of 2-3% or lower (MAC-A-22, MAC-B-24 and MAC-C-31) are enough to obtain significant antimicrobial activity. Moreover, other characteristics, such as MW and DD have to be considered. A valuable tool to correlate the characteristics of chitosan thiomers (DD, MW and DS) and the antimicrobial properties could be chemometrics.

The preliminary biological data presented in this chapter are not yet conclusive. A broader selection of tested bacteria and more reliable and quantitative methods, such as plate counting, should be used.

4.4 Conclusions

Highly substituted TGA samples with sufficient quality for antimicrobial tests could not be obtained from literature protocols. After modifying the synthetic conditions, a maximum DS of 3.54% was achieved via EDC activated synthesis. Alternative reaction pathways led to higher DS values, but most probably some traces of the reagents were present after dialysis. The MTT experiments confirmed that a higher DS of the thiomers is not improving the antibacterial properties, while a DS of 2-3% led to maximum antibacterial activity.

5. Further chitosan functionalization

In this chapter, the synthesis and the characterization of chitosan functionalized with amino acids, salicylic aldehyde and isopropylsulfonyl chloride are reported, alongside with the antibacterial screening of chitosan functionalized with amino-acids against *E. coli and P. aeruginosa*.

5.1 Substitution of chitosan with different amino acids

Chitosan-L-Cysteine (L-Cys) was synthesized and screened together with other thiomers for antibacterial activity. Chitosan-L-Cys exhibited a very low antibacterial activity. Chitosan-L-Cys prepared with chitosan 85/20 (max. DD) at 4 mg/mL even enhanced the growth of the bacterial population over 1 h. Surprisingly, chitosan substituted with D-Cysteine (D-Cys) showed higher antimicrobial efficacy compared to the L-isomer. In view of these results, the antimicrobial activity of chitosan substituted with different L- and D-amino acids (AAs) was investigated. The original idea was to functionalize chitosan both with L and D isomers of cysteine, alanine, serine and lysine. In the end, only chitosan derivatives with L- and D-cysteine/alanine were characterized and tested for antimicrobial activity.

Chitosan was functionalized through EDC-activated amide bond formation, according to similar procedures used to prepare chitosan thiomers.[87] Furthermore, tert-butyloxycarbonyl (BOC) was considered as a protective group and serine-BOC was used to functionalize chitosan. The ^{1}H-NMR spectrum of a synthesized chitosan-serine displayed the signal assigned to BOC, i.e. the de-protection of the amine groups was not complete, probably because of the use of HCl instead of trifluoracetic acid. The signals related to the functionalization with serine were also present. Due to the de-protection problems encountered, it was decided to functionalize chitosan via the direct reaction with the amino acids, avoiding the BOC protection of the amine group. L-Ala-chitosan was synthesized using the protected L-Ala-BOC purchased directly from Sigma-Aldrich.

The synthesis conditions used to functionalize chitosan with AAs were similar to those used for the synthesis of thiomers, aiming for high DS. All the products were purified by dialysis and freeze dried as described in section 4.1.2. The chitosan-AAs prepared from 0.5 g chitosan 85/20 were prepared as reported in Table 5.1.

Table 5.1. Synthesis conditions applied for the preparation of chitosan-AAs.

Substituent	**Label**	**Start. Mat.**	**Reagent** (g)	**EDC** (g)	**T** (°C)	**Time** (h)
L-Cys	MAC-B-2	85/20	0.67	1.1	55	3
D-Cys	MAC-B-25	85/20	1.380	1.2	40	24
D-Cys	MAC-B-26	85/20	0.69	1.2	RT	3
L-Ala	MAC-C-28	85/20	1.012	0.5	RT	23
D-Ala	MAC-C-27	85/20	1.06	0.5	RT	21

Chitosan-L-Cys and -D-Cys were characterized by ^{1}H-NMR spectroscopy, Ellman test and elemental analysis. The ^{1}H-NMR spectrum of chitosan-L-Cys (MAC-B-2) and of chitosan-D-Cys (MAC-B-25) displayed no signals related to the substitution. The ^{1}H-NMR spectrum of chitosan-D-Cys (MAC-B-26) showed a peak at δ 2.72 related to the substitution with cysteine (Figure 5.1). Chitosan-D-Cys syntheses differ through the use of EDC without HCl. The presence in the ^{1}H-NMR spectrum of the signal at δ 2.72 ppm could be explained by the superior catalytic performance the HCl-free EDC. The Ellman test of chitosan-L-Cys and -D-Cys evidenced a low concentration of sulfhydryl groups (70 µmol/g). The DS calculated from elemental analysis data were 5% for chitosan-L-Cys (MAC-B-2) and lower for chitosan-D-Cys (1.3% and 1%, respectively for MAC-B-25 and -B-26).

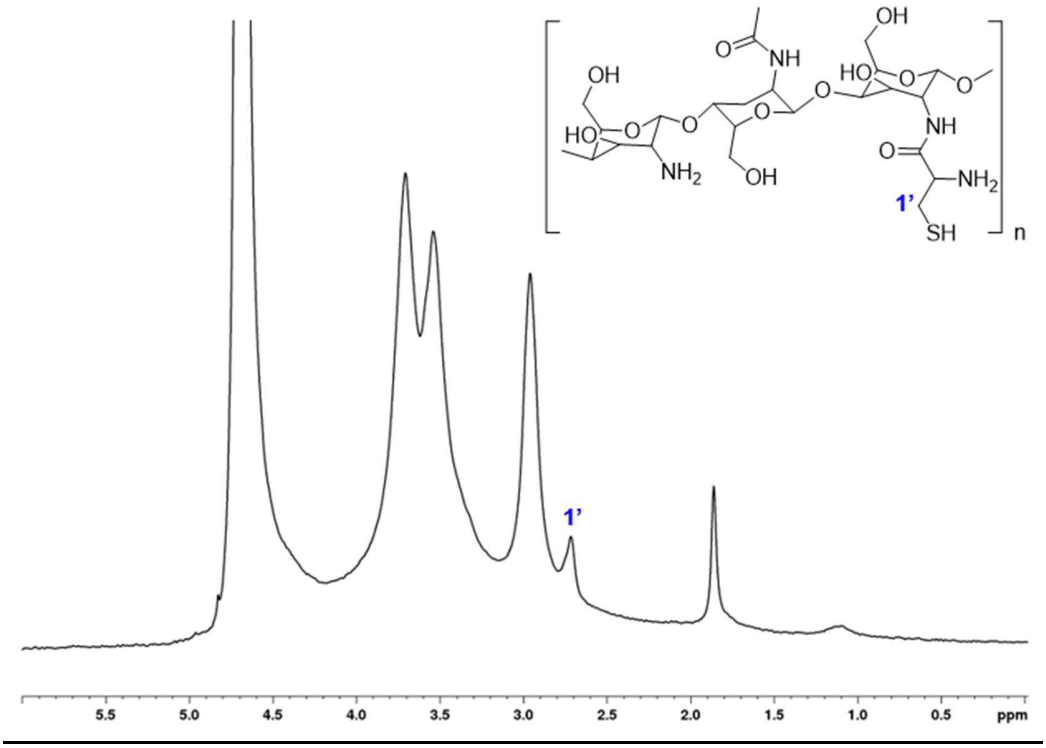

Figure 5.1. ^{1}H-NMR spectrum of chitosan-D-Cys (MAC-B-26) (400 MHz, D_2O, 298 K).

Chitosan-L-Ala and -D-Ala were characterized by ^{1}H-NMR spectroscopy and elemental analysis. The signals in the ^{1}H-NMR spectra related to the substitution were present for both isomers. The signal at δ 1.19 ppm can be assigned to the methyl group of Ala (singlet, doublet in theory) and the signal at δ 3.29 ppm to the proton in position 1' (Figure 5.2). The elemental analysis data of D-Ala (MAC-C-27) confirm the presence of an amino acid by the increased ratio of N/C compared to the pristine chitosan.

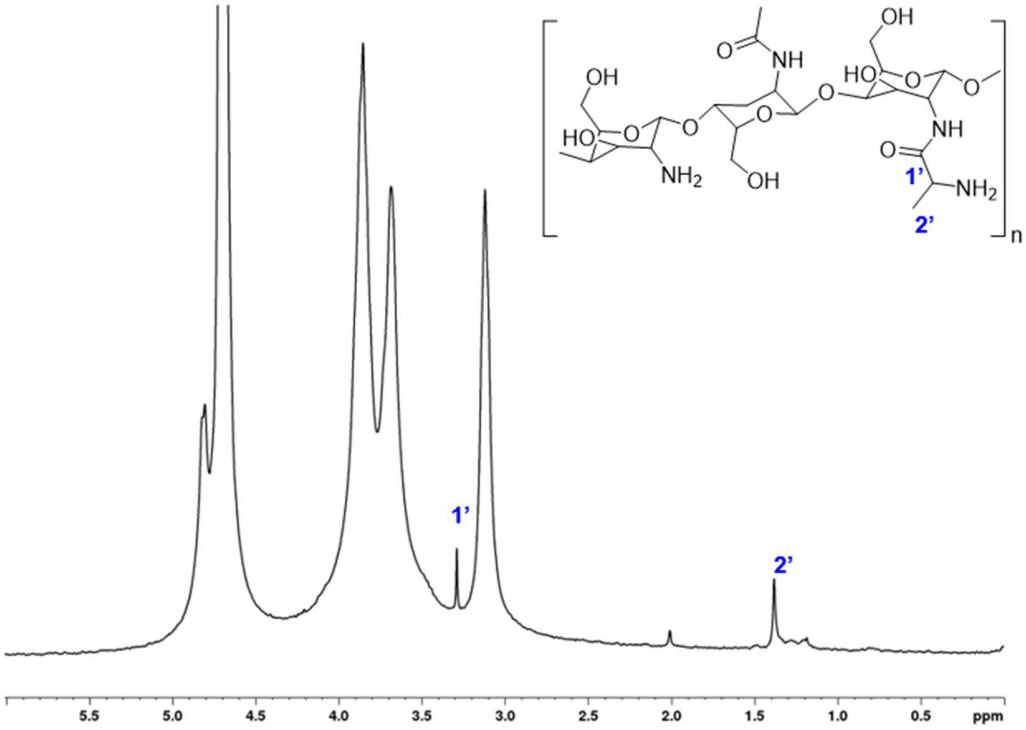

Figure 5.2. ^{1}H-NMR spectrum of chitosan-D-Ala (MAC-C-27) (400 MHz, D_2O, 298 K).

5.1.1 MTT test

Chitosan oligomers were previously functionalized with AAs to investigate the possible enhancement of the antibacterial properties of pristine oligomers,[241] however to the best of our knowledge the R stereoisomers were never considered.

Chitosan-Cys and -Ala were screened with the MTT assay on *E. coli* and *P. aeruginosa* according to the procedure in section 2.2.4. The results are summarized in Figure 5.3. Surprisingly, chitosan derivatives with D- and L- isomers of both Cys and Ala displayed significative different antimicrobial activity, with higher effects in the presence of the D-isomers. Substitution of chitosan with D- and L-Cys led to related behavior trends vs. *P. aeruginosa*.

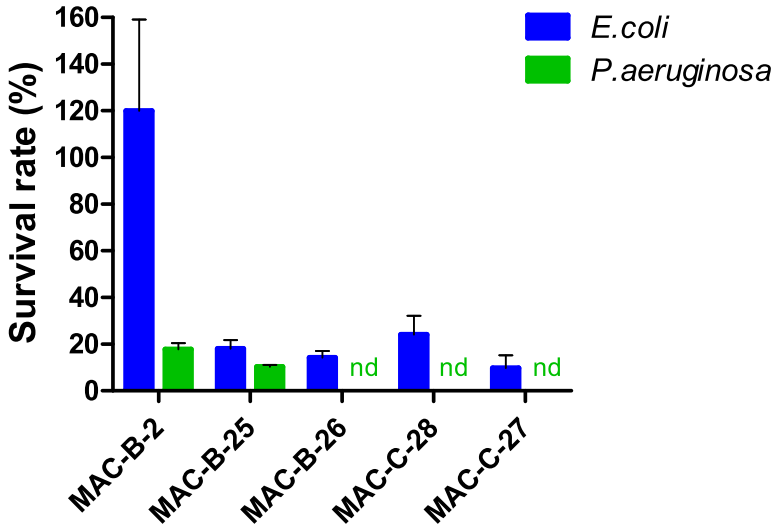

Figure 5.3. MTT results for different chitosan-AAs at 4 mg/mL, 60 min of incubation for E. coli and P. aeruginosa (nd = not determined).

This behavior could be attributed to the impairment of enzymatic metabolism through the D-amino acids. To further investigate the effect of the stereoisomerism of the AAs on the antibacterial activity of chitosan-AAs, PCA experiments would be necessary, as well as the evaluation of antibacterial activity of chitosan substituted with other types of AAs, both as D and L isomers.

5.2 Other functionalized chitosans

Chitosan was functionalized with salicylic aldehyde and with isopropylsulfonyl chloride to investigate the antimicrobial properties of these new compounds.

5.2.1 Chitosan-salicylic aldehyde

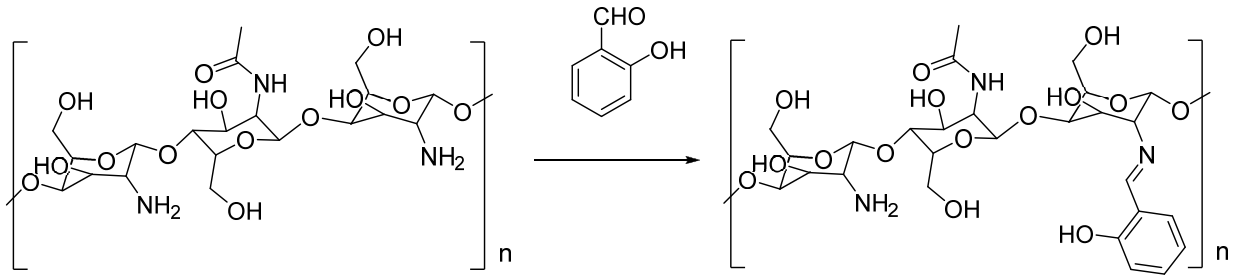

Figure 5.4. Reaction scheme of chitosan functionalization with salicylic aldehyde.

The direct reaction between chitosan and salicylic aldehyde led to the formation of a Schiff base. Chitosan was solubilized in 40 mL acetic acid (1% v/v) over 48 h prior to addition of the aldehyde. After 6.5 h at RT, the reaction mixture was extracted with ethanol. The yellow organic phase was concentrated at the rotary evaporator to give a yellow Plexiglas like polymer. The aqueous phase was dialyzed and freeze dried as reported in section 4.1.2. The FT-IR spectrum of the yellow solid showed the presence of the bands related to chitosan and to the aldehyde. The yellow solid was not soluble in water and therefore its antibacterial activity was not investigated. The ^{1}H-NMR spectrum of the freeze dried solid displayed the only signals of chitosan and none of the substituent.

5.2.2 Chitosan-2-hydrosulfonylpropane

The reaction was performed directly between chitosan, which was previously dissolved in 30 mL acetic acid (1% v/v) and isopropylsulfonyl chloride at RT for 6 h. The reaction mixture was filtered to separate the poorly soluble isopropylsulfonyl chloride, and the filtrate was dialyzed and freeze dried as reported in section 4.1.2. The ^{1}H-NMR spectrum confirmed the substitution, showing a douplet at δ 1.21 ppm corresponding to the methyl groups of the substituent (Figure 5.6).

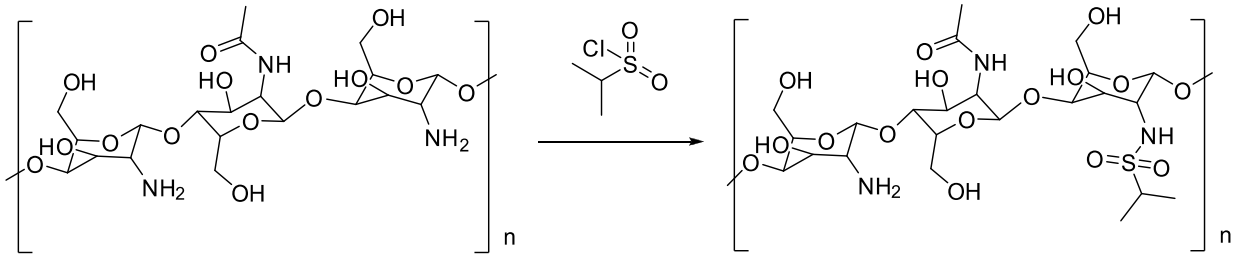

Figure 5.5. Reaction scheme of chitosan functionalization with isopropylsulfonyl chloride.

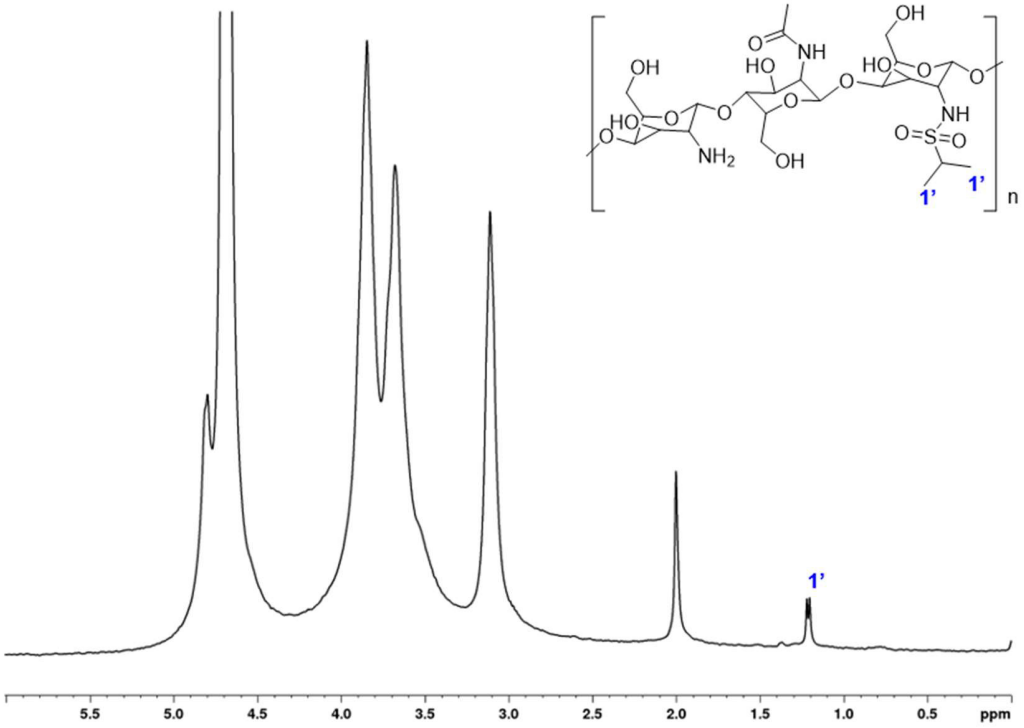

Figure 5.6. ^{1}H-NMR spectrum of chitosan-2-hydrosulfonylpropane (400 MHz, D_2O, 298 K).

Chitosan-2-hydrosulfonylpropane showed poor antibacterial activity in the MTT test against *E. coli* under the conditions reported in section 2.2.4.

5.3 Conclusions

The functionalization of chitosan is often an optimal way to improve chitosan properties, however only definite substituent and degrees of substitution can lead to improved antimicrobial properties. The functionalization procedure should permit to attach the new substituent on the

chitosan backbone and furthermore maintain pristine amine groups, which are essential for the antimicrobial activity of chitosan. The use of D-AAs isomers to functionalize chitosan seems to improve the antibacterial properties compared to the pristine chitosan or to the use of the L-AAs. However, further investigations, such as PCA experiments, are necessary to draw more definitive conclusions on the influence of such stereoisomers on the antimicrobial activity of chitosan.

6. Final remarks and outlooks

Chitosan is an interesting and multi-functional material and can be used for many different scopes and applications, e.g. as coating agent for antimicrobial surfaces or as encapsulating agent. The substitution of chitosan with thiol-bearing substituents could significantly increase the antibacterial properties of pristine chitosan. The new compounds, i. e. chitosan thiomers, are worthy to be investigated further against other different pathogens. The encapsulation of the POMs with chitosan and its derivative CMC does not have a uniform effect, being able to either reduce or enhance the toxicity of the pristine POMs on cancer and normal cells. Further investigations on the different cytotoxicity of the isomers of the POM $\{P_2W_{18}\}$ are necessary to understand the mechanism behind the increased cytotoxicity of the isomeric mixture compared to the pure α-isomer of $\{P_2W_{18}\}$. A rewarding and interesting research project could involve the investigation of chitosan thiomers as encapsulating agents for POMs and the study of their biological properties against cancer cells and bacteria. Further mechanistic studies should be conducted on the feasibility of the two selective cancer targeting approaches proposed in this thesis. The investigation of the antibacterial properties of new functionalized chitosan derivatives and of the anticancer properties of POM-chitosan-based nanocomposites performed in this thesis paved the way for the preparation of new versatile and efficient drug prototypes.

Summary

Bacteria are posing an increasingly serious threat to human health due to their more and more frequent resistance to conventional antibiotics. Infections caused by antibiotic resistant bacteria are on the rise worldwide and raising the costs in health care systems. A possible way to overcome the dangerous infections caused by antibiotic resistant bacteria is the development of new tunable antibacterial drugs which arise from sustainable sources and can be quickly adapted to different strains.

Chitosan is a biopolymer consisting of N-acetyl-D-glucosamine and β-1,4-linked-D-glucosamine with well-known antimicrobial properties. Recently, the versatile antimicrobial properties of chitosan functionalized with thioglycolic acid (chitosan-TGA) were investigated in our group. To further explore and enhance their antibacterial properties, several chitosan thiomers were prepared and tested for antimicrobial activity (Chapter 2). Chitosan was functionalized with several thiol bearing compounds via amide bond formation activated by the carbodiimide EDC. The substituents were mainly alkyl-chain thiomers, such as TGA, thiolactic acid, mercaptopropionic acid (MPA), 2-methyl-3-sulfanylpropanoic acid, mercaptobutyric acid, mercaptohexanoic acid and mercaptooctanoic acid. Moreover, chitosan was functionalized with cysteine, mercaptobenzoic acid and 2-iminothiolane. Four chitosan sources with different degrees of deacetylation DD (87-94%) and molecular weight MW (18-250 kDa) were used as starting materials, and their influence on the antimicrobial activity of the functionalized derivatives was investigated.

Some issues were encountered in the synthesis of chitosan thiomers activated by EDC. The DS of the chitosan-TGA, synthesized according to the original procedure, were lower than expected. Several attempts to increase the DS of chitosan-TGA were made (Chapter 4) through applying and modifying several published procedures. Formation of a Schiff base between chitosan and mercaptoacetaldehyde and the reaction of chitosan with the TGA acyl chloride were also tested. While the DS could be increased compared to the initial attempts, MTT tests on *Escherichia coli* revealed that highly substituted chitosan-TGA did not enhance the antibacterial activity.

Structure-activity relationships between the functionalization of chitosan and the antimicrobial effect was investigated with comprehensive analytical characterization of the polymers (Chapter 2). Special emphasis was placed on the determination of DD, MW and degree of substitution (DS). Chitosan thiomers were characterized by ^{1}H-NMR spectroscopy, gel permeation chromatography, elemental analysis, Ellman test, ζ-potential measurements and FT-IR spectroscopy. The DD and MW strongly depended on the starting material, while the DS was influenced by the functionalizing reagent. The well-known MTT assay was adapted and applied for a fast and reliable screening of the antimicrobial properties of the newly synthesized derivatives.

The antimicrobial activity of the thiomers was tested on two gram-negative strains, *E. coli* and *Pseudomonas aeruginosa*, and on two gram-positive strains, *Streptococcus sobrinus* and *Streptococcus mutans.* MTT results showed superior efficacy of the derivatives produced from chitosan 85/20 (MW ∼ 90 kDa and DD ∼ 93%), probably due to the higher DD. Moreover, a high DS decreased the antibacterial activity, which may be linked to the lower amount of available amine groups. Furthermore, the antimicrobial activity of chitosan functionalized with the D- and L-isomers of cysteine and alanine, respectively, was tested by MTT on *E. coli*. Surprisingly, the D-isomers exhibited superior antibacterial properties (Chapter 5).

The antimicrobial properties of the most promising alkyl thiol substituted chitosans, synthesized from chitosan 85/20, were further investigated by plate counting. Plate counting is a quantitative and reliable method which permits the detection of very few surviving bacterial cells. Under the applied experimental conditions *E. coli* was scarcely affected by the treatment of alkyl thiomers. On the other hand, chitosan alkyl thiomers led to a reduction of the bacterial population by a factor of 5 log or more for *P. aeruginosa*, *S. sobrinus* and *S. mutans*. In particular, at least one chitosan thiomer per strain was able to completely eradicate the bacterial population. Chitosan-MPA was selected as representative example to perform a LIVE/DEAD assay that confirmed the antibacterial action evidenced by the PCA experiments. The above investigation emphasizes the outstanding antimicrobial properties of N-acyl thiolated chitosans and paves the way to the design of new highly efficient, biocompatible and cost-effective antimicrobial compounds.

Cancer is becoming progressively a curable disease through the continuous improvement of innovative therapies and early diagnosis. However, cancer treatments often remain highly expensive and may pose financial issues to many patients worldwide. Polyoxometalates (POMs)

are discrete, negatively charged polyoxoclusters composed mainly of molybdenum, tungsten and vanadium metal centers in their highest oxidation states. Over the past decades, POMs were proposed and frequently investigated *in vitro* as promising inexpensive candidates for new antidiabetic, antiviral, antibacterial and anticancer drugs. However, their clinical applications remain to be explored, because their selectivity, toxicity and stability at physiological conditions needs to be controlled individually. A promising approach to reduce their cytotoxicity, while enhancing their selectivity towards biological targets is their encapsulation into biocompatible polymeric matrices and drug carriers, such as chitosan and its derivatives.

In this work $\{Sb_9W_{21}\}$, $\{Mo_7O_{24}\}$ and $\{P_2W_{18}\}$ were selected as known promising candidates for medical applications, and their nanocomposites with chitosan and carboxymethyl chitosan (CMC) were newly prepared. Chitosan and CMC were selected in order to cover the entire pH range: chitosan is soluble at pH < 6.5 and CMC at pH > 7. The overall goal was to investigate the change in cytotoxicity of POMs upon encapsulation in a biocompatible matrix on bacteria and somatic cells (Chapter 3).

$\{Sb_9W_{21}\}$ as a proven antiviral POM and $\{P_2W_{18}\}$ were synthesized according to the reported procedures and extensively characterized by single-crystal XRD, powder-XRD, elemental analysis and FT-IR spectroscopy. Additionally, ^{31}P-NMR spectroscopy was applied to characterize $\{P_2W_{18}\}$. These techniques confirmed the identity and the phase purity of the compounds. $\{P_2W_{18}\}$ was prepared as α-isomer and as a mixture of the α-, β- and γ-isomers.

POM-chitosan nanocomposites were prepared through cross-linking interaction between the positively charged chitosan and the negatively charged POMs under constant sonication. In comparison, POM-CMC nanoparticles were prepared under constant stirring while applying Ca^{2+} (from $CaCl_2$) as cationic cross-linker between the negatively charged CMC and POM. The nanocomposites were characterized with dynamic light scattering (DLS) and electron microscopy (SEM and TEM) to determine their size range (100-200 nm) and morphology. The morphology observed was partially dependent on the composition of the nanocomposites and on the methodology used for sample preparation.

Moreover, the stability of POMs and of nanocomposites under physiological conditions was addressed as a key issue for future applications. The encapsulation improved the stability of the otherwise unstable $\{Sb_9W_{21}\}$ and did not alter significantly the stability of $\{P_2W_{18}\}$.

The cytotoxicity of the pristine POMs as well as of the nanocomposites was evaluated against bacteria (gram-positive *S. sobrinus* and gram-negative *E. coli*) as well as on mammalian cell lines, namely HeLa and MRC-5. $\{Sb_9W_{21}\}$ and $\{P_2W_{18}\}$ and their as-prepared nanocomposites did not show any particular antibacterial activity, thus highlighting their possible use in bacteria-friendly applications, where the local flora should not be harmed during the treatment. $\{Mo_7O_{24}\}$ showed low cytotoxicity against both the tested cell lines, while α-$\{P_2W_{18}\}$ and $\{Sb_9W_{21}\}$ were more toxic. Surprisingly, the isomeric mixture of α-, β-, and γ-$\{P_2W_{18}\}$ exhibited higher cytotoxicity compared to the pure α-isomer. Furthermore, the cytotoxicity of $(TBA)_4[Mo_8O_{26}]$, $K_7[PTi_2W_{10}O_{40}]$, $K_4[SiMo_{12}O_{40}]$ and $(NH_4)_6[P_2Mo_{18}O_{62}]$, and of the nanocomposites with chitosan or CMC was preliminary tested on HeLa cells.

The modification of cytotoxicity of pristine POMs upon encapsulation was not univocal: the cytotoxicity of the nanocomposite could be either increased or reduced, depending on the POM and the polymeric matrix. Furthermore, the tested cell line plays a role in determining the cytotoxicity. In view of these results the cytotoxicity of POM-chitosan and POM-CMC nanocomposites should be always evaluated individually.

Two possible ways for selective targeting against cancer cells were proposed, based on the pH dependent stability of chitosan and CMC nanoparticles. The first approach involves POMs whose toxicity is increased upon chitosan encapsulation (e.g. $\{Mo_7O_{24}\}$). POM-chitosan nanoparticles are stable at the acidic pH of cancer tissue, so that they could eliminate cancer cells upon local injection. When POM-chitosan nanoparticles diffuse toward the healthy tissue (pH 7.2-7.3), the polymer would precipitate and may eventually impair the transport of nutrients to the cancerous area. The pristine POM may be gradually released from the chitosan nanoparticle, after enzymatic degradation of the polymer. The separated components would be present in the healthy tissue at low, presumably non-cytotoxic concentrations and be cleared by the organism. The second approach to target the cancer cells involves POM-CMC nanoparticles with low toxicity on normal cells compared to the pristine POM (e.g. $\{P_2W_{18}\}$), that could be injected into the bloodstream. Due to their size below 200 nm and their negative surface charge, POM-CMC nanoparticles may accumulate in the cancer tissue due to the EPR effect. Furthermore, at the acidic pH of cancer cells the POM-CMC nanoparticles precipitate and they could release the POM at cytotoxic concentration after enzymatic degradation, thereby eliminating the cancer cells. Further *in vitro*

and *in vivo* experiments are necessary to verify the feasibility of the two proposed targeting approaches and to confirm the applicability of POM-chitosan and POM-CMC nanocomposites as pH sensitive drugs.

The cytotoxicity data collected so far highlight the difficulties in predicting the biological activity of POM-chitosan-based nanocomposites. Substantial research to underpin the structure-activity relationships of these composites is now required. The investigation of the antibacterial properties of new functionalized chitosan derivatives and the anticancer properties of POM-chitosan-based nanocomposites performed in this thesis paves the way for the preparation of new versatile and efficient drug prototypes.

Zusammenfassung

Bakterien, die zunehmende Resistenz gegen die herkömmlichen Antibiotika entwickeln, werden zu einer ernsthaften Bedrohung für die menschliche Gesundheit. Die Zunahme der Infektionen durch antimikrobiell resistente Bakterien verursacht weltweit steigende Kosten für die Gesundheitssysteme. Ein möglicher Ansatz dieses Problem zu bekämpfen ist die Entwicklung von neuen Antibiotika.

Das Biopolymer Chitosan ist bekannt für seine antimikrobiellen Eigenschaften und besteht aus β-1,4-glykosidisch verknüpften *N*-Acetyl-*D*-glucosamin Einheiten. Vor kurzem begann unsere Gruppe mit der Erforschung der antimikrobiellen Eigenschaften von Chitosan, das mit Thioglykolsäure (Chitosan-TGA) funktionalisiert wurde. Zum besseren Verständnis der antibakteriellen Eigenschaften von Chitosan Derivaten wurden mehrere thiolierte Chitosane synthetisiert und auf ihre antimikrobielle Aktivität getestet (Kapitel 2). Dazu wurde die Aminogruppe von vier Chitosanpolymeren, die sich im Deacetylierungs-Grad (Englisch: degree of deacetylation, DD, 87-94%) und Molekulargewicht (MW, 18-250 kDa) unterscheiden, durch Carbodiimide (EDC) aktiviert, um mit Thiolen eine Amidbindung einzugehen. Für die Funktionalisierung der Biopolymere wurden Thiole mit unterschiedlich langen Alkylketten verwendet (TGA, Thiomilchsäure, 3-Mercatoproprionsäure (MPA), 2-Methyl-3-mercaptopropionsäure, 4-Mercaptobutansäure, 6-Mercaptohexansäure und 8-Mercaptooctansäure). Zudem wurde Chitosan mit Cystein, 4-Mercaptobenzoesäure und 2-Iminothiolan funktionalisiert.

Die Synthese von thioliertem Chitosan, aktiviert durch EDC, ging einher mit einigen Schwierigkeiten. Der Substitutionsgrad (Englisch: degree of substitution, DS) des Chitosan-TGA, synthetisiert nach dem Verfahren aus der Literatur, war niedriger als erwartet. Mehrere Versuche zur Erhöhung des DS von Chitosan-TGA wurden durchgeführt (Kapitel 4). Dabei wurden publizierte Verfahren wiederholt und angepasst. Die Bildung einer Schiff'schen Base zwischen Chitosan und Mercaptoacetaldehyden und die Reaktion von Chitosan mit dem TGA-Acylchlorid wurden ebenfalls durchgeführt. Der DS konnte in Bezug auf die ersten Versuche erhöht werden. Der MTT-Test mit *E. coli* ergab allerdings, dass stark substituierten Chitosan-TGA Proben keine höhere antibakterielle Aktivität zeigten.

Die Beziehung zwischen Struktur und Aktivität funktionalisierter Chitosan-Derivate und deren antimikrobieller Wirkung wurde umfassend untersucht. Besonderen Wert wurde auf die Bestimmung von DD, MW und Substitutionsgrad (DS) gelegt. Gesamthaft wurden ^{1}H-NMR-Spektroskopie, Size-Exclusion-Chromatographie, Elementaranalyse, Ellman-Test, ζ-Potential Messungen und FT-IR-Spektroskopie zur Charakterisierung der Biopolymere verwendet. Während DD und MW allein vom Ausgangsmaterial abhängen, wird der Substitutionsgrad von dem funktionalisierenden Reagenz bestimmt.

Die antimikrobielle Aktivität der Biopolymere wurde an zwei Gram-negativen Bakterienstämmen (*Escherichia coli* und *Pseudomonas aeruginosa*) und zwei Gram-positiven Stämmen (*Streptcoccus sobrinus* und *Streptococcus mutans*) getestet. Der MTT Assay wurde auf die jeweiligen Bakterien angepasst und soweit optimiert, dass eine schnelle und zuverlässige Überprüfung der antimikrobiellen Eigenschaften der neu synthetisierten Derivate durchgeführt werden konnten. Die MTT Testresultate zeigten eine überlegene Wirksamkeit der Derivate aus Chitosan 85/20 (MW ∼ 90 kDa und DD ∼ 93%). Weiter konnte gezeigt werden, dass ein hoher DS die antibakterielle Aktivität verringert. Dies kann durch die geringere Menge an verfügbaren Aminogruppen erklärt werden. Darüber hinaus wurde die antimikrobielle Aktivität von Chitosan mit dem D-und L-Isomer von Cystein und Alanin durch MTT-Tests mit *E. coli* getestet. Überraschenderweise zeigten die D-Isomere überlegene antibakterielle Eigenschaften (Kapitel 5). Die antimikrobiellen Eigenschaften der vielversprechendsten Derivate, hergestellt aus Chitosan 85/20, wurden durch das Auszählen von Bakterienkolonien auf Inkubationsplatten (PCA) noch genauer studiert. PCA ist eine zuverlässige Methode, die es erlaubt, auch wenige überlebende Bakterienzellen zu erkennen. Die thiolierten Chitosane hatten in unseren Experimenten kaum eine Wirkung auf *E. coli*. Bei den anderen Bakterienstämmen (*P. aeruginosa, S. sobrinus* und *S. mutans*) wurde hingegen eine Verringerung der bakteriellen Population von mindestens 5 log Einheiten beobachtet. Für alle drei Bakterienstämme wurde jeweils ein thioliertes Chitosan-Derivat gefunden, dass die Bakterienpopulation vollständig auslöschen konnte.

Die bakterizide Wirkung wurde zusätzlich am repräsentativen Beispiel von Chitosan-MPA in Live/Dead Assays überprüft. Die Testresultate bestätigten die Beobachtungen aus dem PCA-Experiment. Die durchgeführten Versuche unterstreichen die hervorragenden

antimikrobiellen Eigenschaften von *N*-Acylthiolierten Chitosan-Derivaten und ebnen den Weg für die Entwicklung von neuen, hocheffizienten, biokompatiblen und kostengünstigen antimikrobiellen Verbindungen.

Krebs wird dank früher Diagnosen und innovativer Therapien zunehmend zu einer heilbaren Erkrankung. Allerdings sind Krebsbehandlungen sehr teuer und für einen grossen Teil der Weltbevölkerung daher oft erschwert zugänglich. Polyoxometallate (POMs) sind diskrete, negativ geladene Metall-Sauerstoff-Cluster, die vorwiegend aus Molybdän, Wolfram und Vanadium in ihren höheren Oxidationszuständen bestehen. POMs wurden als vielversprechende Kandidaten für neue Medikamente gegen virale und bakterielle Infektionen, Diabetes und Krebs vorgeschlagen. Die klinische Anwendung von POMs ist allerdings noch zu erforschen, da die Selektivität, Toxizität und Stabilität dieser Verbindungen unter physiologischen Bedingungen individuell angepasst werden muss. Eine Möglichkeit ihre Zytotoxizität zu reduzieren und gleichzeitige die Selektivität für biologische Ziele zu verbessern ist ihre Einkapselung in eine biokompatible Polymer-Matrix, wie zum Beispiel Chitosan.

In dieser Arbeit wurden die POMs $\{Sb_9W_{21}\}$, $\{Mo_7O_{24}\}$ und $\{P_2W_{18}\}$ als vielversprechende Kandidaten für medizinische Anwendungen ausgewählt und mit Chitosan und Carboxymethyl Chitosan (CMC) eingekapselt. Chitosan und CMC wurden ausgewählt, da diese beiden Biopolymere einen breiten pH-Bereich abzudecken vermögen: Chitosan ist bei pH-Werten < 6.5 löslich, während CMC bei pH-Werten > 7 löslich ist. Anhand dieser Strategie wurde die Veränderung der Zytotoxizität von POMs nach der Einkapselung in eine bioverträgliche Matrix mit Bakterien und somatischen Zellen untersucht (Kapitel 3).

Die Cluster $\{Sb_9W_{21}\}$ und $\{P_2W_{18}\}$ wurden wie in der Literatur beschrieben synthetisiert und ausführlich durch die Röntgenstruktur-Analyse von Einkristallen und mit Röntgen-Pulvermethoden sowie FT-IR-Spektroskopie charakterisiert. Zusätzlich wurde $\{P_2W_{18}\}$ mit ^{31}P-NMR-Spektroskopie untersucht. Alle Analysen bestätigten die Identität und die Phasenreinheit der Verbindungen. Das POM $\{P_2W_{18}\}$ wurde als α-Isomer und als Gemisch aus den α-, β-, γ-Isomeren hergestellt.

Die POM-Chitosan-Nanopartikel wurden durch *cross-linking* zwischen dem positiv geladenen Chitosan und dem negativ geladenen POMs im Ultraschallbad vorbereitet. Die

POM-CMC-Nanopartikel wurden unter ständigem Rühren und der Verwendung von Ca^{2+} (aus $CaCl_2$) als kationisches Quervernetzungsmittel hergestellt. Die Grösse (100-200 nm) und Morphologie der Nanopartikel wurden durch dynamische Lichtstreuung (DLS) und Elektronenmikroskopie (SEM und TEM) bestimmt. Die beobachtete Morphologie war einerseits abhängig von der Zusammensetzung der Nanopartikel und andererseits von der angewandten Methode für die Probenpräparation.

Darüber hinaus wurde die Stabilität von POMs und Nanopartikeln unter physiologischen Bedingungen als ein zentrales Thema für zukünftige Anwendungen untersucht. Die Einkapselung verbesserte die Stabilität des labilen $\{Sb_9W_{21}\}$, hatte aber keinen wesentlichen Einfluss auf die Stabilität von $\{P_2W_{18}\}$.

Die Zytotoxizität der unbehandelten POMs sowie der Nanopartikel wurde auf Bakterien (dem Gram-positiven Stamm *S. sobrinus* und dem Gram-negativen Stamm *E. coli*) sowie auf Säugetierzelllinien, namentlich HeLa und MRC-5, überprüft.

Die POMs $\{Sb_9W_{21}\}$ und $\{P_2W_{18}\}$ sowie die hergestellten Kompositen zeigten keine besondere antibakterielle Aktivität, weshalb sich diese Verbindungen besonders für die Verwendung in bakterienfreundlichen Anwendungen eignen, bei denen die örtliche Flora während der Behandlung nicht geschädigt werden sollte.

Der Cluster $\{Mo_7O_{24}\}$ zeigte eine niedrige Zytotoxizität gegen die beiden getesteten Zelllinien, während α-$\{P_2W_{18}\}$ und $\{Sb_9W_{21}\}$ giftiger waren. Überraschenderweise zeigte die α-, β- and γ-Isomerenmischung $\{P_2W_{18}\}$ eine höhere Zytotoxizität als das α-Isomer.

Darüber hinaus wurden die Zytotoxizität der Cluster $(TBA)_4[Mo_8O_{26}]$, $K_7[PTi_2W_{10}O_{40}]$, $K_4[SiMo_{12}O_{40}]$ und $(NH_4)_6[P_2Mo_{18}O_{62}]$ und ihrer Nanokomposite mit Chitosan oder CMC auf HeLa-Zellen in ersten Experimenten getestet. Bei Vergleich der Zytotoxizität der reinen POMs mit den eingekapselten POMs konnte kein eindeutiger Trend festgestellt werden: die Zytotoxizität des Nanopartikels konnte je nach POM und Polymermatrix entweder erhöht oder reduziert werden. Darüber hinaus spielten die getesteten Zelllinien eine Rolle bei der Bestimmung der Zytotoxizität. Zwei Möglichkeiten zur selektiven Behandlung von Krebszellen wurden vorgeschlagen, basierend auf der pH-abhängigen Stabilität von Chitosan- und CMC-Nanopartikeln. Der erste Ansatz beinhaltet POMs, deren Toxizität bei Einkapselung in Chitosan erhöht wird (e.g. $\{Mo_7O_{24}\}$). POM-Chitosan-Nanopartikel, die im sauren pH-Milieu der Krebszellen stabil sind, könnten bei

lokaler Injektion die Krebszellen eliminieren. POM-Chitosan-Nanopartikel würden dann in Richtung des gesunden Gewebes diffundieren (pH 7.2-7.3), wo das Polymer den Transport von Nährstoffen zum Krebsgewebe beeinträchtigen würde. Das reine POM würde nach dem enzymatischen Abbau des Polymers nach und nach aus den Chitosan-Nanopartikeln freigesetzt. Die beiden getrennten Komponenten lägen im gesunden Gewebe dann in nicht-toxischen Konzentrationen vor und würden durch den Organismus ausgeschieden werden.

Der zweite Ansatz zur Bekämpfung der Krebszellen beinhaltet POM-CMC-Nanopartikel mit geringer Toxizität gegenüber normalen Zellen im Vergleich zu den reinen POMs (e.g. $\{P_2W_{18}\}$), die in den Blutstrom injiziert werden könnte. Aufgrund ihrer Größe unter 200 nm und ihrer negativen Oberflächenladung könnten sich POM-CMC-Nanopartikel aufgrund des EPR-Effekts im Krebsgewebe ansammeln. Darüber hinaus würden diese Komposite im sauren Milieu der Krebszellen ausfallen, wobei dann nach enzymatischem Abbau die POMs freigesetzt und eine lokale cytotoxische Wirkung auf die Krebszellen entfalten würden.

Weitere *in vitro*-und *in vivo*-Experimente sind nun notwendig, um die Realisierbarkeit der beiden vorgeschlagenen Targeting-Ansätze zu überprüfen und POM-Chitosan und POM-CMC-Komposite als pH-sensitive Medikamente zu bestätigen.

Die bisher gesammelten Zytotoxizitäts-Daten unterstreichen die Schwierigkeit, die biologische Aktivität von POM-Chitosan-basierten Kompositen vorherzusagen. Umfangreiche Forschungsarbeiten zur Etablierung der zugrundeliegenden Struktur-Aktivitäts-Beziehungen sind nun erforderlich. Die Untersuchungen zu antibakteriellen Eigenschaften von neuen funktionalisierten Chitosan-Derivaten und zu krebstherapeutischen Eigenschaften von POM-Chitosan-basierten Kompositen in dieser Arbeit ebnen den Weg für die Entwicklung neuer, vielseitiger und effizienter Wirkstoff-Prototypen.

Bibliography

[1] C. R. Woese, O. Kandler, M. L. Wheelis, *Proc. Natl. Acad. Sci. U S A* **1990**, *87*(12), 4576–4579.

[2] M. T. Madigan in *Journey to Diverse Microbial Worlds*; (Ed. J. Seckbach), Springer, **2000**, pp. 61–72.

[3] G. W. Tannock, *Normal microflora*: *An introduction to microbes inhabiting the human body*; Chapman and Hall, London, **1995**.

[4] A. W. Walker, J. Ince, S. H. Duncan, L. M. Webster, G. Holtrop, X. Ze, D. Brown, M. D. Stares, P. Scott, A. Bergerat, P. Louis, F. McIntosh, A. M. Johnstone, G. E. Lobley, J. Parkhill, H. J. Flint, *ISME J.* **2011**, *5*(2), 220–230.

[5] L. V. Hooper, J. I. Gordon, *Science* **2001**, *292*(5519), 1115–1118.

[6] R. S. Gottfried, *Black death;* Simon and Schuster, New York, **2010**.

[7] J. B. Nachega, R. E. Chaisson, *Clin. Infect. Dis.* **2003**, *36*(Supplement_1), S24-S30.

[8] L. Zaffiri, J. Gardner, L. H. Toledo-Pereyra, *J. Invest. Surg.* **2012**, *25*(2), 67–77.

[9] W. C. Wallace, M. E. Cinat, F. Nastanski, W. B. Gornick, S. E. Wilson, *Am Surg* **2000**, *66*(9), 874–878.

[10] a) S. Y. Tan, Y. Tatsumura, *Singapore Med. J.* **2015**, *56*(7), 366–367; b) A. Fleming, *J. Pathol. Bacteriol.* **1932**, *35*(6), 831–842.

[11] H. Otten, *J. Antimicrob. Chemother.* **1986**, *17*(6), 689–690.

[12] B. Spellberg, *Clin. Infect. Dis.* **2008**, *47*(2), 294.

[13] S. Levy, *Lancet* **1982**, *320*(8289), 83–88.

[14] T. Watanabe, *Bacteriol. Rev.* **1963**, *27*(1), 87–115.

[15] V. M. D'Costa, C. E. King, L. Kalan, M. Morar, W. W. L. Sung, C. Schwarz, D. Froese, G. Zazula, F. Calmels, R. Debruyne, G. B. Golding, H. N. Poinar, G. D. Wright, *Nature* **2011**, *477*(7365), 457–461.

[16] R. I. Aminov, R. I. Mackie, *FEMS Microbiol. Lett.* **2007**, *271*(2), 147–161.

[17] K. Bhullar, N. Waglechner, A. Pawlowski, K. Koteva, E. D. Banks, M. D. Johnston, H. A. Barton, G. D. Wright, *PLoS ONE* **2012**, *7*(4); e34953.

[18] J. Davies, D. Davies, *Microbiol. Mol. Biol. Rev.* **2010**, *74*(3), 417–433.

[19] C. L. Ventola, *Pharm. Ther.* **2015**, *40*(4), 277–283.

[20] M. M. Swann, K. L. Baxter, H. I. Field, *Report of the joint committee on the use of antibiotics in animal husbandry and veterinary medicine;* HMSO, London, **1969**.

[21] H. C. Neu, *Science* **1992**, *257*(5073), 1064–1073.

[22] C. Walsh, *Nature* **2000**, *406*(6797), 775–781.

[23] R. Hakenbeck, T. Grebe, D. Zähner, J. B. Stock, *Mol. Microbiol.* **1999**, *33*(4), 673–678.

[24] C. A. Smith, E. N. Baker, *Curr Drug Targets Infect Disord* **2002**, *2*(2), 143–160.

[25] J. R. Knowles, *Acc. Chem. Res.* **1985**, *18*(4), 97–104.

[26] P. A. Lambert, *J. Appl. Microbiol.* **2002**, *92*(s1), 46S–54S.

[27] a) X.-Z. Li, H. Nikaido, *Drugs* **2004**, *64*(2), 159–204; b) S. B. Levy, *Antimicrob. Agents. Ch.* **1992**, *36*(4), 695–703.

[28] G. L. French, *Int. J. Antimicrob. Agents* **2010**, *36*, S3-S7.

[29] a) A. R. Taylor, *Prim. Care* **2013**, *40*(3), 637–654; b) P. S. Pottinger, *Med. Clin. North Am.* **2013**, *97*(4), 601–619.

[30] M. A. Fischbach, C. T. Walsh, *Science* **2009**, *325*(5944), 1089–1093.

[31] R. M. Klevens, M. A. Morrison, J. Nadle, S. Petit, K. Gershman, S. Ray, L. H. Harrison, R. Lynfield, G. Dumyati, J. M. Townes, *Jama* **2007**, *298*(15), 1763–1771.

[32] a) H. W. Boucher, G. H. Talbot, J. S. Bradley, J. E. Edwards, D. Gilbert, L. B. Rice, M. Scheld, B. Spellberg, J. Bartlett, *Clin. Infect. Dis.* **2009**, *48*(1), 1–12; b) C. A. Michael, D. Dominey-Howes, M. Labbate, *Front Public Health* **2014**, *2*; 145.

[33] S. B. Levy, B. Marshall, *Nat. Med.* **2004**, *10*(12), S122–S129.

[34] B. Spellberg, D. N. Gilbert, *Clin. Infect. Dis.* **2014**, *59*(2), S71–S75.

[35] ECDC, *Surveillance of antimicrobial resistance in Europe 2016;* Annual Report of the European Antimicrobial Resistance Surveillance Network (EARS-Net), **2017**. Available at:https://ecdc.europa.eu/en/publications-data/antimicrobial-resistance-surveillance-europe-2016. Accessed April 23, 2018.

[36] J. O'Neill, *Tackling drug-resistant infections globally: Final report and recommendations*; Review on Antimicrobial Resistance, **2016**. Available at:https://amr-review.org/sites/default/files/160525_Final%20paper_with%20cover.pdf. Accessed April 27, 2018.

[37] Z. Golkar, O. Bagasra, D. G. Pace, *J Infect Dev Ctries* **2014**, *8*(2), 129–136.

[38] a) C. L. Ventola, *Pharm. Ther.* **2015**, *40*(5), 344–352; b) B. D. Lushniak, *Public Health Rep* **2014**, *129*(4), 314–316.

[39] F. von Nussbaum, M. Brands, B. Hinzen, S. Weigand, D. Häbich, *Angew. Chem. Int. Ed. Engl.* **2006**, *45*(31), 5072–5129.

[40] a) D. J. Tipper, J. L. Strominger, *Proc. Natl. Acad. Sci. U S A* **1965**, *54*(4), 1133–1141; b) D. J. Waxman, J. L. Strominger, *Annu. Rev. Biochem.* **1983**, *52*(1), 825–869.

[41] I. Chopra, M. Roberts, *Microbiol. Mol. Biol. Rev.* **2001**, *65*(2), 232–260.

[42] D. C. Hooper, *Drugs* **1995**, *49*(2), 10–15.

[43] O. Sköld, *Drug Resist. Updat.* **2000**, *3*(3), 155–160.

[44] M. S. Butler, A. D. Buss, *Biochem. Pharmacol.* **2006**, *71*(7), 919–929.

[45] P. Fernandes, E. Martens, *Biochem. Pharmacol.* **2017**, *133*, 152–163.

[46] The Pew Charitable Trust, *Antibiotics currently in clinical development*, **2014**. Available at:http://www.pewtrusts.org/en/multimedia/data-visualizations/2014/antibiotics-currently-in-clinical-development. Accessed April 24, 2018.

[47] B. M. Kuehn, *JAMA* **2011**, *305*(18), 1845–1846.

[48] I. M. Gould, A. M. Bal, *Virulence* **2013**, *4*(2), 185–191.

[49] R. L. Siegel, K. D. Miller, A. Jemal, *CA Cancer J. Clin.* **2017**, *67*(1), 7–30.

[50] H. Kantarjian, D. Steensma, J. Rius Sanjuan, A. Elshaug, D. Light, *J. Oncol. Pract.* **2014**, *10*(4), 208-211.

[51] D. W. Light, H. Kantarjian, *Cancer* **2013**, *119*(22), 3900–3902.

[52] S. B. Dusetzina, A. N. Winn, G. A. Abel, H. A. Huskamp, N. L. Keating, *J. Clin. Oncol.* **2013**, *32*(4), 306–311.

[53] R. Lopert, A. G. Elshaug, *Health Aff* **2013**, *32*(4), 778–787.

[54] M. Rinaudo, *Prog. Polym. Sci.* **2006**, *31*(7), 603–632.

[55] K. Kurita, *Mar. Biotechnol.* **2006**, *8*(3), 203–226.

[56] S. Kaur, G. S. Dhillon, *Crit. Rev. Microbiol.* **2014**, *40*(2), 155–175.

[57] a) J. Brugnerotto, J. Lizardi, F. Goycoolea, W. Argüelles-Monal, J. Desbrières, M. Rinaudo, *Polymer* **2001**, *42*(8), 3569–3580; b) J. Zawadzki, H. Kaczmarek, *Carbohydr. Polym.* **2010**, *80*(2), 394–400; c) J. Domszy, G. Roberts, *Makromol. Chem.* **1985**, *186*(8), 1671–1677.

[58] A. Zajac, J. Hanuza, M. Wandas, L. Dyminska, *Spectrochim. Acta A Mol. Biomol. Spectrosc.* **2015**, *134*, 114–120.

[59] M. R. Kasaai, J. Arul, G. Charlet, *J. Polym. Sci. B Polym. Phys.* **2000**, *38*(19), 2591–2598.

[60] a) S. C. Tan, *Talanta* **1998**, *45*(4), 713–719; b) R. A. Muzzarelli, R. Rocchetti, *Carbohydr. Polym.* **1985**, *5*(6), 461–472.

[61] L. Heux, J. Brugnerotto, J. Desbrières, M.F. Versali, M. Rinaudo, *Biomacromolecules* **2000**, *1*(4), 746–751.

[62] A. Hirai, H. Odani, A. Nakajima, *Polym. Bull.* **1991**, *26*(1), 87–94.

[63] M. Rinaudo, P. Le Dung, C. Gey, M. Milas, *Int. J. Biol. Macromol.* **1992**, *14*(3), 122–128.

[64] R. A. Muzzarelli, C. Lough, M. Emanuelli, *Carbohydr. Res.* **1987**, *164*, 433–442.

[65] A. C. Wu, *Microb. Pathog.* **1988**, *161*, 447–452.

[66] J. Brugnerotto, J. Desbrières, G. Roberts, M. Rinaudo, *Polymer* **2001**, *42*(25), 9921–9927.

[67] M. X. Weinhold, J. C. M. Sauvageau, N. Keddig, M. Matzke, B. Tartsch, I. Grunwald, C. Kübel, B. Jastorff, J. Thöming, *Green Chem.* **2009**, *11*(4), 498–509.

[68] M. Rinaudo, M. Milas, P. Le Dung, *Int. J. Biol. Macromol.* **1993**, *15*(5), 281–285.

[69] A. Verlee, S. Mincke, C. V. Stevens, *Carbohydr. Polym.* **2017**, *164*, 268–283.

[70] a) T. Han, N. Nwe, T. Furuike, S. Tokura, H. Tamura, *J. Biomed. Sci. Eng.* **2012**, *5*(1), 15–23; b) D. Ren, H. Yi, W. Wang, X. Ma, *Carbohydr. Res.* **2005**, *340*(15), 2403–2410; c) Y. Zhang, Z. Wang, J. Zhang, C. Chen, Q. Wu, L. Zhang, X. Zhang, *Carbohydr. Polym.* **2011**, *85*(3), 554–559.

[71] a) H. Ueno, T. Mori, T. Fujinaga, *Adv. Drug Deliv. Rev.* **2001**, *52*(2), 105–115; b) P. Baldrick, *Regul. Toxicol. Pharmacol.* **2010**, *56*(3), 290–299; c) T. Dai, M. Tanaka, Y.-Y. Huang, M. Hamblin, *Expert Rev. Anti Infect. Ther.* **2011**, *9*(7), 857–879.

[72] a) K. Lee, I. Kwon, Y.-H. Kim, W. Jo, S. Jeong, *J. Control. Release* **1998**, *51*(2-3), 213–220; b) N. Bhattarai, J. Gunn, M. Zhang, *Adv. Drug Deliv. Rev.* **2010**, *62*(1), 83–99.

[73] S. Hirano, C. G. Gebelein, T. C. Cheng, *Cosmetic and pharmaceutical uses of chitin and chitosan*: Cosmetic and Pharmaceutical Applications of Polymers; Plenum Press, New York, **1991**.

[74] R. A. Muzzarelli, *Carbohydr. Polym.* **1996**, *29*(4), 309–316.

[75] K. Shields, N. Smock, C. McQueen, P. Bryant, *Am. J. Health Syst. Pharm.* **2003**, *60*(13), 1310–1312.

[76] a) S. Roller, N. Covill, *Int. J. Food Microbiol.* **1999**, *47*(1-2), 67–77; b) S. Bautista-Baños, A. N. Hernández-Lauzardo, M. G. Velázquez-del Valle, M. Hernández-López, E. Ait Barka, E. Bosquez-Molina, C. L. Wilson, *Crop Prot.* **2006**, *25*(2), 108–118.

[77] H. K. No, S. P. Meyers, W. Prinyawiwatkul, Z. Xu, *J. Food Sci.* **2007**, *72*(5), R87–R100.

[78] L. Orzali, B. Corsi, C. Forni, L. Riccioni in *Biological Activities and Application of Marine Polysaccharides*; (Ed. E. A. Shalaby), InTech, London, **2017**.

[79] M. Rhazi, J. Desbrières, A. Tolaimate, M. Rinaudo, P. Vottero, A. Alagui, M. El Meray, *Eur. Polym. J.* **2002**, *38*(8), 1523–1530.

[80] H. K. No, S. P. Meyers in *Reviews of Environmental Contamination and Toxicology:* Continuation of Residue Reviews; (Ed. G. W. Ware), Springer, New York, **2000**, pp. 1–27.

[81] a) V. K. Mourya, N. N. Inamdar, *React. Funct. Polym.* **2008**, *68*(6), 1013–1051; b) M. N. V. Ravi Kumar, R. A. A. Muzzarelli, C. Muzzarelli, H. Sashiwa, A. J. Domb, *Chem. Rev.* **2004**, *104*(12), 6017–6084; c) N. M. Alves, J. F. Mano, *Int. J. Biol. Macromol.* **2008**, *43*(5), 401–414.

[82] Ö. V. Rúnarsson, J. Holappa, C. Malainer, H. Steinsson, M. Hjálmarsdóttir, T. Nevalainen, M. Másson, *Eur. Polym. J.* **2010**, *46*(6), 1251–1267.

[83] R. Jayakumar, N. Selvamurugan, S. V. Nair, S. Tokura, H. Tamura, *Int. J. Biol. Macromol.* **2008**, *43*(3), 221–225.

[84] a) X. Li, Y. Tushima, M. Morimoto, H. Saimoto, Y. Okamoto, S. Minami, Y. Shigemasa, *Polym. Adv. Technol.* **2000**, *11*(4), 176–179; b) M. M. Issa, M. Köping-Höggård, K. Tømmeraas, K. M. Vårum, B. E. Christensen, S. P. Strand, P. Artursson, *J. Control. Release* **2006**, *115*(1), 103–112.

[85] V. K. Mouryaa, N. N. Inamdara, A. Tiwari, *Adv. Mat. Lett.* **2010**, *1*(1), 11–33.

[86] A. Bernkop-Schnürch, *Adv. Drug Deliv. Rev.* **2005**, *57*(11), 1569–1582.

[87] C. Kast, A. Bernkop-Schnürch, *Biomaterials* **2001**, *22*(17), 2345–2352.

[88] F. Sarti, A. Bernkop-Schnürch in *Chitosan for Biomaterials I*: Advances in Polymer Science; (Eds. R. Jayakumar, M. Prabaharan, R. A. A. Muzzarelli), Springer, Berlin and Heidelberg, **2011**, pp. 93–110.

[89] S. Dünnhaupt, J. Barthelmes, D. Rahmat, K. Leithner, C. C. Thurner, H. Friedl, A. Bernkop-Schnürch, *Mol. Pharm.* **2012**, *9*(5), 1331–1341.

[90] S. Bonengel, A. Bernkop-Schnürch, *J. Control. Release* **2014**, *195*, 120–129.

[91] M. Pope, A. Müller, *Angew. Chem. Int. Ed. Engl.* **1991**, *30*(1), 34–48.

[92] D.-L. Long, R. Tsunashima, L. Cronin, *Angew. Chem. Int. Ed. Engl.* **2010**, *49*(10), 1736–1758.

[93] J. F. Keggin, *Nature* **1933**, *131*(3321), 908–909.

[94] G. M. Brown, M. R. Noe-Spirlet, W. R. Busing, H. A. Levy, *Acta Crystallogr, Sect. B: Struct. Sci* **1977**, *33*(4), 1038–1046.

[95] C. Rocchiccioli-Deltcheff, M. Fournier, R. Franck, R. Thouvenot, *Inorg. Chem.* **1983**, *22*(2), 207–216.

[96] B. Dawson, *Acta Cryst.* **1953**, *6*(2), 113–126.

[97] M. Carraro, S. Gross, *Materials* **2014**, *7*(5), 3956–3989.

[98] M. T. Pope, *Heteropoly and isopoly oxometalates;* Springer, Berlin and New York, **1983**.

[99] M. T. Pope, *Inorganic Chemistry Concept* **1983**, *8*.

[100] D.-L. Long, E. Burkholder, L. Cronin, *Chem. Soc. Rev.* **2007**, *36*(1), 105–121.

[101] Y.-F. Song, R. Tsunashima, *Chem. Soc. Rev.* **2012**, *41*(22), 7384–7402.

[102] M. Sadakane, E. Steckhan, *Chem. Rev.* **1998**, *98*(1), 219–238.

[103] D. E. Katsoulis, *Chem. Rev.* **1998**, *98*(1), 359–388.

[104] S.-S. Wang, G.-Y. Yang, *Chem. Rev.* **2015**, *115*(11), 4893–4962.

[105] a) J. M. Clemente-Juan, E. Coronado, A. Gaita-Ariño, *Chem. Soc. Rev.* **2012**, *41*(22), 7464–7478; b) U. Kortz, A. Müller, J. van Slageren, J. Schnack, N. S. Dalal, M. Dressel, *Coord. Chem. Rev.* **2009**, *253*(19-20), 2315–2327.

[106] T. Yamase, *J. Mater. Chem.* **2005**, *15*(45), 4773–4782.

[107] J. Rhule, C. Hill, D. Judd, R. Schinazi, *Chem. Rev.* **1998**, *98*(1), 327–358.

[108] J. Fang, H. Nakamura, H. Maeda, *Adv. Drug Deliv. Rev.* **2011**, *63*(3), 136–151.

[109] A. V. Narlikar, Y. Y. Fu, D. Maysinger, P. Kujawa, J. Lovrić, *Nanoparticles in medicine;* Oxford University Press, Oxford, **2017**.

[110] a) F. Masood, *Mater. Sci. Eng. C Mater. Biol. Appl.* **2016**, *60*, 569–578; b) J. M. Chan, P. M. Valencia, L. Zhang, R. Langer, O. C. Farokhzad in *Cancer Nanotechnology:* Methods and Protocols; (Eds. S. R. Grobmyer, B. M. Moudgil), Humana Press, Totowa, **2010**, pp. 163–175.

[111] A. P. Alivisatos, *Science* **1996**, *271*(5251), 933–937.

[112] X. Michalet, F. F. Pinaud, L. A. Bentolila, J. M. Tsay, S. Doose, J. J. Li, G. Sundaresan, A. M. Wu, S. S. Gambhir, S. Weiss, *Science* **2005**, *307*(5709), 538–544.

[113] R. A. Sperling, P. R. Gil, F. Zhang, M. Zanella, W. J. Parak, *Chem. Soc. Rev.* **2008**, *37*(9), 1896–1908.

[114] M. Mahmoudi, S. Sant, B. Wang, S. Laurent, T. Sen, *Adv. Drug Deliv. Rev.* **2011**, *63*(1-2), 24–46.

[115] T. Y. Ohulchanskyy, I. Roy, L. N. Goswami, Y. Chen, E. J. Bergey, R. K. Pandey, A. R. Oseroff, P. N. Prasad, *Nano Lett.* **2007**, *7*(9), 2835–2842.

[116] L. Zhang, F. X. Gu, J. M. Chan, A. Z. Wang, R. S. Langer, O. C. Farokhzad, *Clin. Pharmacol. Ther.* **2008**, *83*(5), 761–769.

[117] A. Judge, K. McClintock, J. Phelps, I. MacLachlan, *Mol. Ther.* **2006**, *13*(2), 328–337.

[118] I. Yildiz, S. Shukla, N. F. Steinmetz, *Curr. Opin. Biotechnol.* **2011**, *22*(6), 901–908.

[119] D. Simberg, T. Duza, J. H. Park, M. Essler, J. Pilch, L. Zhang, A. M. Derfus, M. Yang, R. M. Hoffman, S. Bhatia, M. J. Sailor, E. Ruoslahti, *Proc. Natl. Acad. Sci. U S A* **2007**, *104*(3), 932–936.

[120] D. W. Bartlett, H. Su, I. J. Hildebrandt, W. A. Weber, M. E. Davis, *Proc. Natl. Acad. Sci. U S A* **2007**, *104*(39), 15549–15554.

[121] M. Arruebo, M. Valladares, Á. González-Fernández, *J. Nanomater.* **2009**, *2009*(16), 1–24.

[122] A. Elsaesser, C. V. Howard, *Adv. Drug Deliv. Rev.* **2012**, *64*(2), 129–137.

[123] A. Nel, T. Xia, L. Mädler, N. Li, *Science* **2006**, *311*(5761), 622–627.

[124] V. V. Ginzburg, S. Balijepalli, *Nano Lett.* **2007**, *7*(12), 3716–3722.

[125] a) G. Xie, C. Wang, J. Sun, G. Zhong, *Toxicol. Lett.* **2011**, *205*(1), 55–61; b) Q. He, Z. Zhang, F. Gao, Y. Li, J. Shi, *Small* **2011**, *7*(2), 271–280;

[126] M. M. Fernandes, A. Francesko, J. Torrent-Burgués, T. Tzanov, *React. Funct. Polym.* **2013**, *73*(10), 1384–1390.

[127] G. Geisberger, E. B. Gyenge, D. Hinger, A. Käch, C. Maake, G. R. Patzke, *Biomacromolecules* **2013**, *14*(4), 1010–1017.

[128] a) Y. Uchida, *Gekkan Fudo Kemikaru* **1988**, *22*(4), 39–44; b) N. R. Sudarshan, D. G. Hoover, D. Knorr, *Food Biotechnol.* **1992**, *6*(3), 257–272; c) R. Muzzarelli, R. Tarsi, O. Filippini, E. Giovanetti, G. Biagini, P. E. Varaldo, *Antimicrob. Agents. Ch.* **1990**, *34*(10), 2019–2023; d) C. Allan, L. Hadwiger, *Exp. Mycol.* **1979**, *3*(3), 285–287.

[129] P. H. Sette-de-Souza, F. Dantas de Medeiros, M. G. de Oliveira Pinto, J. C. Queiroz, R. I. Maciel de Sousa, P. Meira Bento, D. Pita de Melo, P. Muniz Alves, A. C. Dantas de Medeiros, *Afr. J. Microbiol. Res.* **2015**, *9*(3), 147–154.

[130] H. No, *Int. J. Food Microbiol.* **2002**, *74*(1-2), 65–72.

[131] D. Raafat, K. von Bargen, A. Haas, H.-G. Sahl, *Appl. Environ. Microbiol.* **2008**, *74*(12), 3764–3773.

[132] S.-C. Park, J.-W. Nah, Y. Park, *Macromol. Res.* **2011**, *19*(8), 853–860.

[133] I. Helander, E.-L. Nurmiaho-Lassila, R. Ahvenainen, J. Rhoades, S. Roller, *Int. J. Food Microbiol.* **2001**, *71*(2-3), 235–244.

[134] A. Y. Mansilla, L. Albertengo, M. S. Rodríguez, A. Debbaudt, A. Zúñiga, C. A. Casalongué, *Appl. Microbiol. Biotechnol.* **2013**, *97*(15), 6957–6966.

[135] a) X. Liu, L. Song, L. Li, S. Li, K. Yao, *J. Appl. Polym. Sci.* **2007**, *103*(6), 3521–3528; b) X. Fei Liu, Y. Lin Guan, D. Zhi Yang, Z. Li, K. de Yao, *J. Appl. Polym. Sci.* **2001**, *79*(7), 1324–1335.

[136] a) X. Wang, Y. Du, H. Liu, *Carbohydr. Polym.* **2004**, *56*(1), 21–26; b) X. Wang, Y. Du, L. Fan, H. Liu, Y. Hu, *Polym. Bull.* **2005**, *55*(1-2), 105–113; c) P. S. Jassal, V. P. Raut, *Proc. Indian Natl. Sci. Acad.* **2013**, *79*(1), 31–40.

[137] a) S. Roller, N. Covill, *Int. J. Food Microbiol.* **1999**, *47*(1-2), 67–77; b) R. G. Cuero, G. Osuji, A. Washington, *Biotechnol. Lett.* **1991**, *13*(6), 441–444.

[138] R. Goy, D. de Britto, O. B. G. Assis, *Polímeros* **2009**, *19*(3), 241–247.

[139] H. Liu, Y. Du, X. Wang, L. Sun, *Int. J. Food Microbiol.* **2004**, *95*(2), 147–155.

[140] B. Li, *Asian J. Chem.* **2013**, *25*(18), 10033–10036.

[141] I. Younes, S. Sellimi, M. Rinaudo, K. Jellouli, M. Nasri, *Int. J. Food Microbiol.* **2014**, *185*, 57–63.

[142] Y. Omura, M. Shigemoto, T. Akiyama, H. Saimoto, Y. Shigemasa, I. Nakamura, T. Tsuchido, *Biocontrol Sci.* **2003**, *8*(1), 25–30.

[143] L.-Y. Zheng, J.-F. Zhu, *Carbohydr. Polym.* **2003**, *54*(4), 527–530.

[144] J. C. Fernandes, F. K. Tavaria, S. C. Fonseca, Ó. S. Ramos, M. E. Pintado, F. X. Malcata, *J. Microbiol. Biotechnol.* **2010**, *20*(2), 311–318.

[145] a) M. E. I. Badawy, *J. Appl. Polym. Sci.* **2010**, *117*(2), 960–969; b) R. C. Goy, S. T. Morais, O. B. Assis, *Rev. Bras. Farmacogn.* **2016**, *26*(1), 122–127; c) N. A. Mohamed, M. W. Sabaa, A. H. El-Ghandour, M. M. Abdel-Aziz, O. F. Abdel-Gawad, *Int. J. Biol. Macromol.* **2013**, *60*, 156–164.

[146] M. Hornof, *Eur. J. Pharm. Biopharm.* **2003**, *55*(2), 185–190.

[147] G. Millotti, C. Samberger, E. Fröhlich, D. Sakloetsakun, A. Bernkop-Schnürch, *J. Mater. Chem.* **2010**, *20*(12), 2432–2440.

[148] T. Masuko, A. Minami, N. Iwasaki, T. Majima, S.-I. Nishimura, Y. C. Lee, *Biomacromolecules* **2005**, *6*(2), 880–884.

[149] I. Bravo-Osuna, D. Teutonico, S. Arpicco, C. Vauthier, G. Ponchel, *Int. J. Pharm.* **2007**, *340*(1-2), 173–181.

[150] N. Nakajima, Y. Ikada, *Bioconjugate Chem.* **2002**, *6*(1), 123–130.

[151] G. Ellman, *Arch. Biochem. Biophy.* **1959**, *82*(1), 70–77.

[152] G. Ellman, K. D. Courtney, V. Andres, R. Featherstone, *Biochem. Pharmacol.* **1961**, *7*(2), 88–95.

[153] D. Lee, W. Zhang, S. A. Shirley, X. Kong, G. R. Hellermann, R. F. Lockey, S. S. Mohapatra, *Pharm. Res.* **2007**, *24*(1), 157–167.

[154] a) K. Kafedjiiski, A. H. Krauland, M. H. Hoffer, A. Bernkop-Schnürch, *Biomaterials* **2005**, *26*(7), 819–826; b) R. Singh, L. Kats, W. A. Blättler, J. M. Lambert, *Anal. Biochem.* **1996**, *236*(1), 114–125.

[155] R. Li, H. Lv, X. Zhang, P. Liu, L. Chen, J. Cheng, B. Zhao, *Spectrochim. Acta A Mol. Biomol. Spectrosc.* **2015**, *148*, 369–374.

[156] E. R. M. Sydnor, T. M. Perl, *Clin. Microbiol. Rev.* **2011**, *24*(1), 141–173.

[157] O. Tenaillon, D. Skurnik, B. Picard, E. Denamur, *Nat. Rev. Microbiol.* **2010**, *8*(3), 207–217.

[158] a) G. G. Nicolas, M. C. Lavoie, *Can. J. Microbiol.* **2010**, *57*(1), 1–20; b) M. Sanchez-Acedo, J. Montiel-Company, F. Dasi-Fernandez, J. Almerich-Silla, *Med. Oral.* **2013**, *18*(6), e839–e845.

[159] H. Wang, H. Cheng, F. Wang, D. Wei, X. Wang, *J. Microbiol. Methods* **2010**, *82*(3), 330–333.

[160] H. Y. Lee, S. M. Park, D. H. Ahn, *J. Korean Soc. Food Sci. Nutr.* **2003**, *16*(4), 430–436.

[161] a) G.-J. Tsai, W.-H. Su, H.-C. Chen, C.-L. Pan, *Fish. Sci.* **2002**, *68*(1), 170–177; b) R. Kumar, P. K. Surendan, T. K. Thankappan, *Fish. Technol.* **2006**, *43*(1), 79–84.

[162] a) K. Bae, E. J. Jun, S. M. Lee, D. I. Paik, J. B. Kim, *Clin Oral Investig* **2006**, *10*(2), 102–107; b) Q. X. Ji, D. Y. Zhong, R. Lü, W. Q. Zhang, J. Deng, X. G. Chen, *Carbohydr. Res.* **2009**, *344*(11), 1297–1302; c) E. M. Costa, S. Silva, C. Pina, F. K. Tavaria, M. M. Pintado, *Anaerobe* **2012**, *18*(3), 305–309.

[163] O. Inta, R. Yoksan, J. Limtrakul, *Mater. Sci. Eng. C Mater. Biol. Appl.* **2014**, *42*, 569–577.

[164] P. Sahariah, B. E. Benediktssdóttir, M. Á. Hjálmarsdóttir, O. E. Sigurjonsson, K. K. Sørensen, M. B. Thygesen, K. J. Jensen, M. Másson, *Biomacromolecules* **2015**, *16*(5), 1449–1460.

[165] B. Han, Y. Wei, X. Jia, J. Xu, G. Li, *J. Appl. Polym. Sci.* **2012**, *125*(S2), E143-E148.

[166] a) L. E. Chávez de Paz, A. Resin, K. Howard, D. Sutherland, P. Wejse, *Appl. Environ. Microbiol.* **2011**, *77*(11), 3892–3895; b) Z. Shi, K. G. Neoh, E. T. Kang, W. Wang, *Biomaterials* **2006**, *27*(11), 2440–2449.

[167] a) A. R. Sarasam, P. Brown, S. S. Khajotia, J. J. Dmytryk, S. V. Madihally, *J. Mater. Sci. Mater. Med.* **2008**, *19*(3), 1083–1090; b) C. Virga, C. Landa, D. Beltramo, F. Ausar, S. T. Dorronsoro, *Acta Odontol. Latinoam.* **2003**, *16*(1-2), 9–16.

[168] B. Hasenknopf, *Front. Biosci.* **2005**, *10*(1-3), 275–287.

[169] a) C. Jasmin, N. Raybaud, D. Haapala, F. Sinoussi, J. C. Chermann, C. B. Loustau, C. Bonissol, P. Kona, M. Raynaud, *Biomedicine* **1973**, *18*(4), 319–327; b) S. Shigeta, S. Mori, T. Yamase, N. Yamamoto, N. Yamamoto, *Biomed. Pharmacother.* **2006**, *60*(5), 211–219.

[170] C. Jasmin, G. Herve, A. Teze, P. Souchay, J. C. Chermann, C. Boy Loustau, N. Raybaud, F. Sinoussi, M. Raynaud, *J. Natl. Cancer Inst.* **1974**, *53*(2), 469–474.

[171] J. C. Chermann, F. Sinoussi, C. Jasmin, *Biochem. Bioph. Res. Co.* **1975**, *65*(4), 1229–1236.

[172] C. Cibert, C. Jasmin, *Biochem. Bioph. Res. Co.* **1982**, *108*(4), 1424–1433.

[173] D. Dormont, B. Spire, F. Barré-Sinoussi, L. Montagnier, J. C. Chermann, *Ann. Inst. Pasteur Virol.* **1985**, *136*(1), 75–83.

[174] W. Rozenbaum, D. Dormont, B. Spire, E. Vilmer, M. Gentilini, C. Griscelli, L. Montagnier, F. Barre-Sinoussi, J. C. Chermann, *Lancet* **1985**, *325*(8426), 450–451.

[175] B. L. Moskovitz, *Antimicrob. Agents. Ch.* **1988**, *32*(9), 1300–1303.

[176] M. Burgard, P. Sansonetti, D. Vittecoq, P. Descamps, D. Guetard, S. Herson, W. Rozenbaum, C. Rouzioux, *Aids* **1989**, *3*(10), 665–668.

[177] R. Jee, *Analyst* **1988**, *113*(8), 1321–1324.

[178] T. Yamase, H. Fujita, K. Fukushima, *Inorganica Chim. Acta* **1988**, *151*(1), 15–18.

[179] T. Yamase, K. Tomita, *Inorganica Chim. Acta* **1990**, *169*(2), 147–150.

[180] S. Mitsui, A. Ogata, H. Yanagie, H. Kasano, T. Hisa, T. Yamase, M. Eriguchi, *Biomed. Pharmacother.* **2006**, *60*(7), 353–358.

[181] A. Ogata, S. Mitsui, H. Yanagie, H. Kasano, T. Hisa, T. Yamase, M. Eriguchi, *Biomed. Pharmacother.* **2005**, *59*(5), 240–244.

[182] A. Ogata, H. Yanagie, E. Ishikawa, Y. Morishita, S. Mitsui, A. Yamashita, K. Hasumi, S. Takamoto, T. Yamase, M. Eriguchi, *Br. J. Cancer* **2008**, *98*(2), 399–409.

[183] I. E. León, V. Porro, S. Astrada, M. G. Egusquiza, C. I. Cabello, M. Bollati-Fogolin, S. B. Etcheverry, *Chem. Biol. Interact.* **2014**, *222*, 87–96.

[184] X. Wang, J. Liu, J. Li, Y. Yang, J. Liu, B. Li, M. T. Pope, *J. Inorg. Biochem.* **2003**, *94*(3), 279–284.

[185] H. Stephan, M. Kubeil, F. Emmerling, C. E. Müller, *Eur. J. Inorg. Chem.* **2013**, *2013*(10-11), 1585–1594.

[186] R. Prudent, V. Moucadel, B. Laudet, C. Barette, L. Lafanechère, B. Hasenknopf, J. Li, S. Bareyt, E. Lacôte, S. Thorimbert, M. Malacria, P. Gouzerh, C. Cochet, *Chem. Biol.* **2008**, *15*(7), 683–692.

[187] R. Raza, A. Matin, S. Sarwar, M. Barsukova-Stuckart, M. Ibrahim, U. Kortz, J. Iqbal, *Dalton Trans.* **2012**, *41*(47), 14329–14336.

[188] M. Inoue, K. Segawa, S. Matsunaga, N. Matsumoto, M. Oda, T. Yamase, *J. Inorg. Biochem.* **2005**, *99*(5), 1023–1031.

[189] N. Fukuda, T. Yamase, *Biol. Pharm. Bull.* **1997**, *20*(8), 927–930.

[190] T. Yamase, N. Fukuda, Y. Tajima, *Biol. Pharm. Bull.* **1996**, *19*(3), 459–465.

[191] a) S. Shigeta, S. Mori, E. Kodama, J. Kodama, K. Takahashi, T. Yamase, *Antivir. Res.* **2003**, *58*(3), 265–271; b) S. Ikeda, S. Nishiya, A. Yamamoto, T. Yamase, C. Nishimura, E. D. Clercq, *J. Med. Virol.* **1993**, *41*(3), 191–195.

[192] X.-y. Hu, B.-n. Chen, L. Wang, F.-h. Chen, *Chem. Res. Chin. Univ.* **2012**, *28*(5), 862–865.

[193] S. Hosseini, E. Amini, M. Tavassoti Kheiri, P. Mehrbod, M. Shahidi, E. Zabihi, *Int. J. Mol. Cell. Med.* **2012**, *1*(1), 21–29.

[194] Z. Wenxiu, W. Chuanhua, D. Shunfu, L. Yan, Z. Duo, H. Liqin, *Proceedings 2011 International Conference on Human Health and Biomedical Engineering*: In vitro study on the antitumor activity of several new polyoxometalates, **2011**.

[195] a) X. Wang, J. Liu, M. T. Pope, *Dalton Trans.* **2003,** 5, 957–960; b) X. Wang, L. Xu, Y. Li, F. Li, *J. Nanosci. Nanotechnol.* **2005**, *5*(6), 905–908.

[196] a) Y. Yang, J. He, X. Wang, B. Li, J. Liu, *Transition Met. Chem.* **2004**, *29*(1), 96–99; b) X. Wang, F. Li, S. Liu, M. T. Pope, *J. Inorg. Biochem.* **2005**, *99*(2), 452–457.

[197] F. Zhai, D. Li, C. Zhang, X. Wang, R. Li, *Eur. J. Med. Chem.* **2008**, *43*(9), 1911–1917.

[198] T. Meißner, R. Bergmann, J. Oswald, K. Rode, H. Stephan, W. Richter, H. Zänker, W. Kraus, F. Emmerling, G. Reck, *Transition Met. Chem.* **2006**, *31*(5), 603–610.

[199] G. Geisberger, E. B. Gyenge, C. Maake, G. R. Patzke, *Carbohydr. Polym.* **2013**, *91*(1), 58–67.

[200] D. Menon, R. T. Thomas, S. Narayanan, S. Maya, R. Jayakumar, F. Hussain, V.-K. Lakshmanan, S. V. Nair, *Carbohydr. Polym.* **2011**, *84*(3), 887–893.

[201] H. S. Shah, R. Al-Oweini, A. Haider, U. Kortz, J. Iqbal, *Toxicol. Rep.* **2014**, *1*, 341–352.

[202] H. S. Shah, S. A. Joshi, A. Haider, U. Kortz, N. ur-Rehman, J. Iqbal, *RSC Adv.* **2015**, *5*(113), 93234–93242.

[203] L. de Matteis, S. G. Mitchell, J. M. de La Fuente, *J. Mater. Chem. B* **2014**, *2*(41), 7114–7117.

[204] G. Fiorani, O. Saoncella, P. Kaner, S. A. Altinkaya, A. Figoli, M. Bonchio, M. Carraro, *J. Clust. Sci.* **2014**, *25*(3), 839–854.

[205] M. Michelon, G. Herve, *Comptes Rendus Acad. Sci.* **1972**, *274*(3), 209-212.

[206] I.-M. Mbomekalle, Y. W. Lu, B. Keita, L. Nadjo, *Inorg. Chem. Commun.* **2004**, *7*(1), 86–90.

[207] R. Finke, M. Droege, P. Domaille, *Inorg. Chem.* **1987**, *26*(23), 3886–3896.

[208] P. Roman, A. San José, A. Aranzabe, A. Luque, *Thermochim. Acta* **1992**, *206*, 137–147.

[209] C. Sanchez, J. Livage, J. P. Launay, M. Fournier, Y. Jeannin, *J. Am. Chem. Soc.* **1982**, *104*(11), 3194–3202.

[210] P. J. Domaille, W. H. Knoth, *Inorg. Chem.* **1983**, *22*(5), 818–822.

[211] L. E. Briand, G. M. Valle, H. J. Thomas, *J. Mater. Chem.* **2002**, *12*(2), 299–304.

[212] G. Geisberger, S. Paulus, M. Carraro, M. Bonchio, G. R. Patzke, *Chemistry* **2011**, *17*(16), 4619–4625.

[213] H. Yanagie, A. Ogata, S. Mitsui, T. Hisa, T. Yamase, M. Eriguchi, *Biomed. Pharmacother.* **2006**, *60*(7), 349–352.

[214] T. Yamase, H. Fujita, K. Fukushima, *Inorganica Chim. Acta* **1988**, *151*(1), 15–18.

[215] J. Fischer, L. Ricard, R. Weiss, *J. Am. Chem. Soc.* **1976**, *98*(10), 3050–3052.

[216] R. Finke, M. Droege, P. Domaille, *Inorg. Chem.* **1987**, *26*(23), 3886–3896.

[217] R. Contant, R. Thouvenot, *Inorganica Chim. Acta* **1993**, *212*(1-2), 41–50.

[218] C. L. Hill, M. S. Weeks, R. F. Schinazi, *J. Med. Chem.* **1990**, *33*(10), 2767–2772.

[219] T. Yamase, T. Ikawa, *B. Chem. Soc. Jpn.* **1977**, *50*(3), 746–749.

[220] F. Pu, E. Wang, H. Jiang, J. Ren, *Mol. Biosyst.* **2013**, *9*(1), 113–120.

[221] X.-G. Chen, H.-J. Park, *Carbohydr. Polym.* **2003**, *53*(4), 355–359.

[222] C. He, Y. Hu, L. Yin, C. Tang, C. Yin, *Biomaterials* **2010**, *31*(13), 3657–3666.

[223] F. Alexis, E. Pridgen, L. K. Molnar, O. C. Farokhzad, *Mol. Pharm.* **2008**, *5*(4), 505–515.

[224] K. Greish, *J. Drug. Target.* **2007**, *15*(7-8), 457–464.

[225] S. E. McNeil, *Wiley Interdiscip. Rev. Nanomed. Nanobiotechnol.* **2009**, *1*(3), 264–271.

[226] H. Jonassen, A.-L. Kjøniksen, M. Hiorth, *Colloid Polym Sci* **2012**, *290*(10), 919–929.

[227] S. Kalliola, E. Repo, V. Srivastava, J. P. Heiskanen, J. A. Sirviö, H. Liimatainen, M. Sillanpää, *Colloids Surf. B Biointerfaces* **2017**, *153*, 229–236.

[228] M. Inoue, T. Suzuki, Y. Fujita, M. Oda, N. Matsumoto, J. Iijima, T. Yamase, *Biomed. Pharmacother.* **2006**, *60*(5), 220–226.

[229] M. Inoue, K. Segawa, S. Matsunaga, N. Matsumoto, M. Oda, T. Yamase, *J. Inorg. Biochem.* **2005**, *99*(5), 1023–1031.

[230] G. Geisberger, S. Paulus, E. B. Gyenge, C. Maake, G. R. Patzke, *Small* **2011**, *7*(19), 2808–2814.

[231] C. Goodman, C. McCusker, T. Yilmaz, V. Rotello, *Bioconjugate Chem.* **2004**, *15*(4), 897–900.

[232] a) K. Engin, D. B. Leeper, J.R. Cater, A. J. Thistlethwaite, L. Tupchong, J. D. McFarlane, *Int. J. Hyperthermia* **1995**, *11*(2), 211–216; b) L. E. Gerweck, K. Seetharaman, *Cancer Res.* **1996**, *56*(6), 1194–1198.

[233] a) M. Stubbs, P. M. McSheehy, J. R. Griffiths, C. Bashford, *Mol. Med. Today* **2000**, *6*(1), 15–19; b) P. Swietach, R. D. Vaughan-Jones, A. L. Harris, A. Hulikova, *Philos. Trans. R. Soc. Lond. B Biol. Sci.* **2014**, *369*(1638); 20130099.

[234] J. Wang, D. Hu, Z. Su, *Chin. Sci. Bull.* **2010**, *55*(23), 2497–2504.

[235] M. B. Čolović, B. Medić, M. Ćetković, T. Kravić Stevović, M. Stojanović, W. W. Ayass, A. S. Mougharbel, M. Radenković, M. Prostran, U. Kortz, D. Z. Krstić, *Toxicol. Appl. Pharmacol.* **2017**, *333*, 68–75.

[236] S. Dünnhaupt, J. Barthelmes, S. Köllner, D. Sakloetsakun, G. Shahnaz, A. Düregger, A. Bernkop-Schnürch, *Carbohydr. Polym.* **2015**, *117*, 577–584.

[237] G. W. Anderson, J. E. Zimmerman, F. M. Callahan, *J. Am. Chem. Soc.* **1963**, *85*(19), 3039.

[238] M. D. Cathell, J. C. Szewczyk, F. A. Bui, C. A. Weber, J. D. Wolever, J. Kang, C. L. Schauer, *Biomacromolecules* **2008**, *9*(1), 289–295.

[239] a) M. Stroescu, A. Stoica-Guzun, G. Isopencu, S. I. Jinga, O. Parvulescu, T. Dobre, M. Vasilescu, *Food Hydrocoll.* **2015**, *48*, 62–71; b) X. Jin, J. Wang, J. Bai, *Carbohydr. Res.* **2009**, *344*(6), 825–829; c) S. Kumar, M. Kumari, P. K. Dutta, J. Koh, *Int. J. Polym. Mater. Po.* **2013**, *63*(4), 173–177; d) L. Marin, B. Simionescu, M. Barboiu, *Chem. Commun.* **2012**, *48*(70), 8778–8780.

[240] S. Warren, J. Clayden, *Organic chemistry;* Oxford University Press, Oxford, **2001**.

[241] Y. J. Jeon, *J. Microbiol. Biotechnol.* **2001**, *11*(2), 281–286.


CMSZH
CHEMICAL MOLECULAR SCIENCES ZURICH
GRADUATE SCHOOL